

https://dspace.org/

Kinetic and thermodynamic studies of N-acetyl-cobalt(III)-microperoxidase 8: a vitamin B12a analogue

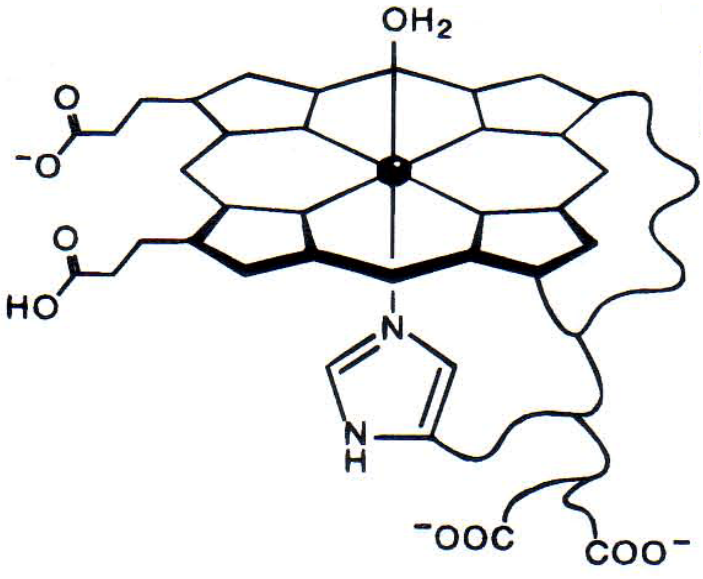
Mathura, Sadhna

2014-02-18
http://hdl.handle.net10539/13846

Downloaded from a DSpace repository. https://dspace.org/

Kinetic and Thermodynamic studies of *N*-Acetyl-Cobalt(III)-Microperoxidase 8: a vitamin B_{12a} analogue

-Sadhna Mathura-



A thesis submitted to the Faculty of Science, University of the Witwatersrand, Johannesburg, in fulfilment of the requirements for the degree of Doctor of Philosophy

June 2013

DECLARATION

I declare that this is my own unaided work. It is being submitted for the Degree of Doctor of Philosophy at the University of the Witwatersrand, Johannesburg. It has not been submitted before for any degree or examination at any other University.

S. Mathura	H. M. Marques	A. S. de Sousa
	Supervisor	**Co-supervisor**

June 2013

PUBLICATIONS

1. Poster Presentation: SACI International Inorganic Chemical Conference, Mykanos, Western Cape, **2007**: Kinetic and Thermodynamic studies of Co(III)MP8: A vitamin B_{12a} analogue.

2. Poster Presentation SACI International Inorganic Chemical Conference, Witwatersrand, Johannesburg, **2011**: Kinetics and Thermodynamic studies of NAcCo(III)MP8: A vitamin B_{12a} analogue.

3. Poster presented by Helder Marques: 40^{th} International Conference on Coordination Chemistry, Valencia, Spain, **2012**: Controlling the Coordination Chemistry of Co(III): corrins and porphyrin.

4. Mathura, S.; de Sousa, A. S.; Fernandes, M. A.; Marques, H. M., **2012**, *Inorg. Chim. Acta*, *392*, 108.

5. Mathura, S.; Sannay, D; de Sousa, A. S.; Marques, H. M., **2012**, *The Preparation of N-Acetyl-Co(III) Microperoxidase-8 (NAcCoMP8) and its Solution Chemistry: Paper 1:* submitted: *J. Inorg. Biochem.*

6. Mathura, S.; de Sousa, A. S.; Perry, C. B.; Navizet, I.; Marques, H. M., **2012**, *The Ligand Substitution Reactions of N-Acetyl-Co(III) Microperoxidase-8 (NAcCoMP8): a Comparison with Aquacobalamin (vitamin B_{12a}): Paper 2:* submitted: *J. Inorg. Biochem.*

ABSTRACT

Comparisons of the kinetic and thermodynamic properties of a Co(III)-porphyrin-containing octapeptide, a model for aquacobalamin (H_2OCbl^+, vitamin B_{12a}), with aquacobalamin are made in order to elucidate the effect the nature of the macrocycle(porphyrin or corrin) has on the properties of Co(III).

The Co(III) porphyrin octapeptide *N*-acetyl-Co(III) Microperoxidase-8 (NAcCoMP8) was prepared by the proteolytic digestion of cytochrome *c*, replacement of Fe(III) by Co(III), and protection of the *N*-terminal group of the peptide by acetylation. In neutral aqueous solution it is monomeric at low concentration with a Soret band at 415 nm with $\varepsilon = 1.61(3) \times 10^5$ M^{-1} cm^{-1}; higher concentrations (> 10 μM), an increase in the ionic strength of the solution, or an increase in temperature above 45 ^oC causes the formation of oligomeric species with a Soret band at 425 nm, usually through intermediacy of a species with a Soret band at 417 nm. Although formation of the latter can be reversed to produce the monomeric 415 nm species on dilution of the solution, or by lowering the temperature or the ionic strength, the formation of the former is irreversible and on standing eventually leads to precipitation of the metallopeptide from solution. NAcCoMP8 has five spectroscopically observable pK_as: at 1.74 ± 0.04 due to protonation and displacement of His-18 either by H_2O or a carboxylate from the peptide; at 4.08 ± 0.02 and 5.80 ± 0.05 due to ionization of the heme carboxylate groups; at 7.81 ± 0.03 due to ionization of coordinated H_2O; and at 12.00 ± 0.03 due to ionization of His-18 to form an imidazolate. NAcCoMP8 provides a means of comparing and contrasting the chemistry of Co(III) porphyrins and corrins and so assessing the influence of the macrocycle on the chemistry of the metal ion.

NAcCoMP8 and aquacobalamin both contain Co(III), an N-donor macrocyclic equatorial ligand (porphyrin, corrin), an imidazole derivative as one axial ligand (His, 5,6- dimethylbenzimidazole) and H_2O in the other axial coordination site. This

allows for an evaluation of the effect of the equatorial macrocyclic ligand on ligand substitution reactions of Co(III). Equilibrium constants (as log K values) for the coordination of anionic (CN^-, N_3^-, NO_2^-, HSO_3^-) and neutral (pyridine, *N*-methylimidazole, methoxylamine and hydroxylamine) ligands were determined spectrophotometrically as a function of temperature and ΔH and ΔS values are reported. The log K value for coordination of pyridine by H_2OCbl^+ is anomalously low. Anionic ligands bind more strongly to H_2OCbl^+ than to NAcCoMP8 while the converse is true for the neutral ligands. It is suggested that the higher residual charge at the metal centre in the corrin (+2) compared to the porphyrin (+1) is primarily responsible. The anionic and neutral ligands behave differently. Log K values for coordination of the anionic ligands by both NAcCoMP8 and H_2OCbl^+ parallel the pK_a of their conjugate acid. In the case of the neutral ligands, log K for coordination by NAcCoMP8 correlates directly with ligand basicity but there is an inverse correlation in the case of H_2OCbl^+. Log K and ΔH values for the reaction with anionic ligands parallel each other in the two systems, but there appears to be an inverse correlation for the neutral ligands.

Kinetics measurements show that H_2OCbl+ is significantly more labile towards substitution by CN^- than NAcCoMP8 (k_{25} = 240 and 103 M^{-1} s^{-1}, respectively) because of a much smaller $\Delta H^‡$ value which is somewhat, but not completely, compensated for by a much more negative $\Delta S^‡$. By contrast, the reaction of *N*-methylimidazole occurs faster with NAcCoMP8 than with H_2OCbl^+ due to a smaller $\Delta H^‡$ and a somewhat larger $\Delta S^‡$. Since the intimate mechanism is probably an interchange mechanism under dissociative activation, the kinetic results are rationalized by the extent of participation of the entering ligand in the transition state. CN^- forms a more stable complex with H_2OCbl^+ (log K > 12) than NAcCoMP8 (log K = 6.04). In its reaction with H_2OCbl^+ the transition state will occur earlier along the reaction coordinate than in its reaction with NAcCoMP8 leading to a lower $\Delta H^‡$. The converse is true for *N*-methylimidazole where its greater affinity for the porphyrin than the corrin (log K = 5.70 and 4.49, respectively) makes its reaction with the former faster (k_{25} = 1300 M^{-1} s^{-1} compared

to 14 M^{-1} s^{-1}). Therefore there is a correlation between the thermodynamic stability of Co(III) complexes of corrin and porphyrins and the rate of substitution of axially coordinated H_2O. The nature of the macrocycle in these Co(III) systems has a profound effect on the chemistry of the metal ion.

In memory of those whom I have lost during my Ph.D.

ACKNOWLEDGEMENTS

I acknowledge:

The National Research Foundation (NRF), the University of the Witwatersrand (Wits) and others for financing this project;

The various institutions, departments, groups, technicians and people whose expertise contributed to this project.

I thank:

Helder Marques and Alvaro de Sousa for their tireless efforts, tutelage, indulgences, merciless editing and after-hours support;

Drew Pullinger, Stuart Smith and Emil Wentzel for essential Mac support;

Chris Perry and Denzel Sannasy for their microperoxidase expertise;

Gert Schoeman for his outstanding Cary and Varian support through my Ph. D;

Susan Chemaly for her vitamin B_{12a} expertise.

I am indebted to:

Nicole. Thank you for sparking my love for the '*Colours of Life*' with my very first pyrrole distillation;

Paradise. In the end, your example saw me through, *one small step at a time*;

Chick, Dan, Steve: thank you for being with me from the very beginning and for enduring until the very end;

Tish, thank you for the *puns*, for indulging me, supporting me and loving me;

Ma, in so many ways this degree would not have reached fruition without you. Thank you for helping me to achieve my dream and for believing in me even when I didn't -- Thank you;

Lois. Thank you for teaching me more about life and about myself than I could ever hope to learn from a Ph. D.

TABLE OF CONTENTS

DECLARATION ii

PUBLICATIONS iii

ABSTRACT iv

ACKNOWLEDGEMENTS viii

LIST OF ABBREVIATIONS xvi

LIST OF TABLES xviii

LIST OF FIGURES xx

CHAPTER 1: INTRODUCTION 1

1.1 INTRODUCTION 1

1.2 METALLOPROTEINS 5

1.2.1 *The significance of metalloproteins* 5

1.2.2 *Biologically important metal ions* 7

1.3 BIOLOGICALLY IMPORTANT MACROCYCLES 11

1.3.1 *Porphyrins* 13

1.3.2 *Corrins* 18

1.3.3 *A comparison of porphyrins and corrins* 20

1.4 MICROPEROXIDASES (MP) 27

1.5 COBALAMINS (Cbl) 37

1.6 PROBLEM STATEMENT, BIOLOGICAL RELEVANCE, SCOPE, AIMS AND ORGANISATION OF THIS WORK 44

1.6.1 *Problem statement* 44

1.6.2 *Biological relevance* 45

1.6.3 *Scope and specific aims* 46

1.6.4 *Organisation of this work* 48

1.7 REFERENCES 49

CHAPTER 2: GENERAL MATERIALS AND METHODS 62

2.1 INTRODUCTION 62

2.2 QUALITATIVE ASSESSMENT OF AGGREGATION EFFECTS ON THE SOLUTION CHEMISTRY OF NAcCoMP8 63

Investigation 1.1: Synthesis, Isolation and Characterisation of NAcCoMP8†

2.2.1 *Synthesis of NAcCoMP8* 65

2.2.1.1 FeMP11 from cytochrome *c* 66

2.2.1.2 NAcFeMP11 by acetylation of FeMP11 67

2.2.1.3 NAcMP11 by reductive demetalation of NAcFeMP11 68

2.2.1.4 NAcCoMP11 by oxidative remetalation of NAcMP11 69

2.2.1.5 NAcCoMP8 by tryptic digestion of NAcCoMP11 70

2.2.2 *Isolation of NAcCoMP8* 71

2.2.2.1 Sep-Pak® cartridges and Millex® filters 71

2.2.2.2 Gel permeation chromatography 72

2.2.3 *Characterisation of NAcCoMP8* 73

2.2.3.1 UV-vis spectroscopy 73

2.2.3.2 HPLC 74

2.2.3.3 Mass spectrometry (MS) 76

2.2.3.4 ICP-OES analysis 76

Investigation 1.2: Solution Behaviour of NAcCoMP8†

2.2.4 *Effects of Time (equilibrium observations)* 77

2.2.5 *Effects of Light* 78

2.2.6 *Effects of Air (oxygen sensitivity)* 78

2.2.7 *Effects of Ionic Strength* 79

2.2.8 *Effects of Concentration (Beer's law investigation)* 79

2.2.9 *Effects of pH (pK_a investigation)* 80

2.2.10 *Effects of Temperature* 82

2.2.11 *Effects of Dispersing Agents and Buffers* 83

2.2.12 *Effects of Reducing Agents* 83

2.3 QUANTITATIVE ASSESSMENT OF THE SOLUTION CHEMISTRY OF NAcCoMP8 84

Investigation 2.1: Thermodynamics of ligand binding reactions of NAcCoMP8†

2.3.1 *Determination of equilibrium constants in NAcCoMP8 with selected donor ligands (pH 7.0; μ = 0.1 M) as a function of temperature* 84

Investigation 2.2: Kinetics of ligand substitution reactions of NAcCoMP8†

2.3.2 *Kinetic of substitution in NAcCoMP8 with selected donor ligands (pH 7.0; μ = 0.1 M) as a function of temperature* 86

2.4 SUMMARY OF MATERIALS 88

2.4.1 *Chemicals* 88

2.4.2 *Equipment* 90

2.5 GENERAL METHODS 91

2.5.1 *pH Measurements* 91

2.5.2 *Buffer Preparations* 91

2.5.3 *Lyophilisation* 92

2.6 MISCELLANEOUS EXPERIMENTS 93

2.6.1 *Synthesis of CoTPPS and CoTMPyP* 93

2.6.2 *Recovery of NAcCoMP8* 95

2.7 REFERENCES 96

CHAPTER 3: MONOMERISATION PART 1: Synthesis Aspects 98

3.1 INTRODUCTION 98

3.2 RESULTS AND DISCUSSION 100

3.2.1 *Optimisation of the acetylation process of NAcCoMP8* 101

3.2.1.1 Percentage yields in NAcCoMP8 synthesis 101

3.2.1.2 General observations of 3 cobalt microperoxidases 105

3.2.2 *Factors influencing aggregation during synthesis* 112

3.2.2.1 Amicon® vs Sep-Pak® observations on NAcCoMP8 112

3.2.2.2 Gel permeation chromatography of FeMP11 116

3.2.2.3 General spectroscopic observations in NAcCoMP8 119

3.3 SUMMARY AND CONCLUSIONS 125

3.4 REFERENCES 127

CHAPTER 4: MONOMERISATION PART 2: Solution Behaviour 130

4.1 INTRODUCTION 130

4.2 RESULTS AND DISCUSSION 133

4.2.1 *Effects of Time (equilibrium observations)* 133

4.2.2 *Effects of Light* 139

4.2.3 *Effects of Air (oxygen sensitivity)* 140

4.2.4 *Effects of Ionic Strength* 142

4.2.5 *Effects of Concentration (Beer's Law investigation)* 147

4.2.6 *Effects of pH (pK_a investigation)* 150

4.2.7 *Effects of Temperature* 158

4.2.8 *Effects of Dispersing Agents and Buffers* 160

4.2.9 *Effects of Reducing Agents* 163

4.3 SUMMARY AND CONCLUSIONS 165

4.4 REFERENCES 170

CHAPTER 5: EQUILIBRIUM CONSTANTS FOR LIGAND BINDING BY NAcCoMP8 174

5.1 INTRODUCTION 174

5.2 RESULTS AND DISCUSSION 177

5.2.1 *A Qualitative Examination of the Physical Data* 178

5.2.1.1 Absorbance spectra observations 178

5.2.1.2 Structural Evidence (from the CSD) 199

5.2.2 *Ligand Binding* 202

5.2.2.1 Log K trends 202

5.2.2.2 ΔH and ΔS trends 210

5.3 SUMMARY AND CONCLUSIONS 224

5.4 REFERENCES 228

CHAPTER 6: KINETICS OF THE LIGAND SUBSTITUTION REACTIONS OF NAcCoMP8 235

6.1 INTRODUCTION 235

6.2 RESULTS AND DISCUSSION 237

6.3 SUMMARY AND CONCLUSIONS 249

6.4 REFERENCES 251

CHAPTER 7: CONCLUSIONS AND FUTURE WORK 253

7.1 INTRODUCTION 253

7.2 STRATEGY USED IN THIS WORK 254

7.3 MONOMERISATION OF NAcCoMP8: Synthesis Aspects 255

7.4 MONOMERISATION OF NAcCoMP8: Solution Behaviour 256

7.5 EQUILIBRIUM CONSTANTS FOR NAcCoMP8 (Thermodynamics) 259

7.6 RATE CONSTANTS FOR NAcCoMP8 (Kinetics) 261

7.7 FINAL CONCLUSION AND COMMENT 263

7.8 REFERENCES 264

APPENDIX 265

2 APPENDIX FOR CHAPTER 2: Materials and Methods 265

A2.1 *Alternative Synthetic Routes* 265

A2.2 *Miscellaneous Synthesis Information* 270

A2.3 *Derivation for Equation 2.4* 275

3 APPENDIX FOR CHAPTER 3: Monomerisation Part 1 279

A3.1 *The Complex Solution Chemistry of CoMP8* 280

A3.2 *Percentage Yield, ICP-OES and Absorptivity Data* 281

A3.3 *FeMP5, FeMP6, FeMP8, FeMP9 and FeMP11* 282

A3.4 *TLC Patterns* 287

A3.5 *Amine Protection Experiments* 288

A3.6 *Characterisation of NAcCoMP8* 291

A3.7 *Synthetic Porphyrins (Publication: Abstract only)* 293

A3.8 *Other Publications (Abstract only)* 294

4 APPENDIX FOR CHAPTER 4: Monomerisation Part 2 298

A4.1 *Derivation of Equation 4.5 and 4.9* 298

† numbering here pertains exclusively to the Investigation sequence- see Chapter 2 for clarity.

LIST OF ABBREVIATIONS

Abbreviation/Symbol	Definition
AdoCbl	Adenosylcobalamin or coenzyme B_{12}
AR	Analytical reagent
B_{12a}	Aquacobalamin or Vitamin B_{12a} or H_2OCbl^+
BP	Biologically pure
CAPS	3-[Cylohexylamino]-1-propanesulfonic† acid
Cbl	Cobalamin(s)
CHAPS	3[(3-Cholamidopropyl)dimethylammonio]-propanesulfonic acid
CHES	3-[*N*-Cylohexylamino]-ethansulfonic acid
CNCbl	Cyanocobalamin or vitamin B_{12}
Co(X)	Cobalt ion where X = I, II or III
Cor	Corrin
CoTPPS	Diaqua-5,10,15,20-tetra-*p*-phenylsulfonyporphinato-cobalt(III)
CoTMPyP	5, 10, 15, Diaqua-5,10,15,20-tetra-*p*-phenyl-N-methyl-4-pyridylporphinato-cobalt(III)
CP	Chemically pure
CR	Commercial reagent
CSD	Cambridge Structural Database
Cys	Cysteine
D	Dissociative mechanism
DMB	5,6-dimethylbenzimidazole
DMAP	4-dimethylaminopyridine
ESI-MS	Electron spray ionisation-mass spectroscopy
FeMP11	Fe(III)-microperoxidase-11
FeMP8	Fe(III)-microperoxidase-8
GR	General reagent
HA	Hydroxylamine
Hb	Hemoglobin††
HEPES	4-(2-hydroxyethyl)-1-piperazineethanesulfonic acid
His or His-18	Histidine or Histidine-18
HOMO	Highest occupied molecular orbital

Abbreviation/Symbo	Definition
HPLC	High performance liquid chromatography
ICP-OES	Inductively coupled plasma optical emission spectrometry
I_d	Dissociative interchange mechanism
k_{25}	Rate constant at 25 ^oC in M^{-1} s^{-1}
LUMO	Lowest unoccupied molecular orbital
Lys	Lysine
Mb	Myoglobin
MES	2-(N-morpholino)ethanesulfonic acid
MeCbl	Methylcobalamin
MOA	Methoxyamine
MOPS	3-[*N*-Mopholino]-propanesulfonic acid
MP	Microperoxidase(s)
MPX	Metal-free microperoxidase where X = 5, 6, 8, 9 or 11
NAcCoMP8	*N*-Acetyl-Co(III)-microperoxidase-8
NAcFeMP8	*N*-Acetyl-Fe(III)-microperoxidase-8
NAcFeMP11	*N*-Acetyl-Co(III)-microperoxidase-11
NMI	*N*-methylimidazole
PDB	Protein databank
PEG	Polyethylene glycol
Por	Porphyrin
Pyr or pyr	Pyridine
RP	Reverse phase
Tris/HCl	Tris-(hydroxymethyl)-aminomethane hydrochloride
Triton X-100	polyethylene glycol p-(1,1,3,3-tetramethylbutyl)-phenyl ether
TWEEN-20	Polyoxyethylene (20) sorbitan monolaurate
Uro'gen III	Uroporphyrinogen III
Val	Valine
$\Delta H^{\ddagger}$ or $\Delta H^{\ddagger}$	Enthalpy of activation
$\Delta S^{\ddagger}$ or $\Delta S^{\ddagger}$	Entropy of activation

---

[†]Sulfur rather than sulphur is the IUPAC-recommended spelling and will be used throughout this thesis for related words
[††]Similarly, hemoprotein rather than haemoprotein is the IUPAC-recommended spelling (http://www.chem.qmul.ac.uk/iupac/)

LIST OF TABLES

Table		Page
1.1	Classification of some biologically significant tetrapyrroles.	3
1.2	Some examples of metalloproteins and their associated functions.	9
1.3	Electronic assignments that accompany Figure 1.13.	36
2.1	Linear gradient HPLC (RP) elution program used for microperoxidase.	75
2.2	A typical ESI-MS LXQ method used for microperoxidase.	76
2.3	Summary of chemicals used in this work.	88
2.4	Summary of equipment and software used in this work.	90
2.5	Summary of the multi-component buffers used in this work.	92
3.1	Percentage yield (by mass) of the various microperoxidases obtained in synthetic Routes A, B, C and D.	102
3.2	Comparison of Amicon® cell and Sep-Pak® cartridge desalting procedures.	113
3.3	Analysis of the bands obtained after FeMP11 gel permeation chromatography.	117
4.1	Rate constants for the conversion of NAcCoMP8 from the 417 to 415 nm species and from 417 to 424 nm species at selected wavelengths.	136
4.2	A comparison of Beer's law limiting slopes for various microperoxidases.	148
4.3	pK_a values for the ionisation of coordinated H_2O in trivalent NAcCoMP8 was a function of monitoring wavelength at 30 ^oC.	155

Table		Page
4.4	Dependence of the pK_a of coordinated H_2O in trivalent NAcCoMP8 as a function of temperature.	156
4.5	Summary of all the results obtained in Chapter 4.	168
4.6	Summary of the qualitative differences observed for the conversion of NAcCoMP8 from 417 to 415 nm species and from 417 to 424 nm.	169
5.1	A comparison of isosbestic points for the replacement of coordinated H_2O with selected ligands in NAcCoMP8 ligand binding studies.	186
5.2	A comparison of isosbestic points for the replacement of coordinated water with CN^- in three NAcCoMP8 species.	194
5.3	Bond length data for some selected corrins and porphyrins.	201
5.4	Equilibrium Constants for the Substitution of Coordinated H_2O in NAcCoMP8 by Some Anionic Ligands.	203
5.5	Equilibrium Constants for the Substitution of Coordinated H_2O in NAcCoMP8 by Some Neutral Ligands.	204
5.6	Thermodynamic trends in some B_{12a}-related compounds with NMI-type ligands.	219
6.1	Rate constants and activation parameters for the reaction of CN^-, NMI and Pyr with NAcCoMP8 and H_2OCbl^+.	244

LIST OF FIGURES

Figure		Page
1.1	Pyrroles.	2
1.2	The biosynthesis of some ‘functional dyes’ showing common ancestry.	4
1.3	Crystal structures of proteins and metalloproteins from PDB.	6
1.4	Illustrating the relationship between metal ion and active enzymes.	6
1.5	The abundance of the elements in the universe relative to Si = 10^4 as a function of atomic number.	10
1.6	Porphin: the backbone of all porphyrins.	14
1.7	Schematic representation of the four porphyrin type isomers.	16
1.8	The cobalt corrin structure.	19
1.9	Comparison of corrin and porphyrin electronic spectra.	20
1.10	Distribution of cobalamin synthesis and utilisation in organisms.	22
1.11	Comparison of corrin and porphyrin biosynthesis.	24
1.12	Hexacoordinate Fe(III) heme fragment from the proteolytic digestion of cytochrome *c*.	28
1.13	Typical UV-vis spectra of ferric (**A**) and ferrous (**B**) iron porphyrins in high (red) and low (blue) spin states.	35

Figure		Page
1.14	Structure and standard view of some important cobalamins.	38
1.15	Pathways of Co-C cleavage in cobalamins.	39
2.1	Flow diagram of the different investigations undertaken in this work.	64
2.2	The four synthetic routes to attain monomeric NAcCoMP8 explored in this work.	66
2.3	Photograph showing the typical reduced pressure/inert atmosphere demetalation set-up.	69
2.4	Photograph showing two purification systems adapted for microperoxidase isolation.	72
2.5	Photograph showing the typical pK_a set-up using a thermostatted cell with an argon line.	81
2.6	The cheaper synthetic Co(III) porphyrins used to develop synthesis protocols in this work.	93
3.1	A flow diagram of the results focused on in Chapter 3.	100
3.2	The effect acetylation on side-chain aggregation in metal-free microperoxidase.	105
3.3	Representation of hemepeptides that may be isolated through the proteolytic digestion of cytochrome *c*.	106
3.4	The UV-vis spectrum of CoMP11 and NAcCoMP11.	107
3.5	The UV-vis spectrum of CoMP8 and NAcCoMP8.	108

Figure		Page
3.6	The UV-vis spectrum of CoMP6 and NAcCoMP6.	109
3.7	Representation of the various *J*-type aggregation forms that may be exhibited by concentrated Co(III) microperoxidases in solution.	111
3.8	The effect of separation technique on the aggregation of NAcCoMP8.	114
3.9	UV-vis spectra of the iron microperoxidase contaminants after FeMP11 purification on gel permeation chromatography.	118
3.10	UV-vis spectrum of NAcCoMP8 at varying pH.	121
3.11	UV-vis spectrum of NAcCoMP8 at varying states of aggregation.	122
3.12	UV-vis spectrum of NAcCoMP8 at varying states of degradation.	123
4.1	A flow diagram of the results focused on in Chapter 4.	132
4.2	The effects of equilibration time on the absorbance of NAcCoMP8 at low and at high concentration in deionised water (pH 6.89; 25 ^{o}C).	137
4.3	Estimated half lives (min) at specific wavelengths for NAcCoMP8 during the equilibration time study at low and high concentration.	138
4.4	The effect of light exposure on the absorbance of NAcCoMP8 (*ca*. 1.25 μM; pH 7; H_2O).	139
4.5	The effects of O_2 exposure on the absorbance of NAcCoMP8 (*ca*. 1.25 μM; pH 7; H_2O).	141
4.6	The effects of ionic strength on the absorbance of NAcCoMP8 at low and high concentration (*ca*. pH 7; 25 ^{o}C).	146

Figure		Page
4.7	The effects of concentration on the absorbance of NAcCoMP8 (*ca*. pH 7; 25 ^{o}C; H_2O).	149
4.8	The effects of pH on the absorbance of NAcCoMP8.	151
4.9	The possible pH-dependent species distribution for NAcCoMP8.	153
4.10	Illustrating the dependence of the Soret region of NAcCoMP8 on pH at 30 ^{o}C.	157
4.11	The effects of temperature on the absorbance of NAcCoMP8 at low and high concentration (*ca*. pH 7; deionised water).	159
4.12	The effects of dispersing agents and buffers on the absorbance spectrum of NAcCoMP8.	162
4.13	The effects of the reducing agent $NaBH_4$ on the absorbance spectrum of NAcCoMP8.	164
5.1	Structures of Vitamin B_{12a} and NAcCoMP8.	175
5.2	Flow diagram of the different aims and results in Chapter 5	176
5.3	Comparison of absorbance spectra of NAcCoMP8 and vitamin B_{12a}	181
5.4	Absorbance spectra of vitamin B_{12a} in the presence of selected anionic and neutral ligands (MOPS 0.1 M; pH 6.8; 25 ^{o}C)	184
5.5	Absorbance spectra of NAcCoMP8 in the presence of selected anionic and neutral ligands (MOPS 0.1 M; pH 6.8; 25 ^{o}C)	185
5.6	Comparison of absorbance maxima (nm) for a Co(III) porphyrin-porphyrin system and for a porphyrin-corrin systems.	188

Figure		Page
5.7	The absorbance spectra of the titration of vitamin B_{12a} in MOPS buffer (0.1 M; pH 6.8; 25 ^{o}C) with selected anionic and neutral ligands.	189
5.8	The titration of NAcCoMP8 415 nm species in MOPS buffer (0.1 M; pH 6.8; 25 ^{o}C) with NaCN (0.1 M) showing 1st and 2nd axial substitutions.	191
5.9	The titration of NAcCoMP8 417 nm species in MOPS buffer (0.1 M; pH 6.8; 25 ^{o}C) with NaCN (0.1 M) showing 1st and 2nd axial substitutions.	192
5.10	The titration of NAcCoMP8 424 nm species in MOPS buffer (0.1 M; pH 6.8; 25 ^{o}C) with NaCN (0.1 M) showing 1st and 2nd axial substitutions.	193
5.11	Proposed methods of the putative tetramer formation in NAcCoMP8.	196
5.12	Examples of NAcCoMP8 spectroscopic data obtained in this work (25 ^{o}C, pH 6.85, 0.1 M MOPS).	205
5.13	Examples of B_{12a} spectroscopic data obtained in this work (25 ^{o}C, pH 6.85, 0.1 M MOPS).	206
5.14	Log K of B_{12a} vs. NAcCoMP8 for neutral and anionic ligands at 25 ^{o}C.	208
5.15	Correlation between ΔH vs ΔS for the substitution of coordinated water in B_{12a} and NAcCoMP8 by neutral and anionic ligands illustrating the enthalpic-entropic compensation effect.	212
5.16	Diagrammatic representation of synergistic bonding between cyanide and Co(III) in B_{12a} in order to explain the remarkable binding affinity in this reaction.	214
5.17	Diagrammatic representation of hydrogen-bonding between bisulfite molecules in relation to Co(III) in B_{12a} to explain the large entropic value in this reaction.	216
5.18	Sources of steric hindrance in the binding of Pyr to Co(III) in $B_{12a.}$	217

Figure		Page
6.1	Flow diagram of the kinetics results focused on in Chapter 6.	237
6.2	Examples of corrected monophasic absorbance/time traces obtained from Cary 300 Bio for the substitution of axially coordinated water with selected probe ligands.	239
6.3	The absorbance/time traces were fit to an equation of the form $A = A_0 + A_1 e^{-k_l^{obs} t}$ for the reaction with selected probe ligands at 25 ^{o}C.	240
6.4	Plots of pH-corrected pseudo first order rate constants k_l against [L] (25 ^{o}C; pH 7; MOPS (0.1 M); μ = 0.1 M by $NaNO_3$).	241
6.5	Eyring plots of corrected $\ln(k_2h/k_BT)$ against T^{-1} (pH 7; MOPS (0.1 M); μ = 0.1 M by $NaNO_3$).	242
6.6	Eyring plots for the rate constant for the reverse reaction of NMI with NAcCoMP8 and with H_2OCbl^+(pH 7; MOPS (0.1 M); μ = 0.1 M by $NaNO_3$).	243
7.1	Flow diagram of the strategy undertaken in this work.	255

---

*There will come a time when you believe that everything is finished. **That** will be the beginning.*

~Louis L'Amour, American author, (1908-1988)~

CHAPTER 1
INTRODUCTION

1.1 INTRODUCTION

Life happens through a series of perfectly executed biological processes. The remarkable level of precision that is required to sustain life through these processes can only be fully appreciated by examining their chemistry. Complex processes such as respiration, digestion and reproduction, and indeed the primary ones such as oxygen and electron transport or photosynthesis are all, at their simplest level, a series of chemical reactions.[1,2] For these chemical reactions, Nature appears to favour the utilisation of heterocyclic compounds and it is generally the heteroatom, oxygen, sulfur or nitrogen, that is responsible for some of their striking chemical properties.[2]

The nitrogen-containing carbon-based heterocyclic rings in particular are extremely versatile[2] which might explain Nature's exploitation of these compounds. They exhibit a broad array of reactivities, conformations and electronic distributions, but mostly it's the heterocycle's ability to form stable complexes with metal ions that is of strong biological significance. Some common biologically significant nitrogen heterocycles include pyridine, imidazole and notably pyrrole.[2,3]

Pyrrole is a five-membered aromatic heterocycle with a sp^2 hybridised nitrogen heteroatom. Pyrroles tend to be extremely weak bases due to the NH group (pK_a = 17.5 under standard conditions).[2,3] However, one of pyrrole's most striking features is it's propensity for polymerisation.[2] Under strongly acidic conditions it readily forms dipyrrins (two pyrroles linked through a methine group), tripyrrins, and of particular biological relevance, the *tetrapyrroles* (**Figure 1.1**).[2,3]

Tetrapyrroles contain four pyrrole rings joined by a carbon and may be linear or cyclic depending on how they have polymerised (**Figure 1.1**).[1,2] Certain conditions favour the formation of open linear chain-like structures such as bilane or bilin.[2,4] However, they may also form an array of closed N-donor macrocyclic structures such as porphyrins, chlorins (reduced porphyrins) and corrins.[4] In addition to the overall chemical versatility of heterocyclic compounds,[2] these macrocycles also allow for metals of various ionic radii to be complexed within this cavity.[2] Such complexes are stable, deeply coloured and form the basis of several natural pigments such as hemoglobin (porphyrin with iron), chlorophyll (chlorin with magnesium) and cobalamin (corrin with cobalt); these pigments share a close functional relationship with many key metalloproteins that are necessary for life (see **Table 1.1** for a list of common tetrapyrrolic 'functional dyes' in Nature).[1,4]

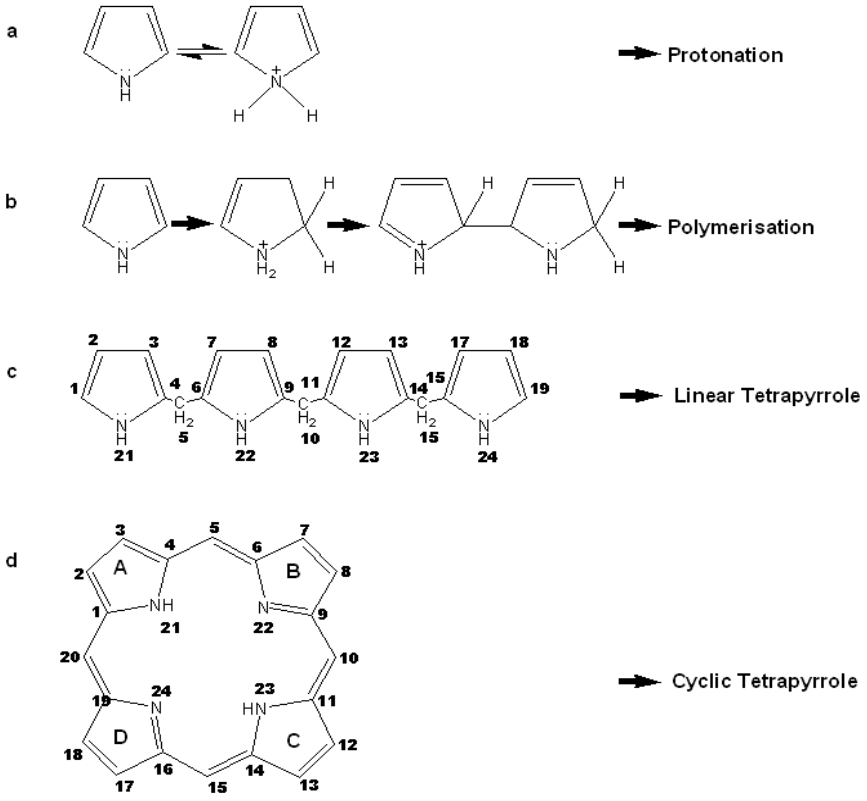
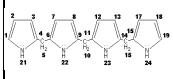
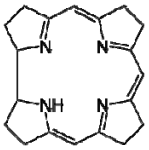
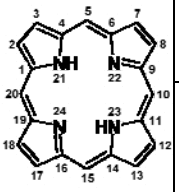
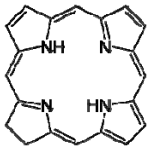


Figure 1.1 Pyrroles. They may be in equilibrium with the protonated equivalent (**a**) or be susceptible to polymerisation in strong acids (**b**) and form linear tetrapyrroles *e.g.* bilanes (**c**) or macrocyclic tetrapyrroles *e.g.* porphyrins (**d**).

Table 1.1 Classification of some biologically significant tetrapyrroles.[1,4,5]

	TYPES OF TETRAPYRROLES			
Linear	**Bilanes or Bilins** 	Bilirubin, biliverdin, Stercobilinogen, Stercobilin, Urobilinogen, Urobilin		
		Phytobilins	Phytochromobilin	
			Phycobilins	-erythrobilin, -cyanobilin, -courobilin, coviolobilin
Macrocyclic	**Corrinoids** 	Cobalamins	Methylcobalamin, Adenosylcobalamin, Cyanocobalamin	
	Porphyrins 	Protoporphyrins	Protoporphyrin IX, Heme† (*b, c, a, o*), Zinc protoporphyrin, Magnesium protoporphyrin	
		Phytoporphyrins	Chlorophyll (c_1, c_2), Protochlorophyllide	
	Reduced Porphyrins 	Porphyrinogens	Uroporphyrinogen (I, III), Coproporphyrinogen (I,III), Protoporphyrinogen IX	
		Chlorins	Chlorophyllide (*a, b*), Chlorophyll (*a, b*), Phaeophytin (*a, b*), Bacteriochlorophyll *c*	
		Bacteriochlorins	Bacteriochlorophyll a	
		Isobacteriochlorins	Siroheme, Sirohydrochlorin	
		Corphins	Cofactor F430	

What is remarkable is that these macrocycles, owing to their common origin (**Figure 1.2**), exhibit a fair degree of structural similarity; yet small changes to these structures lead to a wide array of functionality. For example, the reactions catalysed by natural porphyrins and corrins may be classified either as oxidation-reduction type or as species transfer-type reactions. The two oxidative-reductive models focussed on here are the incorporation of oxygen and the transfer of

electrons and are achieved by the iron porphyrins in hemoproteins.[6] On the other hand, the transfer of free radical groups used in other reactions are achieved by the cobalt-containing corrin macrocycle.[7] Despite their similarities these biological macrocycles have vastly different functions as well as metal ion preferences.

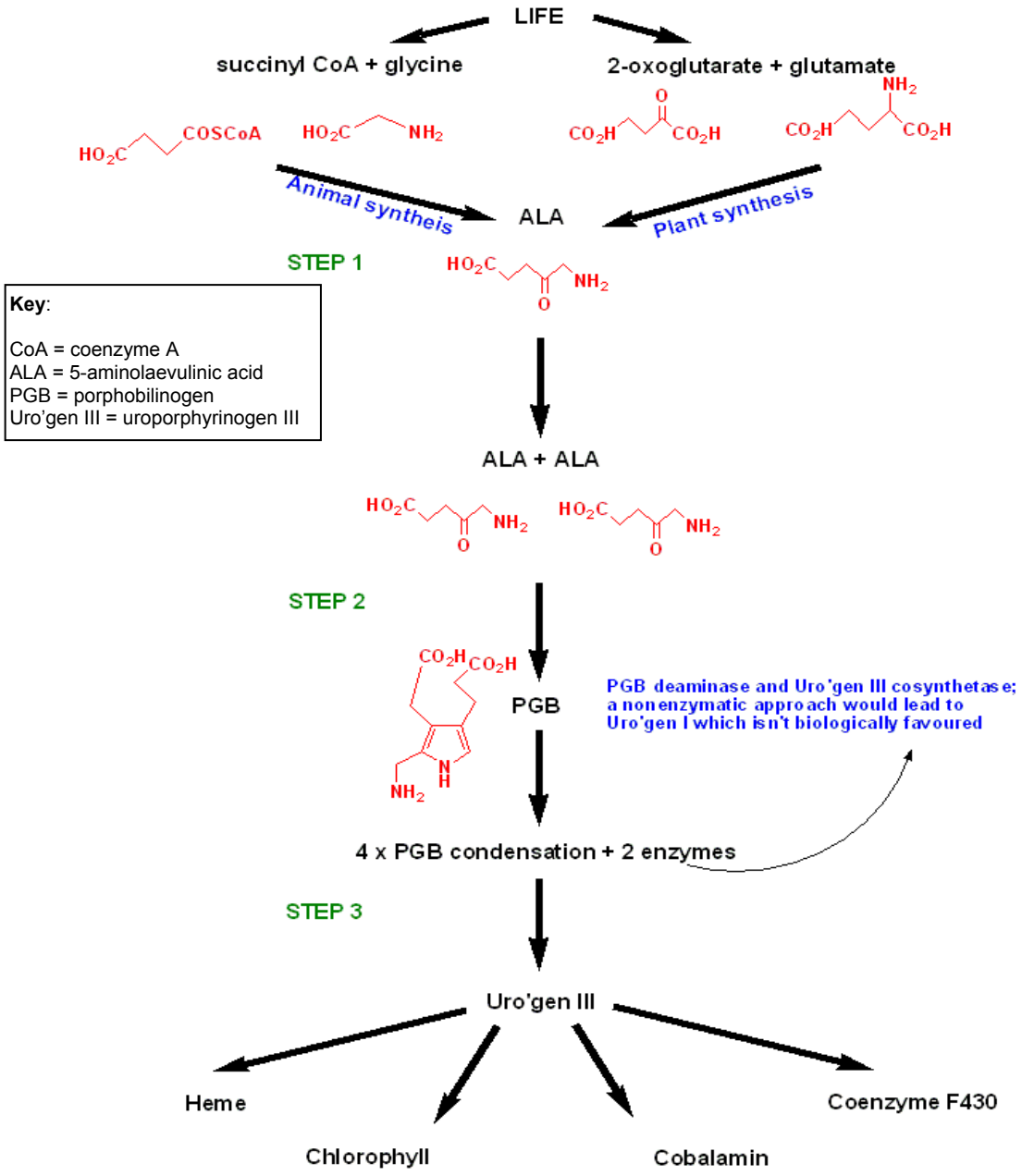


Figure 1.2 The biosynthesis of some 'functional dyes' showing common ancestry (see later for further biosynthesis **Figure 1.9**).[1,4]

1.2 METALLOPROTEINS AND METAL IONS

1.2.1. The significance of metalloproteins

It is estimated that at least one third of all proteins require metal ions to carry out essential life-sustaining functions such as protein transport, signal transduction and particularly enzymatic functions.[8,9] These are generically termed *metalloproteins*. A well-known example is the iron porphyrin structure in hemoproteins.[5] A common type of metalloprotein, a *metalloenzyme*, requires the aid of a metal ion for its catalytic activity such as Mo or V in nitrogenase or the cobalt corrin structure in vitamin B_{12}-dependent enzymes. There are indeed enzymes that are purely proteins and do not require metal ions for their catalytic function such as chymotrypsin and ribonuclease. However, metalloenzymes generally have a metal ion with one labile coordination site for its catalytic activity bound to the protein. Typical of most enzymes, the shape of the active site is important for the function; the metal ion is usually located in a pocket whose shape fits the substrate. Examples of these types of proteins are illustrated (**Figure 1.3**).

Metalloenzymes have been known to complex a wide range of metal ions such as iron, copper, zinc, cobalt and molybdenum, where the metal ions are known to fulfill both structural and catalytic roles.[10-12] These roles can be fulfilled by the metal ion acting alone, in a cluster or by being coordinated to an organic macrocycle.[12] Cofactors, defined here as the metal ions that directly bind to the enzyme (**Figure 1.4**), act as Lewis acids to maximize catalytic activity *e.g.* carboxypeptidase A with a Zn^{2+} cofactor.[5] Coenzymes on the other hand, consist of a metal ion (*e.g.* Co^{3+}) coordinated to an organic molecule (*e.g.* a corrin) which then bind to the enzyme.[5,13,14] Coenzymes are generally not synthesised by the body and have to be obtained from vitamins *e.g*. vitamin B_{12a} which is derived from bacteria.[1]

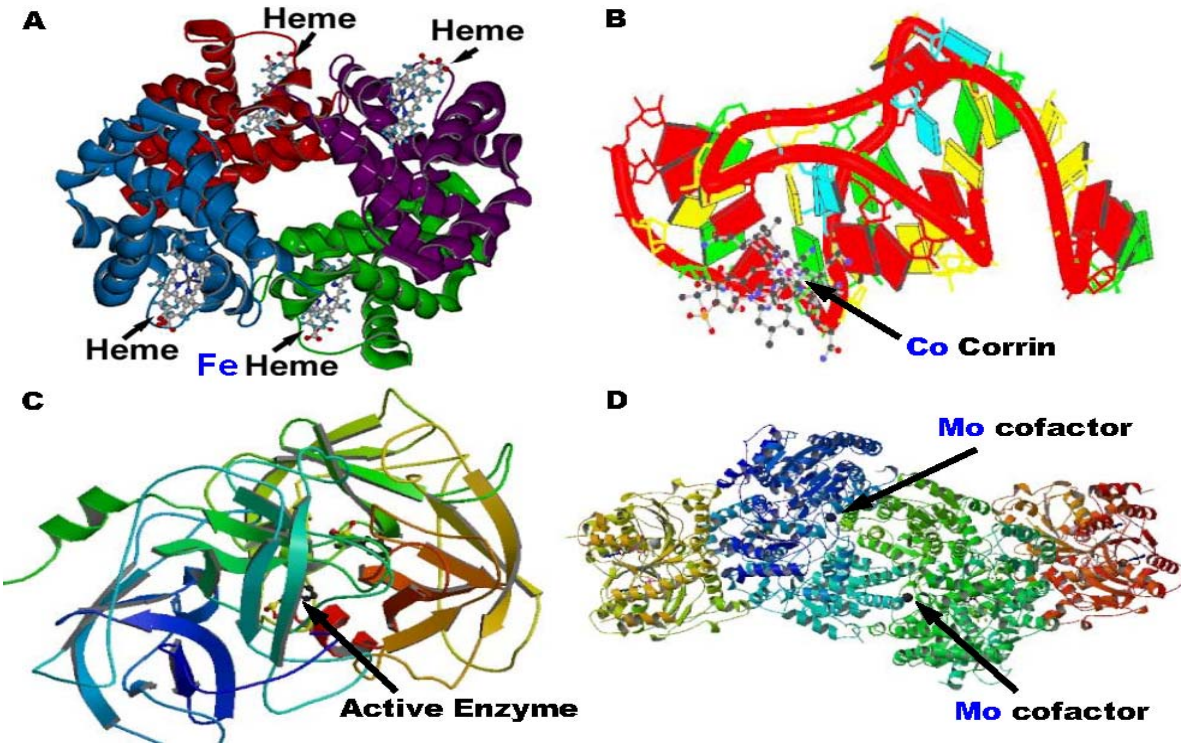


Figure 1.3 Crystal structures of proteins and metalloproteins from PDB.[15] Human deoxyhemoglobin[16] with four heme units (**A**), Co-containing corrin in a vitamin B_{12} RNA aptamer[17] (**B**) and Mo-cofactor nitrogenase[19] (**D**) are examples of metalloproteins whilst the insect chymotrypsin[18] (**C**) is an example of a non metal-containing protein.

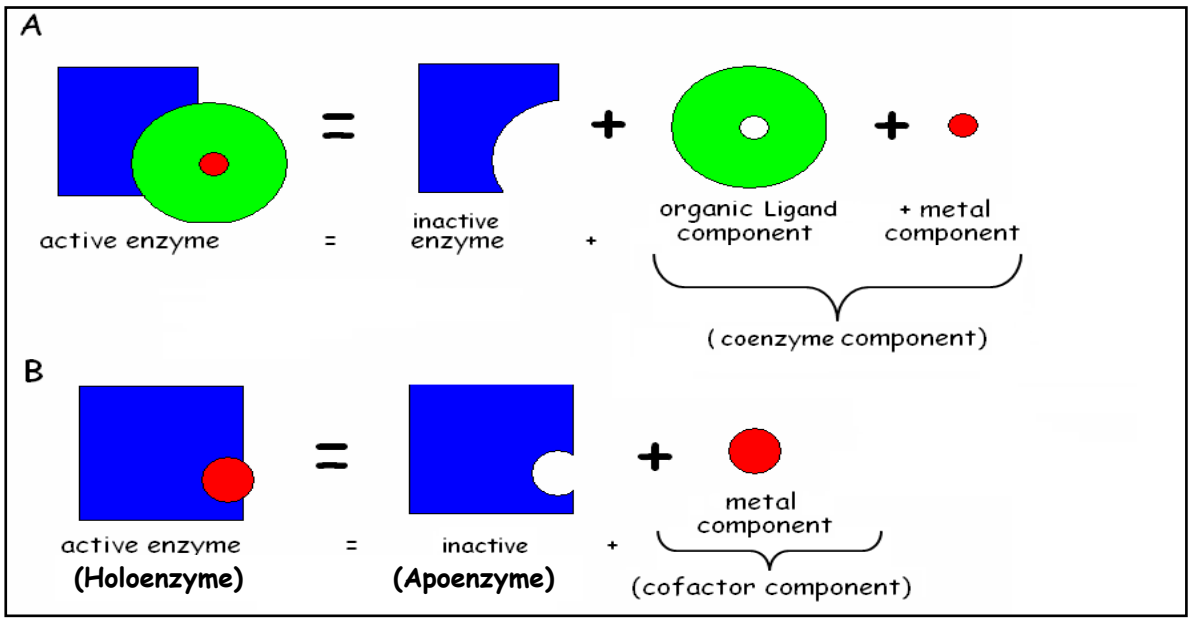


Figure 1.4 Illustrating the relationship between metal ion and active enzymes in this work. The global differences between enzymes, coenzymes and cofactors are shown where (**A**) represents a coenzyme system and (**B**) represents a cofactor system.

Often the truly remarkable functional diversity of metalloproteins is only achieved with porphyrin-type macrocycles as the prosthetic group (see **Section 1.3**). It has been of longstanding interest in bioinorganic chemistry to understand this deeply compatible relationship between metal and macrocycle within a coenzyme, and between coenzyme and enzyme, particularly the precise influence the metal ion has on the structure and function of metalloproteins.[20-25] It is usually difficult to predict how a metal ion will behave in an enzyme; however, the enzyme generally anchors, controls and modifies the fundamental chemistry of the metal ion.[26-28]

1.2.2 Biologically important metal ions

There are at least 30 elements that are essential for life and may be found in macro-, micro- or trace amounts.[29,30] These elements in the form of metal ions are functionally versatile: in the carrying of ionic messages (Na, K, Ca, Cl); the triggering of proteins (Ca, P); for structural integrity (Ca, P, Si); in electron transport (Fe, Cu, Mn); and in catalysis (Fe, Co) (**Table 1.2**).[31-33] The metal ion's interaction with the macrocycle and subsequently the protein determines the direction of the processes taking place. In catalysis for example, without the appropriate metal ion, the reaction the enzyme hopes to catalyse would proceed very slowly, if at all.[26,27]

The way the metal ion binds to the enzyme relates to its function.[28] Usually if the metal ion is on the edge of the protein it serves as a chemical trigger whereas if housed in the centre of the protein (for example, iron in hemoproteins) the action is found to be catalytic and highly ordered.[20,28] Here the metal ion (typically a redox active transition metal and thus biologically significant) is usually coordinated by nitrogen, oxygen or sulfur that originates from amino acid residues on the native protein. Often these donor groups are provided by the side chains from amino acid residues. Of relevance are the imidazole substituents in histidine, thiolate substituents in cysteinyl residues, and carboxylate groups provided by aspartate. In addition to donor groups from amino acids, there are a number of coenzymes with

organic macrocycles that bind a wide selection of metal ions, the most significant being the nitrogen-donor ligands of the porphyrin family (see later, **Section 1.3**).[31]

A striking feature of the macrocyclic part of the coenzyme is the apparent specificity for the metal ion it complexes. Williams posited that each element has had its functional potential raised during evolution through association with particular proteins in order to bring out its optimal value during catalysis.[31] Since DNA is considered to be highly conserved, the changes that happen are in support of life, thus the selection of certain metal ions and pairing with certain proteins is attributed to selection pressure. Williams forwards this as an explanation for why Nature employs several different metal ions in a variety of catalytic roles as well as to explain the peculiarities of the sites selected for each metal ion as is the case in the cobalt-specific corrin macrocycle in cobalamin (**Table 1.2**).[31]

The abundance and bioavailability of Earth's elements, particularly on changing from anaerobic to aerobic atmospheres, is important when trying to rationalise evolutionary selection pressures. Firstly, the most *abundant* elements fall between H and Fe in the Periodic Table whilst the abundance of others like Co, Ni and Cu is considerably lower (**Figure 1.5**).[31] Secondly, *bioavailability* depends on solubility in water and air. Abundant elements such as H, Na, K, Mg, C, Ca and Cl are soluble and readily obtained from sea water or the air. Early atmosphere's sulfuric conditions prompted the formation of insoluble metal sulfides lowering the bioavailability of rare elements *e.g*. Cu, Zn and Cd.[31] On the other hand, Fe, though relatively more abundant than for example Cu or Co,[34-37] may have its bioavailability limited by the formation of insoluble ferric hydroxides. However, Nature has selected for Fe due to its ability to bind dioxygen efficiently; organisms had to evolve in order to tolerate an oxygen-rich environment.[38] Iron can be stabilised[30] over a wide range of oxidation states depending on its coordination environment (-2 to +4); the d^6 Fe(II) ion and d^5 Fe(III) ion being the most common.[39,40] Furthermore, both Fe(II) and Fe(III) can adopt a wide range of geometries and distortions, a feature that was shown to be essential in the

functioning of hemoglobin.[39-42] Were it not for relative abundances, other metal ions such as copper may have rivalled iron's usefulness given its redox properties.[43]

Table 1.2 Some examples of metalloproteins and their associated functions.[11]

Metal	Protein	Function
Cu	Azurin	Electron transport protein (*Alcaligenes xylosoxidans)*
	Rusticyanin	Electron transport protein (*Thiobacillus ferrooxidans)*
	Nitrite Reductase	Reduces NO_2^- in the nitrification pathway (*Alcaligenes xylosoxidans)*
	Superoxide Dismutase	Scavenges superoxide free radicals
	Ceruloplasmin	A ferrooxidase found in the blood
	Hemocyanin	O_2 transport in the blood of molluscs and arthropods
Fe	Hemoglobin	O_2 transport in the blood
	Myoglobin	O_2 storage in muscle tissue
	Transferrins	Iron transport protein found in the blood
	FixL	Heme oxygen sensor protein (*Rhizobium meliloti*)
	Cytochromes	Participate in important electron transfer reactions
	Peroxidase	Protects against uncontrolled H_2O_2 oxidation
	Cytochrome P450	Activation of O_2 with insertion of one of its atoms into the substrate and reduction of the other to form H_2O
Co	Coenzyme B_{12}	Isomerisation, methylation, etc.
Mo	Nitrogenase	Catalyses the ATP-dependent reduction of dinitrogen to ammonia
	ModA	Periplasmic mo-binding proteins (*Azotobacter vinelandii*)
	ModE	Mo-dependent transcription regulator (*E. coli)*
Mn	Catalase	Reduces H_2O_2 to O_2 and H_2O
Ni	Urease	Hydrolysis of urea to ammonia and carbon dioxide
V	Nitrogenase	Catalyses the ATP dependent reduction of dinitrogen to ammonia
Zn	Superoxide Dismutase	Scavenges superoxide free radicals

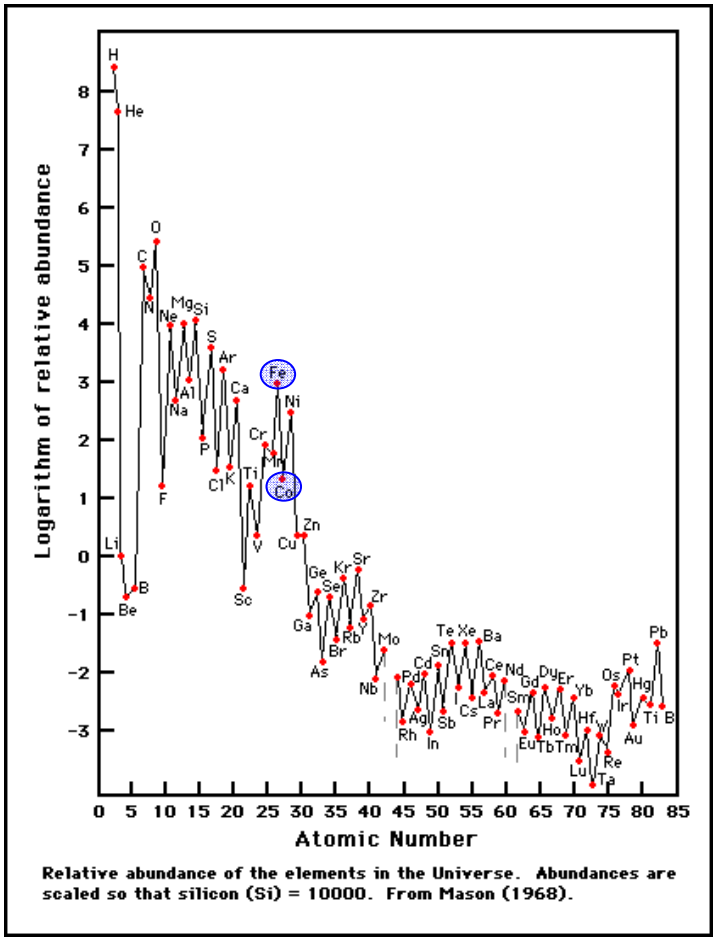


Figure 1.5 The abundance of the elements in the universe relative to Si = 10^4 as a function of atomic number. The relative abundances of Fe and Co are highlighted. Diagram from Williams.[31]

Whilst biological systems may have devised mechanisms to increase bioavailablility of some essential elements[28,31,38,44] it is an energetically costly approach. Nature simply elected to either retain the element by changing its role or in some instances change the element entirely. Ni, W and Co were of value in primitive anaerobic systems.[38,45] However, both Ni and W are of little use in higher life forms. The use of Co has disappeared almost entirely and it has been replaced by other metals as in the case of ribonucleotide reductase.[46] However, the use of Co(III) still persists in a handful of vitamin B_{12}-related compounds. Why this should be the case is not clear, particularly since the more abundant and

electrochemically versatile Fe would be the next logical substitution in its evolution. In fact, Nature has expended so much energy to retain this particular Co-macrocycle complex that where some biochemical pathways have become inactive due to the presence of oxygen, cobalamin has evolved two synthetic pathways for its macrocyclic core: the presumably initial[4] anaerobic synthesis and the likely subsequent aerobic one.[38,47]

Cobalt chemistry appears to be straightforward. Cobalt is found in the first row of the transition elements and typical geometries include tetrahedral and octahedral for a range of oxidation states.[40] Whilst cobalt is known to have a wide range of oxidation states (-3 to +4)[48] the most common are Co(II) and Co(III); the former is considered to be a labile metal ion whilst the latter is classically inert.[40] The inert nature of Co(III) is largely due to the high ligand field stabilization energy associated with low spin d^6 electron configurations. Co(III) is typically a low spin d^6 metal ion except in the case of weak field ligands such as fluoride. Complexes of Co(III) are therefore diamagnetic in the ground state.[29,30] It is interesting to note that, in very particular instances, Co(III) exhibits some semblance of Co(II)-type behaviour, for example, when coordinated by biological macrocycles such as the corrin in cobalamins. [6,49,50]

1.3 BIOLOGICALLY IMPORTANT MACROCYCLES

The porphyrins are the best known example of biologically-important macrocycles.

Porphyrins are steeped in a rich and fascinating history with records that can be traced as far back as the beginning of civilisation. The word itself stems from *porphura,* which refers to the colour purple; porphyrins are renowned for their intensely purple colouring. Whilst the etymology suggests a word of Greek extraction it actually has older Semitic origins (from *purpura*) and was used by the ancient Phoenicians to describe a type of mollusc. They collected thousands of

these snails in order to extract the incredibly rare and coveted pigment called Tyrian Purple, which ironically is not a porphyrin at all. Purple dyes were a rare, carefully guarded commodity in the early civilisations of the Eastern Mediterranean as they were used to indicate people of royal birth as well as high priests, a trend that persists in some monarchies today.[4,51]

In terms of the chemical meaning, 'porphyrin' usually describes a number of deeply coloured fluorescent pigments of natural or synthetic origin that have a substituted tetrapyrrolic macrocyclic ring in common.[4,52] The natural porphyrins are effective at binding metal ions in order to facilitate many biochemical events; they include the hemoproteins, chlorophylls and cobalamins. Strictly speaking, the 'porphyrin' is one member in a list of structurally similar macrocycles that comprise these pigments (see, **Table 1.1**); other members include chlorins and corrins and are found in chlorophylls and cobalamins, respectively. Though the macrocycles used in these pigments have similar biosynthetic origins[4] with small structural differences, these differences are thought to be significant enough to attribute to their functional diversity. It is often thought that this type of design-economy is deliberate and suggests that these functional dyes have a common ancestry.[53]

This work recognises and focuses on the structural distinction between porphyrins and corrins. Furthermore, their unique chemical nuances as a result of these structural differences are examined in order to form a basis for the structure-function relationship in two types of pigments that contain them: the microperoxidases (derived from proteolytic digestion of a hemoprotein) and cobalamins, respectively (see later, **Sections 1.4**, **1.5**).

1.3.1. Porphyrins

The ubiquitous porphyrin macrocycle that has intrigued researchers for decades stems from the porphin structure and consists of four pyrrole rings linked together by methine bridges at their α-carbons.[4,7] According to the IUPAC system α-carbons are at C1, 4, 6, 9, 11, 14, 16 and 19; β-carbons are at 2, 3, 7, 8, 12, 13, 17 and 18; *meso* carbons are at C5, 10, 15 and 20. *Meso* carbons are usually designated for convenience α, β, γ and δ, respectively (**Figure 1.6**).[4,7] These deeply coloured heterocycles exhibit pseudo D_{4h} symmetry and are aromatic (22 π-electrons, with 18 electrons in any one delocalisation pathway). The conjugation is primarily responsible for their deep colouring with intense Soret absorbance bands (*ca*. 400 nm) and very high extinction coefficients.[41,54,55] Their four pyrrolic nitrogen atoms point directly into the ring cavity. When these nitrogens are deprotonated they create a formidable ligand capable of coordinating with almost any transition metal ion as well as some non-metals such as phosphorous.[56] Whilst porphyrins are known to complex an impressive range of metal ions (for example, from the first row of the d block, Ti,[57-59] V,[60-62] Cr,[63,61] Mn,[65-67] Fe,[68-70] Co,[71-73] Ni,[74-76] Cu,[77-79] and Zn[80-82]), it is only the iron porphyrins that have exhibited firm evidence of biological activity and subsequently serve as prosthetic groups (see later in this Section).[2,4,11,37,39,41]

In general, porphyrins are regarded as planar (*e.g*. octaethylporphyrin).[49,50] However, they have been shown to exhibit a fair degree of flexibility, often distorting and changing conformations.[83-85]Understanding what contributes to the changes in porphyrin conformation provides valuable structure-function insight into biological porphyrins. With this in mind, porphyrin molecular mechanics studies[83,84,86-89] are often undertaken as a function of ionic radii (of the central metal), orientation of axial ligands and peripheral substituents.[90]

This flexibility is most apparent on coordination with metal ions as the porphyrin distorts in order to accommodate the ion; the degree of distortion depends on the size of the metal ion.[91] When the metal ion is significantly smaller than the cavity, a 'ruffled' conformation is obtained.[85] The mean planes of opposite pyrrole rings twist such that the *meso* carbon atoms of each pyrrole ring are alternately above and below the mean porphyrin plane; here the nitrogen atoms are closer to metal ion. In the case of a larger metal ion, the opposite pyrrole rings tilt relative to each other in a 'saddle' conformation such that the metal ion is raised out of the porphyrin plane in a 'doming' fashion.[91,92]

Other reasons for porphyrin distortions are also possible. For example metal-free porphyrins distort as a result of repulsions between protonated central nitrogen atoms.[7,52] Bulky substituents on the methine bridging carbons also cause the porphyrin to buckle and twist in order to try and maintain its planar conformation.[93] A loss of aromaticity due to oxidation of the porphyrin also heavily distorts the macrocycle.[4,7]

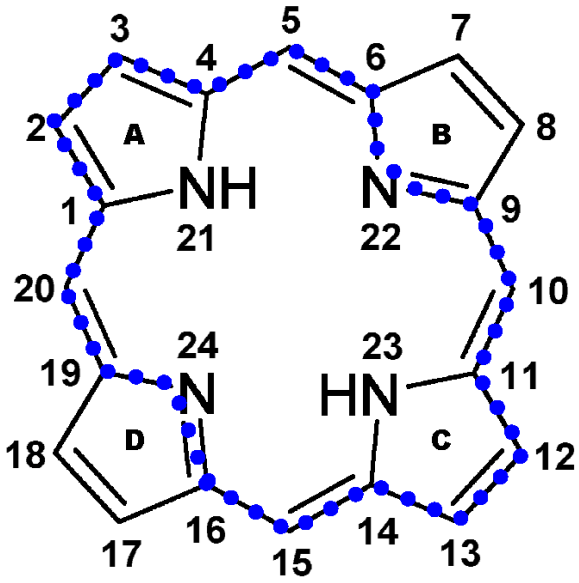


Figure 1.6 Porphin: the backbone of all porphyrins. Substituted porphins are known as porphyrins. The blue pathway indicates the delocalised 18 π electron system. Whilst Hans Fischer is often credited with identifying this structure in 1929, it was originally proposed by Küster in 1912.[1,4]

The basicity of the macrocycle is a physiologically important factor. Porphyrins have two weakly acidic pyrrole nitrogen atoms. Naturally occurring porphyrins have carboxylic acid side chains, mostly propionic or acetic acid side chains, which, when ionised, increase the basicity of the porphyrin ring.[54] The presence of electron-donating substituents on the porphyrin ring also increases the basicity of the porphyrin nitrogen atoms.

Synthetic porphyrins are typically generated through variations on the original Fischer synthesis and are generally stable complexes.[4] They do, however, have a propensity for aggregation and degradation and exhibit solubility difficulties under certain conditions.[7,94,95] These conditions are regulated by the use of detergents and non-aqueous solvents to monomerise the porphyrins.[96] The porphyrin macrocycle, depending on the peripheral substituents, is sometimes light-sensitive and subject to photooxidation and photoreduction reactions; experiments are therefore routinely conducted under low light and low oxygen conditions.[7,52]

In biological porphyrins on the other hand, the peripheral substituents are functionally important and aid in solubility; many are substituted with either acetic- or propionic acid groups on all eight β-positions. They may be arranged to produce four *type isomers* (I, II, III, IV; **Figure 1.7**) of which III is the most functionally significant in biology probably because it is the most abundant.[4] For example, uroporphyrinogen *III* (III to denote the isomer) is a precursor in the biogenesis of hemes, chlorophylls and cobalamins (**Figure 1.2**).[4]

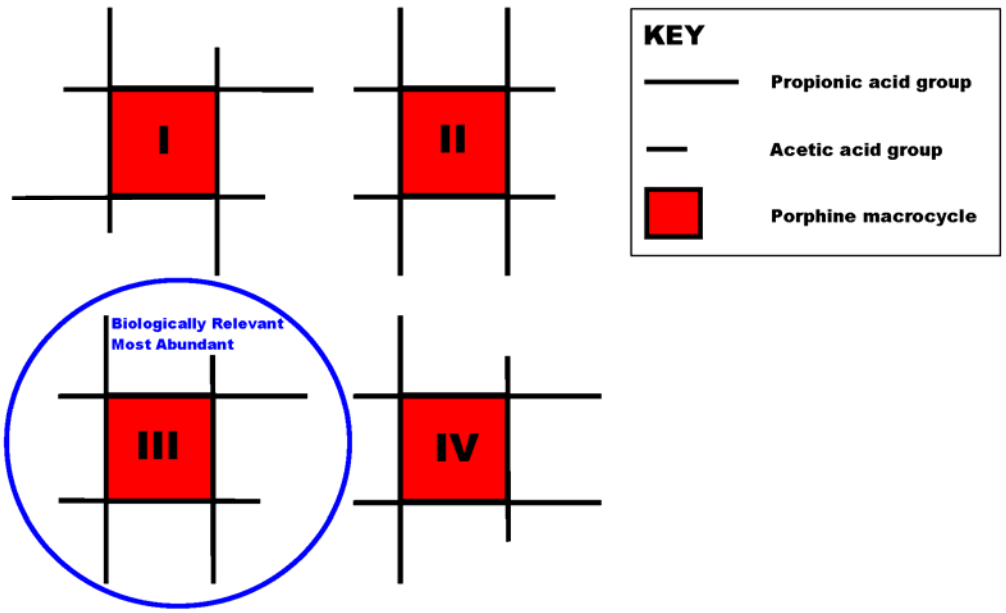


Figure 1.7 Schematic representation of the four porphyrin type isomers.[1,4]

The best known biological porphyrins are the iron-containing hemes found within the native hemoprotein.[4,39,41] These macromolecules serve as fundamental building blocks for self-assembled structures due to their relatively rigid geometry, ease of substitution and selective axial ligand coordination chemistry. The porphyrin dianion binds iron (formally II or III in the resting state) in its preferred octahedral geometry.[29] Here the macrocycle occupies four 'equatorial' coordination sites leaving the two 'axial' coordination sites open for ligand binding. Under normal conditions the 5th or proximal site is coordinated by N (His), S (Cys or Met) or O (Tyr) donors whilst the 6th (distal) site may or may not be occupied; in the latter case it is usually coordinated by water or an amino acid residue.[55] All these features are exploited by hemoproteins to carry out their diverse biological functions such as the transport and storage of dioxygen (hemo- and myoglobin),[97-99] the transfer of electrons (cytochromes),[100,107] oxidation of organic compounds (peroxidases and cytochrome P450),[97,98,101,102] disproportionation of hydrogen peroxide (catalases)[97,98] and the reduction of oxygen (terminal oxidases).[98,100] It is remarkable that such a wide variety in functionality relies predominantely on the

reactivity of a single metal ion immediately suggesting that the ligands (both axial and equatorial) are responsible for modulating the function of the heme iron.

Central to hemoprotein functionality is the ability of the porphyrin macrocycle to modulate the redox potential of the iron.[55] Fine-tuning these redox potentials are achieved in a number of ways.[43,55] These include ligand selectivity, for example, a hard ligand such as N in imidazole favours Fe(III) over Fe(II) whilst the opposite is true in the case of the softer S donor in thioether thereby affecting the redox potentials.[43,55] Another way is by the hydrophobic protein environment destabilising the formation of a positive charge in deeply-buried heme groups. Marchon *et al*., have also shown that the change from CH(S-cysteinyl)CH_3 to $CH{=}CH_2$ to CHO (heme *c* to *b* to *a*) shifts redox potentials (*ca*. 100 mV).[103]

The positions and combinations of the various peripheral substituents in porphyrins[104] and especially in hemes[84,55] invariably lead to electronic differences which in turn have a consequence for the reactivity of the metal ion. The intensely coloured heme *a*, *b* and *c*, are based on the position of their lowest energy absorption band at *ca*. 600 nm, 563 nm and 550 nm, respectively.[2] Heme *a* (*e.g*. cytochrome *c* oxidase) is different to heme *b* in that the methyl side chain is oxidized into a formyl group and one of the vinyl groups has been replaced with an isoprenoid group. Heme *b* is the most prevalent where hemoglobin and myoglobin are the best known examples. Heme *c* (*e.g.* cytochrome *c*) differs from heme *b* in that the two vinyl side chains are covalently bound to the protein itself. Cytochrome *c* is a relatively small heme protein found loosely associated in the inner walls of the mitochondrion and does not bind oxygen. Unlike other cytochromes, it is a soluble protein, essential in electron transfer and is capable of undergoing oxidation and reduction.

Understanding how hemoproteins control and modify the properties of the active site in order to achieve such diverse functionality is of interest. Munro's extensive survey of the available hemoprotein literature demonstrated that there is much that

is unclear in the understanding of their mechanisms and chemistry.[84] The most common way to gather insight into hemoproteins would be to compare the properties of protein-bound and protein-free model heme groups. His survey further indicates that the results obtained from model studies on iron porphyrins cannot be formally separated from those obtained on the actual hemoproteins but are in fact, complementary.[84] For this reason, biomimetic models[105] such as simple iron porphyrins and especially heme fragments have become essential tools in the elucidation of these complex structure-function relationships in biological systems.[7] Attractive biomimetic models for heme studies are the *microperoxidases* (MP) which are the smaller digestion products derived from cytochrome *c*.[106] Since they are derived from a hemoprotein, they have the benefit of being soluble under physiological conditions and contain the same axial ligands as the native protein.[55,84] Commonly studied heme fragments include microperoxidase-11 and microperoxidase-8; the latter will be discussed further (see later, **Section 1.4**).

1.3.2. Corrins

Corrins are another biologically significant tetrapyrrole closely resembling the porphyrins in structure and yet remarkably different in function. The corrin resembles the porphyrin ring in that they are both heterocyclic with four pyrrole subunits orientated into a ring structure with inward-facing nitrogens (**Figure 1.8**). These subunits are joined on either side by a C-CH_3-bridge. In contrast to the porphyrin, the corrin has two pyrrole rings that are directly attached.[1-4]

The missing methine bridge has the effect of lowering the overall symmetry to C_{2v}. Moreover, with 10 saturated carbon atoms at the periphery the conjugation of the outer part of the ring is destroyed and the symmetry is lowered again to C_1.[49] This feature together with the high number of sp^3 hybridised carbon centres makes the corrin ring smaller and considerably more flexible than the porphyrin ring. Corrins are non-planar whilst porphyrins tend to be flat with the ability to adopt various

conformations under certain conditions (**Section 1.3.1**). These features allow for some considerable differences in chemistry of corrins and porphyrins (see **Section 1.3.3**).

Corrins are also partially conjugated through the ring structure with a 14 π-electron system. Relative to porphyrins, they have a '3/4' conjugation with their 'edge carbons' being saturated. These structural features have a profound effect on their colour, electronic spectra and subsequently on ligand binding (**Figure 1.9**).

Corrinoids are seldom metal-free[107,108] and occasionally coordinate to metals such as Pd, Rh, Ni, Zn[109-112] with a strong preference for cobalt, found in Nature as the cobalamins. Cobalamins are remarkably complex, its complexity marked by the inclusion of the rare, inert Co(III) ion. That this Co(III)-complex should be a biological *catalyst* is thus very unusual and suggests that the corrin modifies the chemical properties of Co(III) (see later, **Section 1.5**).

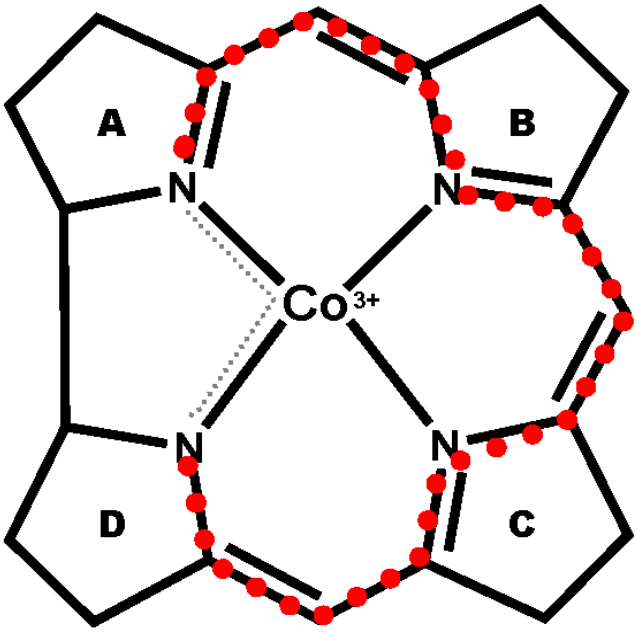


Figure 1.8 The cobalt corrin structure. The red pathway indicates the delocalised π electron system.

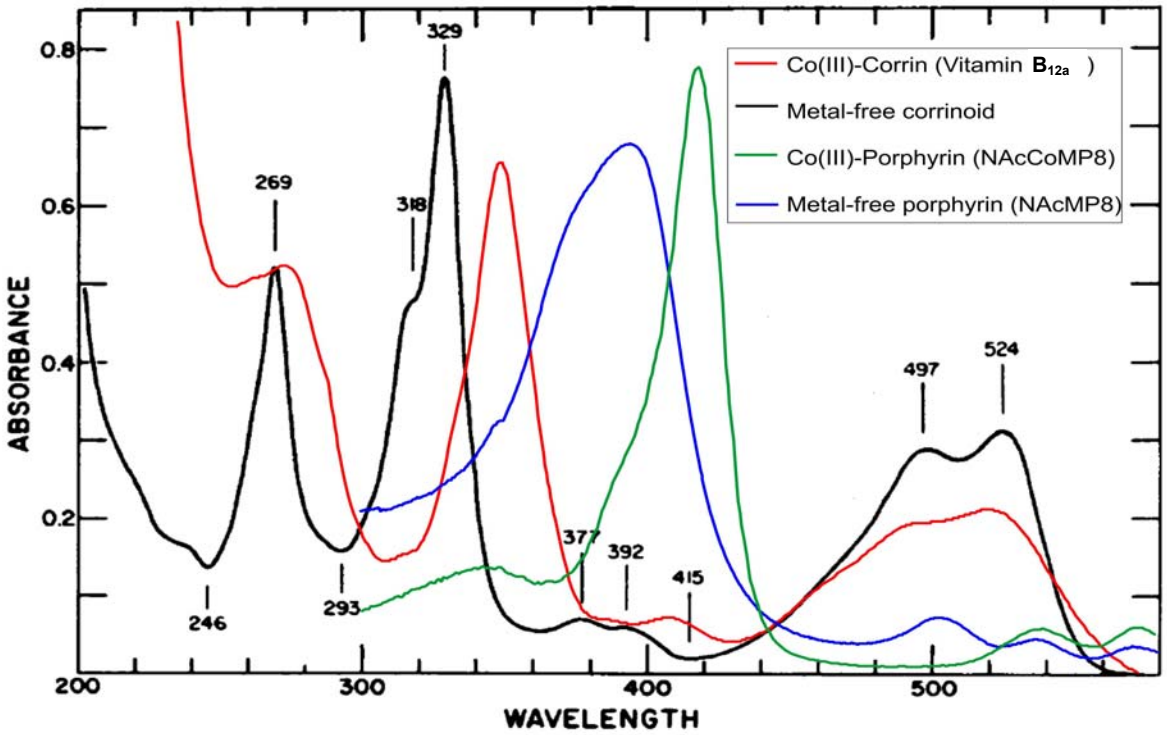


Figure 1.9 Comparison of corrin and porphyrin electronic spectra. The spectrum of the metal-free corrinoid (black) from *Chromatium* is adapted from Toohey[107] and is superimposed against Co(III)-corrin (red), Co(III)-porphyrin (green) and metal-free porphyrin (blue) spectra to compare peaks and relative wavelength shifts but *not* intensities.

1.3.3 A comparison of porphyrins and corrins

Porphyrins and corrins are compared here in three ways. Firstly, the evolutionary implications are examined in relation to their biosynthesis. Secondly, the general structural similarities and differences are summarised in relation to function. Lastly, the chemical properties of each macrocycle are compared.

A longstanding question has been to identify which came first, porphyrins or corrins? It is widely accepted that the early atmosphere was a reducing one with very little free oxygen, consisting of H_2O, methane, CO_2, nitrogen, ammonia and hydrogen.[51,113-119] It therefore seemed unlikely that porphyrins would have been the progenitor given that its synthesis is dominated by a series of controlled oxidation steps. Thus the prevailing view is that corrins, synthesised almost exclusively by

anaerobic bacteria (the evolution of an aerobic pathway was presumably to survive selection pressures in an oxygen-rich atmosphere), is the earlier macrocycle.[38,47,120-131] Further evidence suggests that corrins were functionally significant before porphyrins; key cofactors in early enzymatic reactions such as ribonucleotide reduction involved corrins, not porphyrins.[38,47,124] By examining the distribution of corrins within organisms in relation to evolution and lifestyle adaptations, it seems plausible that corrins came first (**Figure 1.10**).[47]

Georgopapadakou and Scott summarised the most compelling arguments for a corrin progenitor in five critical points.[132] Firstly, they reasoned that most corrins are produced anaerobically and by bacteria only. Secondly, corrins are less oxidised than porphyrins. Next, they are more polar than either hemes or chlorophylls. They then suggested that functionally it is the porphyrin that is involved in free oxygen transfer and transport type reactions, not cobalamins. In contrast, cobalamin's methionine → homocysteine reaction can occur under reducing conditions. Lastly, cobalamins not porphyrins feature in the phylogenetically old hydrogenase reaction.

That said, Miller's classical experiment showed that among the plethora of products in his 'primordial soup' were organic compounds like cyanide, formaldehyde and pyrrole, known precursors of simple laboratory porphyrin synthesis.[51,113-116] Not only were Simionescu and co-workers able to confirm these findings, they also found porphyrin in their experiments albeit in trace amounts.[117] Moreover, they were able to demonstrate the presence of δ-aminolevulinic acid (ALA) under these prebiotic conditions[117] which Scott and co-workers later showed to be crucial in the biosynthesis of porphyrins (**Figure 1.2**).[126-131] Based on this and on Nature's impressive sense of economy, Dolphin had posited that the biosynthesis of cobalt corrins may have in fact arisen from cobalt porphyrins.[133] Cobalt porphyrins have indeed been observed in Nature for example in isobacteriochlorins found in early prokaryotes.[134] But perhaps the most compelling evidence for early porphyrin ancestry was presented by Eschenmoser in the

demonstration of anaerobic porphyrin synthesis using amino nitriles and montmorillonite clay.[118,119] Still, that such a ubiquitous compound would be present in low yields seemed unlikely.

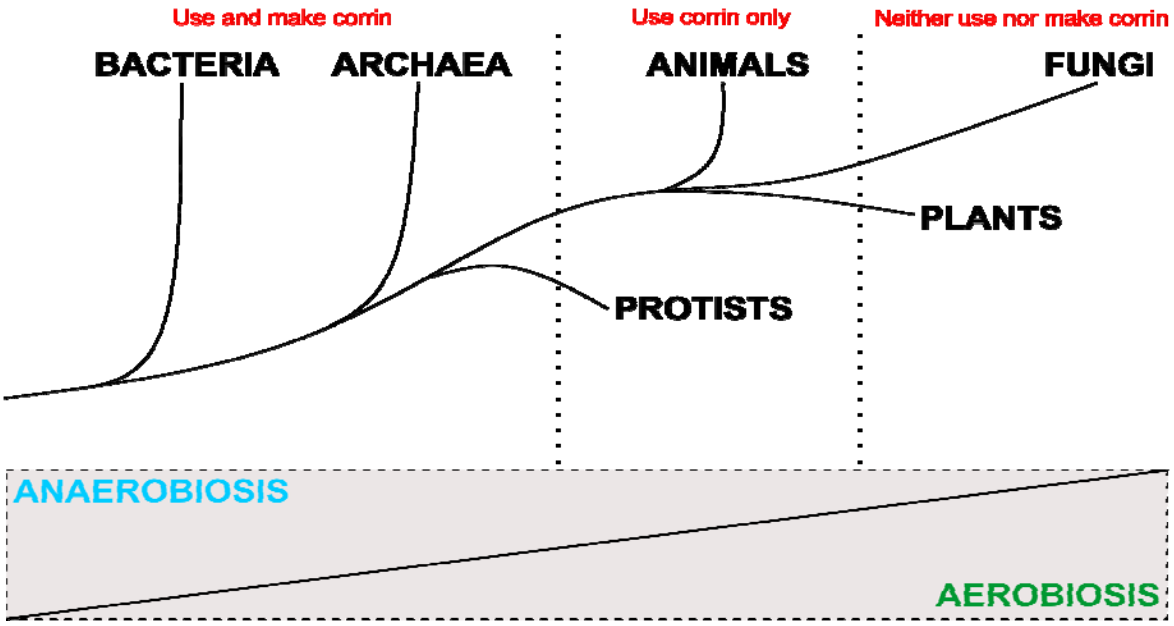


Figure 1.10 Distribution of cobalamin synthesis and utilisation in organisms adapted from Roth *et al*.[47] The wedges show the general direction of evolution in relation to oxygen importance in each type of organism. This diagram shows that corrins are largely associated with anaerobic environments and organisms and thus is a feature of early life.

The biosynthesis of porphyrins and corrins are compared (**Figure 1.11**). Scott and co-workers showed that porphyrins and corrins do indeed share a common biosynthetic pathway up to a point; their respective biosyntheses diverge at uro'gen III (see **Figure 1.2**).[126-131] What is immediately striking is the complexity of the corrin biosynthesis in relation to the porphyrin. The porphyrin has one fairly straightforward aerobic pathway to produce its fully aromatic structure followed by metal complexation and attachment to the native protein. The corrin however, has two pathways (aerobic and anaerobic), each with three parts: synthesis of the corrin ring (different in each pathway), adenosylation and the nucleotide arm. Under aerobic conditions methylation and ring contraction takes more steps (thus energetically more demanding than anaerobic) and cobalt insertion happens much later, after ring contraction.[47, 125] Roth *et al*., suggests that this uro'gen III pathway first evolved to produce the corrin rather than the porphyrin because uro'gen III's asymmetry (**Figure 1.7**) is necessary for the corrin's ring contraction; that porphyrin and chlorophyll biosynthesis branched on later is part of Nature's economy.[47]

The laboratory synthesis of the corrin puts the biosynthesis into perspective. The first (and only) reported full synthesis of a cobalamin in the laboratory was achieved by about 100 researchers in two separate research groups; the entire effort spanned over 90 synthetic steps and took over a decade to complete with each group working on only half a corrin.[4] On the other hand, the synthesis of porphyrins in the laboratory is far less daunting, requiring only a handful of steps.[4]

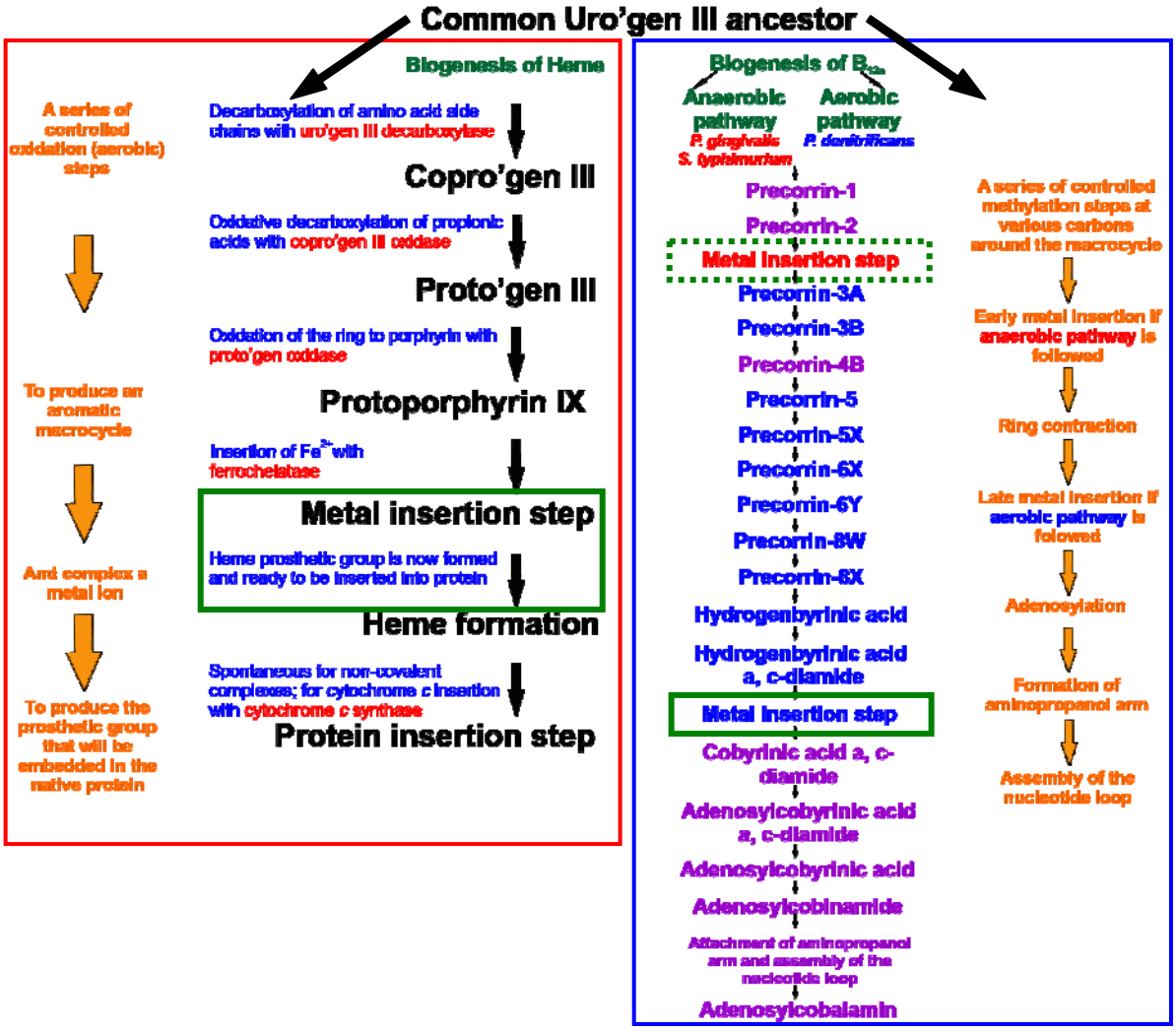


Figure 1.11 Comparison of corrin and porphyrin biosynthesis (following on from **Figure 1.2**).[1,4,6,18,47,120-131] The red box indicates the straightforward heme biosynthetic pathway; the annotations in orange indicate the generalised steps in order to achieve the final hemoprotein from the common Uro'gen III ancestor; blue annotations describe the step; red annotations indicate the main enzymes involved. Similarly, the blue box describes the complex cobalamin biosynthetic pathway. For brevity, the specific actions and enzymes are omitted here. Two biosynthetic pathways produce the corrin ring, the anaerobic pathway with early cobalt-insertion before ring contraction (red) and the aerobic pathway with later cobalt-insertion after ring contraction (blue). The purple annotation indicates steps common to both pathways such as the subsequent adenosylation, formation and attachment of the nucleotide arm. The green box indicates metal insertion steps.

Another common question is if the corrin is indeed an artefact of evolution and succeeded by the porphyrin, why then does the corrin still persist, and more specifically why with cobalt?[134,135] The general structural and chemical aspects of porphyrins and corrins are summarised relative to their function in order to provide some insight (**Section 1.3.1**, **1.3.2**). Some important structural differences that impact on function between these two macrocycles include ring flexibility, cavity size and metal ion preferences.

Porphyrins have four pyrrole rings linked together by methine bridges (**Figure 1.6**). As a result, the structure exhibits D_{4h} symmetry, is fully conjugated (22 π-electrons with an 18 electron conjugation system) with its aromaticity distributed throughout the entire macrocycle. Consequently, there are fewer sp^3 hybridised carbons available to the porphyrin. These features make the porphyrin flatter and more rigid with a larger cavity size than the corrin. The extent of flexibility and resulting conformations depends largely on the type of metal ion the porphyrin tries to complex (**Section 1.3.1**). The corrin on the other hand, has two pyrrole rings directly attached (a 14 π-electrons conjugation system), a feature that lowers the symmetry to C_{2v}; partial conjugation then diminishes the symmetry further to C_1 (**Figure 1.8**). These features together with the number of sp^3 hybridised carbons, destroy planarity, enhances flexibility and creates a smaller central cavity, all of which are functionally significant in cobalt corrins.[50,137]

Corrins exhibit a clear preference for the rare metal cobalt and are seldom found to complex others metal ions. One way to rationalise this preference is from an evolutionary standpoint. Accepting that corrins came first in an early anaerobic reducing atmosphere and that these macrocycles exploit transition metals for their redox properties, then the metal ion best at accessing lower oxidation states would be preferred. Cobalt is commonly found in the +2 and +3 oxidation states. But unlike other first row transition metals like Cr or Fe, cobalt in cobalamins may be reduced further to the lower +1 state in order to perform its catalytic functions. On

changing to an oxidising aerobic environment, abundant metal ions that have access to high valency states and multiple spin states such as iron would then be selected for. Porphyrins, presumably the successor species, are there able to complex a wide variety of transition metal ions with a distinct preference for iron.

However, it still does not explain why corrins persist with Co under contemporary conditions where Fe would be better suited. One theory suggests that the corrin evolved specifically to house the smaller yet redox-versatile cobalt ion.[6,32,119,135] This feature, together with the corrin's flexibility are important in labilising the Co-C bond; selective lability being essential to cobalamin's catalytic functioning (see **Section 1.5**).[50] To this end it has further been suggested that Co(II) in corrin is unique among the 1st row transition metals in that it can provide a stable direct one electron radical.[138] Pratt argues that the Co preference is due to Co(III) being able to form a very covalent M-L bond with low promotion energies.[6,135]

The natural progression is therefore to ask why hasn't the porphyrin replaced the corrin in cobalamins? Although rare, natural cobalt porphyrins are observed in selected isobacteriochlorins.[138] There is clearly something unique about the way the corrin modifies the chemistry of the cobalt ion in order to achieve optimum catalytic functioning by labilising the Co-C bond[137]; a way that cannot be achieved by a cobalt porphyrin. One argument that favours the cobalt corrin specialisation pertains to mechano-chemical trigger mechanisms.[50,42] Enzyme-induced conformational distortions to weaken the Co-C bond are facilitated by the corrin's flexibility, steric crowding and smaller cavity size affording the release of strain energy during catalysis.[50,137] However, evidence suggests that such a conformational change is unlikely to drive cobalamin's catalytic reactions.[139-143] Interestingly, Rovira and co-workers Density Function Theory (DFT) work suggested that one of the reasons Nature may have elected for a cobalt corrin system is because the carbon-ring is capable of enduring some electronic changes without significantly affecting Co-N distances (as opposed to instances in iron porphyrin where the metal moves out-of-plane).[144] This may be facilitated by its

ability to exist in different conformations each with differing redox potentials, a feature unique to the corrin.[134]

Perhaps the most significant contribution in this area was made by Jensen and Ryde using DFT calculations.[49,143,145] Their comprehensive comparison of corrins and porphyrins focussed primarily on the geometric, electronic and functional properties of cobalt and iron porphyrins and corrins. The salient points for the Co-corrin and Fe-porphyrin specificity from their work are summarised.[49,143,145]

Firstly, they showed that Co-corrin and Fe-porphyrin combinations are thermodynamically stable, more so than Co-porphyrins and Fe-corrins. They showed that the reasons for this stability were less chemical and more structural in nature; the differences in cavity size between the two rings (*ca*. 22 pm) contributed significantly towards the selection of metal ions. The smaller corrin ring fits the smaller cobalt ion perfectly and favours cobalt's low-spin oxidation states; Co-corrin species are always low-spin and the strain on the ring is small. This feature is important in labilising the Co-C bond. On the other hand, the porphyrin cavity is too large to accommodate low-spin Co or Fe, thus intermediate spin states are favoured with only small energy differences observed between the spin states. This feature is functionally significant in hemoprotein chemistry, for example in oxygen binding and activation. It was also observed that Co(I)Cor was energetically easier to form than Fe(I)Por. It was also noted that the Co(II/III) couple generated in the cobalt porphyrin is far less suited for electron-transfer reactions than the Fe(II/III) couple in iron porphyrins. Lastly, their work showed that cobalt complexes are more stable towards hydrolysis than iron complexes suggesting that this is why cobalamins are employed by Nature for organometallic transfer-type reactions.

1.4 MICROPEROXIDASES (MP)

The proteolytic digestion of cytochrome *c* leads to the cleavage of the polypeptide

chain at specific sites on either side of the heme moiety. The resulting heme fragments thus comprise a portion of the native protein covalently attached to the heme group. These water-soluble heme fragments, microperoxidases (MP), retain their ability to catalyse the monooxygenation of organic substrates by H_2O_2.[146-150] For these reasons MPs serve as excellent biomimetics for a number of reactions catalyzed by hemoproteins such as the peroxidases and the cytochromes P450.[151-154] Typical MPs obtained from the digestion include FeMP11, FeMP9, FeMP8 and FeMP6 (**Figure 1.12**). MPs are usually derived from horse cytochrome *c*; *Saccharomyces* and *R. rubrum* have been used as alternative cytochrome *c* sources; however sequence variants have been observed.[155,156]

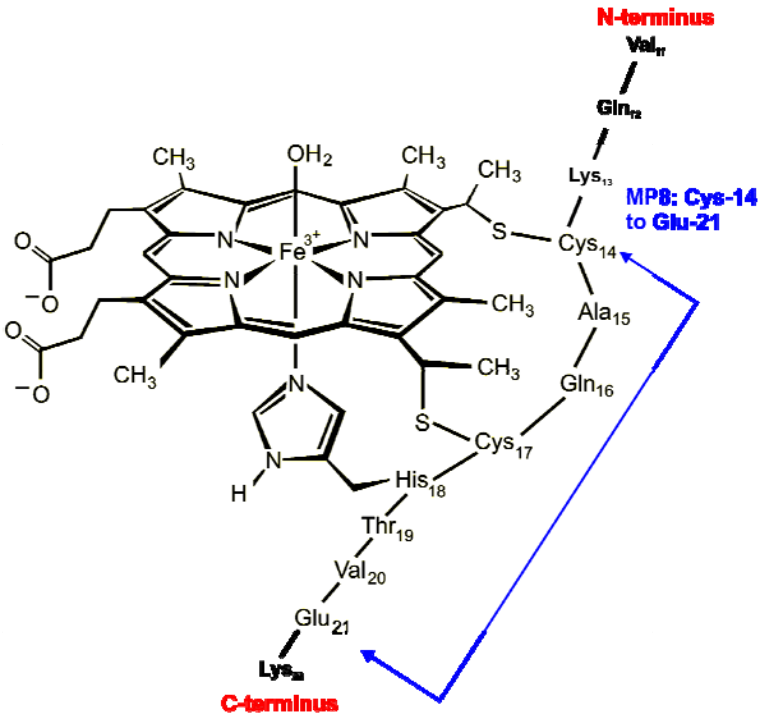


Figure 1.12 Hexacoordinate Fe(III) heme fragment from the proteolytic digestion of cytochrome *c*. Diagram shows the following fragments: FeMP6 (Cys-14 to Thr-19); FeMP8 (Cys-14 to Glu-21); FeMP9 (Cys-14 to Lys-22) and FeMP11 (Val-11 to Glu-21). The amino acid sequence is numbered according to that of horse cytochrome *c*.[84]

Tsou first reported on the proteolytic digestion of horse cytochrome c using pepsin (pH 1.5; 20 ^{o}C; ~20 h). His putative FeMP11 heme-peptide (**Figure 1.12**) had

ascorbate oxidase properties and was able to bind CO and NO.[146-148] Tuppy and Paleus[149] subsequently reported on the preparation of FeMP11 using two pepsin additions (pH 1.55-1.60; 48 hours); this was to overcome inhibition of the enzyme by heme-free peptides in the reaction mixture. Their work showed that proximal coordination site was occupied by His-18. They also found two pK_as: 3.4 and 5.8 at 20 ^oC, which they attributed to the protonation of His-18 leading to the 'base-off' state, and to the deprotonation and intermolecular coordination (and thus aggregation) of either Val-11 (α-NH_2) or Lys-13 (ε-NH_2), respectively. Wilson *et al.,* subsequently confirmed these findings but attributed a third pK_a (7.6 at 20 ^oC) to the aggregation of Lys-13.[157] Aggregation in metalloporphyrins may occur in at least two ways. Firstly, it may occur by covalent intermolecular coordination.[229] Secondly, it may occur by non-covalent π-π stacking. The latter is usually easily resolved by dilution or by the addition of dispersal agents whilst the former often requires structural changes to the coordination site.[158-160]

Harbury and Loach recognised the problem of FeMP11's aggregation by intermolecular coordination as early as 1959. They then reported on the protection of the amino groups on Val-11 and Lys-13 by acetylation (NAcFeMP11) as a means to diminish aggregation.[161,162] Though this method was apparently effective at minimising aggregation it was oddly only really explored about 40 years later at which point the acetylated MP was shown to be monomeric up to 0.6 mM at neutral pH using LCMS and ESR data.[163-165] In the mean time aggregation in FeMP11 has been confirmed by techniques such as Mössbauer,[166-168] EPR,[167,169] Raman,[170] NMR,[171,172] ORD, CD and UV-vis spectroscopy.[173] Solution studies such as ligand binding[157] reactions thus reflect a degree of ambiguity and FeMP11's usefulness as a biomimetic for hemoproteins was compromised.

Obtaining FeMP11 structural information was also complicated by aggregation *e.g.* magnetic studies.[166,167-170,172] There has however, been a single ^1H NMR study on the monomeric cyanide complex of FeMP11. Interestingly, the results show that 25% of the heme moiety (considering both faces) is shielded from solvent because

the bulk of the peptide (Lys-13 to Glu-21) coils underneath in an α-helical conformation similar to that exhibited by cytochrome *c*.[174] However, the α-NH_2 on the Cys-14 is exposed and may able to interact with solvent or allow for intermolecular coordination by a neighbouring heme group to form a low-spin dimer.[175,176] MPs are a classical example of a conformationally fluxional species and are therefore known to resist crystallisation. To date there has been only one MP crystal structure; Ni and Tezcan were able to crystallise FeMP9 by using a molecular host, the so-called 'zinc-directed protein cage', to stabilise the MP through encapsulation.[177]

In 1951 Tsou reported on the tryptic digestion of cytochrome *c*. (pH 8.5; 24 ^{o}C, 20 h).[147,148] The fragment was autoxidisable and the reduced form could bind CO; the fragment was reportedly FeMP9 (**Figure 1.12**). Subsequently, Tuppy and Bodo produced FeMP9, confirmed by degradation methods, through tryptic digestion of cytochrome *c* (pH 8.0; 37 ^{o}C; ~22 h).[178,179] In principle, FeMP9 is readily prepared by a single tryptic digestion and isolated by gel chromatography[180,181], however it has attracted little attention as a biomimetic since its chemistry is dominated by aggregation through intermolecular coordination of the amino groups on Cys-14 and Lys-22.[180-183] Having said that, Baldwin *et al*., demonstrated that FeMP9 may be monomerised in 20% MeOH but at very low heme concentrations (< 1 μM).[182]

FeMP8 was isolated by Tuppy and Paleus as an artefact of the FeMP11 synthesis (**Figure 1.12**).[149] They produced FeMP8 from the tryptic digestion of FeMP11 in dilute ammonia (36 ^{o}C; 23 h). Several modifications[175,184] to this original method[149] have since been made, the most significant of which have been contributed by Adams *et al*.[153] They showed using HPLC, that the maximum yield of FeMP11 from the peptic digestion of horse cytochrome *c* was obtained after only 2 hours (pH 2.1; 40 ^{o}C). The two important steps were firstly the salting-out of FeMP11 at its isoelectric point (~ pH 5) which was stabilised using ammonium sulphate (although the 'salting-out' method has recently been shown to exacerbate aggregation[160,185]). Secondly, this mixture was centrifuged into a pellet; the nonheme-peptides were

separated out into the supernatant and prevented from interfering with the subsequent tryptic digestion (pH 8.5; 40 ^{o}C; 15 min) thereby ensuring quantitative FeMP8 yields. Although FeMP8 is the most commonly studied MP, it is also expensive; Adams' method allows for the production of large quantities (100 – 150 mg) of FeMP8.[153] Under monomeric conditions (< 2 μM) FeMP8 is a promising model for example in the catalytic cycle of peroxidise enzymes.[186-188]

Like most MPs, FeMP8 chemistry is often complicated by aggregation effects though to a lesser extent than FeMP11 or FeMP9. Harbury and Loach showed that the Soret of both FeMP8 and NAcFeMP11 remained fixed at 398 nm on dilution from 20 to 0.2 μM (pH 7).[162] These findings suggested that both species were less susceptible to aggregation by non-covalent π-π stacking than FeMP11; however it is unlikely that dilution would sufficiently monomerise a covalently coordinated aggregate. They later showed that FeMP8 was monomeric at 10 μM; the pH was unspecified.[189] Aron *et al.*, however, demonstrated deviations from Beer's Law as a result of dimerisation at concentrations as low as 2 μM (pH 7.00; 25 ^{o}C); their spectroscopic evidence strongly suggested that the aggregation was through intermolecular coordination of the amine on Cys-14.[175] Urry and Pettegrew confirmed these results using ORC, CD and difference absorption spectroscopy (*ca*. 10^{-6} to 10^{-3} M); their findings also exhibited of non-covalent π-π stacking.[176]

Methods of combating aggregation in FeMP8 may be considered a two-fold approach. Firstly, additives may be used such as detergents[191,192,222] and/or non-coordinating solvents[175,190,191] as surfactants in FeMP8 solution preparation; this works best for non-covalent π-π aggregates. Alcohol solutions such as 20% methanol are commonly used to monomerise MP solutions (*e.g*. in thermodynamic[190-192] and kinetic[193,194] experiments); however this environment no longer mimics physiological conditions and values may differ from those obtained in aqueous systems. For example, three pK_a values for FeMP8 were initially found in 20% methanol at 25^{o}C (pK_a in brackets).[175] These correspond to the deprotonation and coordination of the histidinium cation (4.43), ionisation of the

iron-bound water (8.90) and His-18 to the histindate species (10.48), respectively. However, six pK_a values were found under aqueous conditions.[84] These correspond to the deprotonation and coordination of the C-terminal carboxylic acid group (2.2) and of the histidinium cation (3.5); to the ionisation of the heme propanoic acid subtituents (4.9) and of iron-bound water (8.89), to the deprotonaton of N-terminal ammonium group of Cys-14 (10.42) and of iron-bound His-18 to form histidinate (13.5). These results have two interesting features. Firstly, that the addition of alcohols to MP systems may in fact alter the coordinating environment thereby influencing the values obtained. Secondly, the seemingly remote functional groups on FeMP8 appear to be optically active; their ionisation appears to perturb the electronic structure of the porphyrin in some way.

In the case of intermolecular coordination it is often necessary to structurally modify the coordinating moieties by derivatisation, for example, by acetylation. Acetylation of the α-NH_2 group of Cys-14 on FeMP8 to form NAcFeMP8 suppresses this type of aggregation up to concentrations where it can be conveniently studied by conventional UV-vis spectroscopic methods.[15,163,189,195]
Yang and Sauer were the first to publish evidence that acetylation of FeMP8 minimises aggregation in this species.[196] However, their acetylation and pH methods were unclear. Wang and van Wart[195] subsequently presented Raman work on NAcFeMP8 however their work did not conclusively indicate that acetylation prevented aggregation. The first definitive evidence for the suppression of aggregation by acetylation in FeMP8 was presented by Marques and Munro.[198] Their work showed that NAcFeMP8 remained monomeric up to 30 μM with a self association constant that was an order of magnitude lower than that of FeMP8.[175]

The acetylation of FeMP8 is an attractive means to diminish aggregation because NAcFeMP8 still retains its biomimetic capabilities under physiological conditions and can therefore be directly compared to hemoproteins in aqueous solutions.[198] NAcFeMP11 is water soluble and retains the proximal His-18 ligand above pH 2 whereby the distal coordination site is occupied by a water molecule that is readily

replaced by exogenous ligands from solution.[198]

Metal-substituted enzymes are commonplace in the study of structure-function relationships especially regarding the role of the metal ion.[199] For example, the allosteric analogue of hemoglobin, cobalthemoglobin, showed that it was the motion of the proximal histidine ligand and not the metal ion that triggered allosteric transitions.[199] Thus, another way to examine the significance of iron in the heme system is to replace the iron with another transition metal. The main challenge here is to successfully remove iron without the heme fragment disintegrating. The removal of iron from ferric hemepeptides and the insertion of other metal ions have been reported. Three methods of demetalation have been examined. The first method involves the removal of the entire heme moiety from the polypeptide chain and replacing it with an entirely different metalloporphyrin containing the desired metal ion. This complex method is labour-intensive and less desirable.[208]

The second microperoxidase demetalation method can be effected by treatment with anhydrous HF at –78 ^{o}C[197] or at room temperature[200] to produce the metal-free peptido-porphyrin. Heating with manganous or zinc acetate at 40–55 ^{o}C for 2 h in aqueous solution[197,201] or with nickel acetate at 75 ^{o}C[200] followed by purification by reverse phase chromatography[197,201] or by dialysis[200] leads to the metalated hemepeptide. This method is hazardous as it involves the use of HF.

An alternative procedure that avoids use of HF involves the reductive elimination of iron that occurs on treating a solution of the hemepeptide in deaerated cold acetic acid with ferrous chloride in concentrated HCl.[202-204] Separation of the demetalated hemepeptide from the iron salts is by size exclusion chromatography.[202] Stirring with manganous chloride at 40 ^{o}C in ammonium acetate (pH 5.5) for about 60 h leads to metalation of the porphyrin.[205] Alternatively, metals such as zinc, copper and nickel can be inserted into the metal-free peptido-porphyrin dissolved in 1:3 pyridine:acetic acid by heating with the metal sulfate or chloride at 80 ^{o}C for 10 min under N_2 followed by precipitation of the metallopeptide with acetone.[203,204,231,232]

Porphyrins are extensively-conjugated macrocycles and are thus brightly coloured; they therefore have intense and characteristic electronic spectra. Consequently, electronic spectroscopy is a convenient tool for probing the structure of these molecules. The spectra of iron porphyrins are dominated by the π-electron system. Representative spectra for ferric and ferrous high and low spin iron porphyrins are reported (**Figure 1.13**). Typical hemoprotein examples and representative electronic assignments are shown (**Table 1.3**). Typical low and high spin ferrous- as well as low and high spin ferric hemoproteins include oxymyoglobin (which is analogous to low spin d^6 cobalt porphyrins), deoxymyoglobin, aquometmyoglobin and metmyoglobincyanide, respectively.

There are two main characteristic features in hemoprotein spectra. Firstly, there is an intense band near 400 nm region called the Soret or B band; this is accompanied by a slightly higher energy vibrational overtone, B(1,0), and a broad N band in the UV region (*ca*. 350 nm). Secondly, there are two lower intensity bands near the 550 nm region called Q bands; these are designated Q_o and Q_v or α- and β bands, respectively. These bands are all accounted for by an 18 π-electron model. Q_o and B bands are due to transitions from π (a_{1u}, a_{2u}) to π^* (e_g^*) porphyrin orbitals. Q_v is of vibronic origin and is sometimes denoted as Q(1,0); Q(2,0) bands may also be observed. The N band arises from the a_{2u}, b_{2u} (π) to e_g (π^*) transition. Other lower intensity bands are tabulated (**Table 1.3**). A very characteristic low-intensity band is noted in the 690 nm region (690 nm in azidometMb, and 695 nm in ferricytochrome *c* with His and Met as axial ligands) which is diagnostic of the structural integrity of the heme environment; this arises from the porphyrin to metal charge transfer transition.[55,206-209]

Whilst the spectra of Fe porphyrins may not be very sensitive to the identity of the axial ligand, they are sensitive to their ligand field strength. For example, high-spin Fe(III) porphyrins have distinctive porphyrin to metal charge transfer bands between 650 and 580 nm which is absent in the low-spin complex. [55,206-209]

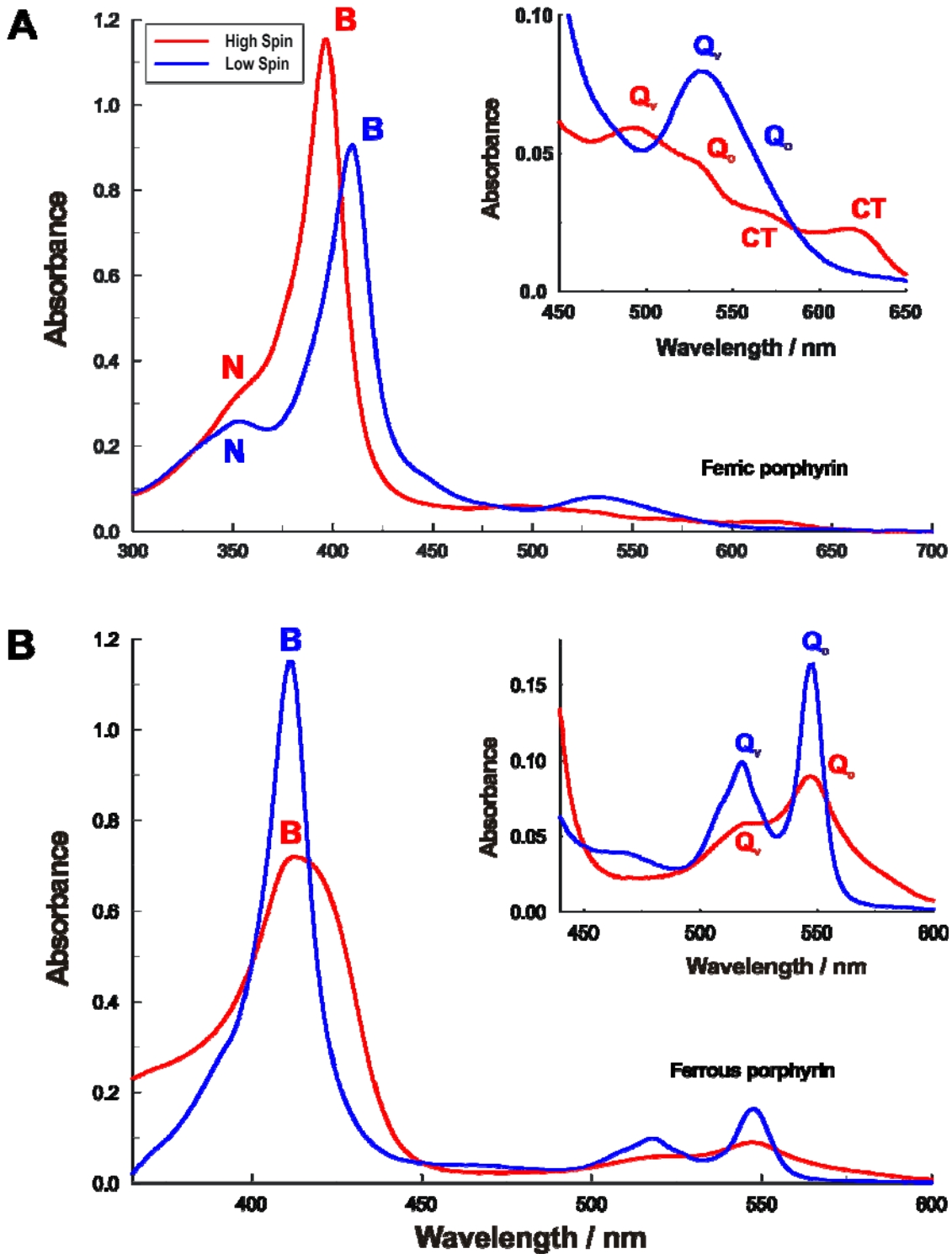


Figure 1.13 Typical UV-vis spectra of ferric (**A**) and ferrous (**B**) iron porphyrins in high (red) and low (blue) spin states. Low spin ferrous porphyrin spectra are also used as a model for low spin d^6 cobalt(III) porphyrin spectra (*e.g.* NAcCoMP8). [55,206-209]

Table 1.3 Electronic assignments that accompany **Figure 1.13.** [55,206-209]

Hemoprotein	λ /nm (solid state)	Assignment
MbO_2	348	N
	398	B(1,0)
	418	B
(Low spin Fe(II))	476	a_{2u} (π) → a_{1g} (d_{z2})
	542	Q_v
	580	Q_o
	645	e_g (dπ) → e_g (π*)
	925	a_{1u}, a_{2u} (π) → O_2 (π_g)
deoxyMb	406	B(1,0)
	433	B
	513	Q(2,0)
(High spin Fe(II))	556	Q_v
	607	Q_o
	626	a_{1g} (d_{z2}) → e_g (π*)
	757	b_{1g} (d_{x2-y2}) → e_g (π*)
	930	e_g (dπ) → e_g (π*)
$metMbH_2O$	357	N
	386	B(1,0)
	408	B
(High spin Fe (III))	467	a'_{2u} (π) → a_{1g} (d_{z2})
	505	Q_v
	545	Q_o
	581	a_{1u} (π) → e_g (dπ)
	633	a_{2u} (π) → e_g (dπ)
$metMbCN^-$	357	N
	400	B(1,0)
	421	B
(Low spin Fe (III))	487	a_{2u} (π) → a_{1g} (d_{z2})
	545	Q_v
	581	Q_o

MbO_2	Oxymyoglobin; shaded region to indicate analogous model for low spin d^6 cobalt porphyrins
deoxyMb	Deoxymyoglobin
$metMbH_2O$	Aquometmyoglobin
$metMbCN^-$	Metmyoglobincyanide

Ligand binding reactions, especially those using UV-vis spectroscopy, are a common method used by researchers in order to probe the nature of the prosthetic group in hemoproteins. Monomeric MPs serve as a useful model for the prosthetic group in hemoproteins. Since the proximal His-18 ligand is retained as part of the amino acid side-chain and the proximal ligand (water) is readily replaced, ligand substitution reactions with a wide variety of ligands may be investigated.[55,206,207]

As mentioned previously, the nature of the distal ligand determines the spin state of the metal ion in the MPs. Strong field ligands tend to produce low-spin complexes including cyanide, imidazoles and pyridines. Weaker field ligands such as azide and sulfite produce complexes that are in spin equilibrium. Predominately weak field ligands give rise to complexes that are high spin, such as those that complex cyanate, thiocyanate and fluoride. [55,190,193,196,206,207]

1.5 COBALAMINS (Cbl)

The relationship between structure and function in relation to cobalamins' remarkable enzymic activity have been the focus of many chemical reviews since the determination of its crystal structure in 1964.[1,4,6,210] Central to this inquiry is the nature and cleavage of the Co-C bond. To this end, the role of the corrin macrocycle is often highlighted together with that of the nucleotide and apoenzyme. This section will therefore focus on how the corrin influences the lability of the Co-C bond in order to achieve its function.

Coenzyme B_{12} (AdoCbl) comprises a Co-corrin macrocycle with an alkyl-bound 5'-deoxyadenosyl and an N(1)-coordinated 5,6-dimethylbenzimidazole (DMB) in the distal and proximal positions, respectively (**Figure 1.14**). The trivalent cobalt (d^6) is therefore a hexacoordinate metal centre; the overall charge is balanced by the corrin's monoanion, the anionic adenosyl group and the negatively charged ribophosphate group on the DMB ligand. Methylcobalamin (MeCbl) has a methyl

group in the distal position whilst cyanocobalamin, the vitaminic form, has a CN^- ligand. On the whole, the corrin is puckered and exhibits a saddle conformation. This conformation is likely due to the rigid DMB as DMB-free corrins are planar.[211] Both the nucleotide chain and the adenosyl group are rigid with a fixed coordination, the latter due to hydrogen bonding and interactions with the corrin ring. One likely function of the adenosyl group is to protect the Co-C bond from exogenous ligands and thereby influence the stereoselectivity of the reactions.

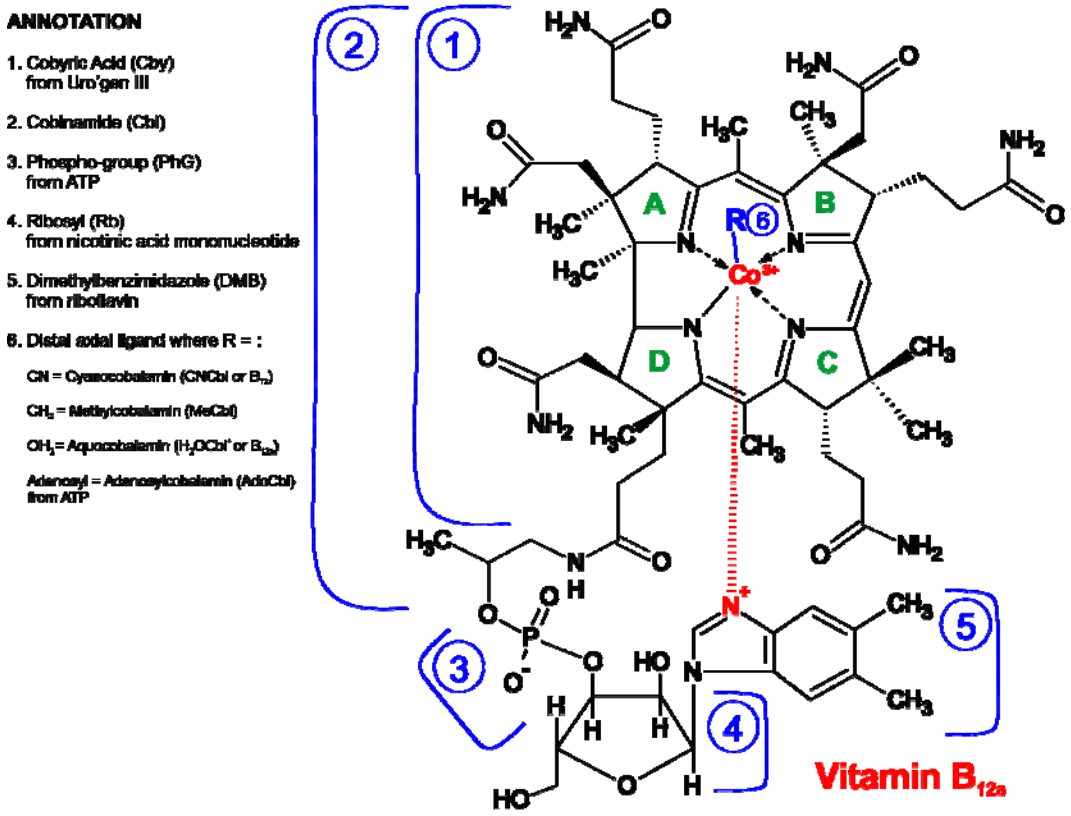


Figure 1.14 Structure and standard view of some important cobalamins. The lower and upper faces are designated α and β face, respectively. The pyrrole rings are labelled A-D.

The most noteworthy feature of AdoCbl (and MeCbl) is the Co-C bond, the only naturally occurring organometallic bond and the determining factor for the enzymic reactions they catalyse. The Co-C bond allows for the enzymically controlled formation of the reactive primary alkyl radicals. Furthermore, the occurrence of cobalt as the metal centre implies very specific functionality; cobalt is the least

abundant first row transition metal in the Earth's crust. Complexation of the relatively small trivalent cobalt ion within the corrin's smaller macrocyclic cavity emphasises the corrin's non-planarity. Were the macrocycle a porphyrin, the non-planarity would be far less pronounced. It is important to note that the cobalt porphyrins do not exhibit the same reactivity as the corrin complexes.[50] This discrepancy implies that cobalt-porphyrins are unable to fulfil the mechanistic requirements of the enzymic reactions involving the cobalt-corrin systems.[50] It therefore becomes necessary to understand how these enzymic reactions work in order to understand the role the corrin structure plays in labilising the Co-C bond.

AdoCbl and MeCbl enzymic functions depend on cobalt-corrin's redox properties. The organometallic bond is relatively inert even under physiological conditions but not so as to prohibit reactions from occurring. Cleavage of the Co-C bond may be homolytic or heterolytic. Homolytic cleavage results in the Co(II) species and a primary alkyl radical. Heterolytic cleavage produces either the low-spin Co(III) species and carbanion or the Co(I) species and carbocation (**Figure 1.15**).[212,213]

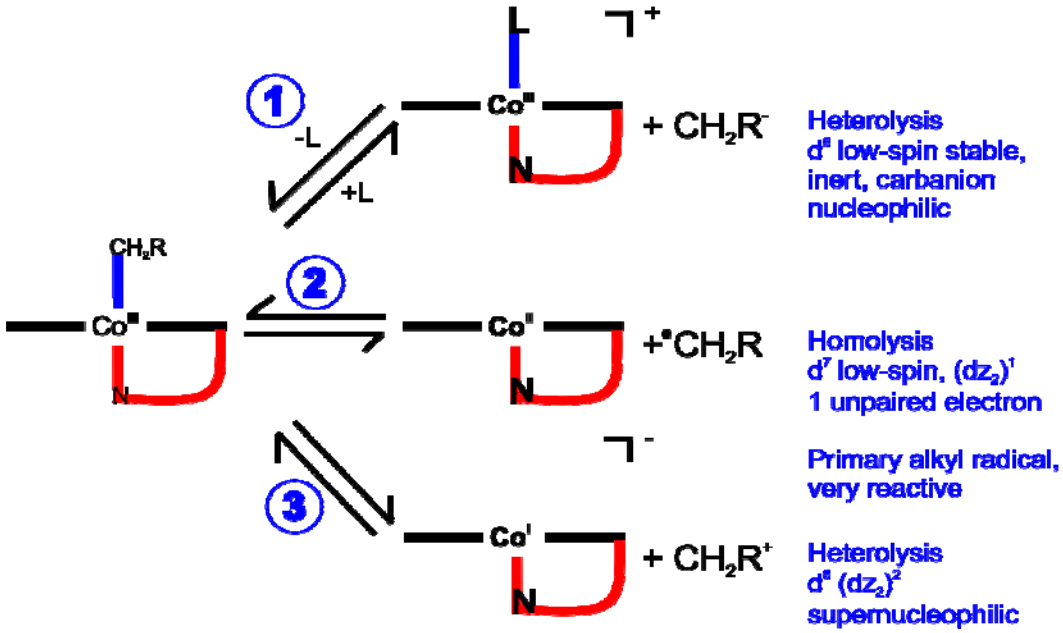


Figure 1.15 Pathways of Co-C cleavage in cobalamins. L = incoming ligand and N = nitrogen atom on DMB.[6] Pathways 1-3 refer to the hetero- and homolytic pathways of Co-C cleavage.[212,213]

The cleavage pathways depend on three aspects: the coordination of the nucleotide, the nature of the substrate and the redox potential. When the nucleotide is not coordinated, then (1) is favoured at positive potentials and (3) at potentials below -0.9 V (vs NHE) (**Figure 1.15**). The homolytic cleavage (2) is important as it occurs at physiological conditions (0 to -0.4 V). The specific redox potential of the reduction steps for AdoCbl is heavily influenced by the *trans* effect of the axial ligands; AdoCbl cleaves Co-C homolytically and the efficiency of which is increased due to the intramolecular coordination of the nucleotide. It has been shown that the Co-C homolysis is 1400 times faster for neopentylcob(III)alamin than for the nucleotide-free derivative; the neopentyl group models deoxyadenosyl.[214] In contrast, Kräutler's examination of the thermodynamic *trans* effect of the nucleotide on the Co-CH_3 bond in MeCbl revealed that the thermal methyl group transfers were in fact, favourable in both cleavage types.[213] In homolytic cleavage, the MeCbl was only marginally more stable than the nucleotide-free derivative suggesting that intermolecular coordination of the base does not significantly affect the thermodynamics (stability) of the organometallic bond. However, in the case of heterolytic cleavage, and more so with nucleophiles, the nucleotide coordination was found to stabilise the Co-C bond significantly.

There is a mutual dependence of the Co-C and Co-nucleotide bonds in AdoCbl and MeCbl in aqueous solution.[212] The degree of substitution of the Co-bound alkyl group has a direct effect of the strength of the nucleotide coordination and thus on the lability of the Co-C bond towards homolysis (in the case of a weak nucleotide coordination). The degree of axial coordination decreases after each one electron reduction step. Martin and Finke's work[215] showed that in the case of MeCbl, Co-C is too strong to support a homolytic mechanism and that the cleavage is initiated rather, by the population of the Co-C σ-antibonding orbital during one electron reduction to form a radical anion. They did this by comparing bond dissociation rates of MeCbl and $MeCbl^{-}$ by thermolysing MeCbl in ethylene glycol in the presence of a radical trap.

Uv-vis was subsequently used to monitor MeCbl/Co(II)B_{12} concentrations and thus kinetic rates. They found that the BDE of Co-C was *ca*. 37 kcal/mol. At the same time, Lexa and Saveant[216] electrochemically induced homolysis from the reduced $MeCbl^{-}$; the results for the homolysis were too fast to compare with those obtained by Martin and Finke,[215] the homolysis of $MeCbi^{-}$ was studied instead. The methyl cobinamide does not have the (marginal) labilising power of the nucleotide and thus the rate could be monitored. The electron that was added to $MeCbi^{-}$ or MeCbl is placed in the σ* orbital along the Co-C bond perpendicular to the macrocycle. This means that the Co-C bond now has three electrons, not two, but effectively only one *bonding* electron and hence 'half a metal bond' results. The comparison of MeCbl and $MeCbi^{-}$ rates confirms that the addition of the antibonding electron more than halves the Co-C bond strength (from *ca*. 37 to *ca*. 12 kcal/mol). An even further drop in bond strength would be anticipated for $MeCbl^{-}$ given the *trans* labilising effect of the nucleotide. This increase in BDE translates into a factor of 10^{15} increase in the homolysis rate and supports the view that the similar rate increase facilitated by the enzyme in AdoCbl dependent reactions could be due to an electron transfer activation mechanism of homolysis. However, the fact that the Co(I) species is not observed in the holoenzyme, but rather the Co(II) species together with the lack of sufficiently reducing biological sources strongly discourages the role of reduction induced homolysis in the enzymic reactions.

Now, even though the application of the reduction mechanism to enzymic reactions has been refuted, it must be noted that such a mechanism could only occur in the case of the corrin ring. This is because the corrin ring, unlike the porphyrin ring, is square planar and able to stabilise the Co(I) state. Under physiological conditions, the Co(I) state is not reversibly accessible for cobalt-porphyrins.[212]

The importance of the Co-C cleavage in organocobalamins may be emphasised by examining the enzymic reactions that they subsequently catalyse in relation to the role of the substrate. The primary step of these enzymic reactions involves the homolysis of the Co-C bond in order to produce a radical ($AdCH_2^{\cdot}$); the radical then

abstracts a hydrogen atom from the substrate. The product radical is obtained by the rearrangement of the substrate radical thereby produced. The catalytic role of the enzyme is therefore fulfilled by the final abstraction by the product radical of a hydrogen from $AdCH_3$.[137,217] Halpern's work confirmed that the rearrangement of the substrate does indeed occur at the free radical stage and that the cobalamin is not involved; the role of the cobalamin is thus to generate (and reabsorb) the free radical.[137] What is important to note here is the significance of the weak Co-C bond (*ca*. 26 kcal/mol)[218]; there are no stable organic molecules which could undergo thermally induced dissociation at the mild physiological conditions in order to generate the highly reactive radical required for the enzymic reactions.

It was also found that the BDE of the organometallic bond is also affected by the basicity of the axial ligand.[137] Since the homolysis of the Co-C involves the reduction of cobalt, the more basic the axial ligand, the greater the stabilisation of the Co(III) species relative to the Co(II) species and so more energy would be required to break it. Additionally, steric factors greatly influence BDE. The model compound used to investigate this effect was $C_6H_5(CH_3)CH\text{-}Co(DH)_2(PR_3)$, where DH = dimethylglyoxime was used as a planar model for the corrin. It was found that as the size of PR_3 increases so too does the cone angle. The relationship between cone angle (and thus size of PH_3) and BDE strongly suggests that size lowers the BDE significantly. X-ray evidence confirmed these findings as large axial ligands result in longer (weaker) Co-C bond lengths. It was also interesting to note that the planar DH ligands were distorted which lends credence to the theory that the Co-C bond weakening is due to the upward distortion of the corrin ring. Lenhert[211] notes that there is significant steric repulsion afforded by the Ado-substituent which thus affects the homolysis of Co-C; since the coenzyme is already sterically crowded, very little distortion would be required to facilitate the dissociation.

Geno and Halpern investigated the differences in bond homolysis between cobalt corrins and porphyrins in order to clarify the role of the corrin in cobalamins.[50] The BDE values for an array of cobalt phospho-porphyrins were determined; the

phosphine substituents differed in sizes and pK_as. There was a linear dependence of BDE on the pK_a of the phosphine which was independent of size. In the corrin model on the other hand, the expected increase in BDE with pK_a was masked by the linear decrease in BDE with increasing phosphine size. As proposed earlier, homolysis is due to the repulsions of the Ado-substituent, induced by the conformational distortions of the corrin ring. The fact that the BDE of the porphyrin derivative is not as affected by the phosphine ligand size suggests that the macrocycle is not as flexible as the corrin even in the presence of bulkier ligands. There is therefore no corresponding steric repulsion with the adenosyl group and subsequently no drop in BDE.

Kräutler *et al*., evaluated the structural changes that occur during Co-C homolysis in order to clarify the role of the corrin ring in this process.[219] He compared the corrin in the coenzyme with that of pentacoordinate cob(II)alamin; the deviations from planarity as well as the orientation of the nucleotide were unchanged. The significant difference was in the displacement of the Co(II) centre from the corrin N-plane, towards the nucleotide. The corresponding decrease in axial Co-N bond length was comparable to those found in both MeCbl and AdoCbl; findings that were supported by earlier work using model compounds.[220] Although the corrin was not significantly bent upwards in the pentacoordinate derivative, the acetamide side groups and the nucleotide sidechain were. Based on these structural changes that the homolytic rate may be increased by the repulsions afforded by the adenosyl group and the corrin due to the upward bending of the corrin side chains which is exacerbated by the concomitant downward displacement of the cobalt centre, a feature that brings the adenosyl group closer to the corrin ring.

The role of the cobalamins in the varied enzymic reactions that they catalyse is heavily dependent upon the cleavage of the Co-C bond; the nature of which readily allows for homo- and heterolysis under mild physiological conditions. The influence of the corrin ring is integral to this labilisation in a way that clearly can not be readily achieved by the porphyrin.

1.6 PROBLEM STATEMENT, BIOLOGICAL RELEVANCE, SCOPE, AIMS AND ORGANISATION OF THIS WORK

1.6.1 Problem statement

Porphyrins and corrins have been compared (**Section 1.3**) and the structural significance of cobalamins has been examined (**Section 1.5**).

The following questions therefore arise:

1. Why has Nature chosen cobalt, one of the least abundant transition metals, as the central metal ion as opposed to iron which is considerably more abundant? Particularly, why has Nature chosen the d^6 low-spin Co(III) ion, a quintessentially inert metal ion to serve as the active site of a number of metalloenzymes, and a metal ion that is unusually labile in this system?

2. What is special about the corrin ligand? What can this ligand offer that a porphyrin ligand cannot especially since porphyrins are more widely observed in Nature than corrins?

3. What is the nature of the metal-ligand interaction and how does the protein use these interactions enzymatically?

There are several approaches that could be undertaken in order to garner insight into these questions. These include extensive examination of cobalt corrins[6,1209,221] and of hemoproteins.[7,84,92] However, an attractive strategy implemented in this work involved the replacement of Fe(III) in the hemepeptide NAcFeMP8 by Co(III) to afford a Co(III) porphyrin complex in which the coordination environment of the metal is not dissimilar to that in cobalamin: the axial ligands are water and an

imidazole derivative (His-18 residue and 5,6-dimethylbenzimidazole, respectively), the equatorial ligands are porphyrin and corrin, respectively. This should then provide the unique opportunity of comparing the effects of porphyrin and corrin on Co(III) in two closely related systems.

1.6.2 Biological relevance

In addition to addressing these fundamental academic questions pertinent to cobalamin chemistry (**Section 1.6.1**), this work may in fact have important medical and pharmacological relevance. A better mechanistic understanding of B_{12a} may lead to more practically useful information in areas such as drug-design in conditions that are commonly associated with cobalamin deficiencies for example, anaemia, cardiovascular disorders and dementia.[223,224]

Current research shows that cobalamin and other B-vitamins have some far-reaching medical implications.[224-232] It has recently been shown that vitamin B_{12a} together with folic acid is important in the prevention of chromosome breakage and hypomethylation of DNA, actions that are associated with cancers.[225,226] The preventative action is compromised in instances of low B_{12a} concentration.[225,226] The use of vitamin B_{12} has been explored as a cheap and effective means of combating gestational diabetes, a condition that often leads to full-on diabetes in the mother and related complications in the infant.[227] Vitamin B_{12a} in combination with thiosulfate administrations are commonly used as a cheap and effective means of treating moderate cases of hydrogen cyanide poisoning.[224,225] Arguably the most compelling medical implication thus far is the correlation of Alzheimer's disease and dementia with a deficiency in B-vitamins.[228-232] Subsequently, the use of cobalamins and other B-vitamins is being investigated as a way of combating associated brain shrinkage and cognitive impairment.[232] High doses of these vitamins have been shown to halve the rate of brain shrinkage in those with early onset Alzheimer's disease.[232]

These examples illustrate the significance that B_{12a} has in current research as well as the importance of acquiring a better understanding of the driving mechanisms that influence these cobalamin-dependent reactions.

1.6.3 Scope and specific aims

The central thrust of this enquiry is aimed at elucidating a pivotal question in vitamin B_{12a} research: *why has Nature elected to retain the corrin ligand*? In attempting to answer this question it is hoped that this work will uncover some of what is unique about the chemistry of Co(III)-corrin systems. Furthermore, it is expected that some insight would be provided as to why this chemistry cannot be performed by Co(III)-porphyrin systems, or for that matter, Fe(III)-porphyrin systems – although this latter question is beyond the scope of this present enquiry.

This project is envisaged to be the first step in a major assault on the three fundamental questions posed previously with the focus being on the macrocycle (**Section 1.6.1**). As such, the scope in this systematic exploration of corrin vs. porphyrin chemistry begins with a brief synthesis component of a suitable B_{12a} analogue containing a porphyrin macrocycle, NAcCoMP8. This is followed by preliminary solution chemistry studies using selected ligands, the results of which are then compared to those obtained for the corrin. In addition, any interesting avenues of inquiry that arise during the course of these investigations are also pursued as the chemistry of this novel compound is explored.

To this end, the following objectives have been proposed in this project:

1. Synthesise microperoxidase-8 (FeMP8), a porphyrin-containing fragment of the protein cytochrome *c*, which retains the proximal His ligand, an excellent model for the proximal 5,6-dimethylbenzimidazole base in the cobalamins. Standard methods for its preparation by proteolytic digestion of cytochrome

c have been developed.[152,153,198] These methods are optimised.

2. Remove Fe(III) from FeMP8 to produce the metal-free MP8 by adapting and optimising the reductive demetalation procedures that were previously outlined.[202]

3. Purify the free-base ligand using size-exclusion chromatography and HPLC.

4. Characterise free-base MP8 using mass spectroscopy (MS).

5. Develop and optimise the protocol for the insertion of Co(III) into MP8 by refluxing with cobaltous acetate followed by aerial oxidation.[226-228]

6. Characterize the CoMP8 by standard techniques, principally MS and UV-vis spectroscopy.

7. If necessary, acetylate the N-terminus of CoMP8 to produce N-acetyl-Co(III)MP8 (NAcCoMP8), a species which is supposedly monomeric in aqueous solution up to concentrations of 50 μM.[208]

8. Characterize NAcCoMP8 by standard techniques, principally MS and UV-vis spectroscopy.

9. Exploit the delineation of the solution chemistry of NAcCoMP8 to find conditions of pH and solvent under which the ligand substitution reactions of coordinated H_2O can be studied.

10. Measure the equilibrium constants for replacement of H_2O in NAcCoMP8 with a variety of neutral N-donor ligands (imidazoles, pyridines, amines), and anionic ligands (CN^-, N_3^-, NO_2^-, HSO_3^- and so on) as a function of temperature, and compare the results with those available for

aquacobalamin, in order to determine what effect the equatorial ligand has on the ligand binding properties of Co(III).

11. Measure the kinetics of ligand substitution of H_2O in NAcCoMP8 with these same ligands, for comparison with equivalent data for aquacobalamin.

1.6.4 Organisation of this work

General methods and details of all materials are given in Chapter 2. Methods relevant only to a particular Chapter are presented in that Chapter.

Each Chapter begins with an introduction in which a summary of the pertinent literature and a statement of the specific aims of the work are presented. This is usually accompanied by a flow chart to clearly illustrate the focus of that particular Chapter. The relevance of the work to porphyrin and corrin chemistry in general and to B_{12a} chemistry in particular, is included in a Discussion in each Chapter. Chapters are concluded with a brief restatement of the initial aims, main findings and conclusions in that Chapter. All references are collected at the end of each Chapter and the numbering is relevant to that Chapter only. A number of Appendices are included which contain details of derivations of equations as well as details of selected synthesis procedures.

1.7 REFERENCES FOR CHAPTER 1

1. Battersby, A. R.; *Nat. Prod. Rep.,* **2000**, *17*, 507.
2. Pozharskii, A.F., Soldatenkov, A.T. and Katritzky, A.R. *Heterocycles in life and society*. John Wiley and Sons, Chichester, New York, Toronto, 1996.
3. Bruice, P.Y.; *Organic Chemistry*, 2nd edition, Prentice-Hall International Inc. London, Sydney, Toronto, New Jersey, 1998.
4. Milgrom, L. R.; *The Colours of Life: An introduction to the chemistry of porphyrins and related compounds,* Oxford University Press, Oxford, 1997.
5. Greenwood, C.; in P. M. Harrison (eds.), *Metalloproteins,* Part 1, Metal Proteins with Redox Roles, MacMillan, London, 1985, pp 43-79.
6. Pratt, J. M.; *Inorganic chemistry of vitamin B_{12}*, Academic Press, London 1972 (and references therein).
7. Dolphin, D., *The Porphyrins*, Academic Press, New York, 1978 (and references therein).
8. Thomson, A. J.; Gray, H. B.; *Curr. Op. Chem. Biol.*, **1998**, 2, 155.
9. Waldron, K. J.; Robinson, N. J., *Nat. Rev. Microbiol.,* **2009**, *7*, 25.
10. Silver, J. B. L.; Morrison, I. E. G.; Barnard, P. W. C., *Inorg. Chim. Acta*, **1983**, *78*, 205.
11. Wrigglesworth, J. M.; Baum, H., *Iron Porphyrins in Biochemistry and Medicine*, Academic Press London, 1980, pp. 45-67.
12. Messerschmidt, A.; Huber, R.; Poulos, T.; Wieghardt, K., *Handbook of Metalloproteins*, John Wiley and Sons, Volume 1, 2001.
13. Karlin, K. D.; *Science*, **1993**, *261*, 701.
14. van Eldik, R., *Chem. Rev.*, **2005**, *105(6)*, 1917.
15. http://www.pdb.org
    Source: Protein Data Bank, Research for Collaboratory Structural Bioinformatics, RCSB PDB, New Jersey, California, Wisconsin, United States, (20-12-2012).
16. Fermi, G.; Perutz, M. F.; Shaanan, B.; Fourme, R., *J. Mol. Biol.*, **1984**, *175*, 159.

17. Sussman, D.; Wilson, C., *Structure Fold. Des.,* **2000**, *8*, 719.

18. Botos, I.; Meyer, E.; Nguyen, M.; Swanson, S. M.; Koomen, J. M.; Russell, D. H.; Meyer, E. F., *J. Mol. Biol.*, **2000**, *298*, 895.

19. Schindelin, H.; Kisker, C.; Schlessman, J. L.; Howard, J. B.; Rees, D. C., *Nature*, **1997**, *387*, 370.

20. Vallee, B. L.; Williams, R. J. P.; *Proc. Natl. Acad. Sci. (U.S.A)*, **1968**, *59*, 498.

21. Williams, R. J. P.; *Chemistry in Britain*, **1996**, *32*, 42.

22. Valuer, B.; Bardez, E.; *Chemistry in Britain*, **1995**, *31,* 216.

23. Beinert, H., *J. Biol. Chem.*, **2002**, *277*, 37967.

24. Bertini, I.; Rosato, A*., Proc. Natl. Acad. Sci., (U. S. A.)*, **2003**, *100*, 3601.

25. Thiel, E. C.; Thorp, H. H., *Curr. Op. Chem. Biol.*, **2005**, *9*, 95.

26. Glusker, J. R.; Katz, A. K.; Bock, C. W., *The Rigaku Journal*, **1999**, *16*, 2.

27. Glusker, J. R., *Adv. Protein Chem.*, 1991, **42**, 1

28. Williams, R. J. P., *Pure and Appl. Chem.*, **1982**, *54*, 1889.

29. Cotton, F. A.; Wilkinson, G., *Advanced Inorganic Chemistry*, 5th Edition, John Wiley and Sons, New York, 1988, Chapters 18, 20 and 30.

30. Cotton, F. A.; Wilkinson, G., *Basic Inorganic Chemistry*, 5th Edition, John Wiley and Sons, New York, 1987, Chapters 18 and 31.

31. Williams, R. J. P., *Proc. Royal Soc. (London)*, **1981**, *B294*, 57.

32. Frausto da Silva, J. J. R.; Williams, R. J. P., *The Biological Chemistry of Elements*, 1991, Claredon Press, Oxford

33. Huheey, J. E., *Inorganic Chemistry*, 3rd Edition, Harper and Row, New York, 1983, Chapters 23 and 31.

34. Thiel, E. C.; Raymond, K. N., *Bioinorganic Chemistry*, University Science Books, California, 1994, Chapter 1.

35. Martin, H.; Gordon, R. M., *Deep Sea Res.*, 1988, **35**, 177.

36. Fox, L. L., *Geochim. Cosmochim. Acta*, 1988, **52**, 771.

37. Aisen, P., *Iron, Biochemistry and Medicine*, 2nd Edition, Academic Press, London, 1980, Chapter 3.

38. Poole, A. M.; Logan, d. T.; Sjoberg, B., *J. Mol. Evol.*, **2005**, *55*, 180.

39. Spiro, T. G., *Proteins of Iron Metabolism*, Grune and Stratton, New York, 1977, 23.

40. Shriver, D. F.; Atkins, P. W.; Langford, C. H., *Inorganic Chemistry*, Oxford University Press, 1994, p. 246.

41. Mankinen, M. W; Churg, A. K., *in Iron Porphyrins*, *Part 1;* Lever, A. B. P., Gray, H. B., Eds.; Addison–Wesley Publishing Company, Inc.: Reading, M. A., 1983, pp.141-235

42. Shelnutt, J. A.; Song, X-Z.; Ma, J-G.; Jia, S-L.; Jentzen, W.; Medforth, C. J., *Chem. Soc. Rev.*, **1998**, *27*, 31.

43. Dunford, H. B.; Dolphin, D.; Raymond, K. N.; Sieker, L., *The Biological Chemistry of Iron*, D. Reidel. Dordrecht. 1982.

44. Williams, R. P. J., *Cell. Mol. Life Sci.*, **1997**, *53*, 816.

45. Chan, M. K.; Mukund, S.; Kletzin, A.; Adams, M. W. W.; Rees, D. C., *Science*, **1995**, *267*, 1463.

46 Reichard, P., *Science*, **1993**, *260*, 1773.

47. Roth, J. R.; Lawrence, J. G.; Bobik, T.A., *Annu. Rev. Microbiol.*, **1996**, *50,* 137.

48. Greenwood, N. N.; Earnshaw, A., *Chemistry of the Elements*, 2nd Edition, Butterworth-Heinemann, pp 1117-1119.

49. Jensen, K.P.; Ryde, U., *Chem. BioChem*. **2003**, *4*, 413.

50. Geno, M.K.; Halpern, J., *J. Am. Chem. Soc.,* **1987**, *109,* 1238.

51. Miller, S. L.; Orgel, L. E., *The Origins of Life on Earth*, Prentice-Hall, New Jersey, 1974 (and references therein).

52. Lavallee, D. K., *The chemistry and biochemistry of N-Substituted porphyrins,* VCH Publishers, Inc., New York, 1987 (and references therein).

53. Shemin, D., *BioEssays*, **1989**, *10*, 30.

54. Smith, K. M., in *Porphyrins and Metalloporphyrins*, Smith, K. M. (eds)., Elserivier Publishing Co., Amsterdam, 1975, pp. 1-200 and 672.

55. Marques, H. M., Ph.D. Thesis, University of the Witwatersrand, Johannesburg, South Africa, **1986** (and references therein).

56. Mangani, S.; Meyer, E. F., Jr.; Cullen, D. L.; Tsutsui, M.; Carrano, C. J., *Inorg. Chem.,* **1983**, *22*, 400.

57. Lecomte, C.; Protas, J.; Marchon, J. C.; Nakajima, M., *Acta Crystallgr., Sect. B,* **1978**, *B34*, 2856.

58. Guilard, R.; Latour, J.-M.; Lecomte, C.; Marchon, J.C.; Protas, J.; Ripoll, D., *Inorg, Chem.* **1978**, *17*, 1228.

59 Berreau, L. M.; Young, V. G., Jr.; Woo, L. K., *Inorg. Chem.*, **1995**, *34*, 527.

60. Drew, M. G. B.; Mitchell, P. C. H.; Scott, C. E., *Inorg. Chim, Acta*, **1984**, *82*, 63.

61. Molinaro, F. S.; Ibers, J. A., *Inorg. Chem.*, **1976**, *15*, 2278.

62. Petterson, R. C., *Acta Crystallogr., Sect. B.,* **1969**, *B25*, 2527.

63. Groves, J. T.; Takahashi, T.; Butler, W. M., *Inorg. Chem.*, **1983**, *22*, 884.

64. Groves, J. T.; Kruper, W. J., Jr.; Haushalter, R. C.; Butler, W. M., *Inorg. Chem.*, **1982**, *21*, 1363.

65. Camenzind, M. J.; Hollander, F. J.; Hill, C. L., *Inorg. Chem.*, **1982**, *21*, 4301.

66. Kirner, J. F.; Reed, C. A.; Scheidt, W. R., *J. Am. Chem., **1977**,* 99*, 1093.*

67. Hill, C. L.; Williamson, M. M., *Inorg. Chem.*, **1985**, *24*, 2836.

68. Kirner, J. F.; Scheidt, W. R., *Inorg. Chem.*, **1975**, *14,* 2081.

69. Hoffman, A. B.; Collins, D. M.; Day, V. W.; Fleischer, E. B.; Srivastava, T. S.; Hoard, J. L., *J. Am. Chem. Soc.*, **1972***, 94,* 3620.

70. Scheidt, W. R.; Osvath, S. R.; Lee, Y. J., *J. Am. Chem. Soc.,* **1987**, *109*, 1958.

71. Scheidt, W. R., *J. Am. Chem. Soc.,* **1974**, *96*, 84.

72. Scheidt, W. R.; Turowska-Tyrk, I., *Inorg. Chem.*, **1994**, *33*, 1314.

73. Doppelt, P.; Fischer, J.; Weiss, R., *J. Am. Chem. Soc.*, **1984**, *106*, 5188.

74. Kirner, J. F.; Garofalo, J., Jr.; Scheidt, W. R., *Inorg. Nucl. Chem. Letters.,* **1975**, *11*, 107.

75. Cullen, D. L.; Meyers, e. F., Jr.; *J. Am. Chem. Soc.*, **1974**, *96*, 2095.

76. Meyers, E. F., *Acta Crystallogr., Sect. B*.; **1972**, *28*, 2162.

77. De Angelis, S.; Solari, E.; Floriani, C.; Chiesi-Villa, A.; Rizzoli, C., *J. Am. Chem. Soc.,* **1994**, *116*, 5691.

78. Moustakali, I.; Tulinsky, A.; *J. Am. Chem. Soc.*, **1973**, *95*, 6811.

79. Hatada, M. H.; Tulinsky, A.; Chang, C. K., *J. Am. Chem. Soc.*, **1980**, *102*, 7115.

80. Bag, N.; Chern, S. S.; Peng, S. M.; Chang, C. K., *Inorg. Chem.,* **1995**, *34*, 753.

81. Collins, D. M.; Hoard, J. L., *J. Am. Chem. Soc.*, **1970**, *92*, 3761.

82. Cullen, D. L.; Meyer, E. F., Jr.; *Acta Crystallogr., Sect. B.,* **1976**, *B32*, 2259.

83. Munro, O. Q.; Bradley, J. C.; Hancock, R. D.; Marques, H. M.; Marsicano, F.; Wade, R. W., *J. Am. Chem. Soc.*, **1992**, *114*, 7218.

84. Munro, O. Q., Ph.D. Thesis, University of the Witwatersrand, Johannesburg, South Africa, **1995** (and references therein).

85. Munro, O. Q.; Marques, H. M.; Debrunner, P. G.; Mohanrao, K.; Scheidt, W. R., *J. Am. Chem. Soc.*, **1995**, *117*, 935.

86. Marques, H. M.; Munro, O. Q.; Grimmer, N. E.; Levendis, D. C.; Marsicano, F.; Pattrick, G.; Markoulides, T., *J. Chem. Soc. Faraday Trans.*, **1995**, *91*, 1741

87. Munro, O. Q.; Marques, H. M.; Debrunner, P. G.; Mohanrao, K.; Sheidt, W. R., *J. Am. Chem. Soc.,* **1995**, *117*, 935.

88. Hancock, R. D.; Weaving, J. S.; Marques, H. M., *J. Chem. Soc. Chem. Commun.,* **1989**, 1176.

89. Marques, H. M.; Brown, K. L., *Coord. Chem. Rev.,* **2002**, *225*, 123.

90. Senge, M. O., *Chem. Commun.,* **2006**, 243.

91. Huheey, J. E., *Inorganic Chemistry*, 3rd Edition, Harper and Row, New York, 1983, Chapters 23 and 31.

92. Prendergast, K.; Spiro, T. G., *J. Am. Chem. Soc.*, **1992**, *114*, 3793.

93. Othman, S.; Lirzin, A. L.; Desbois, A., *Biochemistry*, **1994**, *33*, 15437.

94. Hunter, C. A.; Sanders, J. K. M., *J. Am. Chem. Soc.,* **1990**, *112*, 5525.

95. Kano, K.; Fukuda, K.; Wakami, H.; Nishiyabu, R.; Pasternack, R. F., *J. Am. Chem. Soc.,* **2000**, *122*, 7494 (and references therein).

96. Hambright, P., Porphyrins and Metalloporphyrins , Smith, K. M. (ed)., Elserivier Publishing Co., Amsterdam, 1975, pp.233-278

97. Pratt, J. M., in *Techniques and Topics in Bioinorganic Chemistry*, McAuliffe, C. A. (ed.); The Macmillan Press Ltd., London, 1971; pp 109-204.

98. Hughes, M. N., in *Comprehensive Coordination Chemistry*, Vol. 6; Wilkinson, G. (ed.), Pergamon Press, Oxford, 1987 pp 614-717

99. Makinen, M. W., in *Techniques and Topics in Bioinorganic Chemistry*, McAuliffe, C. A. (ed.); The Macmillan Press Ltd., London, 1971; pp 3-5.

100. Lemberg, R.; Barrett, J., *Cytochromes*, Academic Press, London, 1973.

101. Moore, G. R.; Pettigrew, G. W., *Cytochrome c*. *Evolutionary, Structural and Physicochemical Aspects*, Springer-Verlag, New York, 1990.

102. Murray, R. I., Fisher, M. T., Debrunner, P. G., Sligar, S. G., in *Metalloproteins,* Part 1*;* Harrison, P. (ed.), The Mcmillan Press Ltd., London, 1985, pp 157-206.

103. Marchon, J. C.; Mashido, T.; Reed, C. A. in *Electron Transport and Oxygen Utilization*, Ho. C. (ed.); Elsevier, New York, 1982.

104. Gouterman, M. J., *J. Chem. Phys.*, **1959*,*** *30*, 1139.

105. Holm, R. H.; Solomon, E. I., *Chem. Rev.*, **2004**, *104*, 347.

106. Ricoux, R.; Korri-Youssoufi, H.; Mahy, J-P., *J. Biol. Sci.*, **2005**, 5, 44.

107. Toohey, J. I.; *Proc. Nat. Acad. Sci.*, **1965**, *54*, 934.

108. Muller, P. M.; Farooq, S.; Hardegger, B.; Salmond, W. S.; Eschenmoser, A., *Angew. Chem. Internat. Edit.,* **1973**, *12*, 914.

109. Schiebel, H. M.; Schulten, H. R., *Tetrahedron,* **1979**, *35*, 1191.

110. Yamada, Y.; Miljkovic, E.; Wehrli, P.; Golding, B.; Loliger, P.; Keese, R.; Muller, K.; Eschenmoser, A., *Angew. Chem. Internat. Edit.,* **1969***, 8*, 343.

111. Fischli, A.; Eschenmoser, A., *Angew. Chem. Internat. Edit.,* **1967**, *6*, 866.

112. Bormann, D.; Fischli, A.; Keese, R.; Eschenmoser, A., *Angew. Chem. Internat. Edit.,* **1967**, *6*, 868.

113. Gruber, K.; Puffer, B.; Krautler, B., *Chem. Soc. Rev.*, **2011**, *40*

114. Miller, S. L. *Science*, **1953**, *117*, 528.

115. Miller, S. L., *J. Am. Chem. Soc.*, **1955**, *77*, 2351.

116. Orgel, L. E., *The origins of life: Molecules and Natural Selection,* Chapman and Hall, London, 1973 (and references therein).

117. Simionescu, C. I.; Mora, R.; Simionescu, B. C., *Bioelectr. Bioenerg.*, **1978**, *5*, 1 (and references therein).

118. Ksander, G.; Bold, G.; Lattman, R.; Lehmann, C.; Frah, T.; Xiang, Y. -B.; Inomata, K.; Buser, H. -P.; Schieber, J.; Zass, E.; Eschenmoser, A., *Helv. Chim. Acta.,* **1987**, *70*, 1115.

119. Eschenmoser, A., *Angew. Chem. Int. Ed. Engl.*, **1988***, 27*, 5.

120. Leeper, F. J., *Natural Prod. Rep.*, **1987**, *2*, 441.

121. Roessener, C. A.; Santander, P. J.; Scott, A. I., *Vitam. Horm.*, **2001**, *61*, 267.

122. Heldt, D.; Lawrence, A. D.; Lindenmeyer, M.; Deery, E.; Heathcote, P.; Rigby, S. E.; Warren, M. J., *Biochem. Soc. Trans.,* **2005***, 33*, 815.

123. Roessener, C. A.; Huang, K. X.; Warren, M. J.; Raux, E.; Scott, A. I., *Microbiology*, **2002**, *112548*, 1845.

124. Raux, E.; Schbert, H. L.; Warren, M. J., *Cell. Mol. Life Sci.*, **2000**, *57*, 13.

125. Roper, J. M.; Raux, E.; Brindley, A. A.; Schubert, H. L.; Gharbia, S. E.; Shah, H. N.; Warren, M. J.,128 *J. Biol. Chem.*, **2000**, *275*, 40316.

126. Scott, I. A., *Acc. Chem. Resear.*, **1978**, *11*, 29.

127. Scott, I. A., *Angew. Chem. Int. Ed. Engl.,* **1993**, *32*, 1223.

128. Scott, I. A., *Tetrahedron*, **1994**, *50*, 13315.

129. Scott, I. A., *Pure and Appl. Chem.*, **1996**, *68*, 2057.

130. Battersby, A. R., *Science*, **1994**, *264*, 1551.

131. Battersby, A. R.; McDonald, E.; Cornforth, J. W.; Frydman, B., *Phil. Trans. R. Soc. Lond. B.*, **1976***, 273*, 161.

132. Georgopapadakou, N. H.; Scott, A. I., *J. Theor. Biol.*, **1977**, *69*, 381 (and references therein).

133. Dolphin, D., *BioInorg. Chem.*, **1973**, *2*, 155.

134. Chemaly, S. M.; Jack, L. A.; Yellowlees, L. J.; Harper, P. L. S.; Heeg, B.; Pratt, J. M., *Dalton Trans.*, **2004**, 2125.

135. Pratt, J. M., *Pure and Appl. Chem.*, **1993**, *65*, 1513.

137. Halpern, J., *Science*, **1985**, *227*, 869.

138. Battersby, A. R.; Sheng, Z.-C., *J. Chem. Soc., Chem. Commun.,* **1982**, *24*, 1939.

139. Scheuring, E.; Padmakumar, R.; Banerjee, R.; Chance, M. R., *J. Am. Chem. Soc.*, **1997**, *119*, 12192.

140. Dong, S.; Padmakumar, R.; Banerjee, R.; Spiro, T. G., *J. Am. Chem. Soc.*, **1996**, *118*, 9182.

141. Dong, S.; Padmakumar, R.; Banerjee, R.; Spiro, T. G., *J. Am. Chem. Soc.*, **1999**, *121*, 7063.

142. Sirovatka, J. M.; Rappé, A. K.; Finke, R. G., *Inorg. Chim. Acta.*, **2000**, *545*, 300.

143. Jensen, K. P.; Ryde, U., *J. Mol. Str.*, *Theochem*, **2002**, *585*, 239.

144. Rovira, C.; Kunc. K.; Hutter, J.; Parrinello, M., *Inorg. Chem.*, **2001**, *40*, 11.

145. Jensen, K. P.; Ryde, U., *Coord. Chem. Rev.*, **2009**, *253*, 769.

146. Tsou, C. L., *Nature*, **1949**, 1134.

147. Tsou C. L., *Biochem.*, **1951**, *49*, 362.

148. Tsou C. L., *Biochem.*, **1951**, *49*, 367.

149. Tuppy, H.; Paleus, S., *Acta Chem. Scand.*, **1955**, *9*, 353.

150. Paleus, S.; Ehrenberg, A.; Tuppy, H., *Acta Chem. Scand.*, **1955**, *9*, 365.

151. Marques, H. M., *Dalton Trans.*, **2007**, 4371.

152. Adams, P. A.; Byfield, M. P.; Milton, R. C. L.; Pratt, J. M., *J. Inorg. Biochem.,* **1988**, *34*, 167.

153. Adams, P. A.; Byfield, M. P.; Goold, R. D.; Thumser, A. E., *J. Inorg. Biochem.,* **1989**, *37*, 55.

154. Adams, P. A.; Baldwin, D. A.; Marques, H. M., in Scott, R. A.; Mauk, A. G. (eds.), *Cytochrome c: A Multidisciplinary Approach*, University Science Books, Sausalito, California, 1996, pp. 635-692.

155. Baba., Y.; Mizushima, H.; Wantabe, H., *Chem. Pharm. Bull. Japan*, **1969**, *17*, 82.

156. Paleus, S.; Tuppy, H., *Acta Chem. Scand.*, **1959**, *13*, 641.

157. Wilson, M. T.; Ranson, R. J.; Masiakowski, P.; Czarnecka, E.; Brunori, M., *Eur. J. Biochem.*, **1977**, *77*, 193.

158. Melchionna, S.; Barteri, M.; Ciccotti, G., *J. Phys. Chem.*, **1996**, *100*, 19241.

159. Hunter, C. A.; Sanders, J. K. M., *J. Am. Chem. Soc.,* **1990**, *112*, 5525.

160. Kano, K.; Fukuda, K.; Wakami, H.; Nishiyabu, R.; Pasternack, R. F., *J. Am. Chem. Soc.,* **2000**, *122*, 7494.

161. Harbury, H. A.; Loach, P. A., *J. Biol. Chem.,* **1960**, *12*, 3640.

162. Harbury, H. A.; Loach, P. A., *Proc. Natl. Acad. Sci. U.S.A.*, **1959**, *45*, 1344.

163. Carraway, A. D.; McCollumn, M. G.; Peterson, J., *Inorg. Chem.,* **1996**, *35,* 6885.

164. Marques, H. M.; Perry, C. B., *J. Inorg., Biochem.,* **1999**, *75,* 281.

165. Perry, c. B.; Chick, T.; Ntlokwana, A.; Davies, G.; Marques, H. M., *J. Chem. Soc. Dalton Trans.,* **2002**, 449.

166. Peterson, J.; Silver, J.; Wilson, M. T.; Morrison, I. E. G., *J. Inorg. Biochem.*, **1980**, *13,* 75.

167. Nassif, R.; Baumgartner, C. P.; Sellers, M.; May, L.; *Z. Naturforsch.*, **1976**, *31C*, 232.

168. Baumgartner, C. P.; Sellers, M.; Nassif, R., *Eur. J. Biochem.,* **1974**, *46*, 625.

169. DerVartanian, D. V., *Biochim. Biophys. Res. Commun.,* **1970**, *41,* 932.

170. Loehr, T. M.; Loehr, J. S.; *Biochem. Biophys. Res. Commun.*, **1973**, *55*, 218.

171. Satterlee, J. D., *Inorg. Chim. Acta.*, **1983**, *79*, 195.

172. Jehanli, A. M. T.; Stotter, D. A.; Wilson, M. T., *Eur. J. Biochem.,* **1976**, *71*, 613.

173. Urry, D. W., *J. Am. Chem. Soc.*, **1967**, *89*, 4190.

174. Kimura, K.; Peterson, J.; Wilson, M.; Cookson, D. J.; Williams, R. J. P., *J. Inorg. Biochem.*, **1981**, *15*, 11.

175. Aron, J. A.; Baldwin, D. A.; Marques, H. M.; Pratt, J. M.; Adams, P. A., *J. Inorg. Biochem.*, **1986**, *27*, 227.

176. Urry, D. W.; Pettegrew, J. W., *J. Am. Chem. Soc.*, **1967**, *89*, 5276.

177. Ni, T. W.; Tezcan, F. A., *Angew. Chem. Int. Ed.,* **2010**, *49*, 7014.

178. Tuppy, H.; Bodo, G., *Monatsh.,* **1954**, *85*, 807.

179. Tuppy, H.; Bodo, G., *Monatsh.,* **1954**, *85*, 1024.

180. Peterson, J.; Saleem, M. M. M.; Silver, J.; Wilson, M. T.; Morrison, I. E. G., *J. Inorg. Biochem.*, **1983**, *19,* 165.

181. Marques, H. M.; Shongwe, M. S.; Munro, O. Q.; Egan, T. J., *S. Afr. J. Chem.,* **1997**, *50*, 166.

182. Baldwin, D. A.; Mabuya, M. B.; Marques, H. M., *S. Afr. J. Chem.*, **1987**, *40(2)*, 103.

183. Peterson, J.; Wilson, M. T., *Inorg. Chim. Acta,* **1987**, *135,* 101.

184. Kraehenbuhl, J. P.; Galardy, R. E.; Jamieson, J. D.; *J. Exptl. Med.*, **1974**, *139*, 208.

185. Slavnova, T. D.; Chibisov, A. K.; Gorner, H., *J. Phys. Chem. A*., **2005**, *109*, 4758.

186. Baldwin, D. A>; Marques, H. M.; Pratt, J. M., *J. Inorg. Biochem*., **1987**, *30,* 203.

187. Adams, P. A.; Goold, R. D., *J. Chem. Soc., Chem. Commun.*, **1990**, 97.

188. Adams, P. A., *J. Chem. Soc. Perkin Trans.*, **1990**, 1407.

189. Harbury, H. A.; Loach, P. A., *J. Biol. Chem.,* **1960**, *235*, 3646.

190. Blumenthal, D. C.; Kassner, R. J., *J. Biol. Chem.*, **1979**, *254*, 9617.

191. Huang, Y.-P.; Kassner, R. J., *J. Biol. Chem.*, **1981**, *256*, 5327.

192. Othman, S.; Le Lirzin, A.; Desbois, A., *Biochemistry*, **1993**, *32* 9781

193. Marques, H. M.; Baldwin, D. A.; Pratt, J. M., *J. Inorg. Biochem.*, **1987***, 29*, 77.

194. Smith, M. C.; McLendon, G., *J. Am. Chem. Soc.*, **1980**, *102*, 5666.

195. Wang, J. S.; van Wart, H. E.; *J. Phys. Chem.*, **1989**, *93*, 7925.

196. Yang, E. K.; Sauer, K., in H. Chien (ed.), *Electron Transport and Oxygen Utilization*, Elsevier, New York, 1982.

197. Kim, J. E.; Pribisko, M. A.; Gray, H. B.; Winkler, J. R., *Inorg. Chem.*, **2004**, *43*, 7953.

198. Munro, O. Q.; Marques, H. M., *Inorg. Chem.*, **1996**, *35*, 3752

199. Dickinson, L. C.; Chien, J. C. W., *Biochemistry*, **1975**, *14*, 3526 (and references therein).

200. Ma, J. -G.; Vanderkooi, J. M.; Zhang, J.; Jia, S. -J.; Shelnutt, J. A., *Biochemistry*, **1999**, *38*, 2787.

201. Low, D. W.; Abedin, S.; Yang, G.; Winkler; J. R., Gray, H. B., *Inorg. Chem*. **1998**, *37*, 1841.

202. Primus, J. -L; Boersma, M. G.; Mandon, D.; Boeren, S.; Veeger, C.; Weiss, R.; Rietjens, I. M.C. M., *J. Biol. Inorg. Chem.*, **1999**, *4*, 274.

203. T.P. Henning, T.G. Spring, in: WIPO (Ed.), USA, 1996.

204. T.P. Henning, T.G. Spring, Proc. Proceedings - Electrochemical Society: (New Directions in Electroanalytical Chemistry II); **1999**, *99-5*, 144.

205. Primus, J.L.; Grunenwald, S.; Hagedoorn, P.-L.; Albrecht-Gary, A.-M.; Mandon, D.; Veeger, C., *J. Am. Chem. Soc*., **2002**,*124*, 1214

206. Perry, C. B.; Ph. D. Thesis, University of the Witwatersrand, Johannesburg, South Africa, **2004** (and references therein).

207. Vashi, P. R.; Ph. D. Thesis, University of the Witwatersrand, Johannesburg, South Africa, **2004** (and references therein).

208. Sannasy, D., M.Sc. Dissertation, University of the Witwatersrand, Johannesburg, South Africa, **2005** (and references therein).

209. Knapton, L.; Ph. D. Thesis, University of the Witwatersrand, Johannesburg, South Africa, **2005** (and references therein).

210. Brown, K. L., *Chem. Rev.*, **2005**, *105*, 2075 (and references therein).

211. Lenhert, P. G., *Proc. Roy. Soc. A*, **1968**, *303*, 45.

212. Kaim, W.; Schwederski, B, *Bioinorganic Chemistry: Inorganic Elements in the Chemistry of Life*, Wiley, Chichester, 1994.

213. Krautler, B., *Helv. Chim. Acta.*, **1987**, *70*, 1268.

214. Schrauzer, G. N.; Grate, J. H., *J. Am. Chem. Soc.*, **1981**, *103*, 541.

215. Martin, B. D.; Finke, R. G., *J. Am. Chem. Soc.,* **1992**, *114,* 580.

216. Lexa, D.; Saveant, J. M., *J. Am. Chem. Soc.*, **1983**, *105, 235.*

217. Finke, R. G.; Schiraldi, D. A., *J. Am. Chem. Soc.,* **1983**, *105, 7605*.

218. Kim, S. H.; Leung, T. W., *J. Am. Chem. Soc.,* **1984**, *106,* 8317.

219. Krautler, B.; Keller, W.; Kratky, C., *J. Am. Chem. Soc.,* **1989**, *111,* 8936.

220. Marzilli, L. G.; Toscano, P. J.; Randaccio, L., *J. Am. Chem. Soc.,* **1981**, *103,* 6347.

221. Banerjee, R. (ed.), 1999. *Chemistry and Biochemistry of B_{12}*, Wiley, New York, **1999**.

222. Mazumdar, S.; Medhi, O. K.; Mitra, S., *Inorg Chem.,* **1991**, *30,* 700.

223. http://www.kent.ac.uk/news/stories/vitamin-variants-could-combat-cancer/2012
Source: University of Kent (2012, October 8). Vitamin variants could combat cancer as scientists unravel B12 secrets. *ScienceDaily*; (04-12-2012).

224. Deery, E.; Schroeder, S.; Lawrence, A. D.; Taylor, S. L.; Seyedarabi, A.; Waterman, J.; Wilson, K. S.; Brown, D.; Geeves, M. A.; Howard, M. J.; Pickersgill, R. W.; Warren, M. J., *Nature Chemical Biology*, **2012**, DOI: 10.1038/nchembio.1086

225. Fenech, M., *Mutat. Res.,* **2001**, *475(1),* 57.

226. Fenech, M., *Food Chem. Toxicol.,* **2002**, *40(8)* 1113.

227. http://www2.warwick.ac.uk/fac/med/news/news/could_vitamin_b12/
Source: Saravanan, P.; Department of Metabolic and Vascular Health; Warwick Medical School, The University of Warwick; Coventry, CV4 7AL, United Kingdom; P.Saravanan@warwick.ac.uk; (04-12-2012).

228. Refsum, H.; Smith, A. D., *J. Neurol. Neurosurg. Psychiatry*, **2003**, *74*, 959.

229. Carmel, R.; in: R. Carmel and D. W. Jacobsen (eds.), *Homocysteine in health and disease*, Cambridge University Press, Cambridge, 2001, pp. 289.

230. Smith, A. D., *Am. J. Clin. Nutr.,* **2002**, *75*, 785.

231. Andries, E.; Vogel, T.; Federici, L.; Zimmer, J.; Ciobanu, E.; Kaltenbach, G., *Curr. Geron. And Ger. Research.,***2008**, 1.

232. http://www.bbc.co.uk/news/health-11232356
Source: Hughes, J.; Health Correspondent; BBC News, United Kingdom; Associated specialist: Smith, A. D.; info@pharm.ox.ac.uk; (04-12-2012).

233. Ravikumar, K. A.; Parameswara, A K., *Advances in Natural Science*, **2012**, *5*, 81.

224. Hall, A. H.; Rumack, B. H., *Am. J. Emer. Med.*, **1987**, *5*, 115.

225. Borron, S. W.; Baud, F. J.; Me'garbane, B.; Bismuth, C., *Am. J. Emer. Med.*, **2007**, *25*, 551.

226. Lin, M.; Marzilli, L. G., *Inorg. Chem.,* **1994**, *33*, 5309.

227. Herrmann, O; Mehdi, S. H.; Corsini, A., *Can. J. Chem.,* **1978**, *56*, 1048.

228. Abwao-Konya, J.; Cappelli, A.; Jacobs, L.; Krishnamurthy, M.; Smith, M., *Transition Met. Chem.*, **1984**, *9*, 270.

229. Ehrenberg, A.; Theorell, H., *Acta Chem. Scand.*, **1955**, *9*, 1193.

230. Williams, R. J. P., *J. Mol. Catal.*, **1985**, *30*, 1.

231. Veeger, C., *J. Inorg. Biochem.*, **2002**, *91*, 35.

232. Ryabova, E. S.; Nordlander, E., *Dalton Trans.,* **2005**, 1228.

CHAPTER 2

MATERIALS AND METHODS

2.1 INTRODUCTION

Physical studies of biological systems aim at revealing the exact molecular basis for their function. Due to the complexity surrounding biological systems, it is often useful to examine the molecular behaviour of simpler, relevant model systems. One such biological system in which model design has found wide application is the study of vitamin B_{12a} solution chemistry.[1] Many B_{12a} model systems are based on the use of a conventional chemical species to mimic only the active sites of native proteins.[2] These octahedral organometallic Co(III) models include cobaloximes, Schiff base complexes and simple metalloporphyrins.[2] Few efforts utilise protein fragments as integral parts of model systems.

Described here is the synthesis and solution chemistry of the trivalent cobalt-substituted microperoxidase, NAcCoMP8, a simple biologically-derived vitamin B_{12a} model based on the heme-containing protein fragment of cytochrome *c*. NAcCoMP8 resembles the B_{12a} active site in terms of the axial ligands coordinated to Co(III). However, NAcCoMP8 also offers the unique opportunity for probing the *cis* effect of the equatorial ligand. It achieves this by being a compound in which the coordination environment of Co(III) realistically mimics that of B_{12a} but in which the equatorial corrin ligand has been replaced by porphyrin. The consequences of that change – which ultimately addresses the effect of the corrin ligand on the behaviour of Co(III) – is the central focus of this study.

The synthesis of NAcCoMP8 was performed as previously described.[3] The synthesis was however, re-evaluated and modified to reduce aggregation, a significant obstacle in this work. Once the monomeric NAcCoMP8 was

successfully isolated, the foray into its solution chemistry commenced. This included an examination of its Beer's Law behaviour and determination of the pK_as of the complex before exploring the temperature-dependent thermodynamics and kinetics of ligand substitution reactions, in which axial H_2O water was replaced with a range of exogenous ligands. These were then compared to analogous data obtained (or available) for vitamin B_{12a}.

2.2 QUALITATIVE ASSESSMENT OF AGGREGATION EFFECTS IN THE SOLUTION CHEMISTRY OF NAcCoMP8

The strategy employed in this research project was as follows (**Figure 2.1**):

Investigation 1

The qualitative identification and assessment of aggregation effects in NAcCoMP8 was investigated. This study was approached as two separate investigations:

Investigation 1.1

Firstly, the optimisation of the synthesis, isolation and characterisation of NAcCoMP8 was investigated. Preliminary optimisations included the utilisation of cost-effective options such as synthetic trivalent cobalt-substituted porphyrins.

Investigation 1.2

Secondly, the qualitative assessment of NAcCoMP8's behaviour in solution was investigated. Preliminary studies included procedures for the preparation of monomeric NAcCoMP8.

Investigation 2

A quantitative assessment of the *cis* effect of the equatorial ligand on the properties of Co(III) metal ion was undertaken by comparing the ligand binding properties of Co(III) in NAcCoMP8 and in vitamin B_{12a}. This study was approached as two separate investigations in which the axial H_2O ligand was substituted by a variety of exogenous ligands:

Investigation 2.1

The temperature-dependence of the thermodynamics of ligand substitution reactions.

Investigation 2.2

The temperature-dependence of the kinetics of ligand substitution reactions.

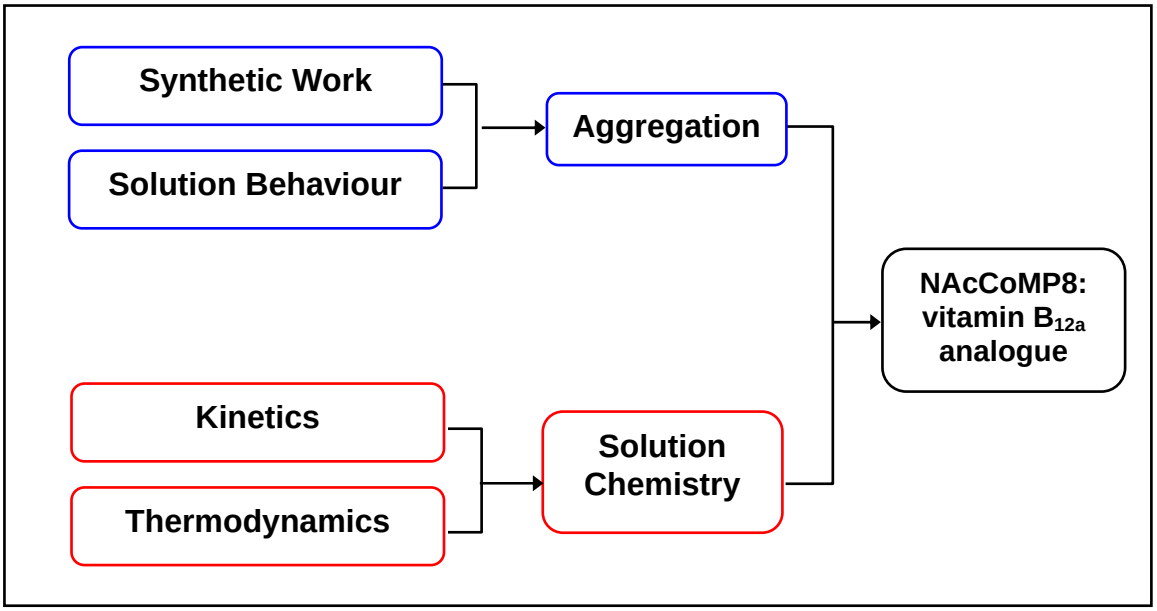


Figure 2.1 Flow diagram of the different investigations undertaken in this work. The blue pathway reflects methods pertaining to the monomerisation of NAcCoMP8 whilst the red pathway reflects the study of the solution chemistry of NAcCoMP8.

2.2.1 Synthesis of NAcCoMP8

The overall synthetic procedure of NAcCoMP8 was conducted as described by Sannasy[3] with modifications. Modifications were explored in order to improve the modest and aggregation-dependent yields.

The original synthesis was elegantly straightforward. It was initiated by the step-wise proteolytic digestion of cytochrome *c* to yield firstly FeMP11 and then on further digestion, FeMP8.[4-6] FeMP8 was then reductively demetalated to afford MP8. This iron-free microperoxidase was subsequently converted into CoMP8 using a cheap cobalt salt. Finally, CoMP8 was acetylated using glacial acetic acid in order to yield NAcCoMP8. In practise, the demetalation and acetylation steps were associated with poor yields and were thus the area of focus of the modifications introduced during this investigation.

The original synthetic procedure could be modified in four viable ways in order to arrive at NAcCoMP8: Routes A, B, C and D (**Figure 2.2**). Routes found to be unviable are not reported here; examples include routes where acetylation was applied directly to the metal-free porphyrin but the porphyrin did not survive the acetylation process. For the sake of brevity, the highest yielding Route C only is reported in detail; the rest may be found in **Appendix 2.1**. The metal ion coordinated to the porphyrin is assumed to be in the trivalent state unless otherwise stated. The term MPX refers to a metal-free microperoxidase where X = 8 or 11. Sources of reagents (**Section 2.4**), technical specifications (**Section 2.4**), specialized (**Sections 2.2.2; 2.2.3**) and general techniques (**Section 2.5**) may found elsewhere

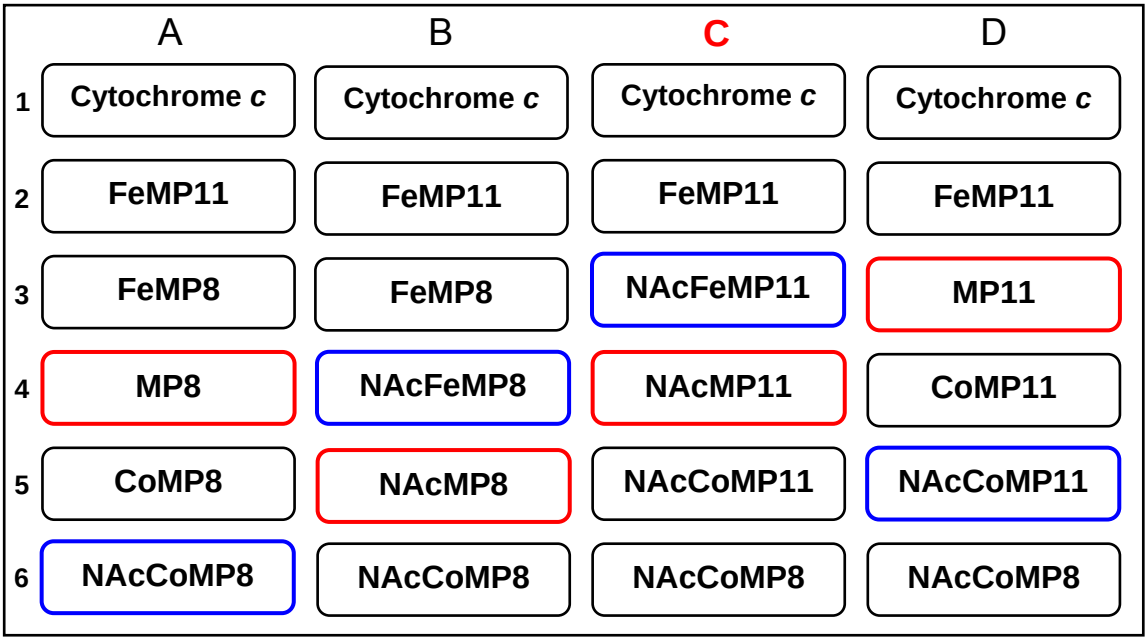


Figure 2.2 The four synthetic routes to attain monomeric NAcCoMP8 explored in this work. Red cells indicate the metal-free porphyrin step. Blue cells indicate primary acetylation step. Route A was used by Sannasy[3]. Routes B, C and D were alternatives explored in this work.

2.2.1.1 Synthesis of FeMP11 from cytochrome *c*

The synthesis of FeMP11 was carried out according to the procedures initially developed by Tsou,[5,6] by Harbury and Loach,[4] and Wilson *et al.*[11] The modifications applied were based on the reports of Adams *et al.*[7,8] and of Munro and Marques[14].

Ferric horse heart cytochrome *c* (300 mg) was treated with pepsin (15 mg; activity: 3200 units mg^{-1}) in 0.1 M phosphate buffer (20 mL) at pH 2.0 in a thermostatted cell at 35 ^{o}C. Care was taken to stir gently to avoid the formation of a stable foam which would alter the overall pepsin concentration in solution. The reaction mixture was incubated for 1 hour, after which a further 15 mg of pepsin was added to counteract the pepsin inhibitor reportedly present in cytochrome *c*[13]. The pH was adjusted to 2.0 at 35 ^{o}C using concentrated phosphoric acid and the solution was incubated for another 3 hours. The reaction was monitored using TLC (3:5:1 MeOH: $CHCl_3$: conc. NH_4OH – 0.2 mm silica gel plates – **Appendix 2.2**).

After 3 hours the reaction vessel was submerged in boiling water for 5 minutes; the pH was then raised to 7.0 at 25 ^{o}C with concentrated NH_4OH, to destroy peptic activity. It was previously demonstrated that increasing ionic strength favours aggregation in microperoxidases[14] and related compounds[22]. The salting-out step was thus circumvented by using column chromatography instead. The bright-red solution was purified by gel permeation chromatography (Sephadex G50, 3.0 cm x 40 cm) eluted with NH_4HCO_3 (0.1 M) at a rate of 10 mL h^{-1}. Two distinctive bands were observed. The first major band off the column was primarily FeMP11. The second minor band off the column was primarily FeMP9. The samples were collected in 0.5 mL fractions with an autosampler and those with >95% purity by high performance liquid chromatography (HPLC) were pooled (**Section 2.2.3.2**; **Appendix 2.2**).

The fractions containing the FeMP11 band, as identified by mass spectroscopy, were loaded onto a Sep-Pak® cartridge for desalting and concentrating. The concentrated FeMP11 solution was then clarified using a Millex® syringe-filter and lyophilized at neutral pH to yield a bright-red spongy solid. The sample was then routinely stored at -20 ^{o}C under argon. Concentration was determined spectroscopically using ε_{395nm} = 1.76 x 10^5 M^{-1} cm^{-1}.[11]

2.2.1.2 Synthesis of NAcFeMP11 by the acetylation of FeMP11

The acetylation procedure was adapted from work done by Munro and Marques[14] for the synthesis of NAcFeMP8. The isolation steps were adapted and modified from work of Carraway *et al*.[9] and Kadnikova and Kostic[12].

FeMP11 (~ 20 mg) was dissolved in 10 mL saturated sodium acetate solution in a thermostatted cell at 5 ^{o}C. A 500 molar excess of acetic anhydride was used to acetylate FeMP11; this was added in 5 aliquots at 10-minute intervals. The evolution of acetic acid *in situ* turned the solution brown-red which was consistent with iron microperoxidase at low pH in this project (**Appendix 2.2**). The reaction mixture was stirred at 5 ^{o}C overnight and then lyophilised. The lyophilised NAcFeMP11 was redissolved in sodium carbonate buffer (2 mL;

0.2M; pH 9.5) and the scarlet compound was desalted on a Sep-Pak® cartridge. Neutral NAcFeMP11 was clarified using a Millex® syringe-filter before being lyophilised. The red-brown product was routinely stored at -20 ^{o}C under argon. The reaction was monitored by TLC (**Section 2.2.1.1**) and HPLC (**Section 2.2.3.2**). NAcFeMP11 was identified by mass spectroscopy. Concentration was determined spectroscopicaly using ε_{397}= 1.48 x 10^5 M^{-1} cm^{-1}.[25]

2.2.1.3 Synthesis of NAcMP11 by the reductive demetalation of NAcFeMP11

The demetalation procedure was adapted from Sannasy[3] and Primus *et al.*[15]. Care was taken to avoid exposure to light and air. The metal-free compound has a tendency to decompose.[3] Thus, once the metal ion was removed, care was taken to complete the subsequent steps in the shortest possible time.

Oven-dried Schlenk apparatus was connected to a high-vacuum line and flooded with argon (**Figure 2.3**). The following reactants were added to the reaction vessel under a blanket of argon: NAcFeMP11 (10.00 mg, 6.64 μmol); 10.00 mL glacial acetic acid; 166 μL concentrated HCl. The brown-red reaction mixture was then frozen under argon using liquid nitrogen. After ensuring that the reactants were thoroughly frozen, the reagents were degassed by three freeze-thaw cycles under vacuum, purging with argon between cycles. After the final freeze-thaw cycle the reaction vessel was covered with aluminum foil to prevent light-exposure. The system was opened briefly under argon to add iron(II)chloride (10.00 mg, 80.16 μmol, 12.07 equiv.) to the reaction mixture and the system was immediately sealed. The reaction was allowed to stir with a magnetic stirrer for about 1 hour at room temperature, resulting in a change of colour from an opaque brown-red solution to a clear bright-purple solution. The reaction was monitored by UV-Vis spectroscopy.

The purification steps were conducted in a dark room. The reaction mixture was diluted by adding deionised water (~ 50 mL) to the Schlenk tube. The sample was immediately loaded onto a Sep-Pak® cartridge for desalting and removal of acids. The neutral purple NAcMP11 solution was then clarified using a syringe-

filter before being frozen with liquid nitrogen and lyophilized in the dark. The light purple spongy solid was stored briefly at -20 ^{o}C under argon before the remetalation step.

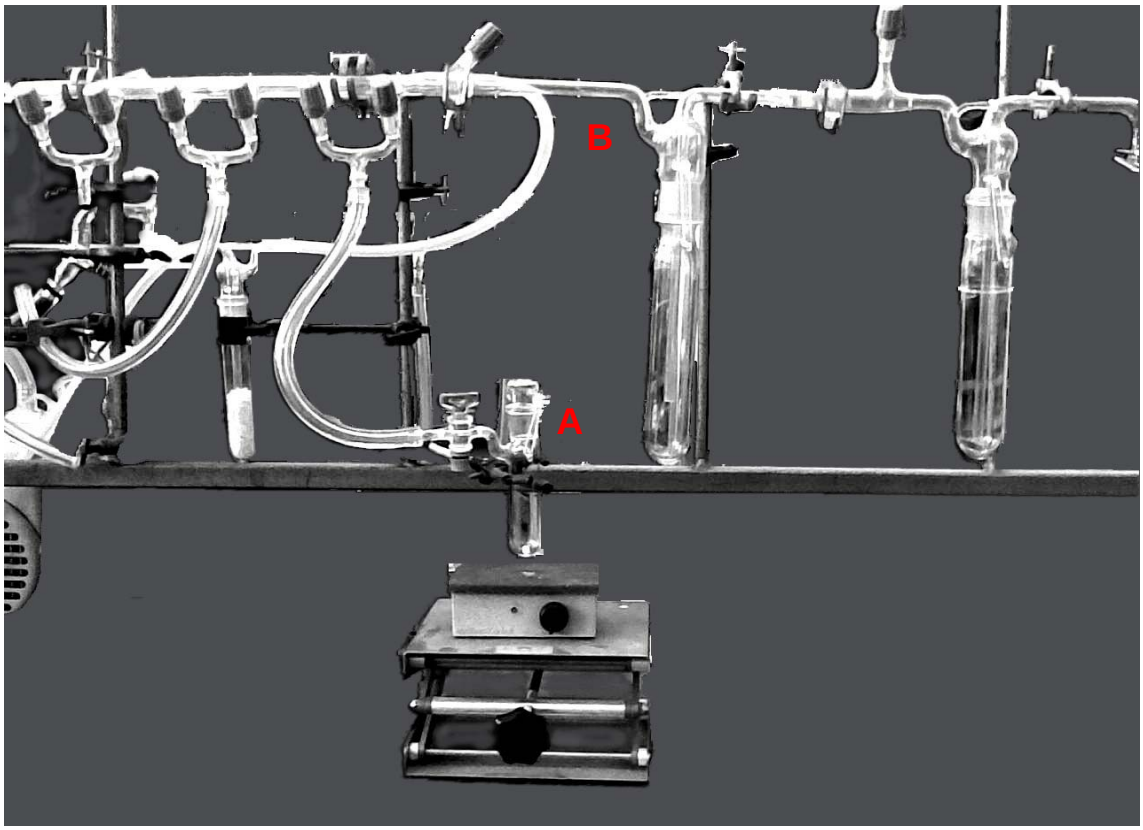


Figure 2.3 Photograph showing the typical reduced pressure/inert atmosphere demetalation set-up. (**A**) Schlenk apparatus usually light-protected using foil attaches to the (**B**) high vacuum line coupled to an argon line..

2.2.1.4 Synthesis of NAcCoMP11 by the oxidative remetalation of NAcMP11

The metalation procedure was adopted from Primus *et al.,*[15] Lin and Marzilli[23] and from Ashley and Au-Young[24] for the syntheses of MnMP8, CoTMPyP and CoTPPS, respectively.

The demetalated NAcMP11 (10 mg) was dissolved in deionised H_2O (5 mL) in a light-protected flask. The pH was adjusted to 8 using concentrated NaOH and the solution was set to reflux. A 100-fold excess of clarified cobaltous acetate dissolved in a minimum volume of MeOH was added to the flask and allowed to stir under reflux (2 hr). The reaction was monitored using UV-Vis spectroscopy.

After the refluxing process the sample could be exposed to white light. NAcCoMP11 was purified and concentrated using a Sep-Pak® cartridge. The purity was assessed using HPLC. The neutral dark-pink NAcCoMP11 solution was clarified using a Millex® syringe-filter and then lyophilized. The pink spongy NAcCoMP11 was routinely stored under argon at -20 ^{o}C and protected from unnecessary light.

2.2.1.5 Synthesis of NAcCoMP8 by the tryptic digestion of NAcCoMP11

NAcCoMP11 (20 mg) was incubated with trypsin (30 mg; activity: 12700 units mg^{-1}) in 0.1 M phosphate buffer (20 mL) at pH 8.5 at 35 ^{o}C in a thermostatted cell for 8 hours under gentle stirring. The reaction was monitored using TLC as reported previously (**Section 2.2.1.1**).

NAcCoMP8 was then precipitated by lowering the pH to 3.5 with dilute H_3PO_4. Solid $(NH_4)_2SO_4$ was added to NAcCoMP8 on ice until saturated. Then a saturated $(NH_4)_2SO_4$ solution was added (*ca*. 15 drops) and the reaction mixture was centrifuged for 45 min at 7000-8000 rpm. If the supernatant was still coloured, the salting-out step was repeated on the said supernatant until colourless. The colourless supernatant was decanted and the NAcCoMP8 pellet was dissolved in 5 mL of deionised water. The pH was readjusted to 7.00 with NaOH and desalted using a Sep-Pak® cartridge. The NAcCoMP8 solution was clarified using a Millex® syringe-filter and then lyophilized. NAcCoMP8 was identified by mass spectrometry (**Section 2.2.3.3**). The dark pink spongy NAcCoMP8 was routinely stored under argon at -20 ^{o}C and protected from unnecessary light. Concentration was determined spectroscopically using[3] ε_{415} = 1.61 x 10^5 M^{-1} cm^{-1}.

This was the final step of a multi-step synthesis. With no further steps pending, brevity allowed for the utilisation of the salting out procedure despite the temporarily increased ionic strength. The final step was also typically carried out on a smaller scale relative to previous steps thus, the salting out procedure was favoured in order to maximize yields on this scale

2.2.2 Isolation of NAcCoMP8

NAcCoMP8 and related products aggregate in solution at high concentrations, pH and ionic strength. It is therefore imperative that the purification steps were performed quickly, at neutral pH where possible and in low salt concentrations. The utilisation of salts and buffers that were easier to remove were also favoured *e.g.* $(NH_4)_2CO_3$ which could be removed by lyophilisation as ammonia and carbon dioxide. Refer to previous sections for materials (**Section 2.4.1**; **2.4.2**).

2.2.2.1 Sep-Pak® cartridges and Millex® filters

The use of Waters Sep-Pak® C18 reverse-phase cartridges (500 mg or 10 g, depending on the quantity of product to be purified) proved to be useful in this regard (**Figure 2.4**). Sep-Pak® cartridges are prepacked plugs containing a silica-based bonded phase with strong hydrophobicity (C18 resin) used to adsorb analytes from aqueous solutions. The products appeared to be immobilized on the C18 resin thereby limiting aggregation during the rapid desalting process.

The utilization of Sep-Pak® cartridges was a five-step process. Firstly, activation was achieved by passing one cartridge-volume of a mobile phase through slowly (50% CH_3CN, HPLC grade). Secondly, equilibration was achieved by passing five cartridge-volumes of the washing-solution through (deionised water). Thirdly, the sample was loaded slowly using 1 mL aliquots to prevent leaching and to anticipate overloading. The best loading occurred when the samples were slightly diluted. Next, the sample was washed exhaustively with deionised water. Washings were tested spectroscopically for sample-leakage and salt (**Appendix 2.2**). Washings were also tested with silver nitrate solution to detect the presence of salt through precipitation (white for chloride; yellow for phosphates and sulfates). Lastly, the sample was eluted using the mobile phase mentioned above.

Prolonged acetonitrile usage at high concentrations has a tendency to degrade

the cartridge and the samples eluted appeared murky, probably because of loss of the C18 from the silica support. Samples were clarified using Millex® syringe-filters (0.45 µm) before lyophilisation (**Figure 2.4**)

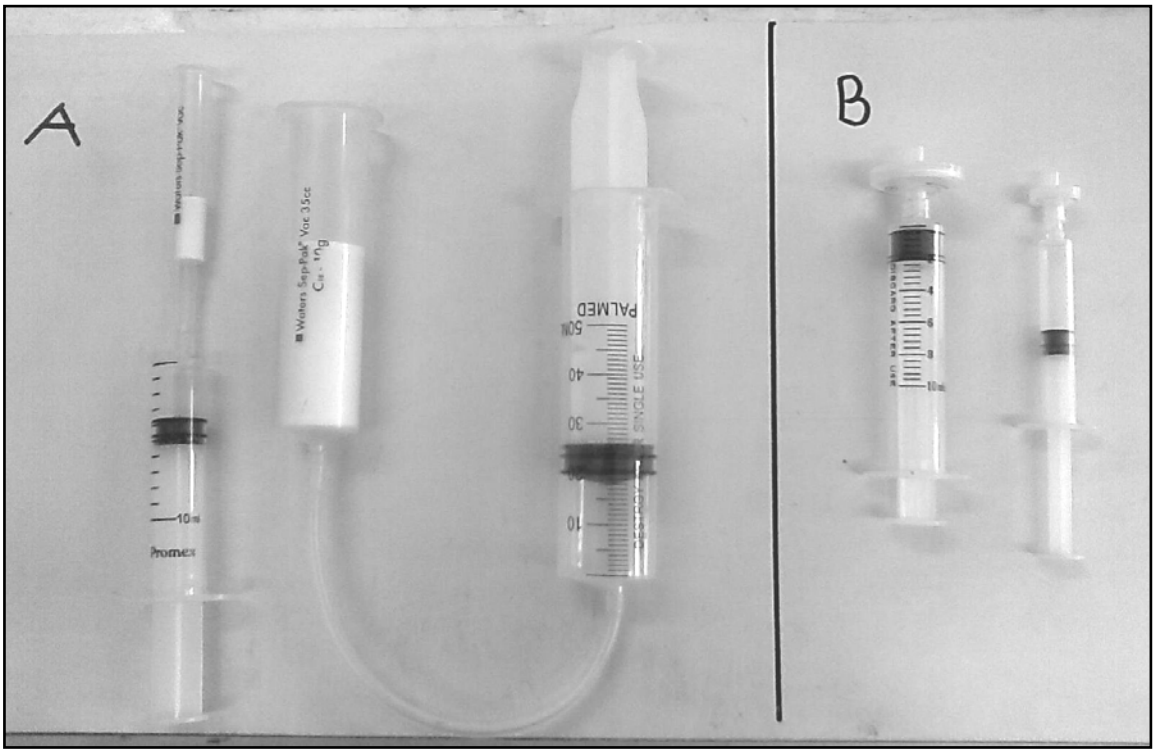


Figure 2.4 Photograph showing two purification systems adapted for microperoxidase isolation. (**A**) Sep-Pak® and (**B**) Millex® set-up for NAcCoMP8 work.

2.2.2.2 Gel permeation chromatography

Proteolytic digestion of cytochrome *c* yields microperoxidases of different sizes.[5,6] Gel permeation chromatography separates molecules on the basis of their size. The smaller molecules enter pores (with specified size) in the solid phase, while the larger molecules travel in the mobile phase and are eluted first. Thus, gel permeation chromatography is a useful way to purify cytochrome *c* digestion products.

The optimal utilization of gel chromatography was achieved in four-steps. Firstly, the appropriate resin for the separation of microperoxidases and impurities was selected. Sephadex G50 was used in a 3 x 40 cm column (Pharmacia Fine Chemicals) allowing small molecules (between 1 500-30 000

Da) to pass through the pores in the solid phase and the larger molecules (> 30 000 Da) to travel in the mobile phase. This allowed for the efficient separation of salts, amino acids (with or without heme) and the various microperoxidases. Secondly, the resin was packed as a slurry using degassed and ultra-filtrated $(NH_4)_2CO_3$ (0.1 M) as the solvent. Care was taken to handle the resin gently so as not to damage the beads as this was shown to lead to false band-separation/merging as well as lengthening of elution times. Damaged beads were removed by "de-fining"; the gel was stirred with a glass rod until the finer (damaged) particles surfaced. These particles were then decanted and the remaining beads were used in the column. Thirdly, equilibration was achieved by passing the solvent through the column at a flow rate of 10 mL h^{-1} over 24 hours. Lastly, the sample was then loaded carefully using a Pasteur pipette and eluted using said solvent. A Watson-Marlow 101U peristaltic pump was used for elution and the fractions were collected using an ISCO 1850 fraction collector

2.2.3 Characterisation of NAcCoMP8

NAcCoMP8's propensity towards aggregation tends to complicate characterization, particularly if sample preparations require high concentrations, pH and ionic strength. Thus characterization methods need to be quick and simple to execute at low concentrations (< 30 μM). Methods used to characterize NAcCoMP8 were UV-vis spectroscopy; HPLC; mass spectroscopy and Inductively Coupled Plasma-Optical Emission Spectroscopy-(ICP-OES). Sources of reagents, technical specifications and specialized methods may be found in sections 2.4.1 (**Table 2.3**), 2.4.2 (**Table 2.4**) and 2.2.2, respectively.

2.2.3.1 UV-Vis spectroscopy

All UV-vis spectra were recorded on Cary spectrophotometers, using quartz cuvettes (Helma, matched sets #284) with a path length of 1.0 cm. Temperature was maintained using a thermostatted cell-holder with a built-in stirrer attached to a Peltier unit. The instruments were allowed to warm up for approximately one-hour prior to use to ensure optimum performance. Samples to be analysed

were degassed and clarified using a Millex® syringe-filter. Depending on the experiment, all samples were run using either Scan® or Kinetics® onboard Cary software. Samples were run against a background applicable to that experimental system (i.e. against the appropriate buffer(s) and ionic strength adjuster). Full spectra were recorded between 300 – 700 nm where possible. These spectra were imported as *.csv files so that they could be opened in Microsoft Excel® spreadsheets and analysed statistically using SigmaPlot® or CurveFit (see later, **Table 2.4**).

Low temperature spectroscopic studies were problematic due to ambient moisture condensing along the cuvette walls as well as on the inner walls of the spectrophotometer chamber. The system had to be best optimized to reduce moisture without allowing additional light into the spectrophotometer chamber. Very thin (5 mm) high quality silicon tubing was used to lead argon into the spectrophotometer chamber from the top of the spectrophotometer whilst nitrogen was used to flood the chamber from below. Drying the chamber air with a heat gun reduced ambient moisture. The floor of the chamber was covered with a calcium chloride 'blanket' (calcium chloride embedded into cotton wool) to absorb any further ambient moisture. The cuvette was wiped dry externally, fitted with a septum and very carefully flooded with argon internally until just before use. The outer cover of the spectrophotometer was covered with a piece of black material to reduce any stray light.

2.2.3.2 HPLC

The assessment of purity of the products was important in instances were co-elutions were suspected (e.g. cytochrome *c* and FeMP9 tend to co-elute[21]). HPLC was useful in this assessment.

All HPLC separations were performed initially with a Spectra-Physics SP8800 ternary gradient pump, a Linear UV-Vis 200 detector (set at 410 nm), and a Varian 4290 integrator. Separations were later performed on a Dionex reverse-phase system using the onboard Chromeleon© software package for analysis.

Phenomenex analytical columns were used (5 µ; 150 X 4.6 mm C18 reverse-phase) coupled to a guard column (4 x 3.0 mm; C18).

All solutions were freshly prepared and filtered (0.45 µm) under vacuum before use. All solvents were HPLC grade. Phosphate buffer was freshly prepared (50 mM; *ca*. pH 7). NaCN (1 mM dissolved in the phosphate buffer) was used as a strongly coordinating ligand in order to monomerize the products being separated. Samples were allowed to reach equilibrium by stirring at room temperature for about an hour. Where possible, samples were prepared in degassed phosphate buffer, and clarified using a Millex® syringe-filter.

The HPLC column was flushed with deionised water for 10 minutes then with phosphate/acetonitrile (98%) for one-hour. A Hamilton gastight HPLC syringe was used to inject 20 µl samples onto the column using a Rheodyne valve and eluted by a linear gradient elution (**Table 2.1**). Blanks (deionised water) were run between samples. The column was flushed with phosphate/acetonitrile (75%) and then water after every five runs (or when necessary) (**Appendix 2.2**).

Table 2.1 Linear gradient HPLC (RP) elution program used for microperoxidases

Time (min)	% Phosphate	% Acetonitrile	Flow Rate (mL min^{-1})
0	98	2	2
2	98	2	2
4	75	25	2
6	65	35	2
8	65	35	2
10	75	25	2
12	98	2	2
18	98	2	2

2.2.3.3 Mass spectrometry

NAcCoMP8 and related products were identified by mass using mass spectrometry. Samples were run on a Thermo® LXQ MS using an ESI source in both positive and negative modes. Where liquid chromatography mass spectrometry (LCMS) analysis was used, the column specifications were the same as that of the HPLC column (**Section 2.2.3.2**). Thermo® standards were used for calibrating the LXQ for high molecular masses. Samples were prepared fresh in methanol (HPLC grade) and clarified using Millex® syringe-filters before running. Samples were typically allowed to stir at room temperature for about 1 hour to reach equilibrium. The LXQ method typically used is shown in (**Table 2.2**).

Table 2.2 A typical ESI-MS LXQ method used for microperoxidases

LXQ Parameter	Setting
Polarity	Positive mode
Ionisation	LC/ESI-MS
Regulation	Field
Resolution	1000
Scan Rate	Continuous scan
Start Mass	2000
End Mass	100
Elution Method	Isocratic
Sample Injection	50 µL

2.2.3.4 ICP-OES analysis

Inductively Coupled Plasma-Optical Emission Spectroscopy-(ICP-OES) was used to determine the extinction coefficient of NAcCoMP8. It was assumed that

the amount of cobalt detected was proportional to the concentration of NAcCoMP8 once a blank correction was taken into account. NAcCoMP8 was accurately weighed out using a six figure Sartorius CP2P balance and transferred quantitatively into a 25 mL A grade volumetric flask kept at 25.0 °C, which was then filled to the mark with distilled water. A set of calibration standards was prepared using a 10 ppm Spectro-multi-element stock solution. The calibrating solutions were sprayed into the plasma and standard curves were obtained (Spectro-Ciros ICP-OES instrument). The samples were then sprayed into plasma and the average concentration of cobalt was determined using data from calibration standards and appropriate dilution factors.

Investigation 1.2: Solution Behaviour of NAcCoMP8

The preparation of a spectroscopically stable monomeric solution of NAcCoMP8 was found to be affected by various factors. These factors included susceptibility to aggregation and degradation. Aggregation was found to be affected by conditions such as increasing ionic strength, high concentration, choice of buffers/dispersal agents and extreme temperature (*ca*. 5-10 ^{o}C and 35-45 ^{o}C). Degradation was found to be affected by exposure to light and air. It was thus necessary to qualitatively investigate the solution behaviour of NAcCoMP8 in relation to these conditions in order to prepare solutions containing a stable monomer. These experiments also defined the limits (pH, ionic strength, concentration etc.) within which further NAcCoMP8 solution chemistry studies could be designed. For brevity, sources of reagents (**Section 2.4**), technical specifications (**Section 2.4**), specialized (**Sections 2.2.2; 2.2.3**) and general techniques (**Section 2.5**) may found elsewhere.

2.2.4 Effects of Time (equilibrium observations)

The absorbance spectrum of a freshly prepared sample of NAcCoMP8 in deionised water was observed to increase over time (hyperchromism) before spectroscopic stability was achieved. Stability is critical for the reproducibility of

subsequent quantitative spectroscopic data. It was thus necessary to determine how long it was required to stir a freshly prepared sample of NAcCoMP8 in order to reach equilibrium.

A stock solution of NAcCoMP8 (*ca*. 1.25 μM; pH 7) was freshly prepared in degassed deionised water. A 2 mL sample was transferred into an argon-filled 1.0 cm pathlength cuvette fitted with a septum. An initial spectrum was recorded between 300 – 700 nm. Thereafter a spectrum was recorded ever 5 minutes for an hour. The sample was protected with aluminum foil between recordings.

2.2.5 Effects of Light

NAcCoMP8 was observed to degrade when exposed to light. The degradation was observed as a systematic decrease in absorbance of the Soret band (hypochromism). It thus became necessary to spectroscopically monitor the effect of light exposure to a sample of NAcCoMP8 as a function of time.

A stock solution of NAcCoMP8 (*ca*. 1.25 μM; pH 7) was freshly prepared in degassed deionised water. A 2 mL sample was transferred into an argon-filled 1.0 cm pathlength cuvette fitted with a septum. An initial spectrum was recorded between 300 – 700 nm. This sample was then systematically exposed to ambient light over a period of 3 days and the absorbance of the Soret band (415 nm) was recorded at various intervals as a function of time.

2.2.6 Effects of Air (oxygen sensitivity)

NAcCoMP8 was observed to degrade when exposed to air (oxygen). The degradation was observed as a systematic decrease in absorbance in the Soret band (hypochromism). It thus became necessary to spectroscopically monitor the effect of air exposure to a known sample of NAcCoMP8 as a function of time

A stock solution of NAcCoMP8 (*ca*. 1.25 μM; pH 7) was freshly prepared in

degassed deionised water. A 2 mL sample was transferred into an argon-filled 1.0 cm pathlength cuvette fitted with a septum. An initial spectrum was recorded between 300 – 700 nm. A gentle stream of O_2 was allowed to bubble into the sample whilst stirring. Absorbance was recorded at Soret band (415 nm) every 5 minutes for 60 minutes. Sample was protected with aluminum foil between readings.

2.2.7 Effects of Ionic Strength

Ionic strength has previously been associated with aggregation in some microperoxidases[14]. It was thus necessary to find ionic strength limits between which monomeric NAcCoMP8 is stable.

These ionic strength limits were determined spectroscopically by the addition of aliquots (between 10 – 100 uL) of a degassed stock solution of $NaClO_4$ (5 M) to a solution of degassed NAcCoMP8 (*ca*. 1.25 μM; pH 7; 1.5 mL) contained in an argon-filled 1.0 cm pathlength cuvette fitted with a septum. After each addition of $NaClO_4$ the sample was gently stirred and allowed to reach equilibrium for 1 minute. An absorbance spectrum was then recorded between 300 – 700 nm using $NaClO_4$ in deionised water as the reference solution. All absorbance readings were corrected for dilution. Total ionic strength was determined (**Equation 2.1**).

$$\mu = \frac{1}{2}\sum c_i z_i^{\,2} \qquad \textbf{Equation 2.1}$$

where μ is total ionic strength of a solution; c_i is the molar concentration of the i^{th} ion ($mol.dm^{-3}$); and z_i is the charge number of that ion, with the sum taken over all ions in the solution

2.2.8 Effects of Concentration (Beer's law investigation)

A concentrated stock solution of NAcCoMP8 (*ca*. 20 μM) was prepared in deionised water. Aliquots (*ca*. 2 - 100 μL) were added successively to a known volume of deionised water in a 1.0 cm pathlength cuvette. After each addition of

NAcCoMP8 the full absorbance spectrum was recorded using a Cary 300 Bio UV-vis spectrophotometer at 25 ^{o}C. After the absorbance reached 2.0 a.u., 200 µl of the final 1.0 cm pathlength curvette mixture was transferred to a 0.1 cm pathlength curvette. Similarly, small increments of stock NAcCoMP8 solution were added to the 0.1 cm pathlength curvette. The absorbance was recorded as before. The data were corrected for dilution and a Beer-Lambert plot of NAcCoMP8 in deionised water was plotted according (**Equation 2.2**)

$$A_{\lambda} = \varepsilon c l \qquad \textbf{Equation 2.2}$$

where A_{λ} is absorbance at some monitoring wavelength λ, ε is the absorbtivity at λ ($M^{-1}.cm^{-1}$), c is the concentration (M) and l is the pathlength (cm).

2.2.9 Effects of pH (pK_a investigation)

The titration procedure for the determination of spectroscopic pK_as of NAcCoMP8 was adopted from Sannasy[3]. Spectroscopic pK_as were determined using a well-insulated continuous flow cell system set up in a thermally-controlled environment as indicated in (**Figure 2.5**). The study was conducted as a function of temperature (10 - 35 ^{o}C) at constant ionic strength (0.1M by $NaNO_3$) by titrating with negligible volumes of either concentrated acid (sulfuric; between pH 1.0-6.5) or base (NaOH; 8 M; between pH 5.5-14).

The pH of NAcCoMP8 (40 mL; 8.01 µM) in a multi-component buffer (**Section 2.5.2**) was adjusted with either acid or base using a drawn out capillary tube and the pH measurements were recorded. After each pH adjustment, the system was allowed to circulate and thermo-equilibrate before a full spectrum (300 – 700 nm) was recorded using a Cary 3E UV-vis spectrophotometer. In this way, a full speciation profile was obtained for NAcCoMP8 at 25 ^{o}C.

Spectroscopic pK_a experiments with NAcCoMP8 were time-consuming. Lengthy experimental times exacerbated the aggregation of NAcCoMP8, particularly at higher temperatures. Thus, the system needed to be re-designed in such a way

as to minimize the experimental time at these temperatures. This was achieved by decreasing the monitored pH and spectroscopic ranges, respectively, since only the pK_a for the aqua/hydroyl species was of primary interest. Thus, subsequent pK_a studies were conducted over shorter wavelength (*ca*. 360 – 450 nm) and pH ranges (*ca*. pH 5-10) in order to reduce the total experimental time.

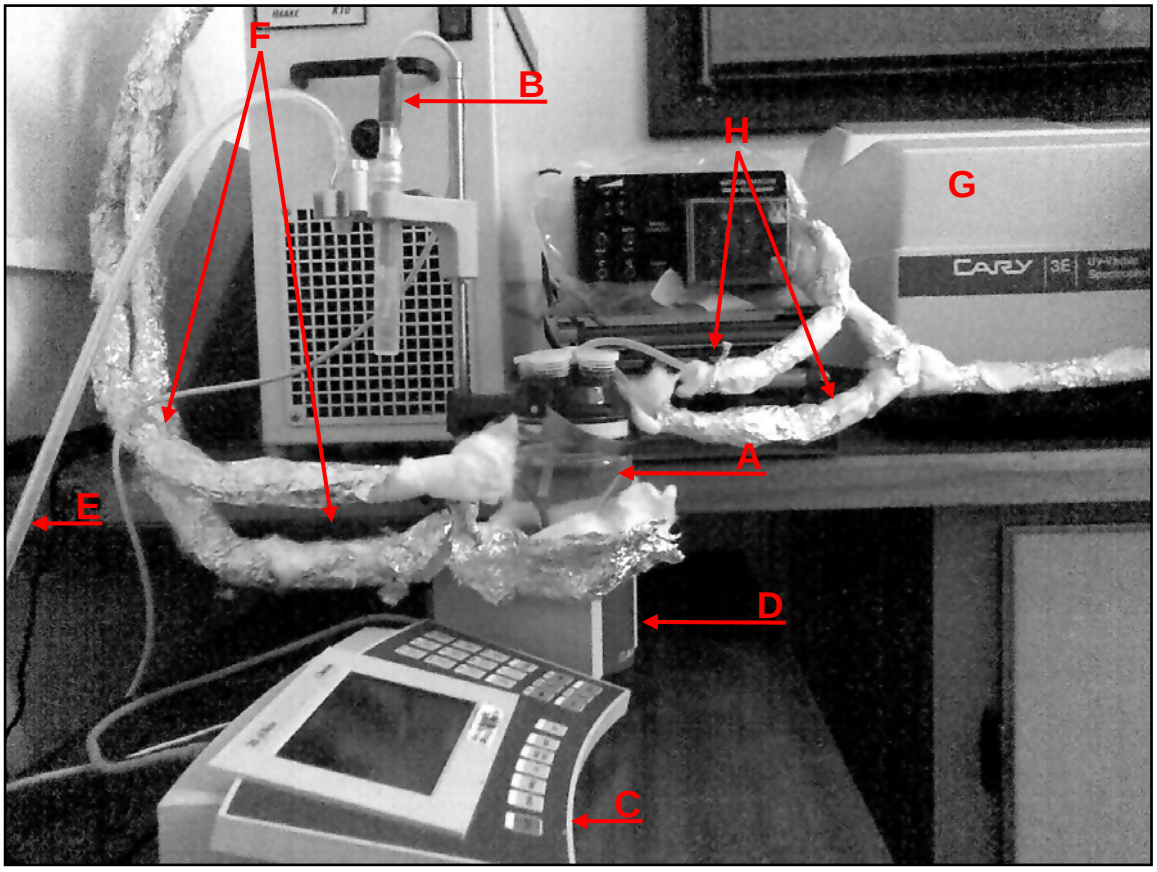


Figure 2.5 Photograph showing the typical pK_a set-up using a thermostatted cell with an argon line. A well-insulated thermostatted cell (**A**) was fitted with an electrode (**B**) attached to pH meter (**C**), stirring unit (**D**) and argon line (**E**) to maintain an inert atmosphere and reduce evaporation. Temperature was maintained by a water bath using high quality silicon tubing (**F**). Sample was circulated into a spectrophotometer (**G**) using a peristaltic pump fitted with high quality silicon tubing (**H**).

For a species A with *n* ionisable functional groups, the following equilibria apply (**Equation 2.3**):

$$\begin{aligned} AH_n &\rightleftharpoons AH_{n-1} + H^+ \quad K_1 \\ AH_{n-1} &\rightleftharpoons AH_{n-2} + H^+ \quad K_2 \\ &\times \\ &\bullet \\ &\bullet \\ AH &\rightleftharpoons A^- + H^+ \quad K_n \end{aligned}$$

Equation 2.3

where the charge on the species AH_i (i = 1 to n) is omitted for convenience. If A_T is the absorbance at the some monitoring wavelength, and A_i the absorbance due to the i^{th} species at that wavelength, then (**Equation 2.4**):

$$A_T = \frac{\sum_{i=0}^{n}\left[A_{i+1}[H^+]^{n-i}\prod_{j=0}^{i}K_j\right]}{\sum_{i=0}^{n}\left[[H^+]^{n-i}\prod_{j=0}^{i}K_j\right]}$$

Equation 2.4

The experimental data were fitted using standard non-linear least-squares methods employing a Newton-Raphson procedure with (**Equation 2.4**) as objective function and all A_i and K_i values as variables (**Appendix 2.3**).

2.2.10 Effects of Temperature

A qualitative temperature study of NAcCoMP8 at various temperatures was attempted in deionised water in order to observe any spectral shifts.

A stock solution of NAcCoMP8 was prepared in deionised water (*ca*. 1.25 μM; pH 7) and degassed using argon. NAcCoMP8 (*ca*. 2 mL) was added to a clean, dry, argon-filled cuvette fitted with a septum. The temperature was increased in 5 ^{o}C increments between 10 – 45 ^{o}C using a Peltier device and the spectrum was recorded between 300 – 700 nm at each temperature.

2.2.11 Effects of Dispersing Agents and Buffers

Various dispersing agents were investigated in the preparation of monomeric NAcCoMP8. These included Triton X-100, PEG, SDS 5% and TWEEN-20. A stock solution of NAcCoMP8 was prepared in deionised water (*ca*. 1.25 μM; pH 7) and degassed using argon. NAcCoMP8 (*ca*. 2 mL) was added to a clean, dry, argon-filled cuvette fitted with a septum. An initial spectrum was recorded from 300 – 700 nm at 25 ^{o}C. To this sample, excess dispersal agent (*ca*. 200 μL in two additions) was added under argon, gently stirred for an hour and the spectrum was recorded every 5 minutes for 30 minutes under these conditions. This procedure was repeated for each dispersing agent listed above. All samples were light-protected when not in immediate use.

Various buffers were investigated for coordination in the preparation of monomeric NAcCoMP8. These included CAPS, CHAPS, HEPES, MES, MOPS and Tris/HCl. Separate stock solutions of NAcCoMP8 (*ca*. 1.25 μM; pH 7) were prepared using Good buffers (*ca*. 0.1 M; pH 7) and allowed to stir for an hour whilst degassed. A 2 mL sample was then transferred into an argon-filled 1.0 cm pathlength cuvette fitted with a septum. One spectrum per hour over 10 hours was recorded between 300 – 700 nm for each sample.

2.2.12 Effects of Reducing Agents

A qualitative study of the reduction of NAcCoMP8 using various reducing agents was attempted in deionised water in order to observe the changes in the electronic spectrum. The reducing agents used were sodium dithionite, sodium borohydride, ascorbic acid and zinc in methanol, respectively.

A stock solution of NAcCoMP8 was prepared in deionised water (*ca*. 1.25 μM; pH 7) and degassed using argon. NAcCoMP8 (*ca*. 2 mL) was added to a clean, dry, argon-filled cuvette fitted with a septum. An initial spectrum was recorded from 300 – 700 nm at 25 ^{o}C. To this sample, previously dried excess reducing agent (*ca*. 0.5 g in two additions) was added under argon, gently stirred and a spectrum was recorded every 5 minutes for 30 minutes under these conditions. This procedure was repeated for each reducing agent listed above.

2.3 QUANTITATIVE ASSESSMENT OF THE SOLUTION CHEMISTRY OF NAcCoMP8

Investigation 2.1: Thermodynamics of ligand substitution reactions of NAcCoMP8

2.3.1 Determination of equilibrium constants in NAcCoMP8 with selected donor ligands (pH 7.0; μ = 0.1) as a function of temperature

Equilibrium constants (log K) were determined for the substitution of the coordinated water in NAcCoMP8 (and in vitamin B_{12a}[†]) by various exogenous ligands. The distally coordinated water was substituted by neutral and anionic ligands, L, and this substitution (**Equation 2.5**) was monitored spectroscopically. The anionic ligands examined were: cyanide, nitrite, sulfite and azide; the neutral ligands were: pyridine, N-methylimidazole, hydroxylamine and methoxyamine. These studies were conducted as a function of temperature (15 – 40 ^{o}C) at constant ionic strength (0.1 M) and pH (pH 7) in order to determine values for ΔH and ΔS. For brevity, sources of reagents (**Section 2.4**), technical specifications (**Section 2.4**), specialized (**Sections 2.2.2; 2.2.3**) and general techniques (**Section 2.5**) may be found elsewhere

$$[Y\text{-}Co(III)Por\text{-}H_2O] + L \longrightarrow [Y\text{-}Co(III)Por\text{-}L] + H_2O \quad \textbf{Equation 2.5}$$

The equilibrium constants for the coordination of NAcCoMP8 (and of vitamin B_{12a}) by exogenous ligand, L, were determined spectroscopically. NAcCoMP8 (2 mL; 3 μM (70 μM for B_{12a}); pH 7) was titrated with ligand (0.1 – 0.001 M) in a 1.0 cm path length cuvette housed in the thermostatted cell block of a UV-vis

[†] Vitamin B_{12a} solutions were made by dissolving a known mass of powder into the relevant buffer. The concentrations were determined spectophotometrically by conversion to the dicyano-complex (ε_{367nm} = 3.04 x 10^4 M^{-1} cm^{-1} from Hill, J. A.; Pratt, J. M.; Williams, R. J. P., *J. Chem. Soc.*, **1964**, 5149.

spectrophotometer. Between 15 and 30 aliquot additions were made in each titration and full absorbance spectra were recorded. All absorbance readings were corrected for dilution. The solutions were buffered with multi-component buffer (**Section 2.5.2**). All solutions were freshly prepared, protected against light with aluminium foil, degassed with argon, clarified and stored at 4 ^{o}C when not immediately in use

The spectrophotometric determination of log K values is often assumed to be independent of the monitoring wavelength. This should indeed be the case if the reactions are simple and the reaction mixture during the course of the titration consists only of the aqua- and exogeneous ligand-ligated form of the metal complexes. In the case of NAcCoMP8, the spectral changes associated with substitution of coordinated water can be quite small and it is not always clear where the greatest signal-to-noise ratio occurs.

To determine whether the values of log K are indeed independent of the monitoring wavelength, and also to average out any possible wavelength-dependence bias in the determinations, spectroscopic data for log K values were obtained at every 1 or 2 nm between 300 and 700 (for titrations with NAcCoMP8 and with B_{12a}) but excluding wavelengths (such as those close to isosbestic points) where the absorbance change was small.

The analysis of absorbance data were fitted by a non-linear least squares method using SigmaPlot.[18] For instances where log K values were small (log K < 4), it is assumed that $[L]_{free} \approx [L]_{total}$ thus, a simple binding isotherm was used (**Equation 2.6**)

$$A_{\lambda} = (A_{o} + KA_{1}[L]) / (1 + K[L]) \qquad \textbf{Equation 2.6}$$

where A_{λ} is the absorbance at some wavelength λ. A_0, A_1 and *K* were the parameters to be optimized. A_0 and A_1 are the absorbance values at λ corresponding to 0 and 100% complex formation.

In the instance where log K > 4, the assumption of $[L]_{free} \approx [L]_{total}$ is no longer valid and an expression for the amount free ligand (LF) in solution has to be compensated for (**Equation 2.7)**.[25]

$$A_{\lambda} = (A_o + KA_1[LF]) / (1 + K[LF]) \qquad \textbf{Equation 2.7}$$

Where $LF = (-a_2 \pm (a_2^2 - 4a_1a_2)^{½}) / 2a_1$ and $a_1 = K$; $a_2 = 1 + K[M]_{total} – K[L]_{total}$; $a_3 = -[L]_{total}$.

Only values of log K obtained from fits for which the correlation coefficient $r^2 > 0.97$ were accepted. *K* was then found from a weighted average, weighted by the reciprocal of the variance, $1/\sigma^2$, where the standard deviation σ = (standard error of the fit)/$n^{½}$ for *n* data points in the titration. Values were corrected for pH (**Equation 2.8**), the temperature-dependent aqua/hydroxo pK_a and for the protonated (non-binding) form of the ligand. This is based on the assumption the hydroxo complex of NAcCoMP8 does not complex the exogenous ligand.

$$K = K_{obs} (1 + 10^{pH - pK_{Co}})(1 + 10^{pK_{Ligand} - pH}) \qquad \textbf{Equation 2.8}$$

Values for ΔH and ΔS were determined from slope and intercept, respectively of van't Hoff plots of ln K vs 1/T.

<u>Investigation 2.2: Kinetics of ligand substitution reactions of NAcCoMP8</u>

2.3.2 Kinetics of substitution in NAcCoMP8 with selected donor ligands (pH 7.0; μ = 0.1) as a function of temperature

For a monomeric Co(III) macrocycle (NAcCoMP8 or B_{12a}) in aqueous solution, the kinetics of substitution reactions with probe ligands is described by (**Equation 2.5**):

$$CoH_2O + L \xrightarrow{k_{II}} CoL + H_2O$$ **Equation 2.5**

where L represents the incoming probe ligand that replaces the axial water with a second order rate constant k_{II}. These absorbances were monitored under pseudo first order conditions where [L] >> [NAcCoMP8]. The rate was monitored spectrophotometrically at selected wavelengths as described below. For brevity, sources of reagents (**Section 2.4**), technical specifications (**Section 2.4**), specialized (**Sections 2.2.2; 2.2.3**) and general techniques (**Section 2.5**) may be found elsewhere.

NAcCoMP8 (*ca*. 3 μM (30 μM for B_{12a})) was added to a 1.0 cm path length cuvette housed in the thermostatted cell block of a UV-vis spectrophotometer. To this a known concentration of the probe ligand was aliquotted and the rate of the reaction was monitored using the onboard Cary Kinetics® software by recording the increase or decrease of absorbance over time at 415 or 425 nm, respectively for NAcCoMP8, and at 350 or 360 nm, respectively for B_{12a}. Five to eight ligand concentrations were used each differing in concentration roughly by a factor of 10. All solutions were freshly prepared, degassed (argon) and buffered with multi-component buffer (pH 7 by NaOH (8 M), μ_{Total} = 0.1 M by $NaNO_3$).

The observed pseudo first order rate constants, k_l^{obs}, was obtained by fitting a standard exponential function employing a Newton-Raphson procedure using SigmaPlot to the absorbance/time traces obtained for each titration (**Equation 2.9**, if the absorbance increases and **Equation 2.10** if it decreases with time).In the equation A_0, A_1 and k_l^{obs} are variables.

$$A_\lambda = A_1 - (A_1 - A_o)e^{(-k_{lobs}t)}$$ **Equation 2.9**

$$A_\lambda = -A_o e^{(-k_{lobs}t)} - A_1 e^{(-k_{lobs}t)} + A_$$ **Equation 2.10**

Thereafter the values for k_I^{obs} were also corrected for dilution and for the pK_a of NAcCoMP8 (**Equation 2.8**) given the assumption that the hydroxo complex of NAcCoMP8 (and of B_{12a}) does not complex the exogenous ligand.

$$k_I^{obs\text{-}corr} = k_{obs}\,(1 + 10^{\,pKa\,-\,pH}) \qquad \textbf{Equation 2.8}$$

Second order rate constants, k_{II}, were obtained from a linear least-square plot of corrected k_I versus [L] where L is the concentration of the incoming ligand. Values of $\Delta H^{\ddagger}$ and $\Delta S^{\ddagger}$ were determined from weighted linear least squares Eyring plots of $\ln(k_{II}h/k_BT)$ against T^{-1}, where h and k_B are the Plank and Boltzmann constants, respectively.

2.4 SUMMARY OF MATERIALS

2.4.1 Chemicals

Table 2.3 Summary of chemicals used in this work.

Chemical	Supplier	Grade
Acids and Bases		
Acetic Acid (glacial)	BDH	AR
Ammonia (as 25% NH_4OH)	Merck	AR
Ascorbic acid	Sigma	AR
Hydrochloric Acid	Saarchem	GR
Nitric acid	Saarchem	GR
Perchloric acid	ACE	CP
Phosphoric acid (99%)	Aldrich	AR
Sodium hydroxide (pellets)	Merck	GR
Sulphuric acid	ACE	GR
Enzymes, Proteins, Metalloporphyrins		
CoTPPS	Frontier Chemicals	CP
CoTMPyP	Frontier Chemicals	CP
Cytochrome *c* (horse heart)	Seravac	BP
Pepsin (porcine)	Sigma	CP
TMPyP	Sigma; Frontier Chemicals	CP
TPPS	Sigma; Frontier Chemicals	CP
Trypsin (bovine)	Sigma	CP
Vitamin B_{12a}	Roussel	BP

Chemical	Supplier	Grade
Fine Chemicals, Reagents, Ligands		
Acetic anhydride	Merck	GR
Ammonium sulphate	Saarchem	AR
Calcium chloride	Sigma	CP
Cobaltous acetate	Saarchem	AR
Hydroxylamine sulphate	Sigma	AR
Iron(II)chloride	Merck	AR
Methoxyamine hydrochloride	Sigma	AR
N-methyl imidazole	Sigma	AR
Potassium chloride	Aldrich	AR
Potassium permanganate	Sigma	AR
Pyridine	Sigma	AR
Silver chloride	Effective lab supplies Ltd	AR
Sodium acetate	Merck	AR
Sodium borohydride	Sigma	AR
Sodium cyanide	Merck	AR
Sodium dithionite	Hopkin & Williams Ltd	AR
Sodium azide	Fluka	AR
Sodium nitrate	Merck	CP
Sodium nitrite	Merck	CP
Sodium perchlorate	Sigma	AR
Sodium sulphite	Merck	CR
Zinc	BDH	GR
Solvents and Gases		
Acetone	Merck	CR
Acetonitrile	Agros-Organics	HPLC
Argon (gas)	Afrox	AR
Chloroform	Sigma	HPLC
Deionised water	Millipore	18 MΩcm
Ethyl acetate	Sigma	CR
Helium (gas)	Afrox	AR
Methanol	BDH	HPLC
Nitrogen (liquid)	Afrox	
Nitrogen (gas)	Afrox	UHP
Oxygen (gas)	Afrox	AR
Buffers and Surfactants		
Ammonium hydrogen carbonate	BDH	AR
Ammonium carbonate	BDH	AR
CAPS	Sigma	AR
CHAPS	Sigma	AR
CHES	Sigma	AR
Dipotassium hydrogen phosphate	Merck	GR
HEPES	Sigma	AR
MES	Sigma	AR
MOPS	Sigma	AR
PEG 1000	BDH	CP

Chemical	Supplier	Grade
Buffers and Surfactants/ continued…		
Potassium dihydrogen phosphate	Merck	GR
Potassium hydrogen phthalate	Saarchem	GR
SDS (5%)	Merck	GR
Sodium hydrogen carbonate	Merck	CP
Sodium carbonate	Merck	CP
Tris	BDH	CP
Triton-100	Merck	GR
Tween-20	Merck	GR
Metrohm Standard Buffer 4.0	Metrohm	
Metrohm Standard Buffer 7.0	Metrohm	
Metrohm Standard Buffer 9.0	Metrohm	

2.4.2 Equipment

Table 2.4 Summary of equipment and software used in this research.

Material	Source	Part No.: / Specification
General Equipment and Instrumentation		
Antistatic gun	Sigma	Zerostat™ Cat. No.: Z108812
Cuvettes	Helma	Quartz; 1 cm; flow cell; #284 set.
Electrodes	Metrohm	6.0258.010 or 6.0234.100
Freeze dryer	Virtis	Unitrap II, Gardiner, NY, 12525
HPLC	Dionex	Reverse phase system
Mass spectrometer	Thermo	Thermo LXQ
Peristaltic pump	*	Watson-Marlow 101U
pH meter	Metrohm	Metrohm 605, 713 or 780
Thermostatted cell	Metrohm	6.1418.150 (5 – 70 mL)
UV-Vis spectrophotometers	Cary, Varian	1E, 3E and 300 Bio
Separation and Filtration		
Amicon® Cell	Millipore	Model 8050. Cat. No. 5122
Deionised Water system	Millipore	DirectQ UV3 18.2 MΩ.cm / 25 °C
Gel filtration columns	Pharmacia	1 m x 0.03 m
HPLC column	Phenomenex	5 µ; 150 X 4.6 mm C18 RP
HPLC guard column	Phenomenex	4 x 3 mm; C18 RP
Millex® syringe-filters	Millipore	0.45 µm, non-sterile, PTFE
Sephadex G50	Sigma	G50; 20 -50 µ M
Sep-Pak® Cartridges	Waters	500 mg and 10 g C18
TLC Plates	Fluka	Silica gel plates 254 nm, 0.2 mm

Software		
Material	**Source**	**Part No.: / Specification**
Excel©	Microsoft®	Ver 11.6.3(101208) 2004
Chromeleon©	Dionex	Ver 2.10(100) 2009
CurveFit©†	Wits	Ver 1.00
Xcalibur®	Thermo®	Thermo Electrons 1998-2005
Kinetics©	Cary, Varian	Ver 3.00(182) 2002
Scan©	Cary, Varian	Ver 3.00(182) 2002
SigmaPlot©	Systat Software	Ver 11.0 (2008)

† Perry, C. B., *CurveFit*, a computer programme for non- linear least-squares fitting using the Marquard algorithm, University of the Witwatersrand, Johannesburg, South Africa, 1998.

2.5 GENERAL METHODS

2.5.1 pH Measurements

All pH measurements were performed using one of the pH meters listed (**Section 2.4.2**) with a combination glass electrode (either 6.0258.010 or 6.0242.101). The instruments were operated according to the respective manufacturer's manual. Instruments were calibrated two hours prior to use with Metrohm standards (pH 4.00, 7.00 or 9.00 at 25.0 °C). Care was taken to ensure thermoequilibration. Electrodes were routinely maintained as per manufacturer's manual.

2.5.2 Buffer Preparations

Buffers were freshly prepared (0.1 M) in degassed deionised water and stored at *ca*. 4 ^{o}C until just before use. The pH of the solutions were adjusted using an acid or base that was appropriate to the experiment being run. All buffers were filtered under pressure. The multi-component buffer was made up to an overall ionic strength of 0.1 M (**Table 2.5**).

Table 2.5 Summary of the multi-component buffers used in this research.

Buffers	pK_a	Useful pH range
$(NH_4)_2CO_3$	7.8	6.8 – 7.0
CHES	9.3	8.6 – 10.0
MES	6.1	5.5 – 6.7
Tris/HCl	8.1	7.0 – 9.0
MOPS	7.2	6.5 – 7.9
Multi-component buffer *	-	4.0 – 10.0

* (CHES, MES, Tris, MOPS, Potassium hydrogen phthalate

2.5.3 Lyophilisation

Lyophilisation is a process of cryo-dessication that allows for the removal of solvent from a sample through sublimation. The lyophilisation process typically requires that the sample be highly concentrated in the smallest possible volume. This however, poses a problem for NAcCoMP8 samples given its propensity towards aggregation at such high concentrations. Thus, samples are not reduced to minimum volume but rather to *ca.* 40 mL with a concentration of *ca*. 2 µM on a UniTrap II Virtis freeze dryer. Furthermore, this volume is frozen around a large round-bottomed flask (250 mL) in order to increase the surface area and thus reduce lyophilisation run-time. All samples must be clarified using a Millex® syringe-filter else NAcCoMP8 tends to lyophilise around the glass as a fine sticky powder as opposed to a spongy solid. The latter is far easier to handle and does not require the use of an anti-static gun. When samples have been dried, they need to be flooded with argon and stored at -20 ^{o}C in a light-protected moisture-free flask. Any moisture will, upon warming up to room temperature, condense and dissolve the extremely hydrophilic NAcCoMP8, forming a highly concentrated solution.

2.6 MISCELLANEOUS EXPERIMENTS

NAcCoMP8 tends to aggregate in solution and is often prepared in small quantities or reclaimed where possible. For this reason, cheaper alternatives are used for all preliminary experimental optimisations. These alternatives are typically synthetic cobalt(III) porphyrins.

2.6.1 Synthesis of CoTPPS and CoTMPyP

Synthetic cobalt (III) porphyrins are typically used as model-systems for vitamin B_{12a}. These include a variety of water-soluble cobalt porphyrins such diaqua-5,10,15,20-tetra-*p*-phenylsulfonyporphinato-cobalt(III) (CoTPPS) and 5, 10, 15, diaqua-5,10,15,20-tetra-*p*-phenyl-N-methyl-4-pyridylporphinato-cobalt(III) (CoTMPyP) (**Figure 2.6**). For brevity, sources of reagents (**Section 2.4**), technical specifications (**Section 2.4**), specialized (**Sections 2.2.2; 2.2.3**) and general techniques (**Section 2.5**) may found elsewhere.

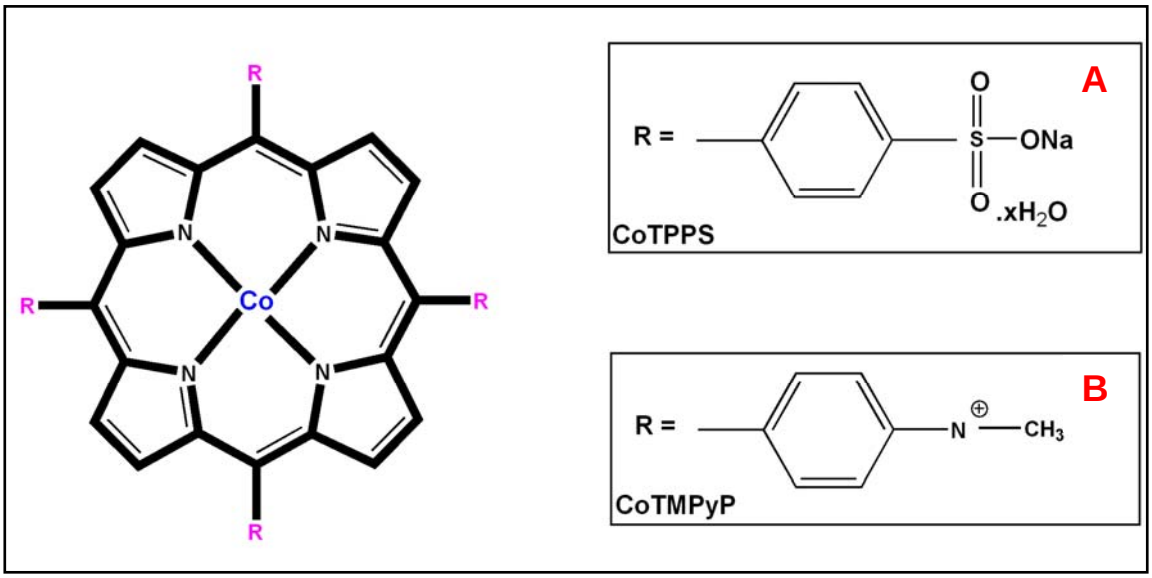


Figure 2.6 The cheaper synthetic Co(III) porphyrins used to develop synthesis protocols in this work. (**A**) CoTPPS and (**B**) CoTMPyP.

The synthesis of CoTPPS was based on the methods employed by Herrmann[27] *et al*., and of Abwoa-Konya[28] *et al*., (CoTMPyP was based on the methods of Lin and Marzilli[23] and Herrmann[27] *et al*.,) with modifications. The notable

modification is against the use of perchlorate salts as these are known to be explosive particularly since synthesis requires heating.

Methods: Freebase porphyrin obtained from Sigma-Aldrich was purified as mentioned below. Freebase porphyrin (10 mg) was dissolved in basic deionised water (*ca*. 2 mL; pH 9 (NaOH)) and refluxed with cobalt acetate (100 fold excess) under argon for 30 minutes in the dark. The cobalt acetate (*ca*. 0.5 g) was prepared by dissolving in dry methanol (*ca*. 1.5 mL) and allowed to stir until dissolved. The cobalt acetate solution was then clarified using a Millex® syringe-filter before addition into reflux vessel (*ca*. 50 uL). Thereafter, the reaction was allowed to stir without heat for three hours in air (*ca*. pH 6 *in vivo*). Synthesis was monitored spectroscopically by the shift in soret from 414 nm to 424 nm (424 nm to 437 nm in CoTMPyP). Once cooled, the metalloporphyrin was precipitated out as dark pink flakes (purple-red in the case of CoTMPyP) using cold acetone. The CoTPPS was recrystallized as dark rhombic purple-black crystals using (2:2:1 ethyl acetate: acetone: water) diffusion system in H-tubes at reduced temperature (*ca*. 4 ^{o}C). CoTPPS was characterized using UV-Vis spectroscopy, NMR and ESI-MS.

Purification: It was typically observed that freebase TPPS (Sigma-Aldrich) was contaminated by the more hydrophobic tri- and di-substituted derivatives as well as water-soluble salts used in the isolation process. TPPS was purified using C18 Sep-Pak® cartridges. The cartridges were activated using HPLC grade CH_3CN (20%) and washed several times with deionised H_2O to equilibrate the column. The TPPS sample was then dissolved in minimal volume deionised water and loaded slowly onto the Sep-Pak® to avoid leaching. Once loaded, the porphyrin was washed several times with deionised water to remove other water-soluble salts used in the isolation process. The porphyrin was then eluted as a single purple band using acetonitrile (20%) and lyophilized overnight. This procedure may also be used to purify the metalloporphyrins if required.

2.6.2 Recovery of NAcCoMP8

NAcCoMP8 had to be recovered from the various experiments in order to be utilized in others. This was more time-efficient than re-making NAcCoMP8. These samples included NAcCoMP8 in various aqueous buffered solutions (*e.g*. Beer's Law, pK_a and other qualitative studies) as well as samples from ligand binding studies where the axial position was not occupied by water. Each of these samples was treated separately to avoid cross-contamination.

NAcCoMP8 in various buffered solutions were adjusted to pH neutral (with either concentrated NaOH or H_2SO_4) if required (*e.g.* in the case of pK_a samples) and concentrated on a C18 Sep-Pak® cartridge primed with HPLC grade CH_3CN and equilibrated with deionised water. The sample was then washed exhaustively with deionised water (*ca*. 1.5 L). Eluents were checked for salts using silver nitrate. The sample was eluted using 50% CH_3CN, filtered using a Millex® syringe-filter and lyophilized. Solid was weighed and identified using HPLC, Uv-Vis and mass spectroscopy.

NAcCoMP8 samples reclaimed from ligand binding studies were diluted and washed with copious amounts of water (*ca*. 5 L per ligand) on an Amicon© cell under pressure (nitrogen) over 24 hours. Samples were routinely checked for salts using silver nitrate. NAcCoMP8 was monitored using Uv-Vis spectroscopy (415 nm). NAcCoMP8 was then concentrated on a C18 Sep Pak® cartridge and treated as before.

2.7 REFERENCES FOR CHAPTER 2

1. Dolphin, D.; McKenna, C.; Murakami, Y.; Tabushi, I., *Biomimetic Chemistry, Advances in Chemistry,* **1999**, *Vol 191* (Monograph), 177th ACS National Meeting, Hawaii.
2. Hamza, M.S.A; Ducker-Benfer, C; van Eldik, R., *Inorg. Chem.*, **2000**, *39*, 3777 (and references therein).
3 Sannasy, D., M.Sc. Dissertation, University of the Witwatersrand, Johannesburg, South Africa, **2005**.
4. Harbury, H. A.; Loach, P. A., *J. Biol. Chem.,* **1960**, *235,* 3640.
5. Tsou, C. L., *Biochem. J.*, **1951**, *49*, 362.
6. Tsou, C. L., *Biochem. J.*, **1951**, *49*, 367.
7. Adams, P. A.; Byfield, M. P.; Raymond, C.; Milton, de L.; Pratt, J. M., *J. Inorg. Biochem.,* **1988**, *34*, 167.
8. Adams, P. A.; Byfield, M. P.; Goold, R. D.; Thumser, A. E., *J. Inorg. Biochem.,* **1989**, *37*, 55.
9. Carraway, A. D.; McCollumn, M. G.; Peterson, J., *Inorg. Chem.,* **1996**, *35,* 6885.
10. Holm, R.H.; Solomon, E.I., *Chemical Reviews*, **2004**, *104 (2)*, 347.
11. Wilson, M.T.; Ranson, R.J.; Masiakowski, P.; Czarnecka, E.; Brunori, M., *Eur. J. Biochem*., **1977**, *77*, 193.
12. Kadnikova, E. N.; Kostic, N. M., *J. Org. Chem.*, **2003**, *68,* 2600.
13. Tuppy, H.; Paleus, S., *Acta Chem. Scand.*, **1955**, *9*, 353.
14. Munro, O. Q.; Marques, H. M., *Inorg. Chem.*, **1996**, *35*, 3752
15. Primus, J.; Marelle, G. B.; Mandon, D.; Boeren, S.; Veeger, C.; Weiss, R.; Rietjens, I. M.C. M., *J. Biol. Inorg. Chem.*, **1999**, *4*, 274
16. Smith, R. M. ; Martell, A. E., *Critical Stability Constants*, Plenum Press, New York, **1986**, Volume 6, Second Supplement, p. 302

17. Merck Catalogue, Chemical Reagents, **2000**.

18. *SigmaPlot,* 11.0; Systat Software, Inc.: San Jose, CA, **2008**.

19. Marques, H. M; Munro, O. Q.; Crawcour, M. L., *Inorg. Chim. Acta*, **1992**, *196*, 221.

20. Martell, A. E.; Smith, R. M.; Motekaites, R. J., NIST *Criticially Selected Stability Constants of Metal Complexes*, V. 8.0. In NIST, Gaithersburg, MD: **2004**.

21. Baldwin, D. A.; Mabuya, M. B.; Marques, H. M., *S. Afr. J. Chem.,* **1987**, *40*, 103.

22. Shelnutt, J. A.; Dobry, M. M.; Satterlee, J. D., *J. Phys. Chem.,* **1984,** *88*, 4980.

23. Lin, M.; Marzilli, L. G., *Inorg. Chem.,* **1994**, *33*, 5309.

24. Ashley, K. R.; Au-Young, S., *Inorg. Chem.*, **1976***, 15(8),* 1937.

25. Marques, H. M.; Perry, C. B., *J. Inorg. Biochem.,* **1999**, *75*, 281.

26. Niederhoffer, E. C.; Timmons, J. H.; Martell, A. E., *Chem. Rev.* **1984,** *84,* 137.

27. Herrmann, O; Mehdi, S. H.; Corsini, A., *Can. J. Chem.,* **1978**, *56*, 1048.

28. Abwao-Konya, J.; Cappelli, A.; Jacobs, L.; Krishnamurthy, M.; Smith, M., *Transition Met. Chem.*, **1984**, *9*, 270.

CHAPTER 3
MONOMERISATION OF NAcCoMP8: SYNTHESIS ASPECTS

3.1 INTRODUCTION

The proteolytic digestion of cytochrome *c* yields a variety of hemepeptides called microperoxidases.[1,2] These microperoxidases at neutral pH typically contain a covalently bound heme that retains a histidine residue in the 5th axial position and a readily replaceable water molecule at the 6th axial position. The availability of this 6th axial position for ligand binding studies demonstrates the attractiveness of microperoxidase as a biomimetic model.[3] However, it has been suggested that ligand binding studies with microperoxidase is often under-utilised.[3] The most apparent reason for this is the propensity of microperoxidase towards aggregation.[3-5]

Microperoxidases are notoriously prone towards aggregation.[3-5] Aggregation has been observed with FeMP11[4,6], FeMP9[7,8], FeMP8[9] and FeMP5[11]. Findings as early as in the 1950s suggested that microperoxidase aggregates could exhibited apparent molecular masses of up to 10 000![12] Thus, the implications towards a complicated solution chemistry is obvious. In this work *aggregation* is referred to as the process whereby a monomer rearranges from dimer to oligomer to polymer and finally to aggregate. Here, *polymer* refers to oligomers of very high masses. *Aggregates*, unless otherwise specified, refer to insoluble polymers that have precipitated, usually irreversibly.

Two types of aggregation have been found amongst microperoxidases: non-covalent π-π interactions and covalent metal–side-chain coordination. Non-covalent π-π interactions occurs through one or more porphyrin faces.[13-15,19]

This may result in a variety of conformations including head-to-tail[16] or plane-to-plane[17]. Metal–side-chain aggregation refers to the coordination of the 6th axial position of one hemepeptide moiety by an amine group of another hemepeptide moiety.[3,19] These co-ordinating amines may be α-amines (*e.g*. Cys-14, Val-11) or ε-amines (*e.g*. Lys-22, Lys-13) and lead to the presence of multiple species in solution.[4,12,20,22]

The various microperoxidase derivatives formed through aggregation tend to significantly complicate the solution chemistry of these species.[3,26,27] The kinetics of disaggregation may further confound ligand binding data. Moreover, aggregation has solubility repercussions that reduce the attractiveness of microperoxidase as biomimetic models.[3] Thus, the need for monomerisation of microperoxidase becomes apparent.

Monomerisation of microperoxidase may be considered a two-fold approach. Firstly, monomerism may be encouraged by regulating the solution environment through the factors that directly influence aggregation. These factors comprise pH, concentration, ionic strength and temperature and regulation may include the utilisation of mixed-solvents, detergents, low ionic strength and so on (see **Chapter 4**).[24,25] Typically, this works well for non-covalent π-π aggregates.[16-18] Secondly, in the case of metal–side-chain coordination it is often necessary to structurally modify the co-ordinating moieties by derivatisation, for example, by acetylation (this **Chapter**). Acetylation of the amines to suppress intermolecular bond formations significantly minimises this type of aggregation. [3,21,22,25]

Aggregation is a feature not exclusive to iron-containing porphyrins but is common in most metalloporphyrins.[15,18,19] These include metalloporphyrins that contain cobalt.[10,13] Thus it was expected that CoMP8 would be prone to aggregation as well. Preliminary work on CoMP8 demonstrated aggregation and revealed complicated, irreproducible solution chemistry data (**Appendix 3.1**). Thus, CoMP8 was aceylated, to produce NAcCoMP8, in which the terminal amino group of Cys-14 is acetylated in order to reduce the effects of aggregation.[21,23] However, despite this, NAcCoMP8 was found to aggregate in

solution under certain conditions (see **Chapter 4**). This then led to the idea of combining various aspects of the two-fold approach towards monomerism mentioned earlier.

The aim of the work presented in this Chapter was therefore to optimise the NAcCoMP8 yields by minimising aggregation during synthesis (*cf*. Investigation 1.1**, Chapter 2**). Aggregation was minimised by employing a two-fold approach towards monomerism: acetylation in order to prevent metal–side-chain co-ordination and by regulating the solution environment with regards to microperoxidase concentration and pH to limit π-π interactions. (**Figure 3.1**).

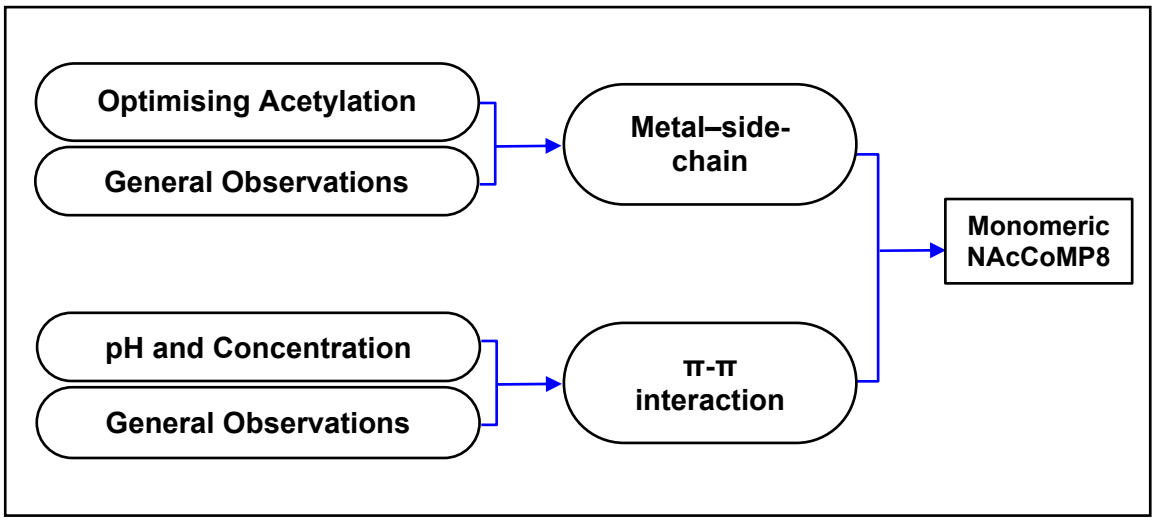


Figure 3.1 A flow diagram of the different aims and results focussed on in Chapter 3. Achieving monomerism involved the minimisation of metal–side-chain interactions by the protection of the co-ordinating moieties through acetylation. Monomerism was also explored by the regulation of the factors that influence aggregation in solution such as pH and concentration.

3.2 RESULTS AND DISCUSSION

The rationale behind the acetylation investigation was prompted by the generally low yields observed in synthetic Route A.[23] The low yields suggested that perhaps aggregation occurred during the synthesis. This led to the idea that perhaps the acetylation step to protect against metal–side-chain coordination occurred too late in the synthesis of NAcCoMP8 and should be effected sooner.

Thus, the first step in this investigation explored when exactly the acetylation step should occur in order to maximise NAcCoMP8 yields (**Figure 3.1**).

The rationale behind the synthesis protocol optimisations was centred on the factors that influenced aggregation in solution such as pH and microperoxidase concentration. The synthesis of NAcCoMP8 often required the intermediate microperoxidases to be at non-neutral pH in high concentration; concentration and pH are both known to promote aggregation.[24, 25] Thus, the second focus of the investigation explored synthetic procedures that minimised high microperoxidases concentrations at non-neutral pH (**Figure 3.1**). Often synthetic cobalt porphyrins were used to optimise these reactions before testing on other cobalt microperoxidases. CoTPPS was utilised for this purpose in this work (**Appendix 3.7**).

3.2.1 Optimisation of the acetylation process of NAcCoMP8

The acetylation of NAcCoMP8 was investigated in terms of (i) a comparative investigation of yields of the various microperoxidases in Routes A, B, C and D, and (ii) a comparative investigation of three different cobalt microperoxidases and their acetylated derivatives.

3.2.1.1 Percentage yields in NAcCoMP8 synthesis

Four different synthetic routes were explored in order to minimise aggregation in NAcCoMP8: Routes A, B, C and D (**Chapter 2; Appendix 2.1**). The primary difference pertained to the position of the acetylation step relative to the demetalation step. Route A represents the original synthesis as described by Sannasy.[23] Routes B and D represents earlier acetylation and demetallation, respectively. Route C represents an amalgamation of the two whereby both acetylation and demetallation are effected earlier relative to Route A. The overall yields for NAcCoMP8 in each route were compared.

Synthesis via Routes A, B, C and D were carried out as described previously (**Chapter 2; Appendix 2.1**). Percentage yields were determined, by mass, for microperoxidases in each route and are reported as a percentage conversion dependent upon the microperoxidase used in the preceding step. Yields could have been estimated by concentration using electronic spectroscopy. However, since absorptivities for some microperoxidases are not known, yields were estimated by mass. The percentage yields reported represent an average of three repeated syntheses for each route (**Table 3.1**). Masses were obtained on a 6-figure balance at reduced temperature to minimise the effects of static (**Appendix 3.2**). In this regard, an anti-static gun was also used as per manufacturer's instructions.

Table 3.1 Percentage yield (by mass, with standard deviations in parentheses) of the various microperoxidases obtained in synthetic Routes A, B, C and D. The underlined synthetic Route C was explored in this work. Percentage yield values for NAcCoMP8 are *italicised* across the synthetic routes

Route A		**Route B**		**Route C**		**Route D**	
FeMP11	84.6(6)	FeMP11	92.7(6)	FeMP11	93.1(7)	FeMP11	91(1)
FeMP8	57.1(5)	FeMP8	57.8(3)	NAcFeMP11	95.1(5)	MP11	90.0(4)
MP8	68.7(5)	NAcFeMP8	87.6(5)	NAcMP11	98.2(1)	CoMP11	85.9(6)
CoMP8	65.1(3)	NAcMP8	76.0(2)	NAcCoMP11	95.1(2)	NAcCoMP11	66.7(9)
NAcCoMP8	*69.0(1)*	*NAcCoMP8*	*72.4(5)*	*NAcCoMP8*	*76.7(7)*	*NAcCoMP8*	*74.9(3)*

The overall yields for the initial peptic digestion product, FeMP11, for Route A, B, C and D were 85%, 93%, 93% and 91%, respectively. The overall yields for the final cobalt(III) substituted digestion product, NAcCoMP8, for Route A, B, C and D were 69%, 72%, 77% and 75%, respectively. The previously reported NAcCoMP8 yield (Route A') was 58%.[23]

Routes C and A were found to have the highest (77%) and lowest (69%) yields,

respectively. Yields for Route B and D were 72% and 75%, respectively; both yields were an improvement on Route A and A'.

Route A yield for NAcCoMP8 reported here (69%) was comparable to that obtained previously for Route A' (58%).[23] The improvement in yield noted (11%) was likely due to the implementation of Sep-Pak® cartridges as opposed to the Amicon® cell during the desalting and concentrating steps (**Section 3.2.1.1**). This improvement was also observed in the FeMP8 synthesis (*ca*. 2%) when FeMP8 was desalted by implementing the Sep-Pak® system rather than the Amicon® system.

Route B yield for NAcCoMP8 (72%) was higher than that obtained for Route A' (58%)[23] and Route A (69%). The increase in yield from Route A' to B (*ca*. 14%) was likely as a consequence of shifting the acetylation procedure ahead of the metal-removal step. Removing the metal allows the His-18 moiety to become uncoordinated from the metal centre. This unbound His-18 moiety now has a greater degree of freedom; side-chain aggregation of the Cys-14 moiety onto another microperoxidase molecule is readily facilitated (**Figure 3.2A**). Thus, protection of the terminal amino groups on the Cys-14 by acetylation prior to removing the metal ion limits the His-18 moiety's propensity for side-chain coordination despite the degrees of freedom (**Figure 3.2B**). Similarly, the process of metal ion-removal requires very concentrated and low pH conditions which promote the formation of metal–side-chain aggregation before the metal is actually removed. Additionally the slight increase in yield from Route A to B (*ca*. 3%) may be attributed to the utilisation of Sep-Pak® cartridges in addition to the shift in acetylation step.

Route D yield for NAcCoMP8 (75%) was higher than that obtained for Route A' (58%)[23] and Route A (69%). The increase in yield from Route A' to D (*ca*. 17%) was likely a consequence of early FeMP11 demetallation, it being the initial precursor in the NAcCoMP8 synthesis. Since the typical overall masses obtained for FeMP11 (*ca*. 40 mg) are larger than those obtained for FeMP8 (*ca*. 20 mg), the errors during synthesis were relatively smaller. Thus the

demetallation and cobalt insertion steps of FeMP11 were easier to manage practically than that of FeMP8. Additionally, the slight increase in yield from Route A to D (*ca*. 6%) may be attributed to the utilisation of Sep-Pak® cartridges in addition to the shift in acetylation step.

Route C yield for NAcCoMP8 (77%) was higher than that obtained for Route A' (58%)[23] and Route A (69%). The increase in yield from Route A' to C (*ca*. 19%) was likely due to a combination effect of both early acetylation and demetallation of FeMP11, the initial precursor in the NAcCoMP8 synthesis. This was the earliest possible step in which acetylation and demetallation could be carried out. Additionally the slight increase in yield from Route A to C (*ca*. 8%) may be attributed to the utilisation of Sep-Pak® cartridges in addition to the shift in acetylation step (**Section 3.2.2.1**).

From this investigation, it is observed that that the position of the demetallation and acetylation steps play an important role in the amount of NAcCoMP8 synthesized. The yield of NAcCoMP8 appeared to be more dependent on the position of the demetallation step rather than the acetylation step. Thus shifting both the acetylation and demetallation steps improved the overall yield of NAcCoMP8 by *ca* 19%.

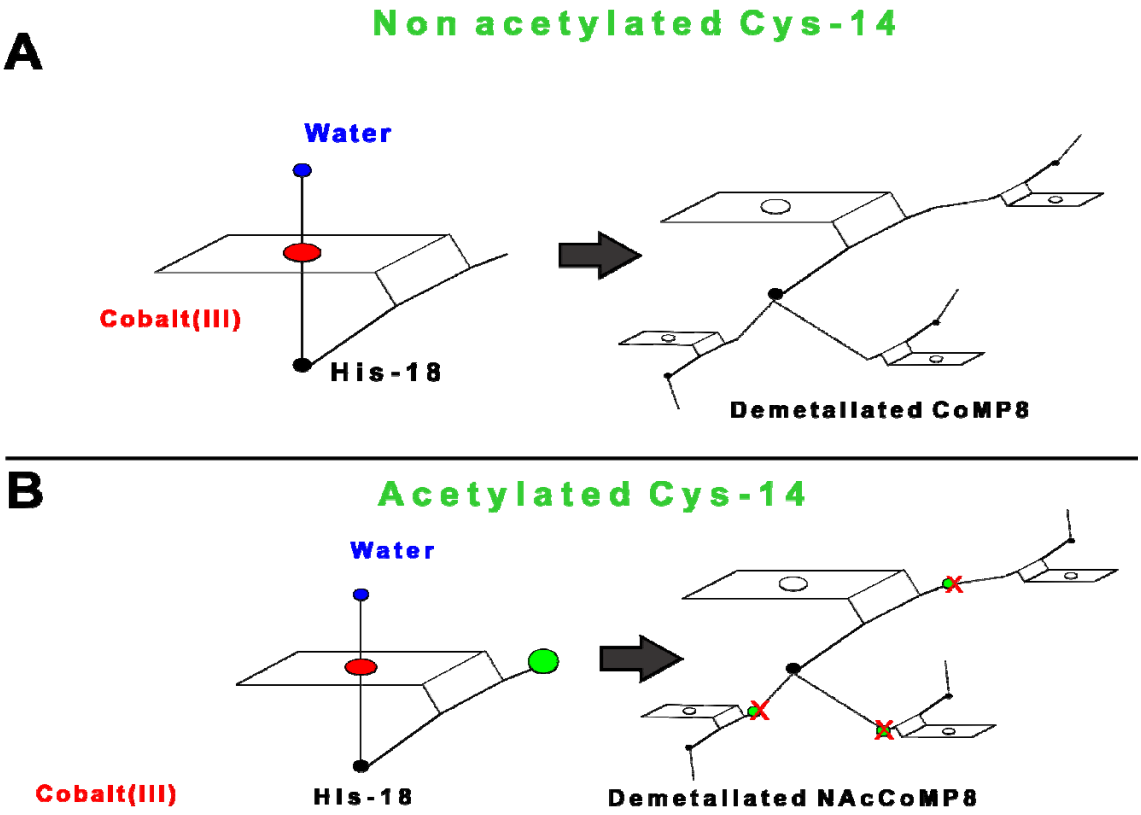


Figure 3.2 The effect of acetylation on side-chain aggregation in metal-free microperoxidase. Metal-free CoMP8 could encounter side-chain aggregation at the non acetylated amines on the Cys-14 group (**A**). However, the demetalated NAcCoMP8 is unable to form those interactions (represented by **X**) due to the acetylation of those amino-groups (**B**).

3.2.1.2 General observations of three cobalt microperoxidases

The proteolytic digestion of cytochrome *c* yields a variety of microperoxidases (**Figure 3.3**). The controlled peptic and tryptic digestion of cytochrome *c* typically yields FeMP8, sometimes with FeMP11, FeMP6 and FeMP5 as impurities. In principle, these microperoxidases could be isolated, demetalated and have cobalt inserted. Thus, two other cobalt microperoxidases were isolated as an artefact of the NAcCoMP8 synthesis (**Section 2.2.1**). These were CoMP11 and CoMP6. Both derivatives were acetylated and qualitatively compared against CoMP8 and NAcCoMP8, respectively. All associated methods, procedures and equipment referred to may be found elsewhere (**Chapter 2; Appendix 2.1**).

A stock solution of each cobalt microperoxidase (*ca*. 1.80 μM; pH 7) was freshly prepared in degassed deionised water. The samples were allowed to stir for about 2 hours to reach equilibrium before filtering with Millex® syringe-filters. Thereafter, a 2 mL sample was transferred into an argon-filled 1.0 cm pathlength cuvette fitted with a septum. A UV-vis spectrum was recorded between 300 – 700 nm (**Figures 3.4 - 3.6**). HPLC and TLC data were recorded using samples recovered whilst monitoring the acetylation reactions at different intervals; chromatograms and TLC examples are included in the Figures.

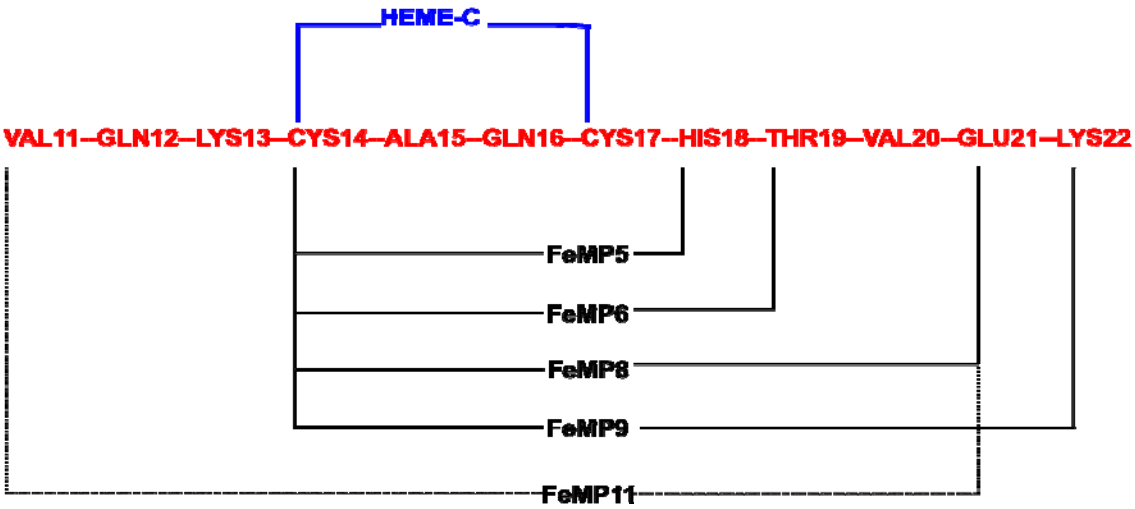


Figure 3.3 Representation of hemepeptides that may be isolated through the proteolytic digestion of cytochrome *c*. The porphyrin moiety (blue) is denoted as *heme-c* to reflect the porphyrin's cytochrome *c* origins. Porphyrin moieties derived from heme-c contain Fe(III) as the metal ion. Adapted from Chuang *et al.*[11]

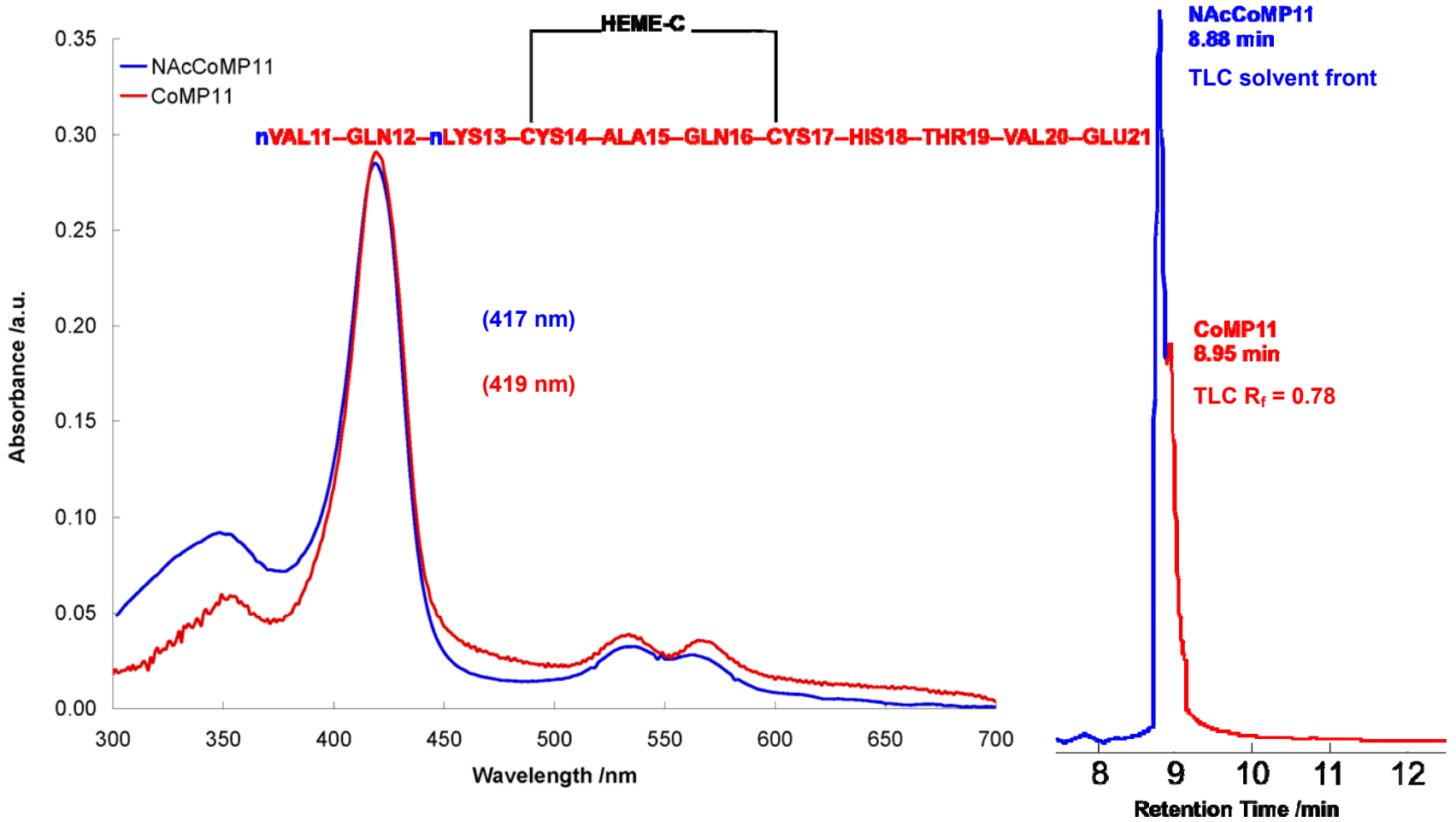


Figure 3.4 The UV-vis spectrum of CoMP11 (red) and NAcCoMP11 (blue). All samples were run in degassed deionised water, *ca*. pH 7, 25 ^{o}C. The corresponding HPLC chromatogram appears alongside with NAcCoMP11 (blue) and CoMP11 (red). The hemepeptide representation refers to CoMP11 (red) with acetylated NAcCoMP11 (blue) represented by n = -$COCH_3$ group. Typically heme-*c* has iron(III) as the central metal ion in the porphyrin moiety. Here this has been replaced by cobalt(III).

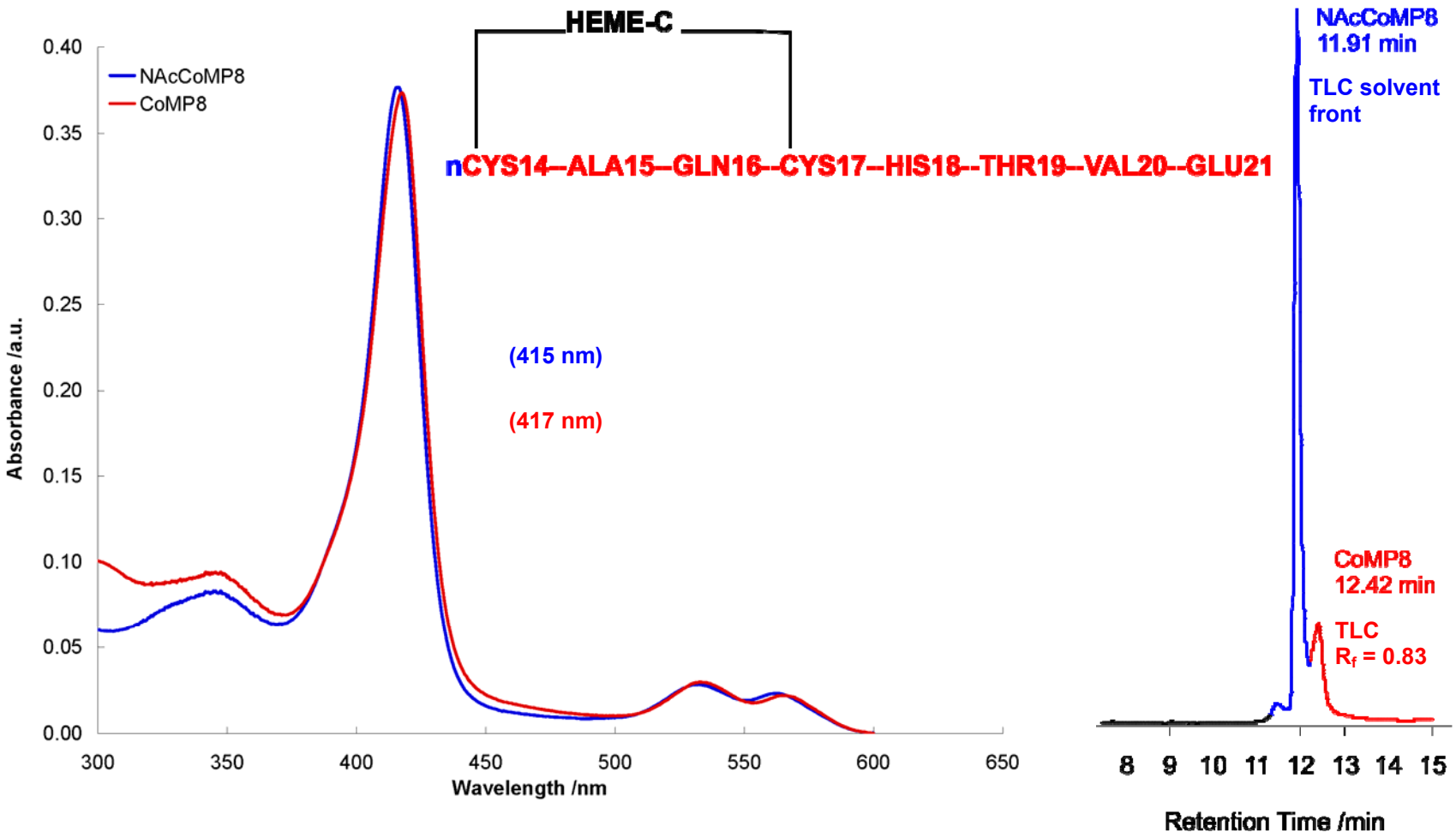


Figure 3.5 The UV-vis spectrum of CoMP8 (red) and NAcCoMP8 (blue). All samples were run in degassed deionised water, *ca*. pH 7, 25 ^{o}C. The corresponding HPLC chromatogram appears alongside with NAcCoMP8 (blue) and CoMP8 (red). The hemepeptide representation refers to CoMP8 (red) with acetylated NAcCoMP8 (blue) represented by n = -$COCH_3$ group. Typically heme-*c* has iron(III) as the central metal ion in the porphyrin moiety. Here this has been replaced by cobalt(III).

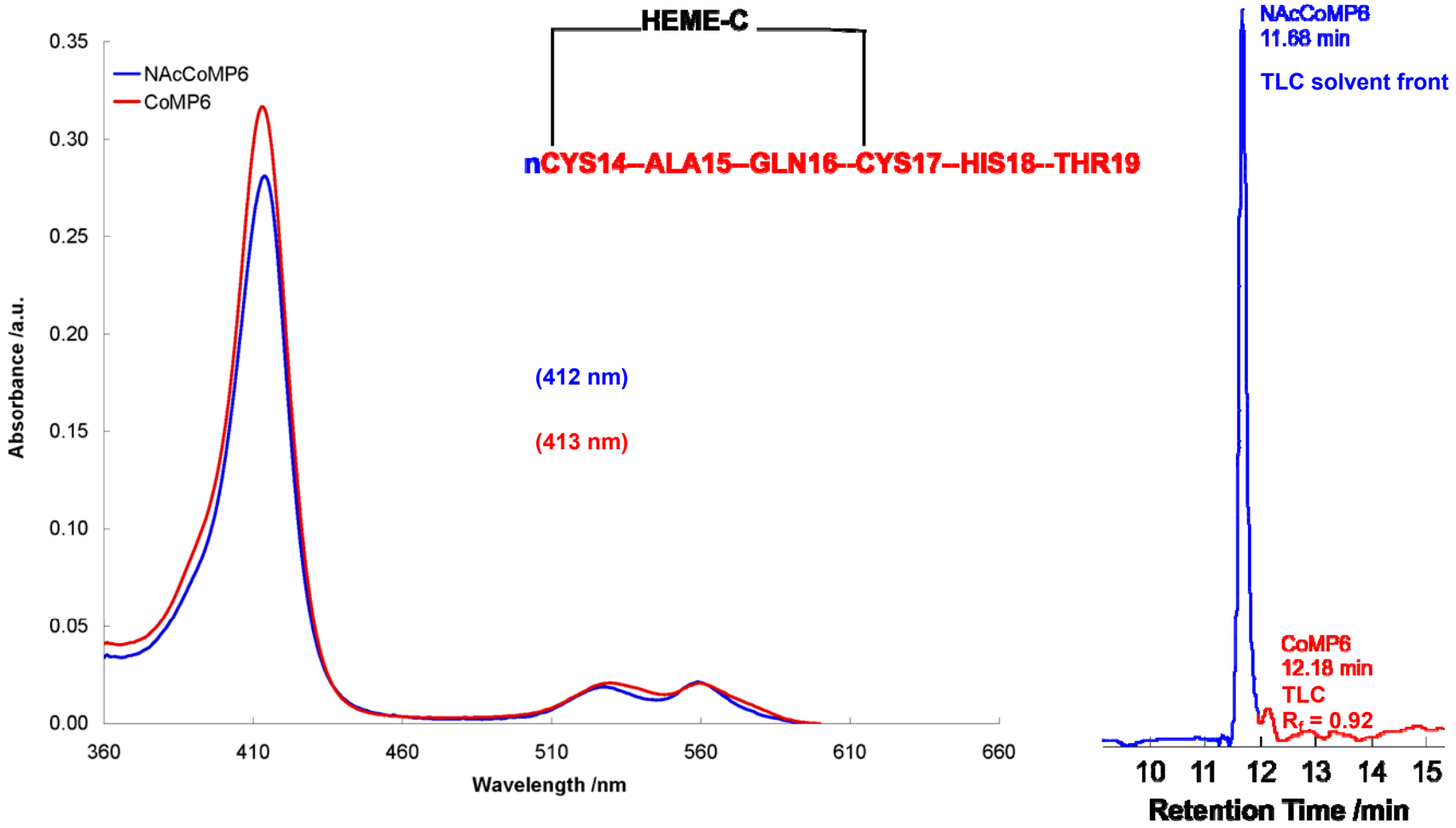


Figure 3.6 The UV-vis spectrum of CoMP6 (red) and NAcCoMP6 (blue). All samples were run in degassed deionised water, *ca*. pH 7, 25 ^{o}C. The corresponding HPLC chromatogram appears alongside with NAcCoMP6 (blue) and CoMP6 (red). The hemepeptide representation refers to CoMP6 (red) with acetylated NAcCoMP6 (blue) represented by n = -$COCH_3$ group. Typically heme-*c* has iron(III) as the central metal ion in the porphyrin moiety. Here this has been replaced by cobalt(III).

The cobalt microperoxidases CoMP11 and NAcCoMP11 were obtained as by-products of NAcCoMP8 synthesis (Route D). These were isolated using Sephadex G-50 gel permeation chromatography. Contaminants were possibly undigested cytochrome *c* and presumably CoMP9.[28] These were present in trace amounts, insufficient for LCMS analysis. CoMP9, though briefly isolated, formed insoluble aggregates and could not be analysed further. Acetylation was attempted on the aggregated CoMP9 sample without success (**Appendix 3.5**).

NAcCoMP6 was obtained as a by-product of NAcCoMP8 synthesis through the trypic digestion of NAcCoMP11 (Route D). CoMP6 was obtained when CoMP8 was synthesized through the tryptic digestion of CoMP11. Both NAcCoMP6 and CoMP6 were purified using Sephadex G-15 gel permeation chromatography. Contaminants were possibly undigested cytochrome *c* and presumably CoMP5.[28] These were present in trace amounts insufficient for LCMS analysis.

Electronic spectra were recorded for all cobalt(III) microperoxidases (**Figures 3.4-3.6**). Spectral features common to all samples were the four distinct bands observed at *ca*. 350 nm, 415 nm, 530 nm and 560 nm. The broad N-band and intense Soret-band (B-band) occurred at *ca.* 350 and 415 nm, respectively. The Soret usually occurred with a vibrational component present as a high-energy shoulder, B(1,0).[35] In contrast, Mn(III)MP8 displayed split Soret-bands which was attributed to inequivalent interactions between the pophyrin p_x and p_y LUMOs and d_p electrons in the manganese ion.[29] In NAcCoMP8 the Q-bands were found at 530 (Q_v) and 560 nm (Q_o), respectively with no charge transfer bands observed in that region. In contrast, FeMP8 species exhibited charge transfer bands in the 550- 650 nm region.[23] Both the Q_o and Soret-bands are due to transitions from π (a_{1u}, a_{2u}) to π*(e_g*) porphyrin orbitals.[35]

Importantly, whilst the Soret was observed to shift (*ca.* 4-5 nm) between the non-acetylated and acetylated species in each cobalt(III) microperoxidase spectrum, the overall spectral profile remained the same. This observation suggested that the acetylation procedure may be an acceptable protection method since the electronic structure of the porphyrin appeared unperturbed.

Interestingly, the Soret exhibited a small *blue* shift when going from a non-acetylated to acetylated cobalt(III) microperoxidase species. If it is assumed that this blue shift is due to the monomerisation of cobalt(III) microperoxidases upon acetylation, then this suggests a red shift (bathochromic) in the electronic spectrum of the *aggregate*. Bathochromic shifts in organic dyes have been associated with the so-called *J*-type aggregation in solution.[30-34] *J*-type aggregates typically undergo supramolecular self-organisation to exhibit a one-dimensional parallel end-to-end type molecular arrangement.[30] This type of molecular arrangement may have several conformations such as 'ladder', 'staircase' and 'brickwork' (**Figure 3.7**).[30] *H*-type aggregates, by contrast, exhibit a perpendicular face-to-face molecular arrangement that conforms to a 'sandwich' type of stacking.[34] Whilst current information pertaining to *H*- and *J*-type aggregates is relatively limited,[34] this information does present an idea of what type of aggregation may be occurring in cobalt(III) microperoxidases in solution (**Figure 3.7**). It is more plausible that cobalt(III) microperoxidases exhibit a *J*- rather than *H*-type aggregation given the positioning of the bulky proximal His-18 ligand. This type of aggregation was suggested and explored in FeMP11 and FeMP8 as well. [16, 17]

The supporting HPLC and TLC data indicate that the acetylated cobalt(III) microperoxidases moved faster through the solid phase than their non-acetylated counterparts, undoubtedly due to interaction between the free amino groups in the latter and the solid support.

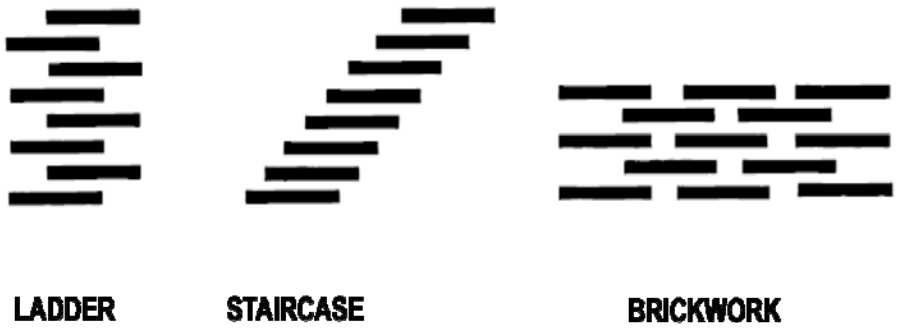


Figure 3.7 An adapted[30] representation of the various *J*-type aggregates that may be exhibited by concentrated cobalt(III) microperoxidases in solution.

3.2.2 Factors influencing the aggregation of NAcCoMP8 during synthesis

The factors influencing aggregation of NAcCoMP8 during synthesis were investigated in terms of (i) a comparative investigation of the effect of aggregation on NAcCoMP8 by varying isolation procedures utilised during synthesis from Amicon® cell to Sep-Pak® cartridges; (ii) a comparative analysis of FeMP11 band separation using gel permeation chromatography and, (iii) a spectroscopic observation of aggregation, degradation and pH in NAcCoMP8.

3.2.2.1 Amicon® vs Sep-Pak® observations on NAcCoMP8

High concentrations of the hemepeptides and a high ionic strength have been reported to promote aggregation.[24.25] Both these conditions are common during the synthesis of NAcCoMP8 and initiate the aggregation effects observed during the solution studies. For example, high microperoxidase concentrations are utilised in the acetylation and demetalation procedures (**Section 2.2.1**). A high ionic strength environment occurs in the ammonium sulphate 'salting-out' step traditionally employed to precipitate proteins and peptides (**Route A**). Both high microperoxidase concentrations and high ionic strengths are found during the desalting step that utilises an Amicon® cell over many hours. Thus, it followed that synthetic strategies needed to be effected in order to limit prolonged exposure to these conditions. One strategy employed to limit these conditions was to replace the Amicon® cell desalting and concentrating step with a Sep-Pak® cartridge.

Synthetic Route C was utilised twice in this investigation (**Section 2.2.1**). The first synthesis utilised the Amicon® cell as the means of isolation, desalting and concentrating whilst the second synthesis utilised the Sep-Pak® cartridge for this purpose. The procedures employed for the utilisation of both isolation procedures were conducted as previously mentioned (**Chapter 2**). The NAcCoMP8 sample obtained from each synthesis was then clarified and

lyophilised. Percentage yields, UV-vis, HPLC and TLC were compared (**Table 3.2; Figure 3.8**).

Table 3.2 Comparison of Amicon® cell and Sep-Pak® cartridge desalting procedures. Percentage yields, HPLC and TLC data for NAcCoMP8 obtained from Amicon® and from Sep-Pak® desalting methods.

Desalting Method	Estimated Procedure Time (Hours)	HPLC R_t (Min)[b]	TLC R_f [b]	% Yield (by mass)
Amicon Cell	5 - 6	15.22	Streak[a]	64.3
Sep-Pak®	1 - 2	13.51	Solvent front	76.1

[a] sample streaked from baseline to solvent front.

[b] methods as previously described (**Chapter 2**).

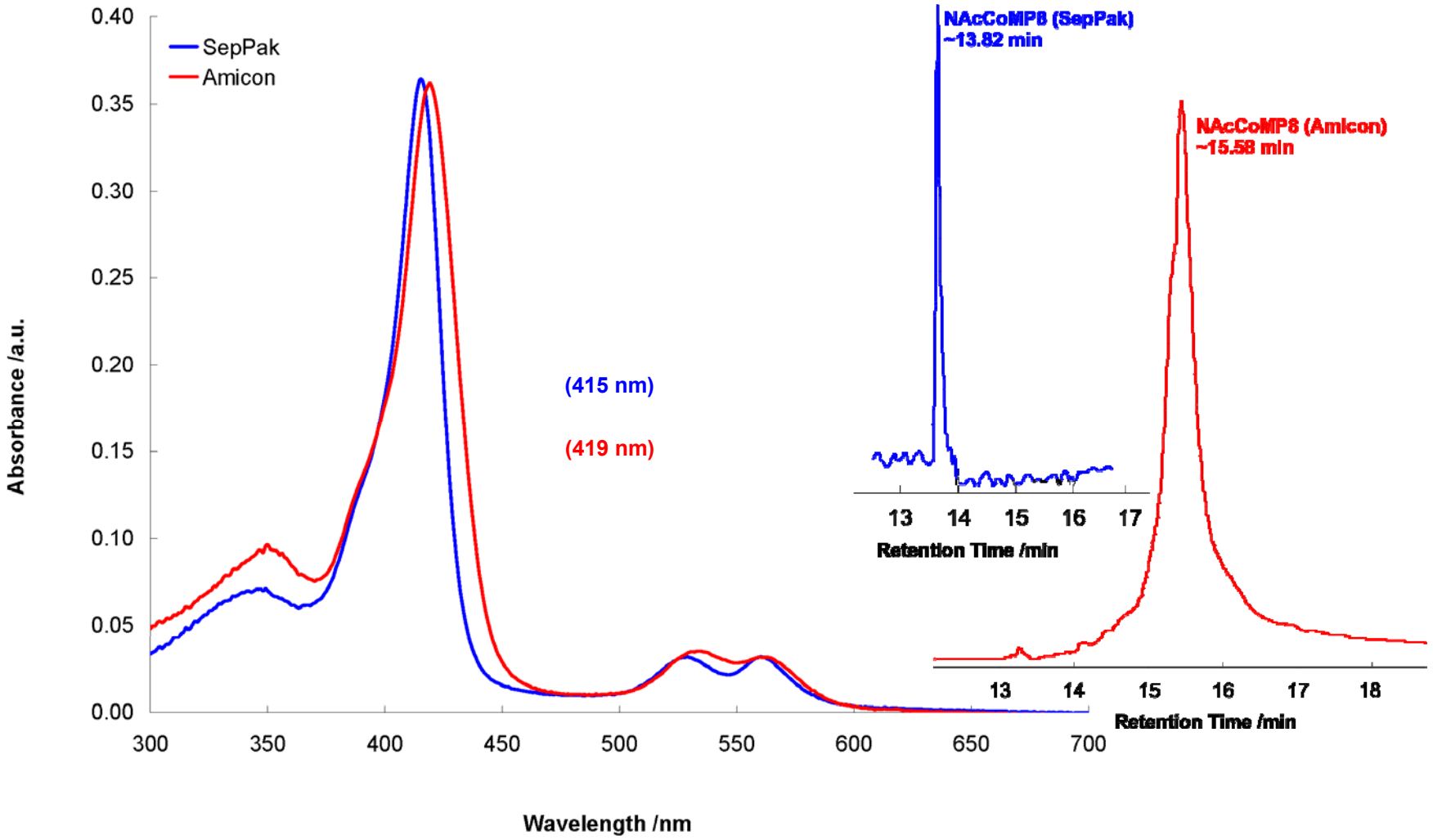


Figure 3.8 The effect of separation technique on the aggregation of NAcCoMP8. UV-vis spectra of NAcCoMP8 from Amicon® (red) and from Sep-Pak® (blue) were obtained in degassed deionised water, *ca*. 25°C, pH 7.

The Amicon® and Sep-Pak® method of desalting and concentrating were investigated using synthetic Route C. HPLC, TLC, masses and electronic spectra were compared for each sample. HPLC data suggested that there was a cleaner separation after the Sep-Pak® system was applied as compared to the Amicon®. In the case of the Amicon® cell, samples had broader peaks that were retained longer (*ca*. 2 minutes longer) by the column than by the Sep-Pak® system.

Supporting TLC evidence suggested that there were mixed species in the Amicon® sample. The Amicon® sample exhibited irreproducible, non-concentration dependent streaking patterns from baseline to solvent front (e.g. feathering, tailing, eclipsing) (**Appendix 3.4**). This streaking may also be attributed to microperoxidase interactions with the solid phase. In the case of the Sep-Pak® system, NAcCoMP8 moved with the solvent front as was consistent with the evidence found in other acetylated cobalt(III) microperoxidases systems (**Figure 3.4-3.6**).

Percentage yield, by mass of NAcCoMP8 using the Sep-Pak® system was consistent with the yield obtained in Route C (**Section 3.2.1.1**). In contrast, the Amicon® system revealed a lowered in yield (*ca*. 12%) as compared to Route C. This lowered yield may be attributed to loss of mass after filtering out the visible insoluble aggregates that were observed during clarification. The Sep-Pak® system showed a significant improvement in yield as compared to the Amicon® system (*ca.* 12%). This improvement was consistent with the yields found in Route A and A' (*ca*. 11%) and Route A and C (*ca.* 8%), where the main synthetic difference was in the use of Sep-Pak® cartridges (**Section 3.2.1.1**).[23]

The electronic spectrum for NAcCoMP8 samples obtained using the Amicon® system were broader relative to the spectrum from the Sep-Pak® system. After purification using the Sep-Pak® system, there was a small blue shift observed in the spectrum (**Section 3.2.1.2**).

Desalting, concentration and purification using the Amicon® cell was estimated

to take about 50% longer than the Sep-Pak® system. This is perhaps the main contributing factor that lowers the yields in the Amicon® system. Lower yields are directly related to the amount of aggregation in the system; aggregation is exacerbated by microperoxidases being in solutions of high concentration and ionic strength over extended periods of time. It is postulated that in the case of the Sep-Pak® system, NAcCoMP8 is immobilised onto the C18 resin thereby limiting self-interactions. The sample is then rapidly washed with fresh aliquots of deionised water in order to swiftly remove salts and lower the overall ionic strength of the system. This is in direct contrast to the Amicon® system where the sample stirs in the same solution of high concentration and ionic strength as the salts are slowly removed by pressure diffusion through a membrane.

3.2.2.2 Gel permeation chromatography of FeMP11

The synthesis of a specific microperoxidase is often contaminated by other digestion products.[25] These digestion products may include unreacted cytochrome *c* or other microperoxidases. These microperoxidases are of varying peptide chain length, but the central porphyrin chromophore is still retained in each. Thus it would be anticipated that the spectroscopic properties of these various microperoxidases in solution would be similar. It therefore becomes critical to remove these contaminating microperoxidases so as not to further complicate the solution chemistry data.

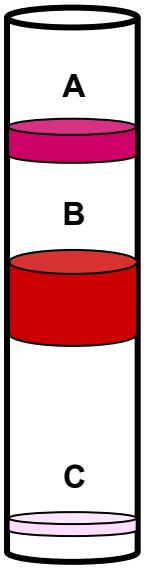
The peptic digestion of cytochrome *c* to synthesize FeMP11 has other digestion products present in very small quantities (*ca*. < 5%) as contaminants. FeMP11 is a precursor to FeMP8 and thus to the target molecule, NAcCoMP8. It is therefore important that the initial precursors are free from contaminants. The contaminants found in FeMP11 may be separated during the gel permeation chromatography (**Section 2.2.2**) part of the synthesis.

Synthesis of FeMP11 and associated procedures were carried out as described previously (**Chapter 2, Route C**). Purification by gel permeation

chromatography revealed three bands (**Table 3.3**). Each band was clarified, lyophilised and weighed (**Section 3.2.1.1**). Masses, HPLC, TLC and UV-vis data were compared. UV-vis data were acquired as described (**Appendix 3.3**).

A stock solution of each band (*ca*. 1.80 μM; pH 7) was freshly prepared in degassed deionised water. The samples were allowed to stir for about 2 hours to reach equilibrium before filtering with Millex® syringe-filters (**Section 2.2.2**). Thereafter, a 2 mL sample was transferred into an argon-filled 1.0 cm pathlength cuvette fitted with a septum. A UV-vis spectrum was recorded between 300 – 600 nm (**Figure 3.9**).

Table 3.3 Analysis of the bands obtained after FeMP11 gel permeation chromatography. Estimated percentage composition, HPLC and TLC data for each component for each band (contaminant) is compared.

G-50 Band Separation [d]	Possible Identity	Estimated Composition (%)[a]	MS (m/z)	HPLC R_t (Min)	TLC R_f
	A				
	FeMP9	3	1635	11.77	0.20[c]
	B				
	FeMP11	97	1863	8.22	0.27
	C				
	Cytochrome-*c*	<1	[b]	12.58	0.00

[a] Estimated over total mass of A, B and C. FeMP11 was lyophilised and weighed before size exclusion chromatography. Each band was collected, lyophilised and weighed separately after lyophilisation. These masses were used to estimate percentage composition of each microperoxidase over the total mass before separation.

[b] Too little sample to obtain reliable data; identity estimated by UV-Vis and TLC.

[c] Irreproducible TLC data due to excessive aggregation; value estimated over 5 plates (**Appendix 3.5**).

[d] The diagram is a schematic representation of the G-50 column after *ca* 90 minutes of elution.

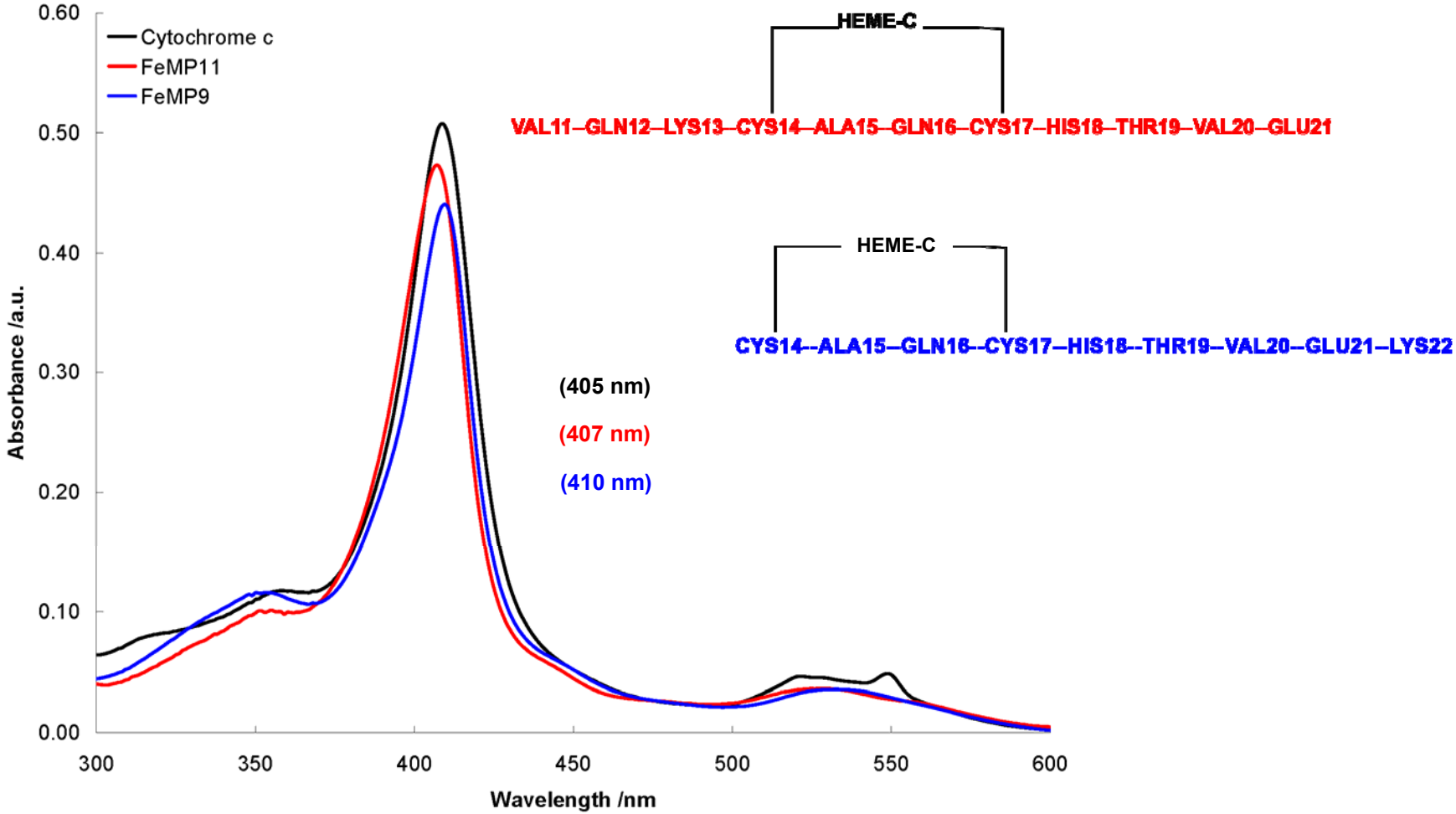


Figure 3.9 UV-vis spectra of the iron microperoxidase contaminants after FeMP11 purification on gel permeation chromatography. UV-vis spectra of cytochrome *c* (black), FeMP11 (red) and FeMP9 (blue) were obtained in degassed deionised water, *ca*. 25°C, pH 7.

FeMP11 was purified using gel permeation chromatography and bands were separated based on molecular size. The separation was not immediately obvious as the bands moved as a unified smear. However, after *ca*. 90 minutes, three bands became apparent: a small dark pink-red band (A); a major thick red-brown band (B); and a very light pink shadow (C). These bands were desalted, clarified, lyophilised, weighed and analysed where possible (**Table 3.3**).

Masses revealed that band B was the major product (*ca.* 97%) of the cytochrome *c* peptic digestion whilst bands A and C were minor products (*ca.* 3%). Band B was confirmed as FeMP11 using MS and UV-vis (**Table 3.3**). Band C was identified as cytochrome *c* by UV-vis spectroscopy and by TLC. Elucidating the identity of band A was problematic as the sample appeared to aggregate almost immediately; this was particularly noticeable on TLC plates. Data for band A were therefore estimated at very low concentrations (**Figure 3.9**).

3.2.2.3 General spectroscopic observations in NAcCoMP8

NAcCoMP8 displayed an array of colours in solution during synthesis. These colours were observed to fluctuate in relation to factors such as pH, states of aggregation and of degradation.

The pH of the solution was found to affect the spectra of NAcCoMP8. A stock solution of NAcCoMP8 (*ca*. 1.80 μM; pH 7, 25 ^{o}C) was freshly prepared in degassed deionised water. The sample was allowed to stir for about 2 hours to reach equilibrium before filtering with a Millex® syringe-filter. A 2 mL sample from the prepared stock solution was transferred into an argon-filled 1.0 cm pathlength cuvette fitted with a septum. An initial UV-vis spectrum of monomerised NAcCoMP8 was recorded between 300 – 700 nm. Thereafter, the pH of this sample was lowered (*ca*. pH 2-3) using negligible amounts of neat perchloric acid. The sample was allowed to stir (*ca*. 15 minutes) under argon

before the UV-vis spectrum stabilised. The procedure was repeated with a fresh sample of NAcCoMP8 for the basic region (*ca*. pH 8-10; NaOH; 8 M). The spectra are reported alongside samples showing the relevant colour changes of NAcCoMP8 in solution. For comparison a photograph of a sample of deionised water is included (**Figure 3.10**).

The effects of aggregation on NAcCoMP8 spectra were observed as follows. An initial UV-vis spectrum of monomerised NAcCoMP8 was recorded as described in the pH experiment above. The NAcCoMP8 sample was then allowed to stir overnight at room temperature and a spectrum was recorded as previously. This procedure was repeated with the same sample over a few days in order to elucidate the different stages of aggregation. No stable spectra were obtained for insoluble aggregates in solution. The spectra are reported alongside samples showing the relevant colours of NAcCoMP8 in solution (**Figure 3.11**).

The effects of degradation on NAcCoMP8 spectra were monitored in a similar manner. An initial UV-vis spectrum of monomerised NAcCoMP8 was recorded as described in the pH experiment above. Thereafter, the sample was transferred to a round-bottomed flask under argon and treated in a sonic bath (*ca*. 30 minutes) to expedite degradation. The sample was transferred back into the cuvette and a spectrum was recorded. This procedure was repeated in order to facilitate complete degradation (a further 30 – 60 minutes). The spectra are shown in (**Figure 3.12**).

The NAcCoMP8 solutions mentioned above were also used to acquire the superimposed supporting data where available (*cf*. TLC and HPLC; **Section 2.2.2**). However, given the various states of speciation, aggregation and degradation in solution as well as related solubility issues, supporting data were found to be irreproducible. As such, the supporting data were typically estimated as an average of 3 repeats.

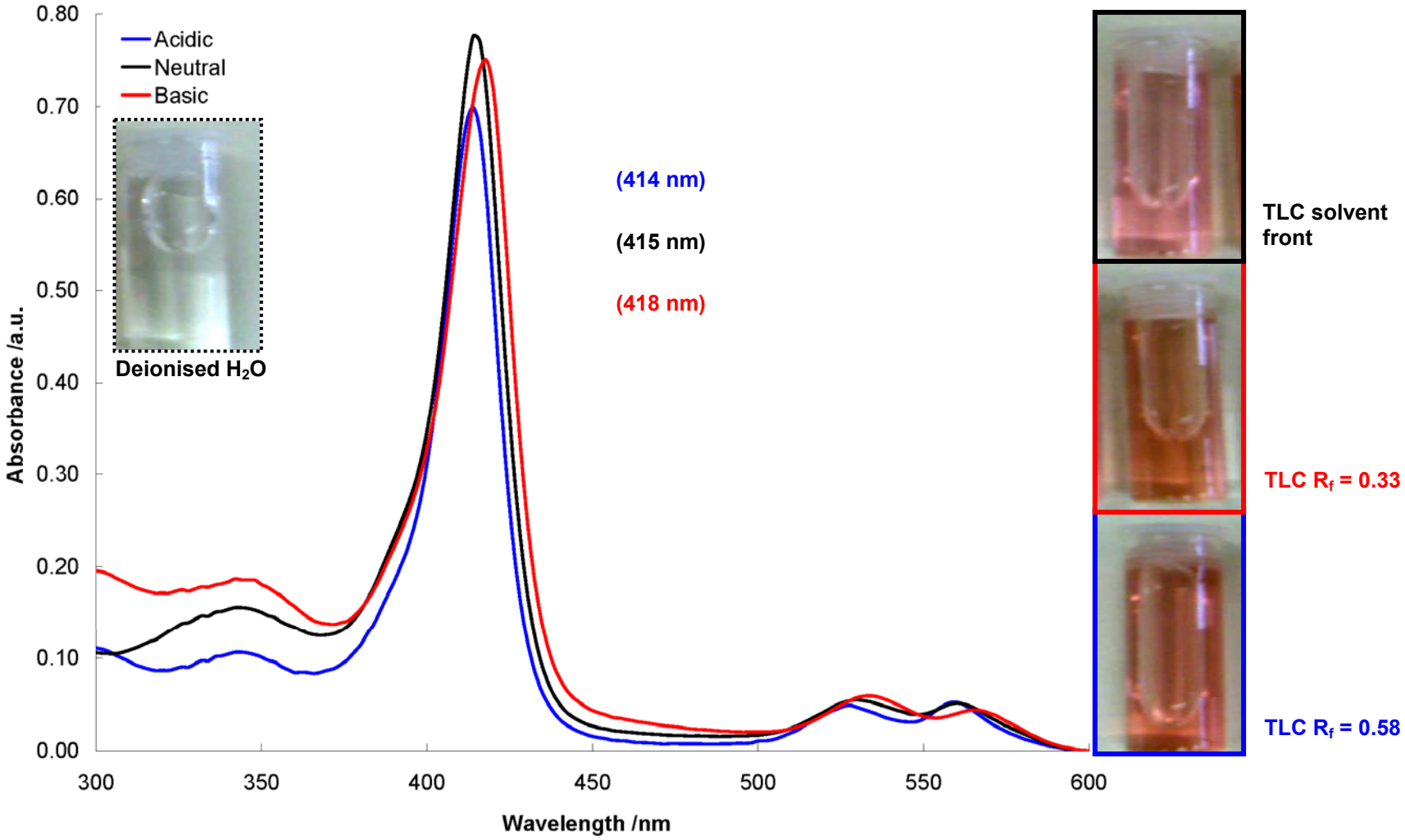


Figure 3.10 UV-vis spectra of NAcCoMP8 at varying pH: (**A**) neutral, (**B**) basic and (**C**) acidic pH in (**D**) deionised water.

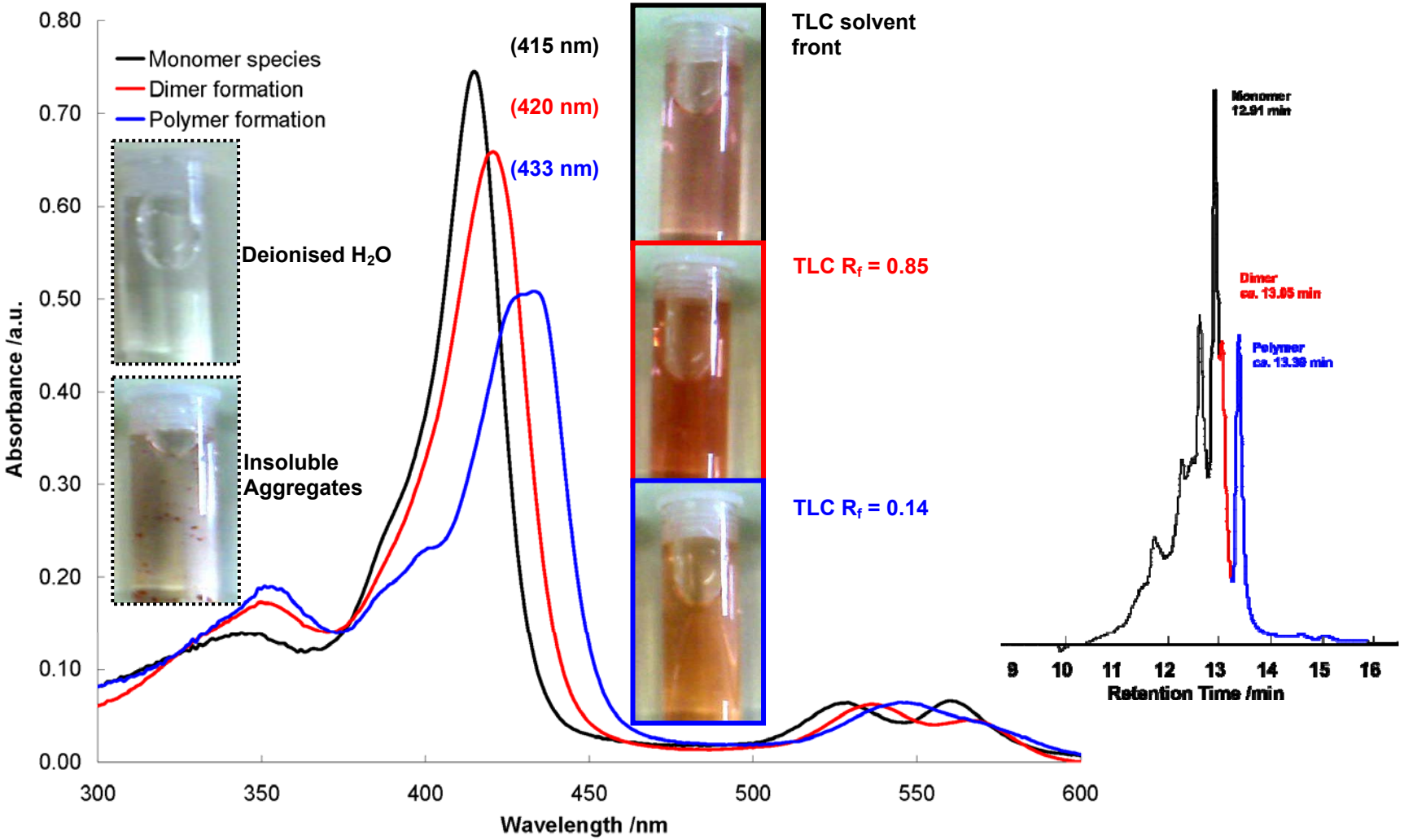


Figure 3.11 UV-vis spectra of NAcCoMP8 at varying states of aggregation: (A) monomer, (B) dimer, (C) polymer in (E) deionised water. Spectrum of (D) visible aggregates could not be obtained.

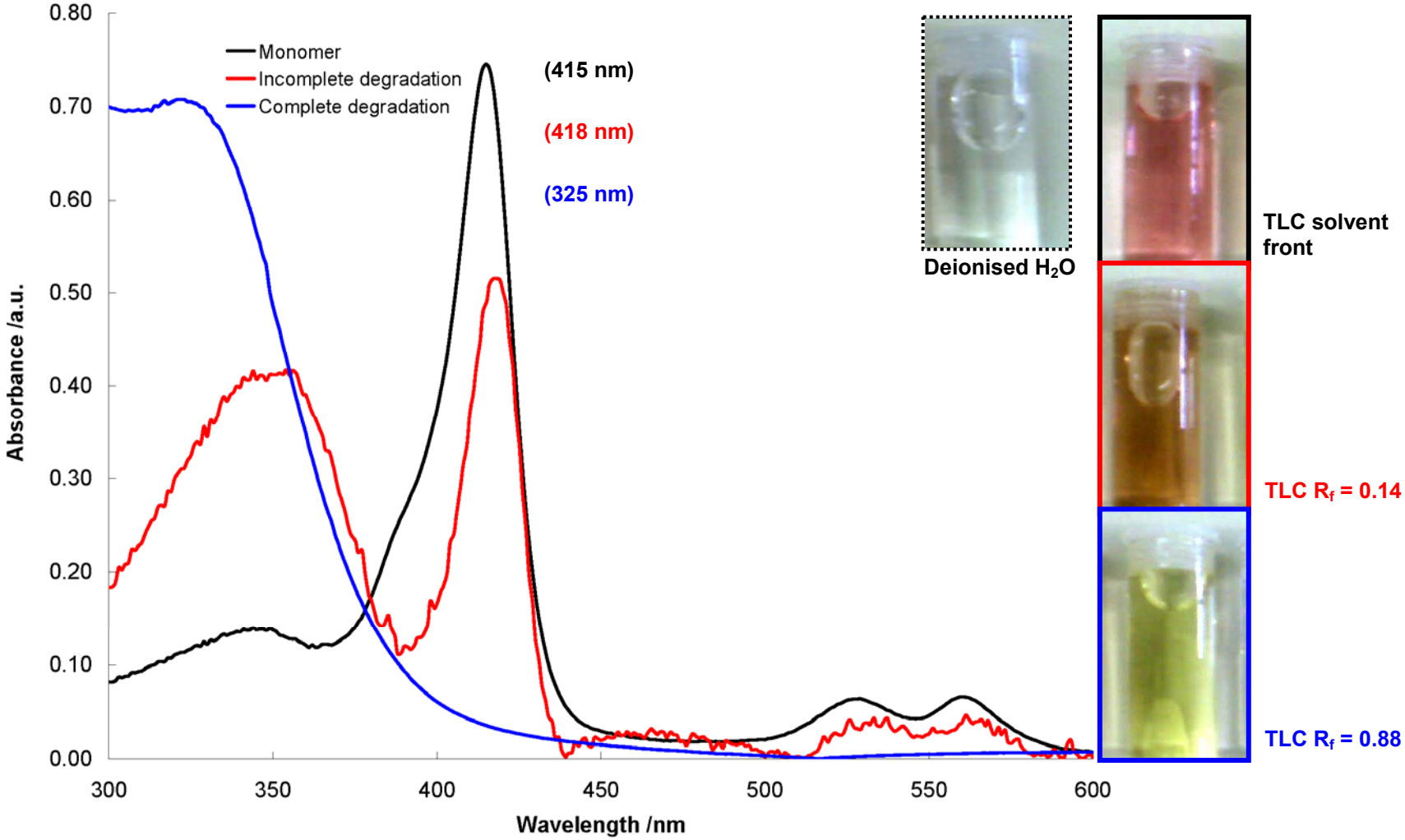


Figure 3.12 UV-vis spectra of NAcCoMP8 at varying states of degradation: (A) clear monomer, (B) turbid incomplete and (C) complete degradation in (D) deionised water.

The effects of pH on NAcCoMP8 UV-vis spectra were observed. The orange-pink basic (*ca*. pH 8 – 10) sample exhibited a slight red shift relative to the clear light-pink neutral species. In contrast, the darker pink acidic (*ca.* pH 2 – 3) sample exhibited a slight blue shift. The TLC data suggests that the basic species travels slower up the solid phase than the acidic species. This may be due to the interaction of the deprotonated carboxylic groups on the microperoxidase with the solid phase.

The dark orange-pink dimer sample exhibited a pronounced red shift and hypochroism relative to the light pink monomer sample. The shift is probably due to initial π-π interactions and subsequent coordination of the His-18 moiety to the cobalt(III) ion of another microperoxidase (see **Chapter 4**). This ordering may be the reason why the dimer moved faster on TLC relative to the disordered polymer. The disordered lighter slightly cloudy orange polymer formation exhibited an even more pronounced red shift coupled to distinct hypochroism, band broadening and N-band formation. When the polymer sample was allowed to reach a higher concentration through slow evaporation, insoluble aggregates became visible.

Sonication of NAcCoMP8 causes its degradation which is clearly observed in the UV-vis spectra. The orange-brown partially degraded solution exhibits a distinct red shift relative to the light pink monomer sample. Furthermore, a band formation was observed in the UV region (*ca.* 350 nm). The solution itself became turbid, producing a noisy spectrum. The completely degraded solution turned bright yellow with a complete disappearance of the Soret. This is likely caused by the oxidation and cleavage of the porphyrin ring resulting in the formation of the bright yellow biliverdin.[36]

3.3 SUMMARY AND CONCLUSIONS

This Chapter dealt with the optimisation of NAcCoMP8 yields by minimising aggregation during synthesis. Aggregation was minimised by optimising the acetylation step to limit metal–side-chain interactions and by regulating the solution environment with regards to concentration and pH in order to limit π-π interactions. This was achieved by investigating the effects of acetylation on percentage yield of NAcCoMP8; by observing the spectral changes of three different acetylated cobalt(III) microperoxidases; by observing the effects of desalting and concentrating procedures on the yield of NAcCoMP8; and by observing spectral changes in NAcCoMP8 relative to pH, aggregation and degradation.

Acetylation and demetallation steps of NAcCoMP8 were investigated in terms of percentage yield. Percentage yields for NAcCoMP8 syntheses suggested that acetylating and demetallating the precursor FeMP11 as soon as possible in addition to utilising the Sep-Pak® system afforded the greatest increase in yield (*ca*. 19%).

Three cobalt(III) microperoxidases were investigated in relation to their acetylated counterparts. These were CoMP11, CoMP8 and CoMP6; and their acetylated counterparts, NAcCoMP11, NAcCoMP8 and NAcCoMP6. UV-vis data suggests that although a slight blue shift may be observed in the acetylated species, the spectral profile remains consistent with the non-acetylated species. TLC and HPLC data suggested that the acetylated species moved faster through the solid phase than the non-acetylated species.

The effects of desalting and concentrating procedures on the yield of NAcCoMP8 were investigated. The utilisation of Sep-Pak® cartridges increased the yield by *ca*. 12% relative to the Amicon® cell. This is likely due to the immobilisation of NAcCoMP8 onto the C18 resin followed by the rapid desalting procedure as compared to the previously utilised Amicon® cell.

The spectral changes in NAcCoMP8 relative to pH, aggregation and

degradation were investigated. Distinctive colour changes were observed in acidic and basic solutions as compared to neutral solutions; in monomer, dimer and polymer solutions; and in partially degraded and fully degraded solutions (see **Chapter 4**).

3.4 REFERENCES FOR CHAPTER 3

1 Tsou, C. L., *Biochem. J*, **1951**, *49*, 362.

2 Tsou, C. L., *Biochem. J.*, **1951**, *49*, 367.

3 Carraway, A. D.; McCollumn, M. G.; Peterson, J., *Inorg. Chem.,* **1996**, *35,* 6885.

4 Wilson, M. T.; Ranson, R. J.; Masiakowski, P.; Czarnecka, E.; Brunori, M., *Eur. J. Biochem*., **1977**, *77*, 193.

5 Othman, S.; Le Lirzin, A.; Desbois, A., *Biochemistry*, **1993**, *32* 9781

6 Verbaro, D.; Hagarman, A.; Kohli, A.; Schweitzer-Stenner, R., *J. Biol. Inorg. Chem.*, **2009**, *14(8)*, 1289.

7 Riposati, A.; Prieto, T.; Shida, C. S.; Nantes, I. L.; Nascimento, O. R., *J. Inorg. Biochem*., **2006**, *100(2)*, 226.

8 Baldwin, D. A.; Mabuya, M. B.; Marques, H. M., *S. Afr. J. Chem.*, **1987**, *40(2)*, 103.

9 Aron, J. A.; Baldwin, D. A.; Marques, H. M.; Pratt, J. M.; Adams, P. A., *J. Inorg. Biochem.*, **1986**, *27*, 227.

10 Pasternack, R. F.; Parr, G. R., *Inorg. Chem*., **1976**, *15*, 3087

11 Chuang, W. J.; Chang, Y. D.; Jeng, W. Y., *J. Inorg. Biochem*., **1999**, *75(2)*, 93.

12 Ehrenberg, A.; Theorell, H., *Acta Chem. Scand.*, **1955**, *9*, 1193.

13 Pasternack, R. F.; Francesconi, L.; Raff, D.; Spiro, E., *Inorg. Chem.*, **1973**, *12*, 2606.

14 Brown, S. B.; Hatzikonstantinou, H., *Biochim. Bophys. Acta*, **1979**, *585*, 143.

15 Scheer, H.; Katz, J. J.; in K. M. Smith (ed.), *Porphyrins and Metalloporphyrins*; Elsevier Scientific Publishing Company, Amsterdam, 1975, pp 399-524

16 Urry, D. W.; Pettegrew, J. W., *J. Am. Chem. Soc.*, **1967**, *89*, 5276.

17 Urry, D. W., *J. Am. Chem. Soc.*, **1967**, *89*, 4190.

18 White, W. I., in D. Dolphin (ed.), *The Pophyrins*, vol. 5, Academic Press, London, 1978, pp. 303-339.

19 Medford, C. J., in K. M. Kadish, K. M Smith, R. Guilard (eds.), *The Porphyrin Handbook*, vol 5, Academic Press, London, 2000, pp 46-60

20 Peterson, J.; Silver, J.; Wilson, M. T.; Morrison, I. E. G., *J. Inorg. Biochem.*, **1980**, *13,* 75.

21 Wang, J. S.; van Wart, H. E.; *J. Phys. Chem.*, **1989**, *93*, 7925.

22 Munro, O. Q.; Marques, H. M., *Inorg. Chem.*, **1996**, *35*, 3752

23 Sannasy, D., M.Sc. Dissertation, University of the Witwatersrand, Johannesburg, South Africa, **2005**.

24 Harbury, H. A.; Loach, P. A., *Proc. Natl. Acad. Sci. U.S.A.*, **1959**, *45*, 1344.

25 Harbury, H. A.; Loach, P. A., *J. Biol. Chem.*, **1960**, *235*, 3640.

26 Marques, H. M.; Shongwe, M. S.; Munro, O. Q.; Egan, T. J., *S. Afr. J. Chem.,* **1997**, *50*, 166.

27 Adams, P. A.; Baldwin, D. A.; Marques, H. M., in Scott, R. A.; Mauk, A. G. (eds.), *Cytochrome c: A Multidisciplinary Approach*, University Science Books, Sausalito, California, 1996, pp. 635-692.

28 Peterson, J.; Saleem, M. M. M.; Silver, J.; *J. Inorg. Biochem.*, **1983**, *19,* 165.

29 Low, D. W.; Abedin, S.; Yang, G.; Winkler; J. R., Gray, H. B., *Inorg. Chem*. **1998**, *37*, 1841.

30 http://www.dstuns.iitm.ac.in/teaching-and-presentations/teaching/undergraduate%20courses/cy306-structure-and-energetics-of-biomolecules/presentations/H-%20and%20J-%20Aggregates.pdf *Source*: Pradeep; T.; DST Unit of Nanoscience, Department of Chemistry, Indian Institute of Technology, Madras, Chennai, India; pradeep@iitm.ac.in; (06-11-2011).

31 Jelley, E. E., *Nature,* **1936**, *138*, 563.

32 Scheibe, G.; Kandler, L., *Angew. Chem.,* **1936**, *49*, 563.

33 Maiti, N. C.; Mazumdar, S.; Periasamy, N., *J. Phys. Chem. B,* **1998**, *102,* 1528.

34 Gadde, S.; Batchelor, E. K.; Weiss, J. P.; Ling, L.; Kaifer, A.E., *J. Am. Chem. Soc.,* **2008**, *130*, 17114.

35 Marques, H.M., Ph. D. Dissertation, University of the Witwatersrand, Johannesburg, South Africa, **1986**.

36 Frakenberg, N.; Lagarias, J. C.; in K.M. Kadish; K. M. Smith; R. Guilard; (ed.), *The Porphyrin Handbook Volume 13*; Elsevier Scientific Publishing Company, Amsterdam, 2003, pp 211-233

CHAPTER 4
MONOMERISATION OF NAcCoMP8: SOLUTION BEHAVIOUR

4.1 INTRODUCTION

Microperoxidases[1-10], like most metalloporphyins[11-15] have a tendency to aggregate in solution. In the context of this work, a*ggregation* refers to the process whereby a monomer rearranges from dimer to oligomer to polymer and finally to aggregate. As previously described, two types of aggregation were found to be prevalent amongst microperoxidases: non-covalent π-π interactions and covalent metal–side-chain interactions. Also emphasised previously was the need to limit such interactions in order to produce reliable and reproducible solution chemistry data (**Section 3.1**).

The limiting of such interactions is particularly significant if the basis of the technique used for data acquisition is sensitive towards aggregation. For example, electronic spectroscopy of FeMP11 (10 μM, pH 6.9) showed time-dependent spectral changes on dilution, and this was attributed to metal–side-chain aggregation.[31] In addition to electronic spectroscopy[19] other techniques such as Mössbauer,[34] ESR,[46] Raman,[49] NMR,[42,45] optical rotatory dispersion,[19] circular dichroism[19] and magnetic studies[34,45-48] were reported to confirm the presence of FeMP11 aggregation, either in solution or in the solid state. Whilst methods to limit aggregation with these techniques exist, they ideally need to mimic physiological conditions without additional optical interference. Thus, understanding the factors that contribute to each type of interaction assists in forging an experiment-specific plan to limit aggregation relevant to that particular technique.

Non-covalent π-π interactions are common in metalloporphyrins[15-17] and certainly in microperoxidases.[18,19] In the case of microperoxidases, this form of aggregation was observed using spectroscopic techniques such as optical rotation, circular dichroism and difference absorbance spectroscopy.[18,19] Those studies indicated that in the case of FeMP11 and FeMP8, non-covalent π-π interactions occurred between the distal faces of two or more moieties (**Section 3.1**).[18,19] Further studies suggested that those interactions were strongly influenced by concentration, ionic strength, temperature and pH.[20-23] Evidence also indicated that, in general, this type of aggregation might be minimised by dilution[18,19] and elevated temperatures.[18,19] Though not always ideal in mimicking physiological conditions, the use of detergents,[24,25] non-aqueous[26,27]and mixed solvents[28-29] have also been used to limit aggregation in microperoxidases.

Instances of covalent metal–side-chain interaction in microperoxidases are common.[2,31-37] As described previously, this aggregation refers to the coordination of the 6th axial position of one hemepeptide moiety by an amino group of another hemepeptide moiety[2,31-34] thereby leading to multiple species in solution.[2,10,34,35] For example, in the case of FeMP11, the involvement of Val-11 and/or Lys-13 amino groups in aggregation are well documented.[2,33,45] Interestingly, however, when these amino groups are removed, as in the case of FeMP8, the aggregation is observed to diminish relative to FeMP11 thereby leading to a simpler solution chemistry.[40,31,32,36] However, aggregation in FeMP8 is still expected to occur via the terminal Cys-14[8] (**Section 3.1**).

This evidence suggests two important observations: firstly, that these particular amino groups are instrumental in microperoxidase aggregation (*cf*. CoMP9 data, **Appendix 3.1**); and secondly, the removal or alternatively, *protection*, of these amines should minimise aggregation.[31,32] The protection of these coordinating amines through acetylation to successfully limit aggregation in microperoxidases has been well documented (**Section 3.2.1**).[1,4,31,32,35,43,44] This type of aggregation was also found to be strongly influenced by pH, concentration and

temperature.[10,31,32] Interactions were minimised further by the introduction of strongly coordinating axial ligands that compete for the distal coordination site, though this approach is less than ideal and indeed is inappropriate for ligand binding studies.[10,31,32,41,42]

Reproducible data relies upon the cobalt(III) microperoxidase† being monomeric in solution (*cf*. CoMP8 data, **Appendix 3.1**). The overall strategy towards attaining a monomeric cobalt(III) microperoxidase solution was discussed previously (**Section 3.1**). Monomerisation was first approached from a synthesis perspective whereby CoMP8 was structurally modified by acetylation (NAcCoMP8) to suppress metal–side-chain aggregation (**Section 3.2.1**). Additionally, the synthesis was tailored to minimize high temperature, concentration and ionic strength conditions (**Section 3.2.2**). However, despite these modifications, NAcCoMP8 was found to aggregate and/or degrade, in solution under certain conditions (**Figure 4.1**).

The aim of the work presented in this Chapter was therefore to qualitatively investigate the conditions under which a spectroscopically stable and monomeric NAcCoMP8 solution may be prepared (*cf.* Investigation 1.2, **Chapter 2**).

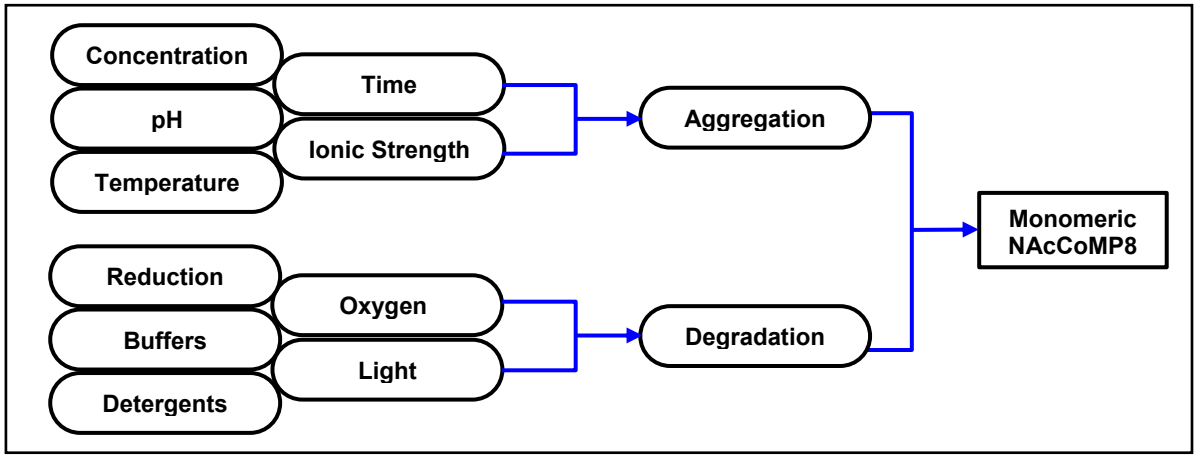


Figure 4.1 A flow diagram of the results focussed on in Chapter 4. In order to achieve a spectroscopically stable and monomeric NAcCoMP8 solution, the factors affecting aggregation and degradation were qualitatively explored in solution.

† It was anticipated that cobalt(III) microperoxidase would be susceptible to aggregation based on the precedence set by FeMP8[35] and other cobalt(III) porphyrins[39] in this regard (**Section 3.1**).

4.2 RESULTS AND DISCUSSION

The rationale behind this investigation was prompted by the initially irreproducible and unstable spectral behaviour of NAcCoMP8 in solution. NAcCoMP8 displayed *apparently* time-dependent spectral shifts (*ca*. 25^{o}C, pH 6.89, deionised water; *cf*. Figure 3.11, **Chapter 3**). In some instances, these spectral shifts were either small or large and the resulting solution was either dark pink or yellow-orange.

The disparity in spectral shifts indicated that the preparation of a spectroscopically stable monomeric solution of NAcCoMP8 may be affected by various factors which influenced the compound's susceptibility to aggregation and to degradation. As noted previously, aggregation was found to be affected by conditions such as ionic strength, concentration, pH, equilibration time and temperature. Degradation was affected by exposure to light, air, reducing agents, dispersants and buffers (**Section 3.2.2.3**). It was thus necessary to qualitatively investigate the solution behaviour of NAcCoMP8 in relation to these conditions in order to prepare solutions containing a stable monomer (**Figure 4.1**). Sources of reagents (**Section 2.4**), technical specifications (**Section 2.4**), specialized (**Sections 2.2.2; 2.2.3**) and general techniques (**Section 2.5**) are given elsewhere.

4.2.1 Effects of Time (equilibrium observations)

At 25 ^{o}C a sample of NAcCoMP8 in deionised water at neutral pH exhibited *apparently* time-dependent spectral shifts (*cf*. Figure 3.11, **Chapter 3**). These spectral shifts appeared to be irreproducible. The spectroscopic stability of NAcCoMP8 is critical for the reproducibility of subsequent quantitative solution chemistry data. It was thus necessary to determine how long, and under what conditions, a freshly prepared sample of NAcCoMP8 was required to stir in order to reach equilibrium.

UV-visible spectra were recorded for NAcCoMP8 over a period of an hour so as to observe any time-dependent spectral shifts at low and at high concentration (**Figure 4.2**). As described previously (**Section 2.2.4**), a 2 mL sample of freshly prepared NAcCoMP8 (*ca*. 1.25 μM; pH 6.89; degassed deionised water, 25 ^{o}C) was transferred into an argon-filled 1.0 cm pathlength cuvette fitted with a septum. An initial spectrum was recorded between 300 – 700 nm. Thereafter a spectrum was recorded ever 5 minutes for an hour (**Figure 4.2A**). The sample was protected from light with aluminium foil between recordings. This procedure was then repeated with a higher NAcCoMP8 concentration (*ca*. 10.0 μM; **Figure 4.2B**).

Spectral features common to all samples were the four distinct bands observed at *ca*. 350 nm, 415 nm, 530 nm and 560 nm. These correspond to the N, B (Soret) and two Q bands (**Section 3.2.1.2**; **Section 5.2.1**). However, what is immediately obvious is the distinct hypochromic red shift at the Soret (417 → 424 nm) observed at the higher NAcCoMP8 concentration with a well-defined isosbestic point at 422 nm (**Figure 4.2B**). There are also distinctive shifts in the Q band region (530 → 538 nm and 560 → 568nm, respectively) with isosbestic points observed at 533, 554, 570 nm (**Figure 4.2B**, insets). The final pink-orange solution was reminiscent of those observed previously (*cf.* Figure 3.11, **Chapter 3**).

This is in stark contrast to the slight hyperchromic blue shift observed at the lower NAcCoMP8 concentrations (417 → 415 nm) (**Figure 4.2A**). There are two poorly-defined isosbestic points observed at 417 and 418 nm, suggesting the presence of multiple equilibria (**Figure 4.2A**, insets). However, an important observation is that despite this initial solution complexity, NAcCoMP8 at low concentration exhibits only small changes to the overall spectral profile. Furthermore, this 415 nm species reproducibly exhibits spectroscopically stability after an hour. The final solution was a slightly darker pink product (*cf*. Figure 3.11, **Chapter 3**).

The equilibration times are compared in **Figure 4.3**. At high NAcCoMP8 concentration (**Figure 4.3B**) the appearance of the 424 nm species and the decay

of the 417 nm species follow apparently simple first order kinetics with k_1 = 0.096 ± 0.002 and 0.087 ± 0.002 min^{-1}, respectively, and a half life of between 7.2 and 8.0 min. The rate constants appear to be wavelength-independent. In contrast, at low concentration these parameters show a distinct wavelength-dependence (**Table 4.1**). This dependence supports the spectroscopic findings in Figure 4.2A that suggested the presence of multiple equilibria. Thus, k values for the appearance of the 415 nm species and decay of the 417 nm species were averaged for selected wavelengths on either side of the Soret (k_{1ave} = 0.030 ± 0.010 and 0.080 ± 0.03 min^{-1}, respectively). Apparent half life values at low NAcCoMP8 concentrations were between 8.7 and 23.1 min (**Figure 4.3A**, showing absorbance data at 407 and 424 nm as an example). Therefore an hour at neutral pH is sufficient time to allow a dilute aqueous solution of NAcCoMP8 at 25 ^{o}C to reach equilibrium.

These observed complexities in the solution behaviour of NAcCoMP8 may be an artefact of isolation (**Section 2.2.2.1**). NAcCoMP8 is typically eluted off C18 solid phase cartridges (Sep-Pak®) using CH_3CN. The purified highly concentrated NAcCoMP8 solution is then frozen and lyophilised in this non-coordinating, dispersing solvent. Under these conditions, it seems plausible that NAcCoMP8, through non-covalent π-π interactions, [18,19] lyophilises as a mixture of weakly associated and disordered oligomers; very likely dimers and tetramers (*cf*. ionic strength evidence, **Section 4.2.4**). On dilution, these moieties then disperse at different rates depending on the identity of the moiety and the mixed dispersal is reflected by the presence of different isosbestic points.

At low concentration, monomeric NAcCoMP8 forms a spectroscopically stable solution with λ_{max} = 415 nm. At sufficiently high monomer concentration, NAcCoMP8 associates further and forms a tightly packed dimer, similar to those observed by Munro and Marques in NAcFeMP8.[35] This likely occurs covalently through metal–side-chain coordination and is observed spectroscopically as a well-defined isosbestic point at 422 nm. Once formed, the 424 nm species does not revert to the 417 nm (or the 415 nm species) on dilution with water or methanol.

Table 4.1 Rate constants (min^{-1}) for the observed conversion of NAcCoMP8 from the 417 to the 415 nm species at low concentration and the conversion of the 417 nm species to the 424 nm at high concentration for selected wavelengths (nm) averaged on either side of the Soret band.

Low [NAcCoMP8]			High [NAcCoMP8]		
λ (nm)	**k_1 (min^{-1})**	**k_{1ave} (min^{-1})**	**λ (nm)**	**k_1 (min^{-1})**	**k_{1ave} k (min^{-1})**
415	0.017(8)		419	0.082(2)	
414	0.024(7)		418	0.085(2)	
413	0.028(7)		417	0.087(2)	
412	0.030(7)		416	0.089(2)	
411	0.034(7)		415	0.091(2)	
410	0.033(7)		414	0.093(2)	
409	0.034(7)		413	0.095(2)	
408	0.033(8)		412	0.098(2)	
407	0.035(9)	0.030(10)	411	0.099(2)	0.091(2)
427	0.062(9)		432	0.079(3)	
426	0.066(9)		431	0.081(3)	
425	0.070(9)		430	0.082(3)	
424	0.073(9)		429	0.083(3)	
423	0.078(9)		428	0.084(3)	
422	0.08(10)		427	0.086(3)	
421	0.09(10)		426	0.087(4)	
420	0.11(20)		425	0.090(5)	
419	0.13(40)	0.080(30)	424	0.096(9)	0.089(6)

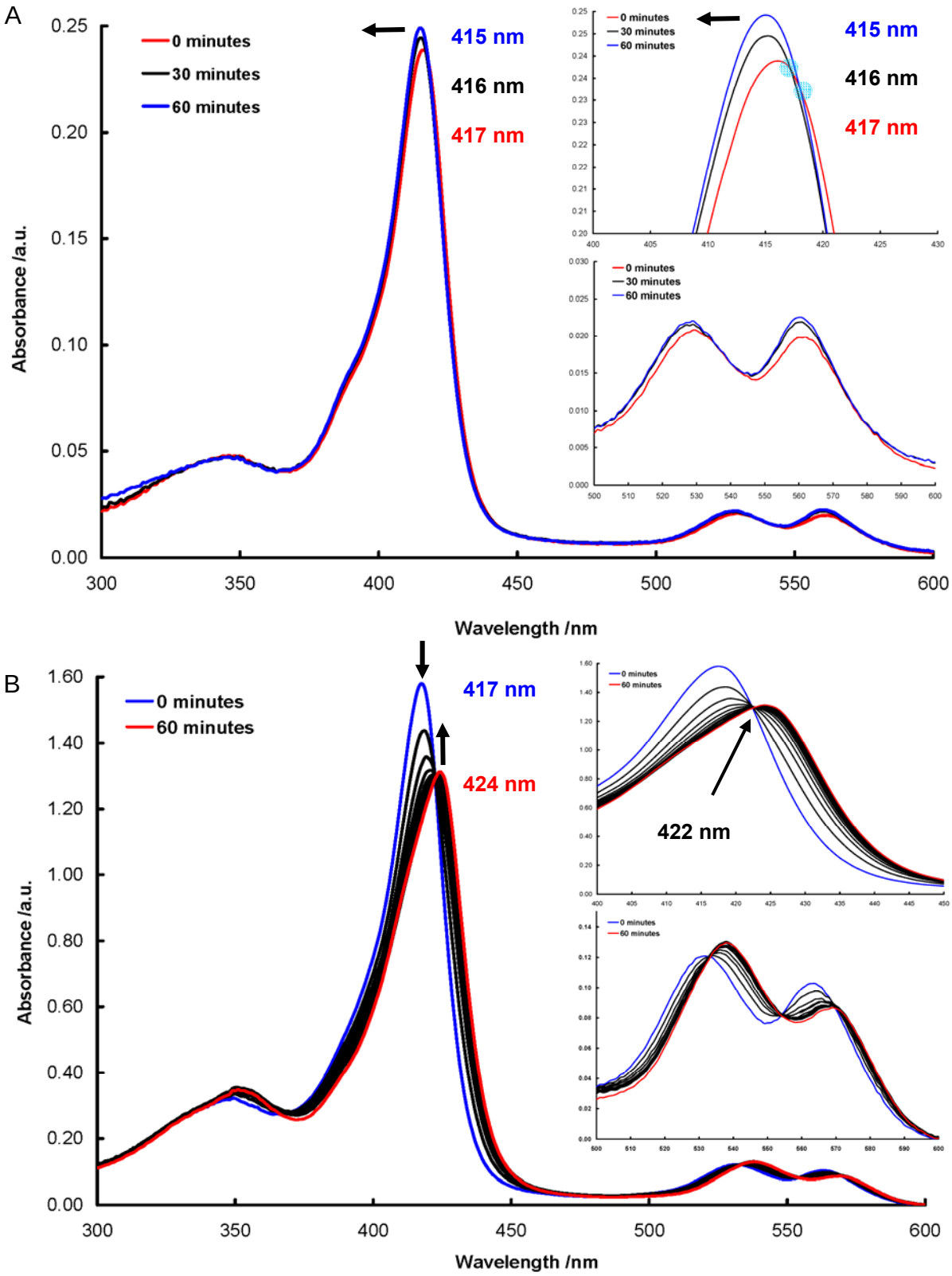


Figure 4.2 The effects of equilibration time on the absorbance of NAcCoMP8 at (**A**) low (*ca*. 1.25 μM) and (**B**) high (*ca*. 10.0 μM; irreversible) concentration in deionised water pH 6.89.

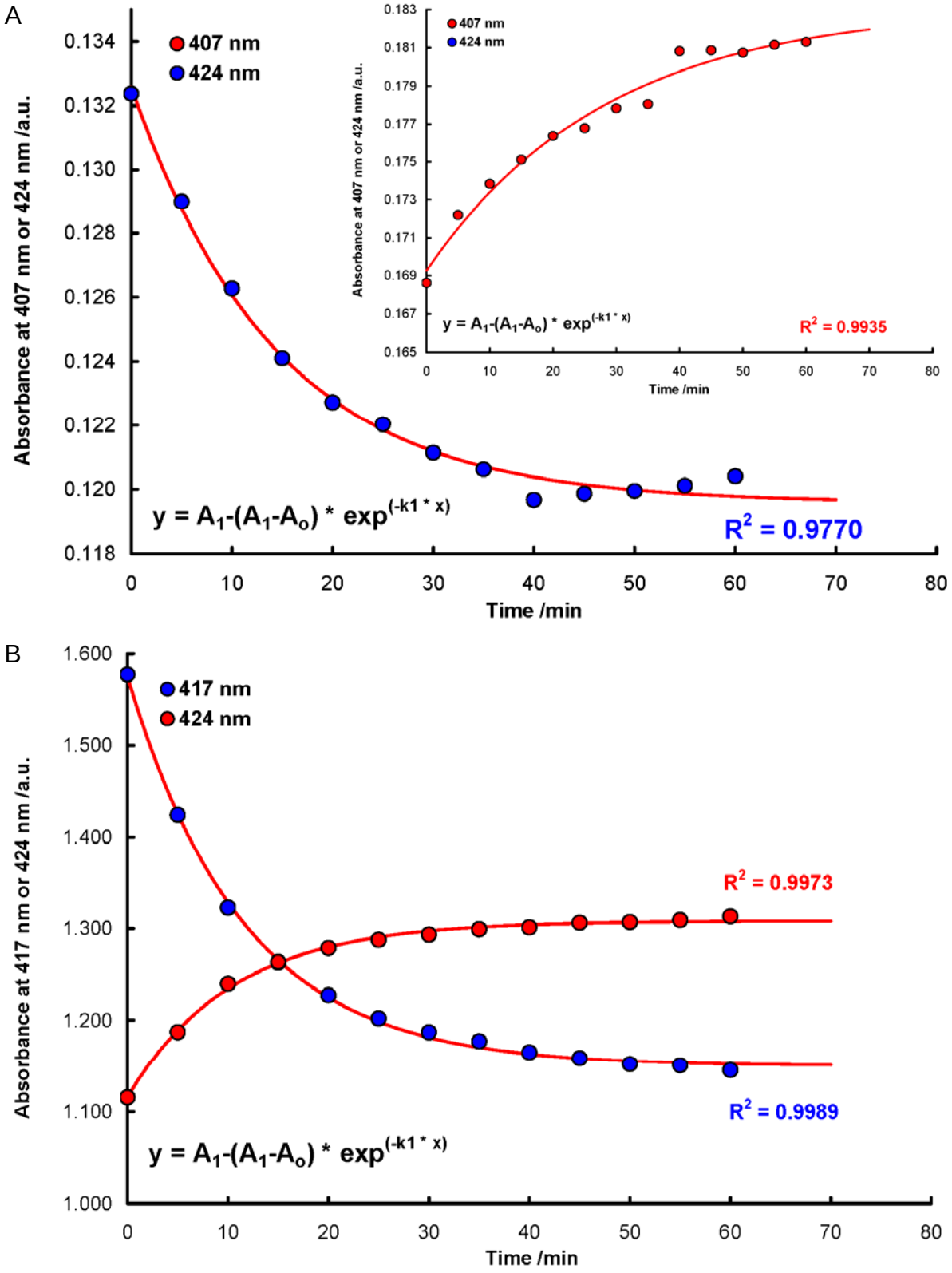


Figure 4.3 Estimated half lives (min) at specific wavelengths for NAcCoMP8 during the equilibration time study at low (**A**) low (*ca*. 1.25 μM) and (**B**) high (*ca*. 10.0 μM) in deionised water at pH 6.89.

4.2.2 Effects of Light

NAcCoMP8 was observed to degrade when exposed to light (*cf*. Figure 3.12, **Chapter 3**). The degradation was observed as a systematic decrease in absorbance of the Soret band (hypochromism). It thus became necessary to spectroscopically monitor the effect of light exposure to a sample of NAcCoMP8 as a function of time.

A stock solution of NAcCoMP8 (*ca*. 1.25 μM; pH 7) was freshly prepared in degassed deionised water (**Section 2.2.5**). A 2 mL sample was transferred into an argon-filled 1.0 cm pathlength cuvette fitted with a septum. An initial spectrum was recorded between 300 – 700 nm. This sample was then systematically exposed to ambient light over a period of 3 days and the absorbance of the Soret band (415 nm) was recorded at various intervals as a function of time (**Figure 4.4**).

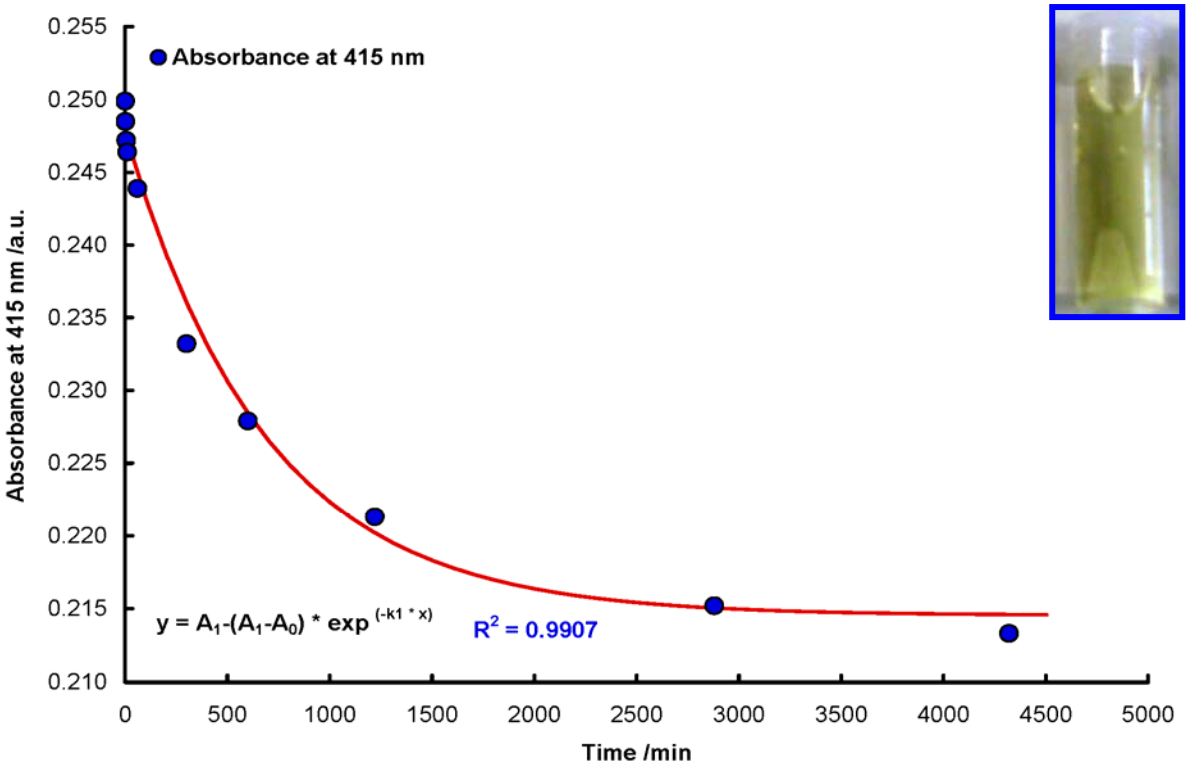


Figure 4.4 The effect of light exposure on the absorbance of NAcCoMP8 at 415 nm (*ca*. 1.25 μM; pH 7, deionised H_2O).

Initially, a small decrease in absorbance was observed over the first hour of light exposure (*ca*. 2.5%.). After the first hour however, there was a significant decrease in absorbance (*ca*. 15%.). The overall decrease in absorbance at 415 nm was *ca*. 15%. This suggests that the chromophore is rapidly disintegrating, the products of which appear to exacerbate the degradation process. The apparent half life for the overall process was found to be $t_{1/2apparent}$ = 478 min for $k_1 = 0.0015 \pm 0.0002$ min^{-1}.

Cobalt porphyrins are routinely light-protected during synthesis and solution chemistry experiments.[51,52] There has been evidence to suggest that cobalt porphyrins that are exposed to light undergo slow photo-reduction and/or photolysis.[50] However, the final product was a turbid solution and exhibited a pale yellow colour with a slight green tinge. Whilst this solution was too turbid to obtain a stable and realistic absorbance spectrum for comparison[59] (*cf*. Figure 3.12, **Chapter 3**), the colouring is typical of bile pigments or *bilins.*[56] Bilins are typical open-chain tetrapyrrolic porphyrin decomposition products. Common bilins include the initial green-yellow water-soluble biliverdin and the final yellow-orange water-insoluble bilirubin.[56-58] The turbidity of the sample is probably due to a mixture of biliverdin and bilirubin as a result of incomplete photo-degradation.[56]

4.2.3 Effects of Air (oxygen sensitivity)

An aerated aqueous solution of NAcCoMP8 exhibited a systematic decrease in absorbance over time. It thus became necessary to spectroscopically monitor the effect of air exposure to a known sample of NAcCoMP8 as a function of time.

A stock solution of NAcCoMP8 (*ca*. 1.25 μM; pH 7) was freshly prepared in degassed deionised water (**Section 2.2.6**). A 2 mL sample was transferred into an argon-filled 1.0 cm pathlength cuvette fitted with a septum. An initial spectrum was recorded between 300 – 700 nm. A gentle stream of O_2 was allowed to bubble into the sample whilst stirring. Absorbance was recorded at Soret band (415 nm) every

5 minutes for 60 minutes (**Figure 4.5**). The sample was protected from light with aluminium foil between readings.

There was a significant decrease in absorbance after the first 10 min of oxygen exposure (*ca*. 10%.). Thereafter, the decrease in absorbance appeared to level off after 30 min (*ca*. 15%). The overall decrease in absorbance was *ca*. 16%. This suggests that the decomposition of the chromophore upon exposure to dioxygen proceeds rapidly with an apparent half life of $t_{1/2apparent}$ = 7.81 min for k_1 = 0.089 ± 0.009. The yellow-orange colour is typical of the porphyrin decomposition product, bilirubin (**Section 4.2.2**).[56]

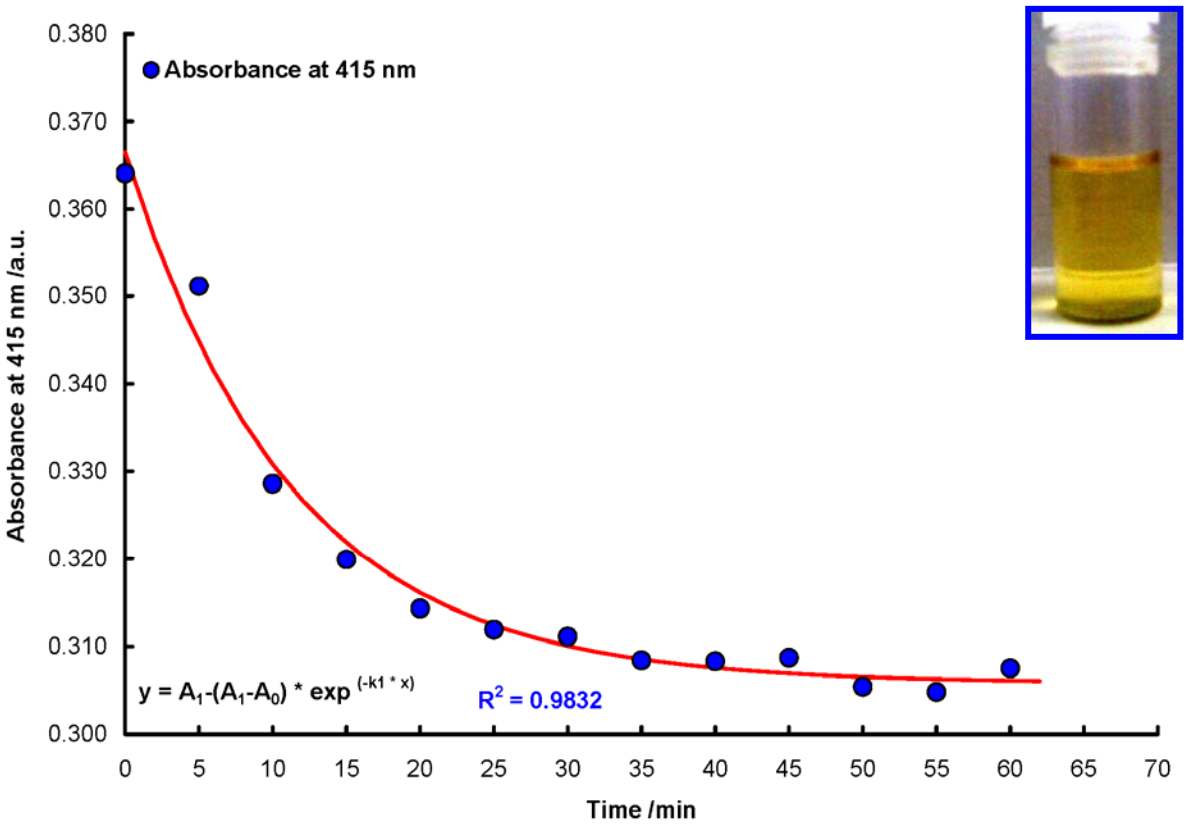


Figure 4.5 The effects of oxygen exposure on the absorbance of NAcCoMP8 at 415 nm over one hour (*ca*. 1.25 μM; pH 7, deionised H_2O).

4.2.4 Effects of Ionic Strength

Ionic strength has previously been associated with aggregation in some metalloporphyrins[53-56] and microperoxidases.[35] It was thus necessary to determine the effects of ionic strength on absorbance of aqueous NAcCoMP8 at neutral pH. These observations were made at both high and at low NAcCoMP8 concentrations.

These ionic strength limits were determined spectroscopically as described previously (**Section 2.2.7**). Aliquots of degassed $NaClO_4$ (5 M; between 10 – 100 uL) was added to degassed NAcCoMP8 (*ca*. 1.25 μM; pH 7; 1.5 mL, 25 ^oC) in an argon-filled 1.0 cm pathlength cuvette fitted with a septum. After each addition of $NaClO_4$ the sample was gently stirred and allowed to reach equilibrium for 1 minute. An absorbance spectrum was then recorded between 300 – 700 nm using $NaClO_4$ in deionised water as the reference solution. Absorbance data were corrected for dilution (**Figure 4.6**). The experiment was subsequently repeated at higher NAcCoMP8 concentration (*ca*. 10.0 μM; pH 7; 1.5 mL, 25 ^oC)

UV-visible spectra were recorded for both high and low NAcCoMP8 concentrations with increasing ionic strength (0 – 4 M) so as to observe any spectral shifts (**Figure 4.6**). What is immediately obvious is the red shift of the Soret band (417 → 424 nm) observed at high NAcCoMP8 concentrations with a well-defined isosbestic point at 422 nm (**Figure 4.6B**); this is accompanied by a small decrease in the intensity of the Soret band. There are also distinctive shifts in the Q band region (530 → 538 nm and 560 → 568nm, respectively) with isosbestic points observed at 533, 554, 570 nm. The final solution was pale yellow-orange.

This is in stark contrast to the slight red shift observed at low NAcCoMP8 concentrations (415 → 417 nm) (**Figure 4.6A**) which is accompanied by a very large decrease in the intensity of the Soret band. There are no readily discernable isosbestic points. The final diluted solution was a lighter pink colour.

Clearly two different equilibria are present at low and at high concentration of NAcCoMP8. These equilibria were thus explored by comparing the ionic strength dependence of the Soret bands at each concentration (**Figure 4.6,** insets); this was found to be distinctly sigmoidal.

If we assume that at low NAcCoMP8 concentration an increase in ionic strength induces a simple dimerisation process (**Equation 4.1**; **Appendix 4.1**),

$$2M \rightleftharpoons D_1 .....(D_1 = \text{dimer})$$ **Equation 4.1**

then:

$$2M + nL^+ \xrightarrow{K_1} D_1$$ **Equation 4.2**

where M refers to monomeric NAcCoMP8 at pH 7.0, D_1 represents the dimer formation on binding of n cations (L^+) by M.

The total absorbance A_T is given by (**Equation 4.3**):

$$A_T = \sum_{m=1}^{2} A_m \alpha_m$$ **Equation 4.3**

where A_m is the absorbance of the m^{th} species, and α_m is the fraction of that species in solution.[35]

Thus, a non-linear least squares fit of the data with

$$\alpha_M = \frac{-1+\sqrt{1+8K_1[L]^n}}{4K_1[L]^n}$$ **Equation 4.4**

$$\alpha_{D_1} = \frac{1-[M]}{2}$$ **Equation 4.5**

in Equation 4.3 (**Figure 4.6A**, inset) at 25 ^oC gave K_1 = (0.080 ± 0.008) M^{-4}, n = 3.4 ± 0.3, and there is a good fit of this simple model to the experimental data.

At high NAcCoMP8 concentration sigmoidal behaviour is again observed. It seems likely that the process at high concentration is that of the aggregation of two dimers since the spectroscopic end product in the low concentration study spectroscopically is the same as the starting product in the high concentration study (both at 417 nm). If the assumption is made that the dimeric species D_1 forms a tetramer (**Equation 4.6**; **Appendix 4.1**):

$$2D_1 \rightleftharpoons T_L \qquad \textbf{Equation 4.6}$$

then:

$$2D_1 + jL \xrightarrow{K_2} T_L \qquad \textbf{Equation 4.7}$$

where T_L represents a tetramer on binding of j cations (L^+) by D_1.

The total absorbance A_T is given by (**Equation 4.3**). The values obtained from a non-linear least-squares fit with

$$\alpha_{D_1} = \frac{-1+\sqrt{1+8K_2[L]^j}}{4K_2[L]^j} \qquad \textbf{Equation 4.8}$$

$$\alpha_{T_L} = \frac{1-[D_1]}{2} \qquad \textbf{Equation 4.9}$$

at 25 ^oC gave $K_2 = (2.19 \pm 0.09)\ M^{-5}$, $j = 3.7 \pm 0.1$

These findings show that the spectrum of NAcCoMP8 is strongly dependent on ionic strength. The simplest model consistent with the experimental data suggests that this dependence is the consequence of the presence of two equilibria, the first being the formation of a dimer at low concentration (415 → 417 nm) which is driven by the binding of 3 cations ($n = 3.4 \pm 0.3$) which is subsequently followed by a second equilibrium, the formation of a putative tetrameric species (417 → 424 nm), driven by the binding of approximately 4 further cations ($j = 3.7 \pm 0.1$).

There are striking similarities between the ionic strength dependence work presented here and those in the equilibrium time study (**Section 4.2.1**). Comparatively, both studies show distinctly different solution behaviour at low and at high NAcCoMP8 concentrations. This indicates a significant concentration-dependence (*cf*. Beer's Law investigation, **Section 4.2.5**). At high NAcCoMP8 concentrations for both ionic- and equilibrium studies, there is an irreversible hypochromic redshift with a well-defined isosbestic point at 422 nm. In both studies the shift did not revert back on dilution with methanol or other dispersing agents. This suggests that the type of species formed (putatively a tetramer) may involve interaction between the metal of one dimeric species and the polypeptide side-chain of another. In a similar study with NAcFeMP8 the second equilibrium was attributed to a tighter packed π-π dimer species.[35]

Interestingly, disparity between the two studies is observed at *low* NAcCoMP8 concentration. Here, NAcCoMP8 over time shows a small hyperchromic blueshift (417 → 415 nm) with two indistinct isosbestic points (417 and 418 nm). In contrast, the ionic strength study exhibits no discernable isosbestic points but rather a remarkably hypochromic yet small redshift in the opposite direction (415 → 417 nm) is noted. Whilst the latter is consistent with aggregation,[35] the former may be attributed to the monomerisation of a loosely packed π-π dimer species.[35] Monomer–π-π dimer equilibriums are not uncommon in metalloporphyrins. The diminished electrostatic repulsions due to charge neutralisation on the porphyrins by the binding of cations facilitates the formation of π-π dimers.[20,22,35]

This evidence suggests two important features in the preparation of a spectroscopically stable monomeric NAcCoMP8 solution. Firstly, the formation of the irreversible NAcCoMP8 species at high concentration occurs more as an artefact of concentration-dependence than ionic- or time-dependence. Yet, the reversible species at low NAcCoMP8 concentration shows distinctive ionic strength dependence and is a precursor to the 424 nm species. Thus, it is not sufficient to prepare NAcCoMP8 at low concentrations but at low ionic strength as well.

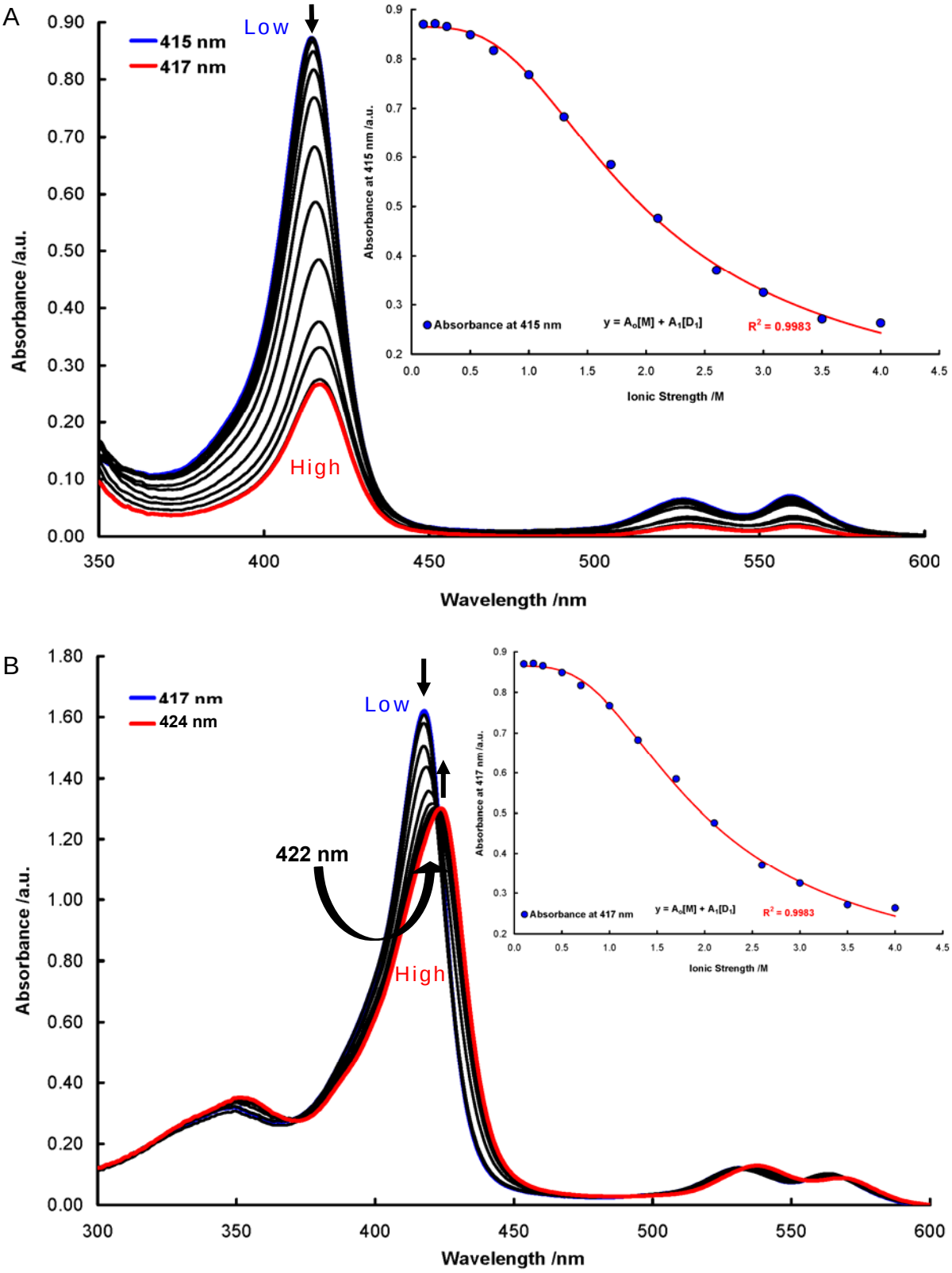


Figure 4.6 The effects of ionic strength on the absorbance of NAcCoMP8 at (**A**) low (*ca*. 1.25 μM) and (**B**) high (*ca*. 10.0 μM; irreversible) concentration in deionised water pH 6.89

4.2.5 Effects of Concentration (Beer's Law investigation)

The solution behaviour studies of NAcCoMP8 thus far suggest a distinct concentration dependence of its properties. It was thus necessary to determine the effects of concentration on absorbance of aqueous NAcCoMP8 at neutral pH. An effective method for assessing concentration-dependence of aggregation in microperoxidases is through the extent of adherence to Beer's Law.[12] Deviation from Beer's Law signals aggregation of the absorbing species whilst a single set of isosbestic points denote a simple equilibrium, such as that of a monomer-dimer.[35]

The Beer's law study was conducted as previously described (**Section 2.2.8**). A known volume of deionised water was titrated with aliquots of concentrated NAcCoMP8 stock solution (*ca*. 20 μM; 25 ^{o}C; between 2 - 100 μL) in 1.0 cm pathlength cell. The full absorbance spectrum from 300 – 700nm was recorded after each addition. The data were corrected for dilution and then a Beer-Lambert plot was constructed for NAcCoMP8 in deionised water (**Figure 4.7B**). Similar studies were conducted for CoMP8, NAcCoMP11 and CoMP11 (**Figure 4.7A**). There were however, insufficient quantities of NAcCoMP6 and CoMP6 for a comparative study.

The absorbance of the acetylated species was found to be slightly higher than that of the non-acetylated species in both sets of cobalt(III)microperoxidases (**Figure 4.7**). This might suggest monomerism of the acetylated species relative to the non-acetylated species since aggregation diminishes the absorbance (for example, in **Figure 4.6A**). Nevertheless, a plot of absorbance as a function of concentration for both CoMP11 and CoMP8 give apparently good straight lines (r^2 > 0.999 in both cases); in the absence of other evidence (*cf*. CoMP8 irreproducibility, **Appendix 3.1**) monomerism of a species in solution might be erroneously concluded. It is therefore concluded that the apparent adherence to Beer's Law in these systems is in itself an insufficient reason for concluding that the species is monomeric. The

limiting slope for NAcCoMP11, CoMP11, NAcCoMP8 and CoMP8 were recorded (25 ^{o}C, deionised water, neutral pH; x 10^5 M^{-1} cm^{-1}): (2.13 ± 0.01), (1.84 ± 0.01), (1.94 ± 0.01) and (1.81 ± 0.01), respectively. This suggests that the acetylation process is an effective means of limiting the formation of aggregating species, particularly by metal–side-chain coordination.

The limiting slopes of various microperoxidases are compared (**Table 4.2**). In this work the values for the limiting slope were found to be higher in cobalt microperoxidases than the iron species. Sannasy's NAcCoMP8 work corroborates this finding.[60] This suggests that changing the central metal ion from iron to cobalt significantly changes the limiting slope. Furthermore, the data in Table 4.2 suggests that the limiting slope is affected by ionic strength.

Table 4.2 A comparison of Beer's law limiting slopes for various microperoxidases (pH 7.0, 25 ^{o}C).

Microperoxidase Species	**Ionic Strength (M)**	**Limiting slope (10^5 M^{-1} cm^{-1})**
FeMP8[8]	0.1 M ($NaClO_4$)	1.57 ± 0.01
NAcFeMP8[35]	0.50 M ($NaClO_4$)	1.55 ± 0.01
NAcCoMP8[60]	0.0 M (H_2O)	1.80 ± 0.01
NAcCoMP8[60]	0.1 M ($NaClO_4$)	1.66 ± 0.01
CoMP8†	0.0 M (H_2O)	1.81 ± 0.01
CoMP11†	0.0 M (H_2O)	1.84 ± 0.01
NAcCoMP11†	0.0 M (H_2O)	2.13 ± 0.01
NAcCoMP8†	0.0 M (H_2O)	1.94 ± 0.01

† this work

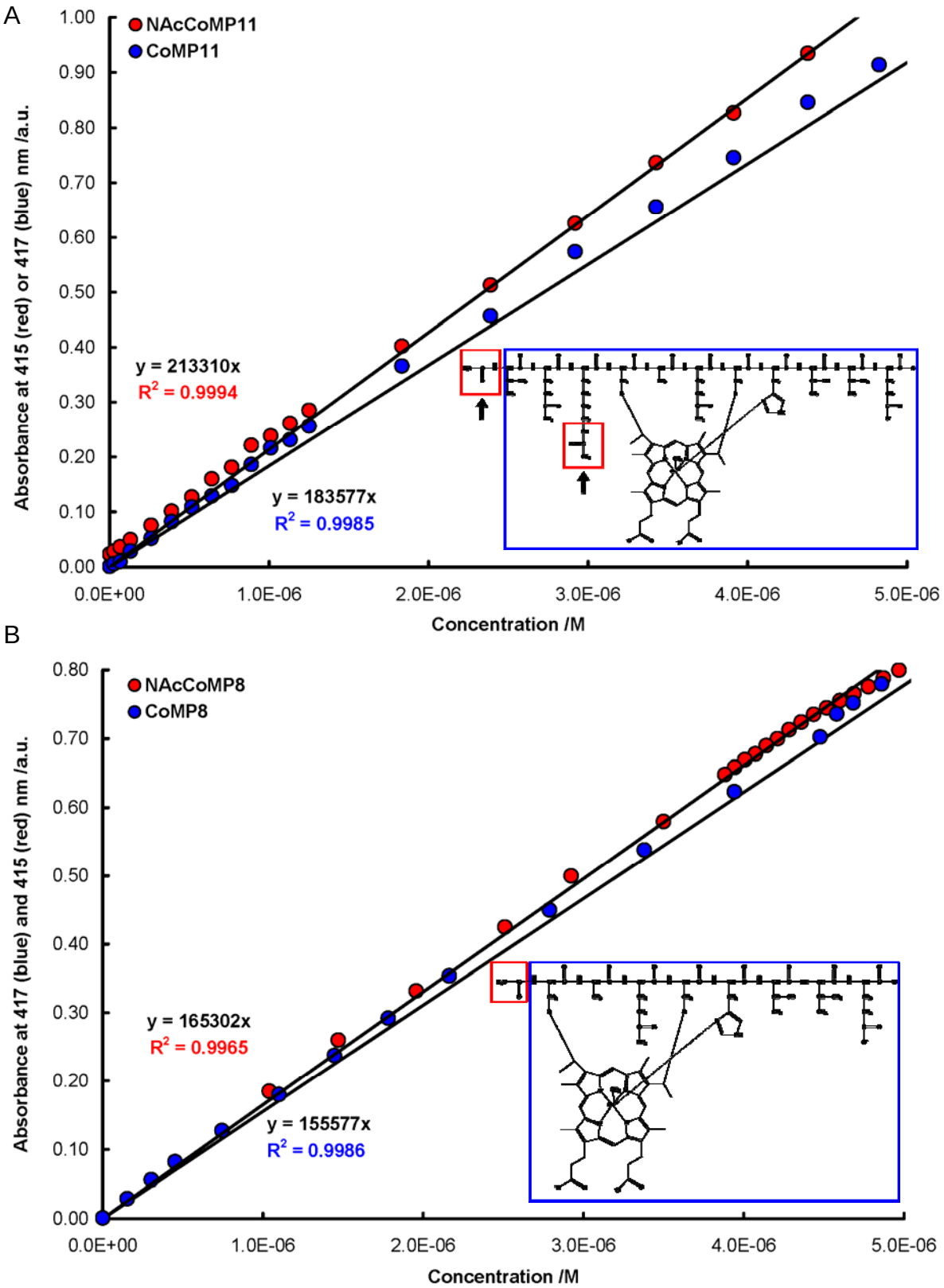


Figure 4.7 The effects of concentration on the absorbance of NAcCoMP8 in deionised water (pH 7.0, 25 °C).

4.2.6 Effects of pH (pK_a investigation)

The titration procedure for the determination of spectroscopic pK_as of NAcCoMP8 was described previously[60] (**Section 2.2.9**). The study was conducted as a function of temperature and ionic strength (10 - 35 ^oC; 0.1 M by $NaNO_3$) by titrating NAcCoMP8 (40 mL; 8.01 μM) with negligible volumes of either concentrated acid (sulfuric; between pH 1.0-6.5) or base (NaOH; 8 M; between pH 5.5-14). After each pH adjustment, the system was allowed to thermo-equilibrate before a full absorbance spectrum (300 – 700 nm) was recorded at 25 ^oC. For temperatures other than 25 ^oC, the absorbance and pH were recorded only in the region of interest (*ca*. 360 – 450 nm; pH 5-10) (**Section 2.2.9**).

The absorbance of NAcCoMP8 was found to vary with pH (**Figure 4.8A, Figure 4.8B**). At low pH the spectral features are consistent with those expected for NAcCoMP8 (**Figure 4.8A**; *cf***.** Figure 3.10**, Section 3.2.2.3**). As pH decreases from neutral to acidic, the Soret band undergoes a blue shift from 415 → 410 nm with a possible isosbestic point at 413 nm. This is accompanied by band broadening especially at *ca.* pH 1. On the other hand, the Q-bands exhibit greater differentiation as the pH is lowered (hyperchromism at 560 nm with isosbestic points at 530, 570 and 590 nm). These shifts were consistent with those reported previously.[60]

This type of spectral behaviour is contrasted to that observed at higher pH values (**Figure 4.8B**). The Soret band shows a red shift (415 → 418 nm) whilst the Q-bands exhibit hyperchromism with increasing pH. These band shifts consistent with those observed previously.[60] The bands are also broader than those observed at lower pH values. Whilst both the acidic and basic solutions are a darker pink than the original neutral solution, the latter solution exhibits an orange tinge (*cf***.** Figure 3.10**, Section 3.2.2.3**).

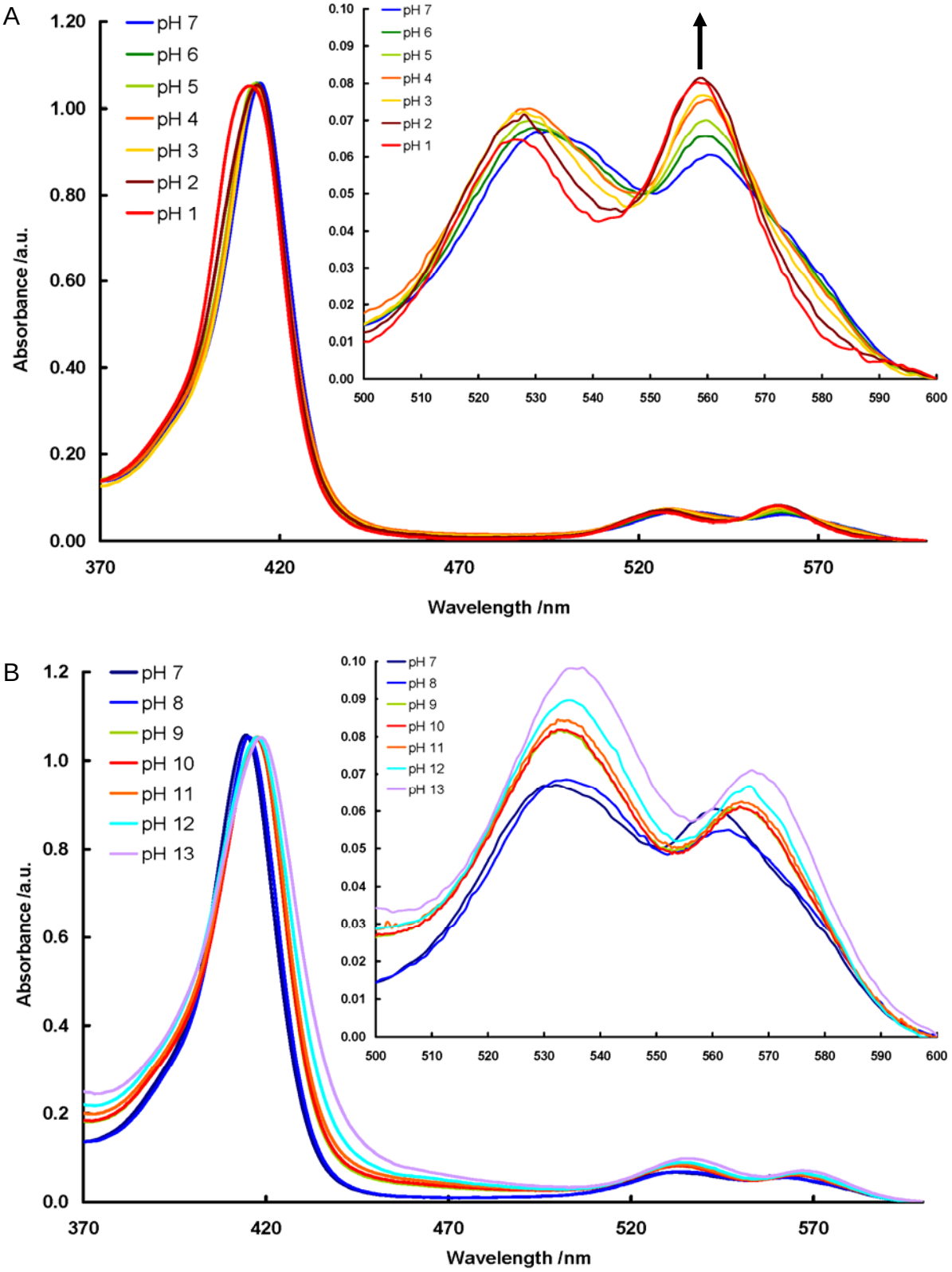


Figure 4.8 The effects of pH on the absorbance of NAcCoMP8 (*ca*. 1.25 μM; pH 7, multi component buffer). The acidic (**A**) and basic (**B**) regions are reflected.

The pH dependence of absorbance in NAcCoMP8 was observed at 415 nm in the 25 ^{o}C study (**Figure 4.9A**). This curve was fitted to an ionisation isotherm in order to calculate the acid dissociation constants (pK_a) for NAcCoMP8. The experimental data in the acid region (*ca*. pH 1 – 7) were fitted to an ionisation isotherm involving 3 pK_as whilst the basic region (ca. pH 7 – 12) was fitted to 2 pK_as (**Equation 2.3** and **Equation 2.4**, **Section 2.2.9**). Five pK_a values are discernible for NAcCoMP8 across the pH range at 25 ^{o}C (**Figure 4.9A**).

The pK_as were assigned by analogy with the trivalent NAcFeMP8 system (**Figure 4.9B**).[35] The pK_as were thus attributed to the deprotonation of the imidazole of His-18 and its displacement of H_2O (or possibly the C-terminal carboxylate, or that of the side chain of Glu-21) from the proximal coordination site of Co(III) (pK_a = 1.74 ± 0.04), successive deprotonation of the heme carboxylates (4.08 ± 0.02 and 5.80 ± 0.05); ionisation of the axial H_2O ligand 7.81 ± 0.03; and ionisation of the imidazole of His-18 to form an imidazolate (12.00 ± 0.03).

These values were then compared to those observed in trivalent NAcFeMP8. The analogous pK_a values in trivalent NAcFeMP8 are 2.1(2) and 3.12(7) — only one pK_a, at 1.74(4) is observed in the present system; 4.95(7) and 6.1(3); 9.59(1); and 12.71(5). The acid dissociation constant for the ionisation of the axial water is of significance as it is the value used in pK_a corrections in the subsequent NAcCoMP8 ligand binding studies. The pKa value for the ionisation of the distally coordinated water in vitamin B_{12a} is 8.10(12).[61,62] This is only marginally higher than that observed here for trivalent NAcCoMP8 (7.81(3)). This suggests that the metal ion is more polarising towards coordinated H_2O in the porphyrin system than in the corrin system, despite the net formal charge at the metal centre being lower, *viz.* +1 in the porphyrin system (Co^{3+} and a porphyrin dianion) but +2 in the corrin system (Co^{3+} and a corrin mono-anion). Also, the higher acidity of H_2O coordinated to low spin Co(III) compared to high spin Fe(III) is consistent with the smaller ionic radius (and hence higher Lewis acidity) of the former (0.545 Å) than the latter (0.645 Å).[63]

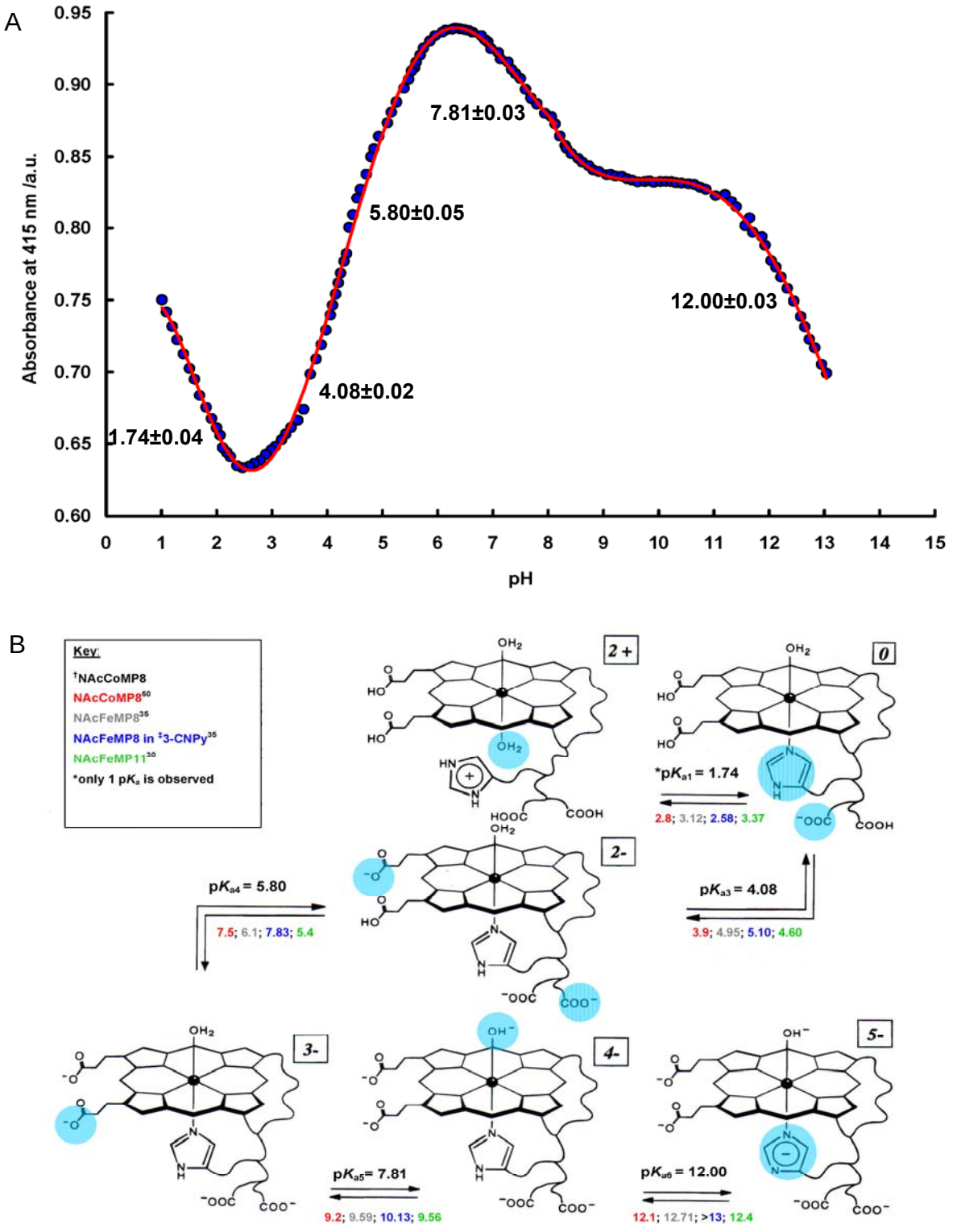


Figure 4.9 Possible species distribution for NAcCoMP8. Five pK_a values are discernible for NAcCoMP8 across the pH range at 25 °C (**A**) NAcCoMP8 species (**B**) assignment as a function of pH (*ca*. 1.25 μM; pH 7, multi component buffer). (†) refers to this work and (‡) refers to 3-cyanopyridine. Diagram adapted from literature.[30, 35]

It is essential to know the pK_a for the ionisation of the bound axial water in NAcCoMP8. Knowing this pK_a enables corrections to be made to all kinetic and thermodynamic data such that pH-independent values are obtained. However, two factors made it difficult to obtain reliable data. Firstly, to ensure a monomeric 415 nm species, low concentrations of NAcCoMP8 had to be used. This inevitably meant that the spectroscopic data was noisier than might be hoped for (**Figure 4.10A**, showing data at 30 ^{o}C, as an example). Secondly, there is a relatively small change in the spectrum on ionisation of the axially coordinated H_2O (in contrast to B_{12a} itself, or indeed trivalent NAcFeMP8 where ionisation is accompanied by a spin change in the metal ion).

The ionisation occurs with a well-defined isosbestic point at 415 nm with a shift of the Soret band from 415 nm to 418 nm with an increase in its intensity. Above pH 9.1, the intensity of the Soret decreases and it undergoes a red shift as His-18 ionises to form an imidazolate. In order to average out the noise, the spectral changes 10 nm on either side of the isosbestic point were fitted with to an equation (**Equation 2.4**) involving a single pK_a. The values obtained from twenty such fits at each temperature were then averaged. **Figure 4.10B** and **Figure 4.10C** show absorbance data against pH at 30^{o}C as an example. The values obtained are given in Table 4.3.

Table 4.3 pK_a values for the ionisation of coordinated H_2O in trivalent NAcCoMP8 was a function of monitoring wavelength at 30 ^oC.

λ (nm)	**pK_a**	**σ**	**r^2**
403	7.78	0.05	0.979
404	7.79	0.05	0.981
405	7.77	0.04	0.985
406	7.79	0.04	0.987
407	7.78	0.04	0.992
408	7.75	0.04	0.991
409	7.77	0.04	0.992
410	7.76	0.04	0.991
411	7.77	0.04	0.993
412	7.82	0.05	0.987
419	7.78	0.03	0.993
420	7.79	0.03	0.995
421	7.80	0.02	0.995
422	7.80	0.02	0.995
423	7.82	0.02	0.996
424	7.83	0.02	0.997
425	7.83	0.03	0.996
426	7.84	0.03	0.994
427	7.86	0.03	0.995
428	7.87	0.04	0.993
429	7.88	0.04	0.992
430	7.90	0.05	0.990
Mean	7.83		
σ	0.04		

The mean pK_a values obtained by a similar procedure between 10.0 and 39.5 ^oC is given in Table 4.4.

Table 4.4. Dependence of the pK_a of coordinated H_2O in trivalent NAcCoMP8 as a function of temperature.

T (^oC)	mean pK_a	σ
10.0	7.55	0.10
15.0	7.67	0.16
20.3	7.88	0.10
20.0	7.93	0.16
25.0	7.57	0.14
30.1	7.83	0.04
34.9	7.28	0.06
39.5	7.43	0.11

There is no clear dependence of pK_a on temperature. This means that the temperature-dependence of this value is small compared to the uncertainty in the measurement. Hence, an average value for the pK_a, *viz.*, 7.64, was used for all determinations of rate and equilibrium constants.

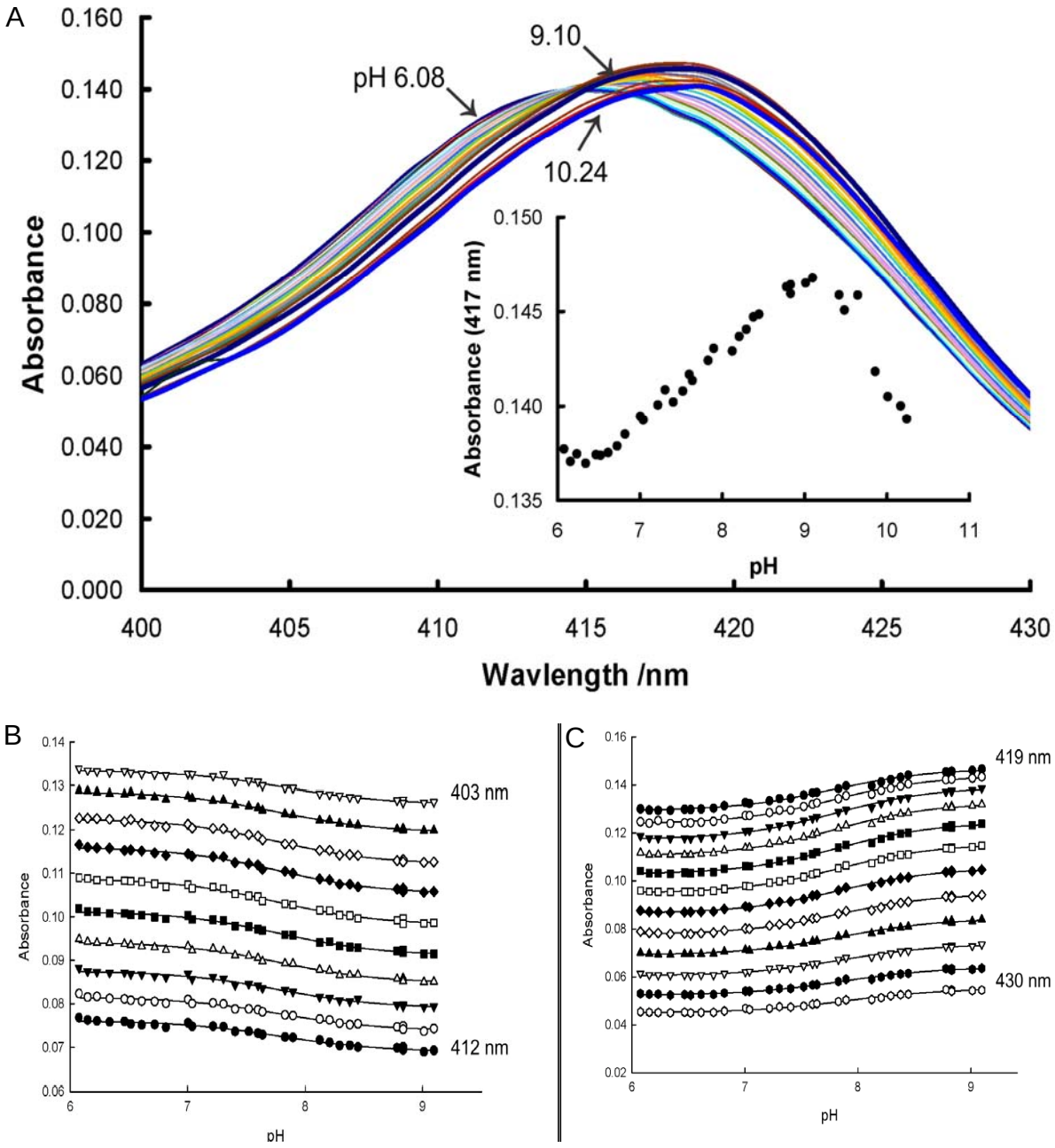


Figure 4.10. (**A**) Illustrating the dependence of the Soret region of NAcMP8 on pH at 30 ^{o}C. The insert shows the absorbance at 417 nm was a function of pH. (**B**) Fits of the change in absorbance between 403 and 412 nm, and between (**C**) 419 and 430 nm, for NAcMP8 at 30 ^{o}C to an equation involving one single pK_a

4.2.7 Effects of Temperature

The thermal stability of NAcCoMP8 in deionised water was assessed as previously described (**Section 2.2.10**). A stock solution of NAcCoMP8 was prepared in degassed deionised water (*ca*. 1.25 µM; pH 7). NAcCoMP8 (*ca*. 2 mL) was added to a clean, dry, argon-filled cuvette fitted with a septum. The temperature was increased in 5 ^{o}C increments between 10 – 45 ^{o}C using a Peltier device and the spectrum was recorded between 300 – 700 nm at each temperature.

The absorbance changes as a function of temperature were observed at low and high NAcCoMP8 concentrations in deionised water (**Figure 4.11**). At low NAcCoMP8 concentrations (**Figure 4.11A**) a small redshift of the Soret band was observed as temperature increased (415 → 417 nm); this was accompanied by a systematic decrease in absorbance, together with band broadening (**Figure 4.11A,** inset). Interestingly however, the 417 nm species present at *ca*. 50 ^{o}C reverted back to the 415 nm species when diluted with 50% methanol.

This is in stark contrast to the spectral changes observed at high NAcCoMP8 concentrations (**Figure 4.11B**). At high NAcCoMP8 concentrations the spectral profile changed significantly with an increase in temperature (**Figure 4.11B,** inset**;** 415 → 422 nm; 527 → 537nm; 560 → 574 nm). Discernable isosbestic points were observed at 420, 530, 553 and 567nm.

The observations at low NAcCoMP8 are consistent with the formation of the loosely packed π-π dimer already observed in the concentration-dependence study (**Section 4.2.5**) and the effect of ionic strength (**Section 4.2.4**). Similarly, at higher NAcCoMP8 concentrations and increase in temperature promotes the formation of a species with a Soret at 422 nm, very close to that observed to the putative tetramer found in the study of the effect of ionic strength.

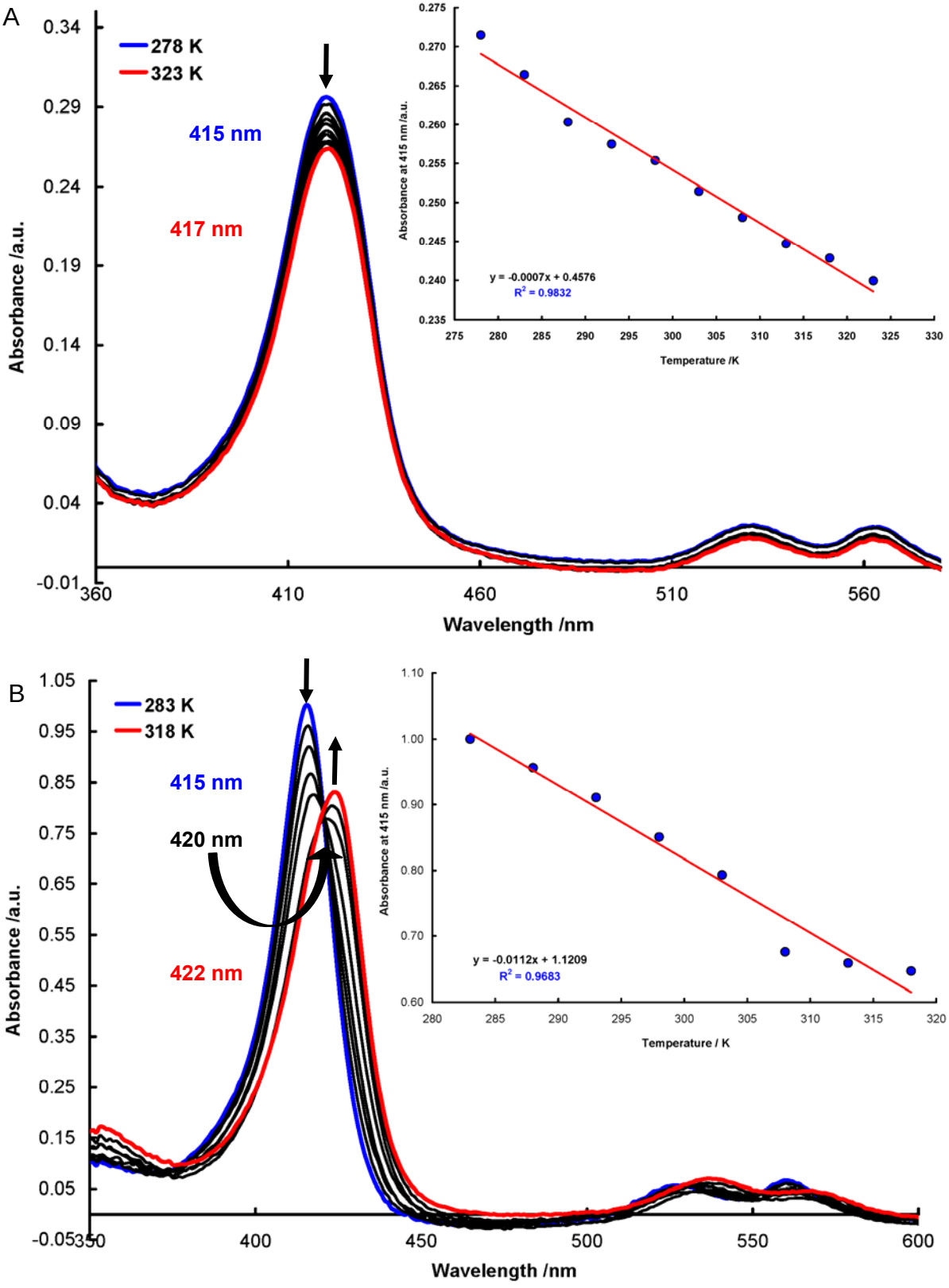


Figure 4.11 The effects of temperature on the absorbance of NAcCoMP8 at (**A**) low (*ca*. 1.25 μM) and (**B**) high (*ca*. 10.0 μM; irreversible) concentration in deionised water pH 6.89

4.2.8 Effects of Dispersing Agents and Buffers

Metalloporphyrins are readily solubilised in detergents, mixed solvents, biological buffers and crown ethers.[24-29] However, these alternatives need to be applied judiciously as they may not be practical a alternative. This is particularly true in the case of biomimetic systems and the biological environments they aim to mimic. Certainly with the complex biomimetic system, NAcCoMP8, they should be screened for possible optical interference before any spectrophotometric-based solution studies are conducted. To this end, various dispersal agents and biological buffers were screened for optical interference and/or binding in NAcCoMP8.

Various dispersing agents were investigated in the preparation of monomeric NAcCoMP8 as described previously (**Section 2.2.11)**. These included Triton X-100, PEG, SDS 5% and TWEEN-20. A stock solution of NAcCoMP8 was prepared in deionised water (*ca*. 1.25 μM; pH 7) and degassed using argon. A 2 mL sample of this stock solution was then added to a clean, dry, argon-filled cell fitted with a septum. An initial spectrum was recorded from 300 – 700 nm at 25 ^{o}C. To this sample, excess dispersal agent (*ca*. 200 μL in two additions) was then added to the cell under argon. This solution was gently stirred and allowed to reach equilibrium for one hour. Thereafter, a spectrum was recorded every 5 minutes for 30 minutes under the same conditions. This procedure was repeated for each dispersing agent listed above. All samples were light-protected when not in immediate use.

Similarly, various buffers were also investigated in the preparation of monomeric NAcCoMP8 (**Section 2.2.11**). These included CAPS, CHAPS, HEPES, MES, MOPS and Tris/HCl. Separate stock solutions of NAcCoMP8 (*ca*. 1.25 μM; pH 7) were prepared using Good buffers (*ca*. 0.1 M; pH 7) and allowed to stir for an hour whilst degassed. A 2 mL sample was then transferred into an argon-filled 1.0 cm pathlength cuvette fitted with a septum. One spectrum per hour over a 10 hour-

period was recorded between 300 – 700 nm for each sample. Only the samples showing any significant spectroscopic changes were reported here.

The dispersing agents explored in this study exhibited varying degrees of optical interference on the absorbance spectrum of NAcCoMP8 (**Figure 4.12A**, with the dispersing agents inset). These interferences were observed mainly in the near UV region and may be attributed to two features. Firstly, the dispersing agents explored could be spectrophotometrically active in the UV region. This could be particularly problematic in the case of nitrite binding studies for example, whereby a distinctive band is observed in the UV region. Furthermore, some metalloporphryins have been observed to take a longer time to reach spectroscopic stability when certain detergents were used.[39] This was certainly the case with the NAcCoMP8 sample that contained SDS 5%.

Secondly, some dispersing agents exhibited evidence of binding as suggested by the distinct Soret shifts. For example, this may be observed in the SDS 5% study where the Soret shifted significantly from 415 → 418 nm. Presumably the coordination is by a hydroxyl group on the SDS 5% moiety as it competes for the distal position on NAcCoMP8. This is especially problematic when trying to design ligand binding experiments in a system such as NAcCoMP8. The addition of any unknown potentially competing ligands should be avoided as they only add spectroscopic interference to an already complex system.

In the case of buffers, it was found that HEPES (0.1 M, pH 7.0, 25 ^{o}C) effected a blueshift in the Soret band (415 → 413 nm) again suggesting coordination of the metal ion (**Figure 4.12B**, with the structure of HEPES and possible point of coordination with Co(III) in NAcCoMP8 inset). HEPES consists of hydroxyl and sulfonate moieties. The other sulfonate-containing buffers and Tris exhibited no evidence of coordination. This suggests that HEPES then likely coordinated through the terminal hydroxyl group as it is sterically unhindered.

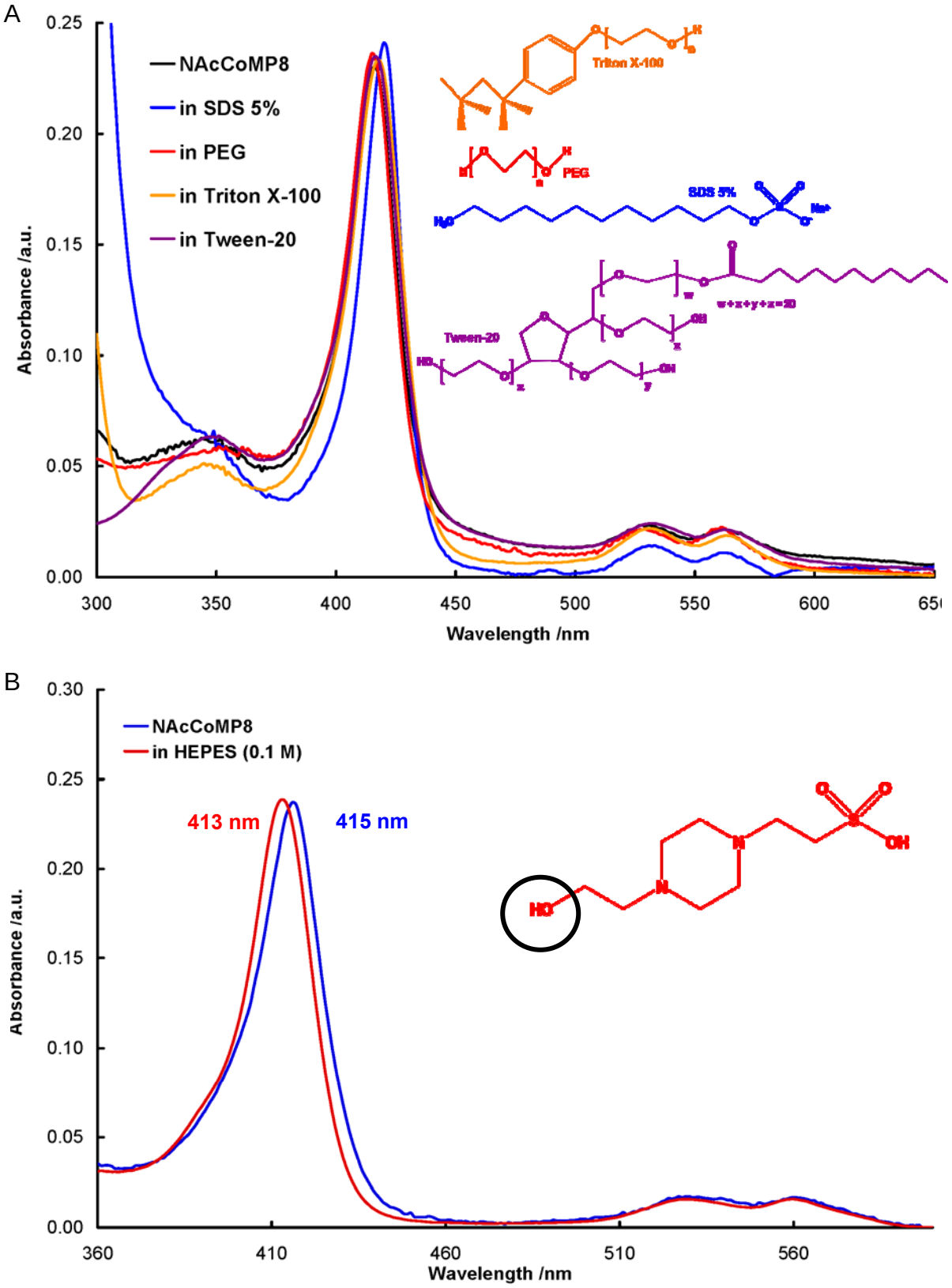


Figure 4.12 The effects of dispersing agents (**A**) and of 0.1 M HEPES buffer (**B**) on the absorbance spectrum of aqueous NAcCoMP8 (pH 7.0, 25 °C).

4.2.9 Effects of Reducing Agents

A qualitative study of the reduction of NAcCoMP8 using various reducing agents was attempted in deionised water in order to observe the changes in the electronic spectrum. The reducing agents used were sodium dithionite, sodium borohydride, ascorbic acid and zinc in methanol, respectively. The study was conducted as described previously (**Section 2.2.12**).

A stock solution of NAcCoMP8 was prepared in deionised water (*ca*. 1.25 μM; pH 7) and degassed using argon. NAcCoMP8 (*ca*. 2 mL) was added to a clean, dry, argon-filled cuvette fitted with a septum. An initial spectrum was recorded from 300 – 700 nm at 25 ^{o}C. To this sample, previously dried excess reducing agent (*ca*. 0.5 g in two additions) was added under argon, gently stirred and a spectrum was recorded every 5 minutes for 30 minutes under the same conditions. This procedure was repeated for each reducing agent listed above.

The absorbance spectrum of NAcCoMP8 only exhibited significant spectral changes in the presence of $NaBH_4$. It was therefore the only reducing agent spectrum reported here (**Figure 4.13**). There was considerable difficulty in obtaining a well-defined absorbance spectrum of NAcCoMP8 with $NaBH_4$. After the first $NaBH_4$ addition the sample bubbled vigorously and thus contributed significantly to the spectral noise. However, after the second addition of $NaBH_4$, solution became slightly yellow-pink and turbid.

The spectral changes observed in the $NaBH_4$ study were rapid and occurred in two main regions. Firstly, the addition of $NaBH_4$ prompted the disappearance of the Soret band at 415 nm. This was followed by the brief emergence of a band at 395nm which also subsequently disappeared. The final band formed was at 345 nm. There were also noticeable shifts in the UV region as compared to the initial NAcCoMP8 sample, but these were masked by spectral noise. Secondly, the Q

band region exhibited significant albeit noisy shifts. Both the Q bands disappeared after 1 minute and were replaced by a band at 540 nm and possibly by a band in the 500 nm region (**Figure 4.13**, inset).

The spectral shifts observed in NAcCoMP8 on the addition of $NaBH_4$ appeared to be consistent with the reduction of the trivalent CoTPPS[52] and CoTMPyP[64] It is thus plausible that the cobalt metal ion in NAcCoMP8 was rapidly reduced from Co(III)→Co(II) (red trace). The short-lived putative Co(II) species was then further reduced from Co(II)→Co(I) (blue trace). The re-oxidation of the putative Co(I)→Co(II)→Co(III) should be observed by the re-emergence of the initial NAcCoMP8 spectrum (black trace). The initial Soret band attempted to re-emerge at 415 nm when the cuvette was exposed to air (gray trace) however the yellow solution suggests degradation..

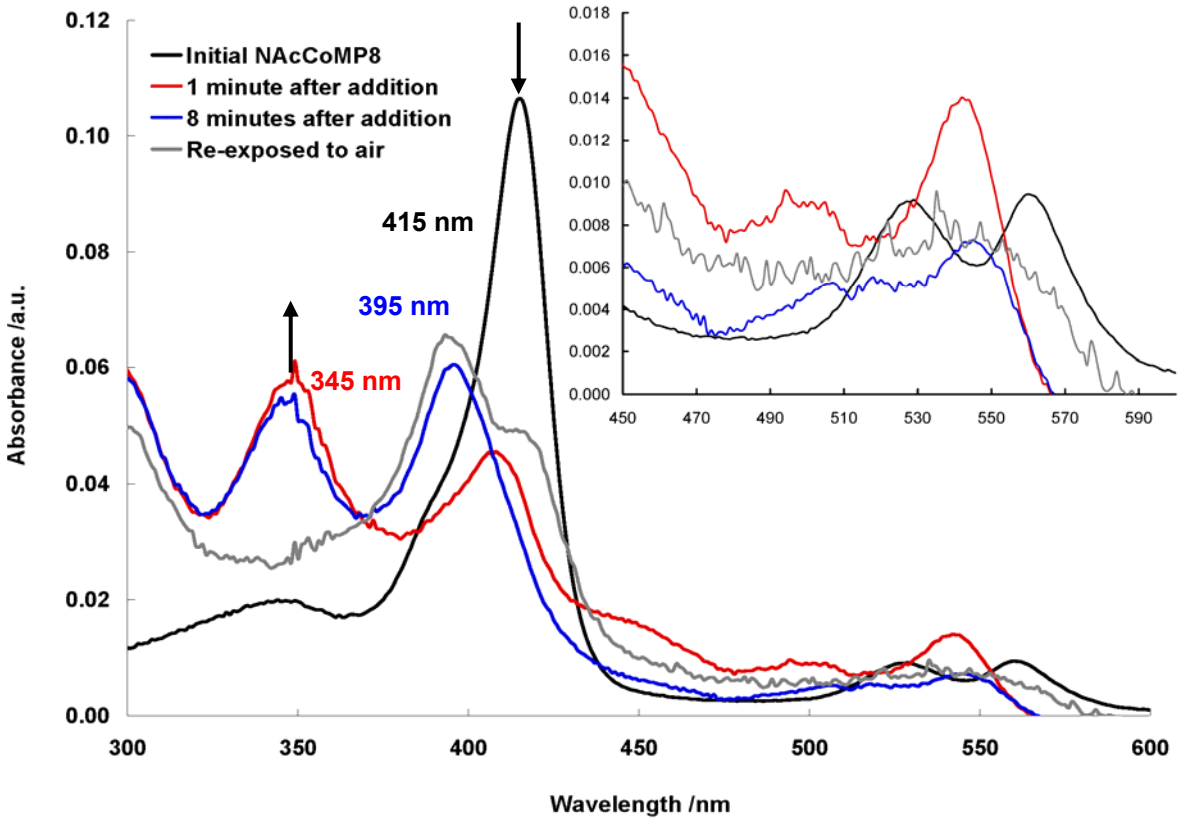


Figure 4.13 The effects of the reducing agent $NaBH_4$ on the absorbance sof NAcCoMP8 (degassed using argon, deionised water, 25 ^{o}C, pH 7.0).

3.3 SUMMARY AND CONCLUSIONS

This Chapter deals with the preparation of a spectroscopically stable monomeric NAcCoMP8 solution. A monomeric solution of NAcCoMP8 was obtained by qualitatively assessing the factors that affected aggregation and degradation, respectively. Aggregation was found to be affected by factors such as ionic strength, concentration, pH, equilibration time and temperature. Degradation was affected by exposure to light, air, reducing agents, dispersants and buffers. All these spectroscopic findings and qualitative observations are summarised (**Table 4.5**, **4.6**). Whilst this Chapter dealt with the solution preparation conditions of monomeric NAcCoMP8, it would be remiss not to comment on the interesting solution behaviour exhibited by this compound during these experiments.

The solution behaviour of NAcCoMP8 is complex; it appears to exist as three concentration-dependent species. These are tentatively termed the monomeric 415 nm species, the intermediate 417 nm species and the irreversible 424 nm species. When solid NAcCoMP8 is dissolved in deionised water, the first species observed is at 417 nm. This transient light pink species then transforms depending on its concentration in solution. If the solution is concentrated (*ca*. 10 μM or with an absorbance >0.7 a.u.) the 417 nm species converts rapidly to the 424 nm species. This orange-pink 424 nm species exhibits broad absorbance spectra and is spectroscopically unstable, especially towards ligand binding (see Chapter 5 where all three species were exposed to a test ligand, cyanide, and their respective binding behaviours were qualitatively compared). Furthermore, the formation of the 424 nm species appears to be irreversible when external pressures were applied (temperature, dilution with 50% MeOH and extreme changes in pH). When this species is left standing at room temperature for a few days, visible aggregates form (**Figure 3.11**) and characterisation data were irreproducible (**Table 4.5, 4.6**).

On the other hand, at low concentration, the 417 nm species converts *slowly* to the

415 nm species (*ca*. 1-2 μM or with an absorbance <0.3 a.u.). This slightly darker pink species was the most spectroscopically stable and reproducible characterisation data were obtained (**Appendix 3.6**). This species also responded reproducibly to ligand binding studies using a test ligand (**Chapter 5**) and was thus isolated for use in other solution chemistry studies. The characterisation data obtained for this species was also comparable to those observed previously.[60]

Some fascinating observations were noted about the 417 nm species. It appears as though this species is always in equilibrium with either 424 or 415 nm species depending on its concentration. Though seemingly short-lived, the 417 nm species could be promoted by external factors such as changes in temperature and ionic strength (**Section 4.2.4**; **Section 4.2.7**) but *only from the 415 nm species*. This suggests that it may be possible to isolate higher concentrations of the 415 nm species by diluting an intermediate concentration of the 417 nm species (*ca*. 3-6 μM or with an absorbance *ca*. 0.4-0.6 a.u.) with a non-coordinating and dispersing solvent at this stage such as 50% methanol. However, this approach was not explored as it lacks the practicality in mimicking the physiological conditions necessary for the comparative vitamin B_{12a} studies it was intended to provide insight into.

This peculiar and irreversible solution behaviour of the 424 nm species also provides some interesting insights towards the preparation of monomeric NAcCoMP8. It suggests that the formation of this species is entirely concentration dependent and its formation at high ionic strength and temperature is merely an artefact of the transient 417 nm species being at sufficiently high concentration and rapid kinetics at this concentration (a half life of formation of under 10 minute). There is no wavelength dependence and one set of neat isosbestic points suggests a simpler reaction. It is likely that the species formed occurs through covalent metal–side-chain interaction.

Subsequently, the abovementioned behaviour provides ample insight into the

formation of the *monomeric* 415 nm species. Its formation is complex and the evidence suggests mixed equilibria. It seems plausible that since NAcCoMP8 lyophilises at high concentrations in dispersing solvents such as acetonitrile, it forms a mixture of loosely packed π-π dimers and/or tetramers. These species then monomerise at different rates when diluted. The monomerisation of the dimer is expected to be simpler than that of the tetramer and hence faster which accounts for the large discrepancy in half life values (between 10 – 20 minutes).

However, once the 415 nm species is formed, it is spectroscopically stable enough to perform solution-based experiments on. It was found that monomeric NAcCoMP8 has 5 pK_a values at 25 ^{o}C. The pK_a of interest, the aqua/hydroxyl equilibrium, occurs at 7.81 ± 0.03 which is lower than both that of vitamin B_{12a} and NAcFeMP8. It was also observed that acetylation was important in the facilitation of monomerism and that adherence to Beer's Law is not a sufficient indicator of monomerism in this case. Additionally, NAcCoMP8 shows a greater sensitivity towards air exposure than light exposure and degrades to a mixture of presumably biliverdin and bilirubin under prolonged exposure to both conditions. NAcCoMP8 may be reduced chemically with $NaBH_4$. This reduction is reversible. Detergents add optical interference and HEPES buffer provides a competing ligand.

Thus, a spectroscopically stable and monomeric NAcCoMP8 solution can be prepared by dissolving lyophilised NAcCoMP8 to degassed deionised water or low ionic strength buffer (<0.1M). Solid NAcCoMP8 should be stored under argon and handled whilst still frozen, possibly with the aid of an antistatic gun. Buffers and/or detergents should be pre-screened for spectroscopic interferences. Solutions should be stirred before use to promote the monomeric aqua species (1-2 hours; 25 ^{o}C; pH 7; λ_{max} = 415 nm at *ca* 0.3 a.u.; *ca*. 1-2 μM). Extreme light-, oxygen- and heat exposure should be avoided. Extreme oxygen and light exposure promotes degradation to bilins whilst extreme temperatures promote 417 nm species contamination. Samples should be clarified with a syringe filter before experiments and should be distinctly pink in colour.

Table 4.5 Summary of all the results obtained in Chapter 4.

Factor	Condition	Final Colour	†Shifts /nm		‡‡Intensity /%		Data obtained from study
			Soret	Q-bands	Soret	Q-bands	
AGGREGATION	↓ [Time]	Dark pink	417→415	None	↑ (5)	↑ (5), ↑ (10)	$t_{1/2(424nm)}$ = 7.24 min; $t_{1/2(417nm)}$ = 7.98 min $k_{1(424nm)}$ = 0.096 ± 0.002; $k_{1(417nm)}$ = 0.087 ± 0.004
	↑ [Time]	Pink orange	417→424 (422)	530→538; 560→568; (533, 554, 570)	↓ (30)	↓ (10), ↓ (20)	$t_{1/2(424nm)}$ = 9.97 min; $t_{1/2(417nm)}$ = 19.57 min $k_{1(424nm)}$ = 0.070 ± 0.007; $k_{1(417nm)}$ = 0.035 ± 0.005
	↓ [Ionic]	Light pink	415→417	None	↓ (70)	↓ (70), ↓ (75)	K_1 = 0.080 ± 0.008 M^{-3}, n = 3.4 ± 0.3
	↑ [Ionic]	Yellow orange	417→424 (422)	530→538; 560→568; (533, 554, 570)	↓ (30)	↓ (10), ↓ (20)	K_1 = 2.19 ± 0.09 M^{-3}, n = 3.7 ± 0.8
	↓[Temp]	Dark pink	415→417	None	↓ (10)	↓ (5), ↓ (10)	Linear dependence limiting slope (-7.0 x 10^{-4})
	↑[Temp]	Pink orange	415→422 (420)	527→537; 560→574; (530, 553, 567)	↓ (30)	↓ (10), ↓ (15)	Linear dependence limiting slope (-1.12 x 10^{-2})
	Conc.	Dark pink	415→418	None	††	††	Linear dependence limiting slope 1.94 x 10^5 M^{-1} cm^{-1}
	↓pH	Dark pink	415→410	530→526; (530, 570, 590)	-	-	pK_as = 1.74 ± 0.04, 4.08 ± 0.02, 5.80 ± 0.05
	↑pH	Pink orange	415→418	530→538; 560→568	-	-	pK_as = 7.81 ± 0.03 and 12.00 ± 0.03.
DEGRADATION	Light	Pale yellow	‡	‡	↓ (15)	‡	$t_{1/2(415)}$ = 478 min k_1 = 0.0015 ± 0.0002
	O_2	Yellow orange	‡	‡	↓ (15)	‡	$t_{1/2(415)}$ = 7.81 min k_1 = 0.089 ± 0.009
	Buffer	Bright Pink	415→413 (414)	530→528; 560→558	none	↓ (5), ↓ (5)	Qualitative; HEPES
	Red. A	Pale yellow	415→395→ 345(400, 384, 370)	560→545→540;530 →490→diminished	↓ (60)	↓ (50), ↓ (60)	Qualitative; $NaBH_4$

↑[x] refers to study [x] conducted at high NAcCoMP8 concentrations where X refers to time, temperature, pH etc.

↓[x] refers to study [x] conducted at low NAcCoMP8 concentrations where X refers to time, temperature, pH etc.

† isosbestic point(s) in brackets

†† the study involved monitoring a shift in absorbance intensity so reporting it here will not be an authentic reflection of intensity change in relation to concentration; see rather Time studies.

‡ absorbance values recorded at Soret only

‡‡ Intensity increase or decrease denoted by arrows with estimated percentage in brackets

Table 4.6 Summary of the qualitative differences observed for the conversion of NAcCoMP8 from the 417 to 415 nm species and from 417 to 424 nm.

	OBSERVED EQUILBRIA	
	417 → 415 nm	**417 → 424 nm**
1.	Light pink to dark pink solution	Light pink to orange-pink solution
2.	Complex (mixed) equilibria	Simple equilibria
3.	Wavelength dependence	No wavelength dependence
4.	Poorly defined isosbestic points	Well defined isosbestic points
5.	Slow kinetics	Rapid kinetics
6.	Reversible	Not reversible
7.	By high ionic strength and temperature	No effect
8.	Forms putative dimer/tetramer by π-π stacking	Forms putative tetramer by covalent metal–side-chain interaction

4.4 REFERENCES FOR CHAPTER 4

1. Carraway, A. D.; McCollumn, M. G.; Peterson, J., *Inorg. Chem.,* **1996**, *35,* 6885.
2. Wilson, M. T.; Ranson, R. J.; Masiakowski, P.; Czarnecka, E.; Brunori, M., *Eur. J. Biochem*., **1977**, *77*, 193.
3. Othman, S.; Le Lirzin, A.; Desbois, A., *Biochemistry*, **1993**, *32* 9781
4. Wang, J. S.; van Wart, H. E.; *J. Phys. Chem.*, **1989**, *93*, 7925.
5. Verbaro, D.; Hagarman, A.; Kohli, A.; Schweitzer-Stenner, R., *J. Biol. Inorg. Chem.*, **2009**, *14(8)*, 1289.
6. Riposati, A.; Prieto, T.; Shida, C. S.; Nantes, I. L.; Nascimento, O. R., *J. Inorg. Biochem*., **2006**, *100(2)*, 226.
7. Baldwin, D. A.; Mabuya, M. B.; Marques, H. M., *S. Afr. J. Chem.*, **1987**, *40(2)*, 103.
8. Aron, J. A.; Baldwin, D. A.; Marques, H. M.; Pratt, J. M.; Adams, P. A., *J. Inorg. Biochem.*, **1986**, *27*, 227.
9. Chuang, W. J.; Chang, Y. D.; Jeng, W. Y., *J. Inorg. Biochem*., **1999**, *75(2)*, 93.
10. Ehrenberg, A.; Theorell, H., *Acta Chem. Scand.*, **1955**, *9*, 1193.
11. Pasternack, R. F.; Parr, G. R., *Inorg. Chem*., **1976**, *15*, 3087
12. White, W. I., in D. Dolphin (ed.), *The Pophyrins*, vol. 5, Academic Press, London, 1978, pp. 303-339.
13. Marks, T. J., *Science*, **1985**, *227,* 881.
14. Pasternack, R. F.; Lee, H.; Malek, P.; Spencer, C., *J. Inorg. Nucl. Chem.*, **1977**, *39,* 1865.
15. Pasternack, R. F.; Francesconi, L.; Raff, D.; Spiro, E., *Inorg. Chem.*, **1973**, *12*, 2606.

16. Brown, S. B.; Hatzikonstantinou, H., *Biochim. Bophys. Acta*, **1979**, *585*, 143.

17. Scheer, H.; Katz, J. J.; in K. M. Smith (ed.), *Porphyrins and Metalloporphyrins*; Elsevier Scientific Publishing Company, Amsterdam, 1975, pp 399-524

18. Urry, D. W.; Pettegrew, J. W., *J. Am. Chem. Soc.*, **1967**, *89*, 5276.

19. Urry, D. W., *J. Am. Chem. Soc.*, **1967**, *89*, 4190.

20. Shelnutt, J.A.; Dobry, M. M.; Satterlee, J. D., *J. Phys. Chem.*, **1984**, *88*, 4980.

21. Satterlee, J. D.; Shelnutt, J. A., *J. Phys. Chem.*, **1984**, *88*, 5487.

22. White, W. I.; Plane, R. A., *Bioinorg. Chem*., **1974**, *4*, 21.

23. Satterlee, J. D.; Shelnutt, J. A., *Inorg. Chim. Acta.*, **1985**, *106*, 165.

24. Medhi, O. K.; Houlton, A.; Silver, A., *J. Inorg. Chim. Acta.*, **1989**, *161*, 213.

25. Mazumdar, S.; Medhi, O. K.; Mitra, S., *Inorg Chem.,* **1991**, *30,* 700.

26. Bowyer, J. R.; Odell, B.; *Biochem. Biophys. Res. Commun.*, **1985**, *127*, 828.

27. Marques, H. M.; Munro, O. Q.; Crawcour, M. L., *Inorg. Chim. Acta.,* **1992**, *196,* 221.

28. Baldwin, D. A.; Marques, H. M.; Pratt, J. M.; *J. Inorg. Biochem.*, **1986**, *27*, 245.

29. Fuhrhop, J.; Smith, K. M., in Smith, K. M. (eds.), *Porphyrins and Metalloporphyrins,* Elsevier Scientific Publishing Company, Amsterdamn 1975, pp 757-869.

30. Marques, H. M.; Perry, C. B., *J. Inorg., Biochem.,* **1999**, *75,* 281.

31. Harbury, H. A.; Loach, P. A., *Proc. Natl. Acad. Sci. U.S.A.*, **1959**, *45*, 1344.

32. Harbury, H. A.; Loach, P. A., *J. Biol. Chem.*, **1960**, *235*, 3640.

33. Peterson, J.; Saleem, M. M. M.; Silver, J.; *J. Inorg. Biochem.*, **1983**, *19,* 165.

34. Peterson, J.; Silver, J.; Wilson, M. T.; Morrison, I. E. G., *J. Inorg. Biochem.*, **1980**, *13,* 75.

35. Munro, O. Q.; Marques, H. M., *Inorg. Chem.*, **1996**, *35*, 3752

36. Marques, H.M., Ph. D. Dissertation, University of the Witwatersrand, Johannesburg, South Africa, **1986**.

37. Marques, H. M.; Shongwe, M. S.; Munro, O. Q.; Egan, T. J., *S. Afr. J. Chem.,* **1997**, *50*, 166.

38. Neta, P., *J, Phys. Chem.,* **1981**, *85,* 3678.

39. Abwao-Konya, J.; Cappelli, A.; Jacobs, L.; Krishnamurthy, M.; Smith, M., *Transition Met. Chem.*, **1984**, *9*, 270.

40. Adams, P. A.; Baldwin, D. A.; Marques, H. M., in Scott, R. A.; Mauk, A. G. (eds.), *Cytochrome c: A Multidisciplinary Approach*, University Science Books, Sausalito, California, 1996, pp. 635-692.

41. Kimura, K.; Peterson, J.; Wilson, M. T.; Cookson, D. J.; Williams, R. J. P., *J. Inorg. Biochem.*, **1981**, *15*, 11.

42. Satterlee, J. D., *Inorg. Chim. Acta.*, **1983**, *79*, 195.

43. Yang, E. K.; Sauer, K., in H. Chien (ed.), *Electron Transport and Oxygen Utilization*, Elsevier, New York, 1982.

44. Wang, J. S.; Tsai, A. L.; Heldt, J.; Palmer, G.; van Wart, H. E., *J. Biol. Chem.,* **1992**, *267,* 15310.

45. Jehanli, A. M. T.; Stotter, D. A.; Wilson, M. T., *Eur. J. Biochem.,* **1976**, *71*, 613.

46. Nassif, R.; Baumgartner, C. P.; Sellers, M.; May, L.; *Z. Naturforsch.*, **1976**, *31C*, 232.

47. Baumgartner, C. P.; Sellers, M.; Nassif, R., *Eur. J. Biochem.,* **1974**, *46*, 625.

48. DerVartanian, D. V., *Biochim. Biophys. Res. Commun.,* **1970**, *41,* 932.

49. Loehr, T. M.; Loehr, J. S.; *Biochem. Biophys. Res. Commun.*, **1973**, *55*, 218.

50. Hatano, K.; Usui, K.; Ishida, Y., *Bull. Chem. Soc. Jpn.,* **1981**, *54*, 413.

51. Pasternack, R. F.; Cobb, M. A., *Biochem. Biophys. Res. Commun.,* **1973**, *51(3),* 507.

52. Mosseri, S.; Neta, P.; Harriman, A.; Hambright, P., *J. Inorg. Biochem.,* **1990**, *39*, 93.

53. Endisch, C.; Fuhrhop, J. H.; Buschmann, J.; Luger, P.; Siggel, U., *J. Am. Chem. Soc.*, **1996**, *118*, 6671.

54. Ruhlmann, L.; Nakamura, A.; Vos, J. G.; Fuhrhop, J. H., *Inorg. Chem.*, **1998**, *37*, 6052.

55. Sawaguchi, T.; Matsue, T.; Itaya, K.; Uchida, I., *Electrochim. Acta*, **1991**, *36*, 703.

56. Milgrom, L. R.; *The Colours of Life: An introduction to the chemistry of porphyrins and related compounds,* Oxford University Press, Oxford, 1997, pp 156-175.

57. King, R. F. G. J.; Brown, S. B., *Biochem. J.,* **1978**, *174*,103.

58. Kumar, D.; de Visser, S. I. P.; Shaik, S., *J. Am. Chem. Soc*., **2005**, *127*, 8204.

59. Bhakta, M. N.; Olabisi, A.; Wimalasena, A.; Wilks, A., *J. Inorg. Biochem.*, **2008**, *102*, 251.

60. Sannasy, D., M.Sc. Dissertation, University of the Witwatersrand, Johannesburg, South Africa, **2005**.

61. Reenstra, W. W.; Jencks, W. P., *J. Am. Chem. Soc.*, **1979**, *101*, 5780.

62. Marques, H. M.; Brown, K. L.; Jacobsen, D.W., *J. Biol. Chem*., **1988**, *263*, 12378.

63. Shannon, R. D., *Acta Cryst*., **1976**, *A32*, 751.

64. Pasternack, R. F.; Cobb, M. A.; Sutin, N., *Inorg. Chem.*, **1975**, *14*, 866**.**

CHAPTER 5
Equilibrium Constants for Ligand Binding by NAcCoMP8

5.1 INTRODUCTION

Studying metal-ligand interactions often reveals important coordination information about the nature of the central metal ion in macrocyclic compounds.[1,2,3] These metal-ligand interactions may be probed using a three-fold approach. Firstly, the interactions may be investigated by comparing physical properties such as spectral shifts in the Uv-vis spectrum, and bond lengths and angles in the ground state of each compound (the so-called ground state '*cis*- and *trans*-influences'). Secondly, the comparison of chemical equilibria, which measure the difference in free energy between the ground states of these compounds, may be compared ('thermodynamic influences'). Lastly, by comparing the rates of reactions exhibited by these compounds, the difference between the ground- and transition states may be observed ('kinetic effects' – see **Chapter 6**).[1]

Ligand binding studies offer a useful means of acquiring data pertaining to metal-ligand interactions.[2,4,5] In these binding studies a metal complex is typically reacted with selected ligands and the metal-ligand interactions are monitored spectrophotometrically or by some other technique such as NMR or potentiometry. By performing comparative ligand binding studies of two related compounds with varied *cis* ligands (such as the corrin in vitamin B_{12a} and the porphyrin in NAcCoMP8), the (in this case) *macrocyclic influence* exerted on the metal ion may also be observed (*cis* influence). This forms the basis of the hypothesis used to elucidate the macrocyclic influence on the nature of cobalt(III) in vitamin B_{12a} in this work (**Chapter 1**).

In this study, water *trans* to histidine was substituted with various exogenous ligands as a function of temperature in a simple cobalt(III) porphyrin, *NAcCoMP8*. NAcCoMP8 serves as a biomimetic model[6] for B_{12a} (**Chapter 1**) and thus presents an excellent candidate for comparative ligand binding studies. Cobalt(III)-containing vitamin B_{12a} corrin macrocycle has 5,6-dimethybenzimidazole (DMB) and water in α and β positions, respectively,[7] whilst the analogous NAcCoMP8 porphyrin has water and histidine, (His) respectively.[8] The equilibria involving the binding of a single ligand can be readily observed using a wide range of exogenous ligands whilst being conveniently monitored using uv-vis spectroscopy.[6,9] Furthermore, the chemistry is not complicated by the formation of *cis*-*trans*-isomers as one of the axial ligands (DMB and His-18, in B_{12a} and NAcCoMP8, respectively) is tethered to the macrocycle (**Figure 5.1**).[10,11]

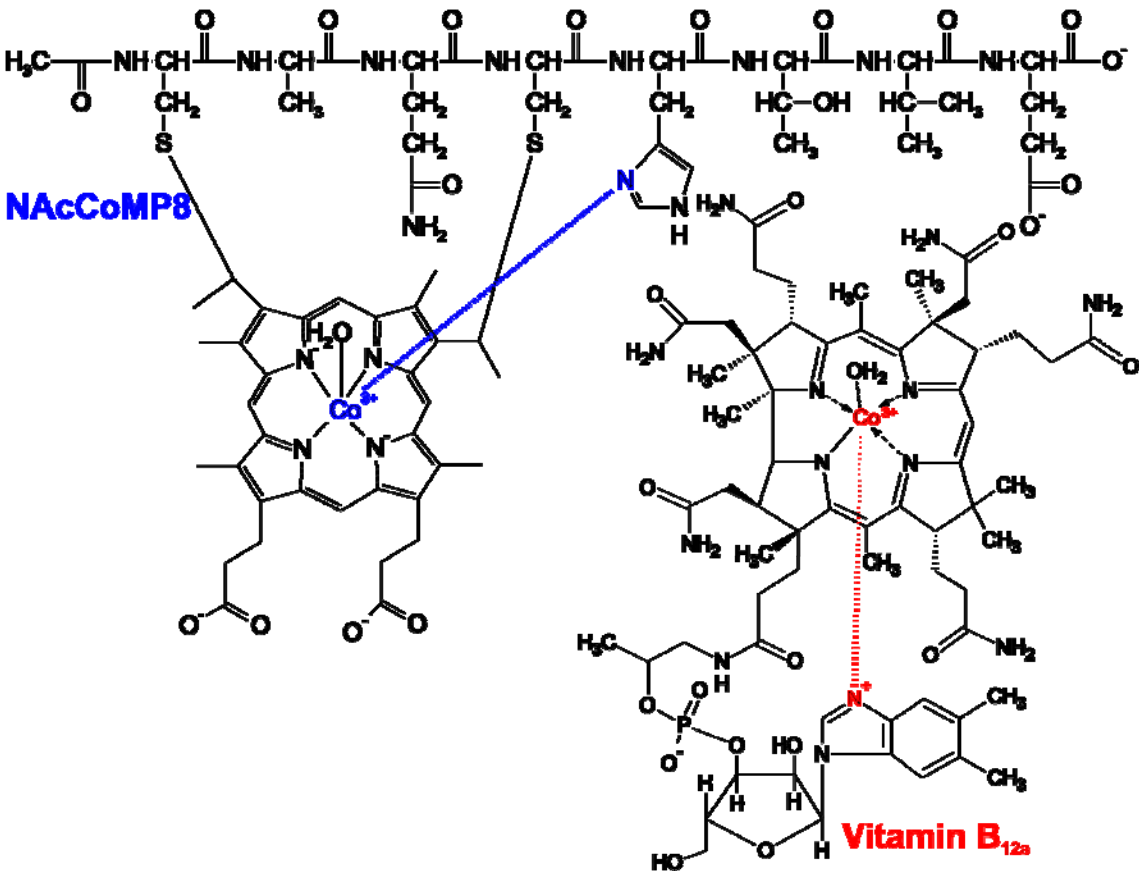


Figure 5.1 Structures of Vitamin B_{12a} and NAcCoMP8. Vitamin B_{12a} axially bound to N-donor DMB (red) and NAcCoMP8 axially bound to N-donor His-18 (blue); both ligands *trans* to axially coordinated water.

The aim of the work reported in this Chapter is therefore to qualitatively and quantitatively assess the *cis* effects of the equatorial ligand on the metal ion by comparing the ligand binding properties of Co(III) in NAcCoMP8 and in B_{12a}. Quantitatively, this was achieved by reacting NAcCoMP8 with selected ligands in order to observe absorbance changes, from which thermodynamic (log K, ΔH and ΔS) data were obtained. The absorbance spectra were also qualitatively compared. The anionic ligands examined were: cyanide, azide, nitrite and sulfite; the neutral ligands* were: pyridine, N-methyl imidazole, methoxyamine and hydroxylamine. These data were then compared to analogous B_{12a} data in order to elucidate the effects of the corrin ring on the ligand binding properties of the centrally-bound cobalt(III). These data were acquired as a function of temperature (*ca*. 15 – 40 ^{o}C) at constant ionic strength (μ = 0.1 M) and pH (*ca*. pH 7; except in HSO_3^-, which was obtained at *ca*. pH 5 using acetate buffer[12]) (**Investigation 2.1**, **Figure 5.2**).

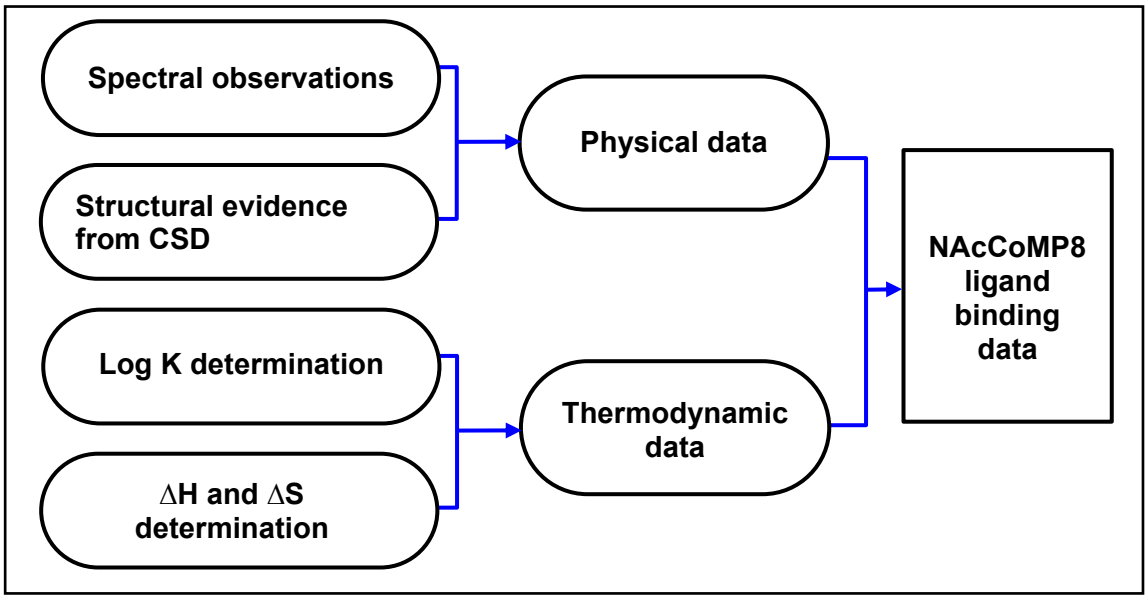


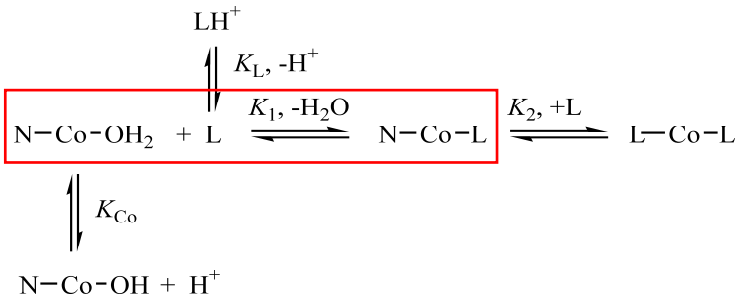
Figure 5.2 Flow diagram of the different aims and results in Chapter 5

* Here and elsewhere vitamin B_{12a} and neutral ligands are abbreviated: B_{12a}, pyridine (Pyr); n-methyl imidazole (NMI); methoxyamine (MOA) and hydroxylamine (HA).

5.2 RESULTS AND DISCUSSION

Absorbance spectra (300 – 700 nm) and thermodynamic data (log K, ΔH and ΔS) for the substitution of coordinated water by selected anionic (CN^-, N_3^-, NO_2^-, HSO_3^-) and neutral (Pyr, NMI, MOA, HA) ligands were obtained for NAcCoMP8 and for B_{12a} (15 – 40 °C; μ = 0.1 M; pH 7). Reagents (**Section 2.4**), technical specifications (**Section 2.4**), specialized (**Sections 2.2.2; 2.2.3**) and general techniques (**Section 2.5**) may found elsewhere (**Chapter 2**).

The following pH-dependent equilibria occur for a monomer in solution:



Equation 5.1

where N represents the proximal ligand (His-18 in NAcCoMP8 and DMB in B_{12a}) Overall charges have been ignored for convenience. The equilibrium of interest refers to the highlighted reaction in **Equation 5.1**. The incoming ligand L, replaces the distally bound water in the coordination sphere of the cobalt ion.

Absorbance spectra were recorded for these ligand-binding reactions and then used in two separate investigations. Firstly, spectra were qualitatively compared to observe any ligand-dependent spectral shifts (**Section 5.2.1.1**). Secondly, wavelength specific absorbance data were fitted using non-linear least squares methods in SigmaPlot[13] in order to find log K (**Section 5.2.2.1**) by applying the corrections mentioned previously (**Equation 2.6-2.8**). Often factors influencing log K (*i.e.* ΔH and ΔS values) are left unexplored by performing binding studies at one temperature only.[7] In this work, studies were therefore conducted as a function of temperature and values for ΔH (kJ mol^{-1}) and ΔS (J K^{-1} mol^{-1}) were determined from slope and intercept, respectively from van't Hoff plots (ln K vs 1/T) (**Section 5.2.2.2**).

Monomeric NAcCoMP8 is only spectroscopically stable at very low concentrations (see **Chapter 4**). These low NAcCoMP8 concentrations in addition to the small ligand binding absorbance shifts no doubt increased the experimental error. Thus, some statistical considerations had to be effected in order to average out the inevitable experimental errors. Total absorbance changes were found to be small; thus monitoring absorbance at a single wavelength would lead to unduly large errors. This potentially wavelength-dependent[14] bias was mitigated by averaging absorbance data across a set of wavelengths, typically 20 nm on either side of the isosbestic point in the Soret region. The Q-band region was unusable due to the very small absorbance changes in that region. However, since some wavelengths give log K values with larger errors than others, a weighted averaging procedure† was employed in order to compensate for this observation. Furthermore, all absorbance values were corrected for dilution, free ligand- and pK_a- effects (**Section 2.3.1**).

5.2.1 A Qualitative Examination of the Physical Data

A qualitative assessment of the binding of NAcCoMP8 (and of B_{12a}) with various exogenous ligands was made in terms of absorbance spectra (Section **5.2.1.1**) and solid state bond length evidence (Section **5.2.1.2**) obtained from the CSD‡.

5.2.1.1 Absorbance spectra observations

The influences of binding a selected group of exogenous ligands to cobalt(III)-containing macrocycles with different equatorial ligands may be observed by comparing the absorbance spectra obtained during these studies. These may be termed ground state *cis* influences.

† The weighting factor was equal to the reciprocal of the residual standard error of the estimate. This was then used to find the fractional weighted contribution (relative to the sum of all the weighting factors) of log K for each wavelength. The weighted log K was then the sum of these contributions such that the absorbance with the higher errors contributed less to the average than those values that were within error.[15]

‡ Cambridge Structural Database, V. 5.32 (updated: Nov 2010), CCDC, Cambridge, UK, 2010.

In this Section the ground state *cis* influences exerted by the porphyrin (and corrin) on the binding properties of Co(III) were qualitatively investigated. These qualitative investigations were achieved by comparing the absorbance profiles of NAcCoMP8 with selected exogenous ligands against similar data obtained for vitamin B_{12a}. Since it is the hypothesis that the equatorial ligand imparts some unique electronic properties onto cobalt(III), a general overview of the electronic influences on the absorbance spectrum of the corrin and porphyrin moieties is thus necessary.

There are usually five types of electronic transitions that occur in coordinated macrocycles. Firstly, there are the d-d transitions of the central metal ion. Then there are transitions predominantly associated with the macrocycle. Thirdly, there are internal transitions within the axial ligands (*e.g*. base on/off in the case of DMB in B_{12a} or His-18 in NAcCoMP8). There are also charge transfer transitions from the macrocycle to the metal or vice versa (equatorial MLCT or LMCT) and lastly from axial ligand to metal or vice versa (axial MLCT or LMCT).

In the case of B_{12a}, the important spin-allowed $\pi \rightarrow \pi^*$ transitions are observed above 300 nm (**Figure 5.3A**, red).[7] The bands with decreasing intensity are: γ band (350–370 nm), αβ bands (420–600 nm), δ bands (300-330 nm) and the lowest intensity D and E bands (390–420 nm) with no consensus on the δ band assignment.[7,16,17] These complex transitions were resolved using Gaussian analysis;[2] however, the simplified version adapted from Kuhn *et al*.,[18] is illustrated (inset). The bands below 300 nm are due to either protonated or coordinated DMB (280-290 nm).[7] Particularly noteworthy is the dependence of the absorbance spectrum on the identity of the axial ligands (see later **Figure 5.4**).[7] This ligand dependence, seen as shifts in the γ band,[1,17,19] correlate to the extent of *cis* and *trans* influences observed.[7] The γ band tends to exhibit a red shift as the donor strength of the axial ligands increase. [2,7,20]

Similarly, the porphyrin electronic transitions are also predominately spin-allowed $\pi \rightarrow \pi^*$.[7] The visible bands with decreasing intensity are: B or Soret band (390-420 nm) region, N (330-350 nm) and Q bands (500 – 600 nm)

(**Figure 5.3A**, blue).[9] Gouterman[21] first rationalised these transitions using the 'four-orbital model' where the absorption bands originate from transitions between the frontier orbitals, HOMO and HOMO-1, and LUMO and LUMO+1. The energies of these transitions are acutely affected by the identity of the metal ion and by the porphyrin substituents (see later **Figure 5.5**).[22] There are also strong vibronic bands in the UV-vis region.[22] The model used for the porphyrin electronic transitions in Figure 5.2 is for a low spin Fe(II) hematoporphyrin.[9] However the available spin states in iron tend to affect transitions most notably in the Q band region.[23] Given that cobalt(III) is in the low spin state, these transitions are not observed.[6]

One way to assess the macrocyclic effects on the metal ion would be to qualitatively compare the absorbance spectra of each macrocycle. In this case, NAcCoMP8 is compared with B_{12a} (**Figure 5.3A**, blue and red, respectively). Both macrocycles exhibit similar absorbance profiles as might be expected since their chromophores are strikingly similar.[17,22,24] They both have intense bands in the 350-400 nm and the 500-600 nm region. These bands correspond to γ and Soret bands, and αβ and Q bands, in corrin and porphyrin, respectively. However, the αβ bands are more prominent than the Q bands and exhibit a significant blue shift relative to the porphyrin bands. This may be a consequence of B_{12a} being the lesser conjugated system.[17]

Another way to observe the effect the macrocycle has on the metal ion would be to compare metal- and metal-free spectra (**Figure 5.3B**). Here, NAcCoMP8 (blue) is compared to metal-free acetylated microperoxidase (black). The corresponding corrin comparison (inset) has B_{12a} (red) superimposed on Toohey's[25] metal-free corrinoid (black). Immediately obvious is the distinctive blue shift in both the corrin and porphyrin metal-free spectra relative to the metallated species. Removal of the metal ion also seems to have a more profound effect on the Q bands rather than the αβ bands where the former splits into four Q bands in the metal-free porphyrin.

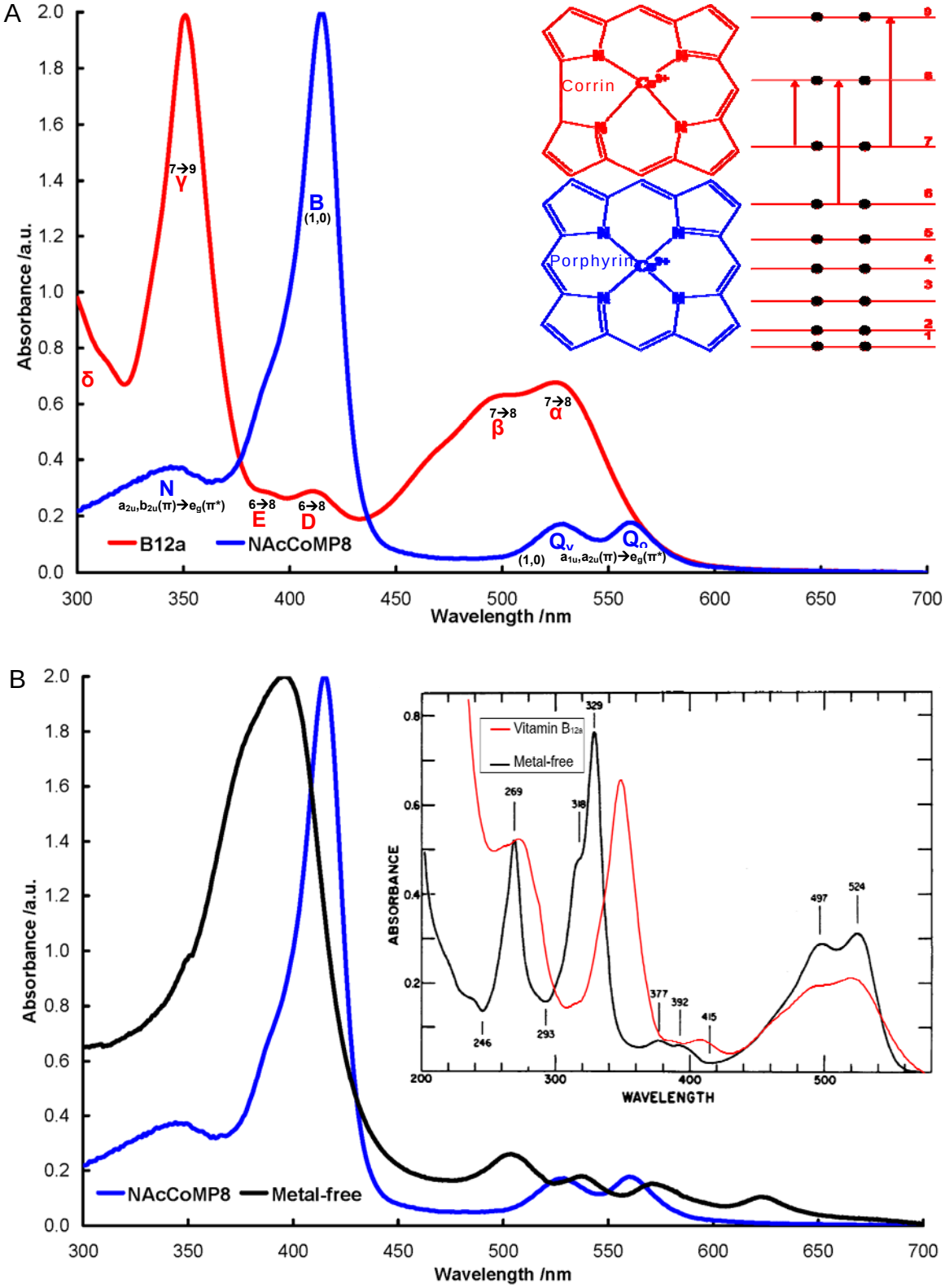


Figure 5.3 Comparison of absorbance spectra of NAcCoMP8 (blue) and vitamin B_{12a} (red) in deionised water illustrated with possible band assignments for porphyrin[9,23] and corrin [7,18] (**A**). These are then compared with the corresponding metal-free analogues at neutral pH (**B**). The spectrum of the metal-free corrinoid from *Chromatium* is adapted from Toohey[25] with the spectrum of vitamin B_{12a} superimposed in order to compare peaks and relative wavelength shifts but *not* intensities.

The absorbance profiles of NAcCoMP8 with selected neutral and anionic ligands were qualitatively compared to corresponding vitamin B_{12a} data. Spectra were obtained as previously described (**Chapter 2**). Aliquots of degassed ligand were added to NAcCoMP8 (and similarly to B_{12a}) in an argon-filled 1.0 cm pathlength cuvette fitted with a septum. The sample was gently stirred and allowed to reach equilibrium for 1 minute. An absorbance spectrum was then recorded between 300 – 700 nm. All spectra were run in MOPS (0.1 M; 25 ^{o}C *ca*. pH 6.8; spectra for HSO_3^- were obtained at pH 5 using $NaCH_3COO$ buffer).

Absorbance spectra were obtained for NAcCoMP8 with selected neutral and with anionic ligands so as to observe any qualitative spectral trends (**Figure 5.5**). It is immediately apparent that the extent of the red shift observed at the Soret is far more prominent with the anions than with the neutral ligands. In the case of the anionic ligands (**Figure 5.5B**) the Soret shift (415 → 425 nm) is double than the shift observed with the neutral ligands (**Figure 5.5A**) (415 → 420 nm). This trend is approximated in the Q band region as well however, to a lesser extent due to the instrument noise present at low porphyrin concentrations. This evidence suggests that there is significantly more metal-ligand interaction with anionic than neutral ligands in NAcCoMP8.

This significant red shift trend is far more apparent in the corresponding B_{12a} spectra (**Figure 5.4**). Here the anionic ligands (**Figure 5.4B**) exhibit a red shift in the γ band (350 → 367 nm) that is *ca*. 65% greater than the equivalent shift in the neutral ligands (350 → 361 nm). Additionally, the αβ bands exhibit far more prominent red shifts than the analogous Q bands in the porphyrin. It is even more interesting to note that the overall γ red shift observed in B_{12a} with the anionic ligands (17 nm) is *ca*. twice that observed in the analogous NAcCoMP8 data (10 nm). This trend is also seen with the neutral ligands where the γ red shift in B_{12a} (11 nm) was *ca*. twice that observed in NAcCoMP8 (5 nm). This evidence suggests that there is significantly more electronic metal-ligand interaction in the corrin than the porphyrin and more so with the anionic ligands than with the neutral ligands.

Other spectral observations include those that pertain to the anionic ligands cyanide and bisulfite in both macrocycles. In the case of the anionic ligand cyanide, both vitamin B_{12a}[7,26] (**Figure 5.4B**, red trace) and NAcCoMP8 (**Figure 5.5B**, red trace) show distinct red shifts relative to the other anionic spectra. It is in fact the largest red shift observed in both cases in this work. This significant red shift suggests that the strong-field cyanide ligand is promoting a smaller HOMO-LUMO gap relative to the other ligands in the study. The implication is that cyanide, presumably coordinating through the carbon atom,[7] is transferring significant amounts of electron density onto the cobalt ion in both cases. Furthermore, the red shift observed in B_{12a} due to cyanide is *ca*. 50% greater than that observed in NAcCoMP8. This significant disparity in red shift implies that the corrin facilitates a much smaller HOMO-LUMO gap with the trivalent cobalt ion than the porphyrin. In turn, this suggests that the corrin-cobalt system is accepting electron density more efficiently than the porphyrin-cobalt system.

In the case of the bisulfite ligand, coordination is presumably through the soft sulfur atom.[7] Here, vitamin B_{12a} exhibits a spectrum that is distinctly dissimilar to the others in the anionic series (**Figure 5.4B**, green trace). It may be argued that the cobalamin is being reduced since bisulfite is a known reducing agent however the reported sulfitocobalamin spectrum is not consistent with that of a reduced cobalamin.[7] It seems likely that the soft polarisable S-donor ligand influences nature of this spectrum; “atypical” vitamin B_{12a} spectra were previously documented as being common in soft polarisable ligands bound to trivalent cobalt,[1,2,12,27] in some organo-ligands complexes[7] or with linkage isomerism.[7,12] On the other hand, NAcCoMP8 does not exhibit this “atypical” spectral behaviour with bisulfite (**Figure 5.5B**, grey trace). There is, in fact, a great deal of similarity amongst the NAcCoMP8 spectra in this study. However, it is once again interesting to note that the red shift exhibited by B_{12a} is approximately 50% greater than that of NAcCoMP8.

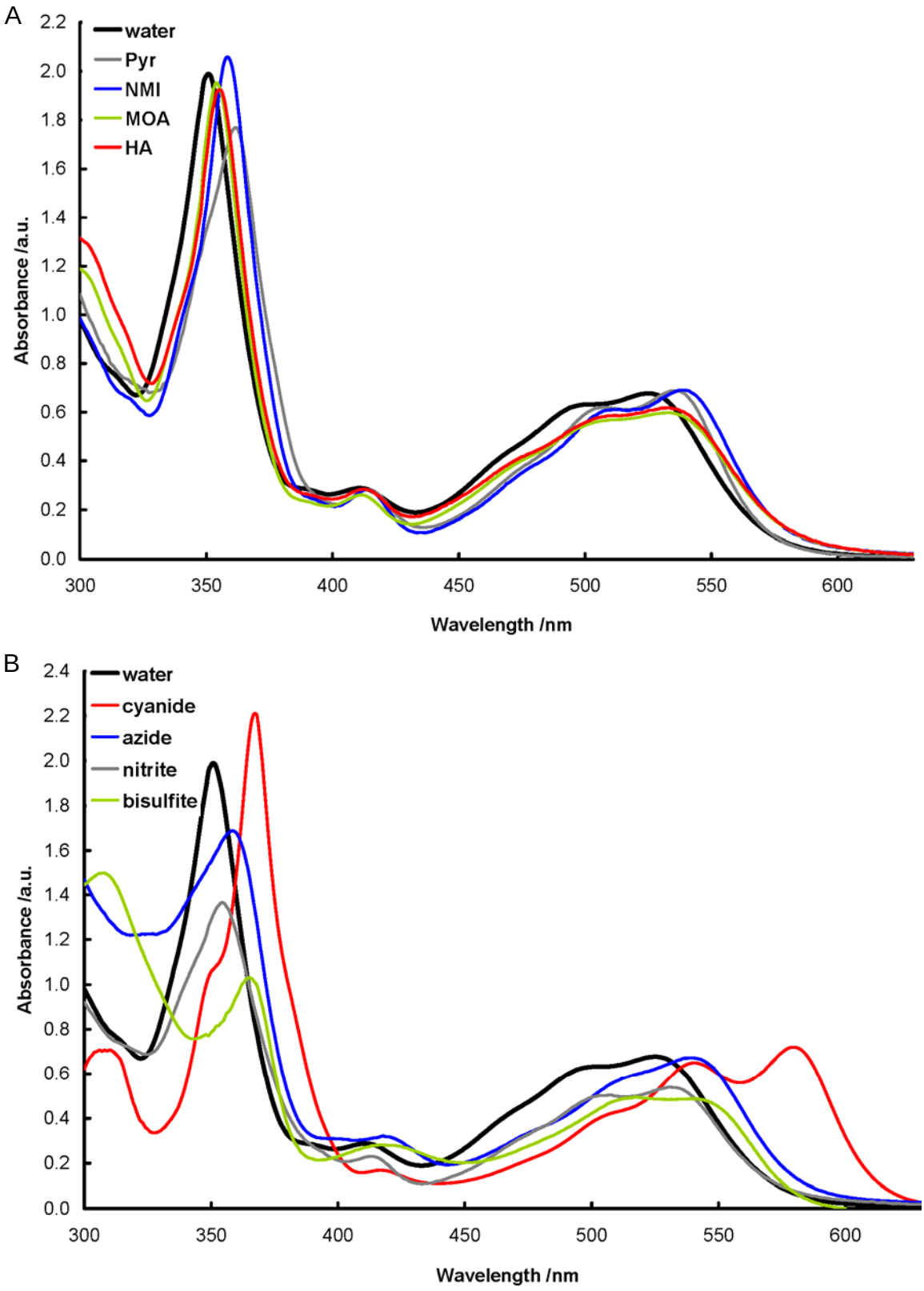


Figure 5.4 The comparison of spectral data in vitamin B_{12a} in MOPS buffer (0.1 M; pH 6.8; 25 °C) for some neutral (**A**) and anionic ligands (**B**). See Table 5.1 for isosbestic points relative to the aqua-species.

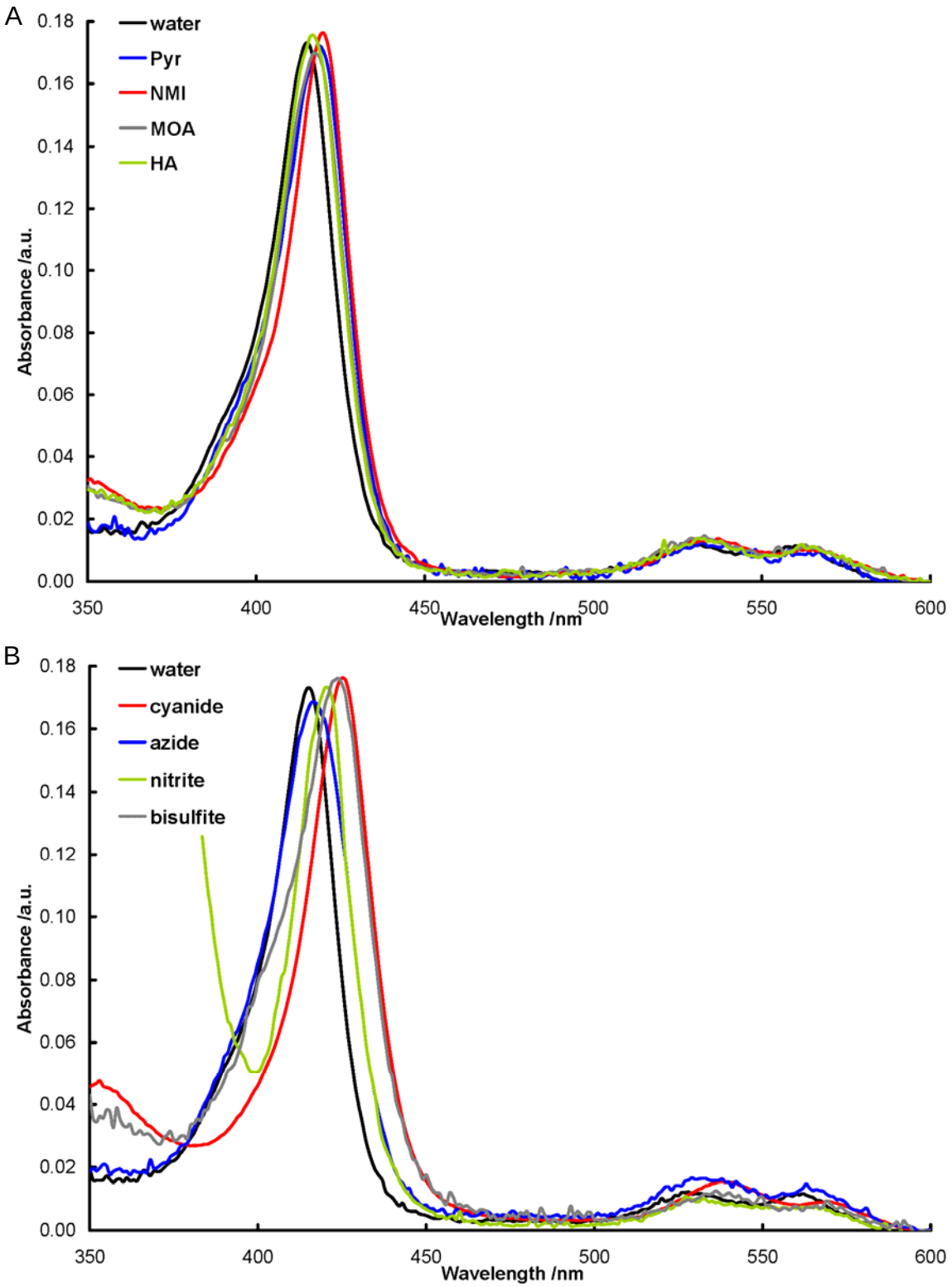


Figure 5.5 The comparison of spectral data in NAcCoMP8 in MOPS buffer (0.1 M; pH 6.8; 25 ^{o}C) for some neutral (**A**) and anionic ligands (**B**). See Table 5.1 for isosbestic points relative to the aqua-species.

Table 5.1 Isosbestic points for the replacement of coordinated water with selected exogenous ligands in NAcCoMP8 ligand binding studies

Ligand	Isosbestic points /nm	
	Vitamin B_{12a}	**††NAcCoMP8**
CN^-	†(1st) 325; 356; 386; 418; 533 †(2nd) 319; 359; 400; 531	†(1st) 373; 420; 500; 532; 551; 596 †(2nd) 383; 431; 544; 564
N_3^-	341; 356; 439; 531	360; 421; 470; 530; 547; 574
NO_2^-	340; 356; 404; 420; 494; 519	418; 440; 530; 543; 566
HSO_3^-	337; 361; 455; 502; 525	420; 530; 552; 574
Pyr	325; 357; 392; 418; 529	418
NMI	311; 355; 387; 411; 420; 508; 529	367; 418; 548; 567
MOA	323; 350; 383; 407; 418; 530	417
HA	325; 353; 383; 406; 421; 444; 528	416; 430; 550

† refers to 1st and 2nd substitution of cyanide, respectively (see later in the text, **Equation 5.2**; **5.3**)

†† refers to the monomeric 415 nm NAcCoMP8 species only (see later in this Section)

Another way to assess the macrocyclic influence of trivalent cobalt corrins and porphyrins on their electronic spectra would be to compare λ_{max} values of each system. Here, λ_{max} is used to indicate the wavelength (nm) at which the maximum absorbance value occurs. This may be at either the γ band in B_{12a} or at the Soret in NAcCoMP8. To achieve this, λ_{max} from the previous ligand binding spectral data are compared. Firstly, the λ_{max} values of NAcCoMP8 are compared to those obtained from NAcCoMP11 in order to have a cobalt(III)-porphyrin-porphyrin (Co^{III}-por-por) system for comparison (**Figure 5.6A**). Secondly, the NAcCoMP8 λ_{max} values were compared to those obtained for vitamin B_{12a}[12] such that a cobalt(III)-porphyrin-corrin (Co^{III}-por-cor) system may be compared (**Figure 5.6B**).

The shifts in wavelength in relation to selected anionic and neutral ligands are compared in the Co^{III}-por-por system (**Figure 5.6A**). This system reveals a reasonably linear relationship (R^2 = 0.89). This correlation suggests that the additional peptides present in NAcCoMP11 do not affect the electronic transitions on the chromophore to any appreciable degree. Thus, in general,

NAcCoMP11 and NAcCoMP8 show similar spectroscopic behaviour in solution. Both cobalt(III) porphyrins exhibit the largest wavelength deviation with the strong-field ligand, cyanide (relative to their respective aqua-complexes). The greatest deviation in the linear trend is contributed by the neutral ligand, pyridine followed by the anionic ligand, azide.

In contrast, the Co^{III}-por-cor system exhibits considerably more scatter (**Figure 5.6B**). The poorer wavelength correlation in the Co^{III}-por-cor system (R^2 = 0.66) emphasises the electronic dissimilarity between the macrocycles. This suggests that the corrin macrocycle affects the metal-ligand interaction differently than in the porphyrin macrocycle. Whilst the range in wavelength shifts in the Co^{III}-por-por system, relative to NAcCoMP11, is 11 nm, the range in the Co^{III}-por-cor system relative to vitamin B_{12a} is 17 nm. Despite this obvious disparity both macrocyclic systems exhibit the largest wavelength deviation with cyanide (relative to their respective aqua-complexes).

However, in the Co^{III}-por-cor system the greatest deviation in the linear trend is due to nitrite and *not* pyridine as anticipated from the Co^{III}-por-por system. In this B_{12a} study (*ca*. 25 ^{o}C, pH 7, μ = 0.1 M) the shift in λ_{max} from the aqua to the 'nitro' species was 350 → 354 nm. This was in agreement with the crystallographic evidence[54] which indicated that Co(III) in B_{12a} binds NO_2^- through the relatively softer N-donor atom. This is consistent with the corrin-Co(III) affinity for the softer donor atom in an ambidentate nucleophile inferring a more Co(II)-type nature in this macrocycle.

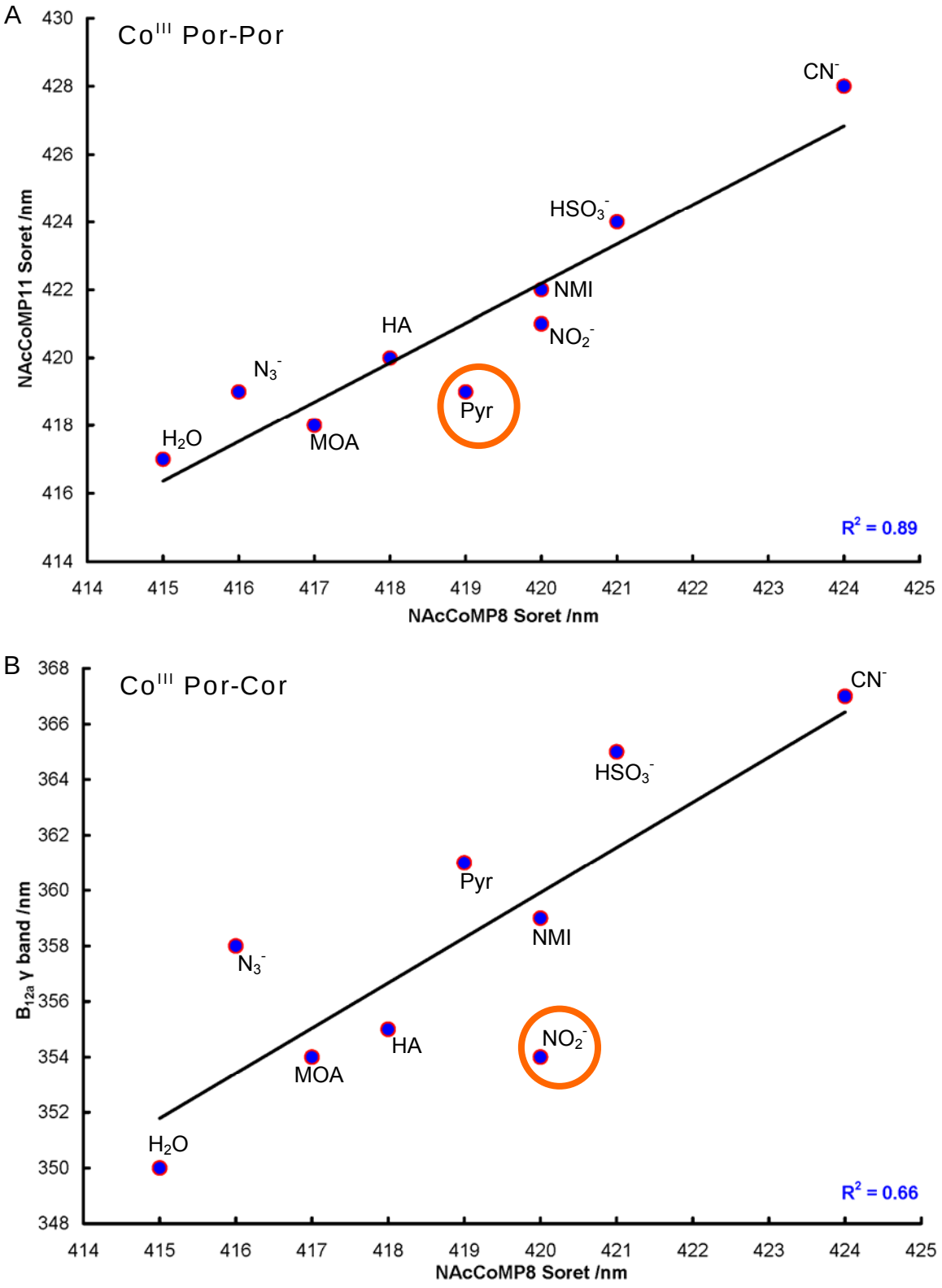


Figure 5.6 Comparison of Sorets (nm) for NAcCoMP8 and NAcCoMP11 (**A**) and for NAcCoMP8 and vitamin B_{12a} (**B**). The B_{12a} wavelength shifts were consistent with values reported previously.[12] See Table 5.1 for isosbestic points relative to the aqua-species.

Some examples of the absorbance spectra collected during the titration of B_{12a} with the various ligands explored in this work are illustrated below (**Figure 5.7,** isosbestic points in **Table 5.1**). The titration involving the anionic ligand bisulfite exhibited the interesting so-called 'atypical' vitamin B_{12a} spectra mentioned previously. These spectral profiles are common with B_{12a}-sulphur compounds.[2,7] There is significant absorbance in the δ band region and a distinct hypochromism of the γ band, which is considerably red shifted.[27] To compare the corresponding NAcCoMP8 spectra here would be meaningless given the small and noisy spectral shifts. However, the spectral shifts pertaining to the binding of the test ligand, cyanide, to NAcCoMP8 revealed some interesting spectral differentiation and were subsequently reported on.

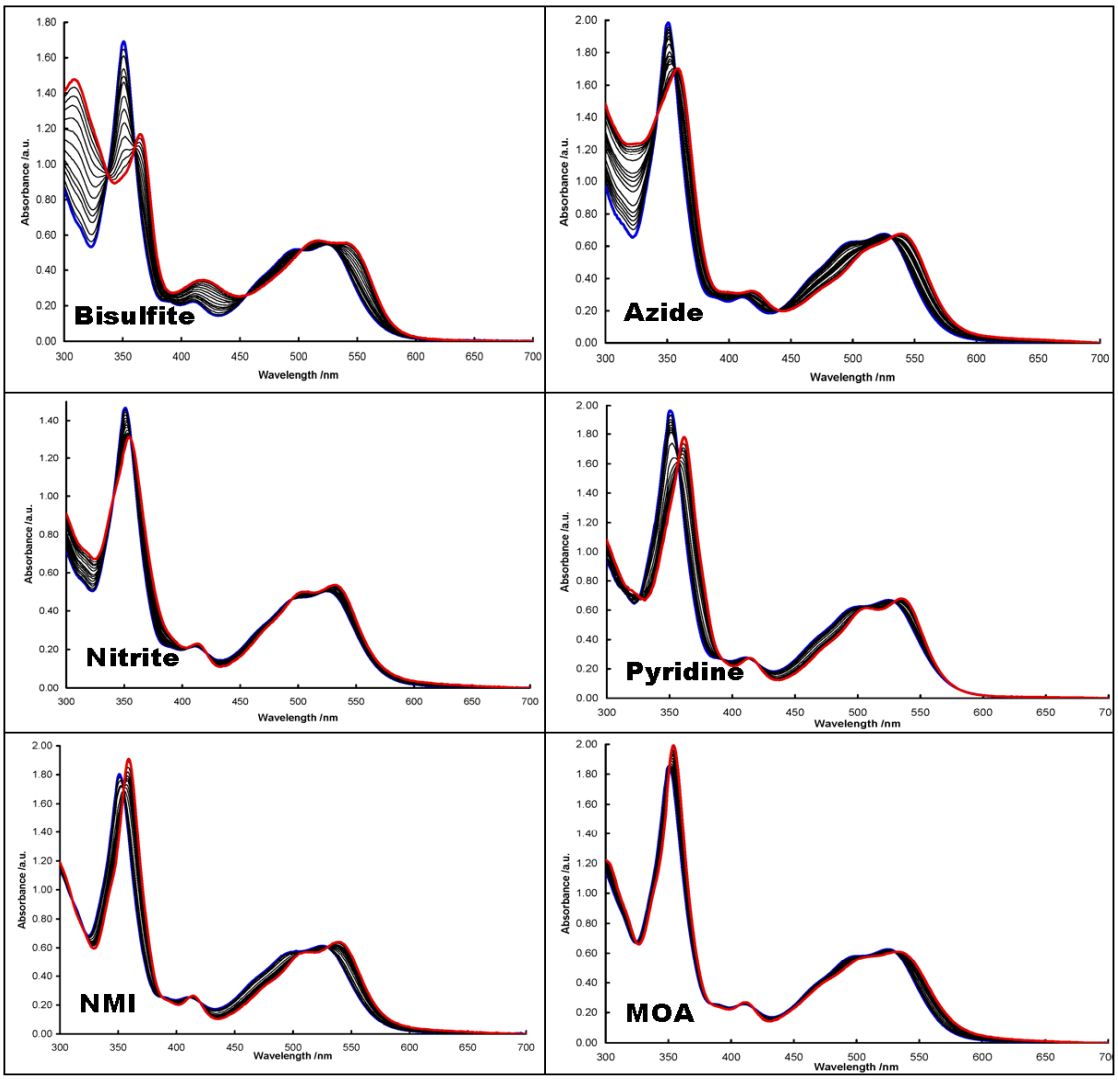


Figure 5.7 The titration of vitamin B_{12a} in MOPS buffer (0.1 M; pH 6.8; 25 ^{o}C) with some examples of anionic and neutral ligands. Refer to Table 5.1 for isosbestic points.

Like other microperoxidases,[28-30] NAcCoMP8 is prone to aggregation and exists as three concentration-dependent species in solution (**Chapter 4**). These are the monomeric 415 nm species present at very low concentrations; the transient 417 nm species and the irreversible 424 nm species that occurs at higher concentrations. These species were reacted with cyanide as a test ligand in order to compare the ligand binding behaviour of each species.

The ligand binding of cyanide with each NAcCoMP8 species was conducted at 25 ^{o}C as previously described (**Chapter 2**). With each species, aliquots of freshly prepared NaCN solution were added to NAcCoMP8 in a 1.0 cm pathlength cuvette under argon. The sample was allowed to reach equilibrium for 1 minute (**Section 4.2.1**) after which an absorbance spectrum was recorded between 300 – 700 nm (MOPS 0.1 M; *ca*. pH 7). The wavelength-specific absorbance data were then fitted using non-linear least squares methods in SigmaPlot[13] in order to find log K (**Section 5.2.2.1**; **Equation 2.6**; **2.7**). It is appreciated that since the 417 nm species is only briefly isolated that it represents a mixture of 424 nm and/or 415 nm species as well.

Each NAcCoMP8 species exhibits two sets of spectral data, **A** and **B** (see **Figures 5.8**-**5.10**). Here, **A** and **B** presumably corresponds to the 1st and 2nd ligand substitutions, respectively (**Equation 5.2**; **5.3**, where L is the incoming cyanide ligand). It is immediately obvious that the equilibrium observed in the 415 nm species (**Figure 5.8**) is unique relative to the 417 (**Figure 5.9**) and 424 nm species (**Figure 5.10**), certainly at the first substitution. At the first substitution only the 415 nm species exhibits 3 well-defined, spectroscopically stable isosbestic points in the Q band region (**Figure 5.8A**). In contrast, the 417 and 424 nm species exhibited poorly defined isosbestic points suggesting the existence of mixtures in solution. Thus, it was the monomeric 415 nm species that was used for subsequent ligand binding studies.

$$\textbf{His-Co(III)-H}_2\textbf{O} + \textbf{L} \rightleftharpoons \textbf{His-Co(III)-L} + \textbf{H}_2\textbf{O} \qquad \textbf{Equation 5.2}$$

$$\textbf{His-Co(III)-L} + \textbf{L} \rightleftharpoons \textbf{L-Co(III)-L} \qquad \textbf{Equation 5.3}$$

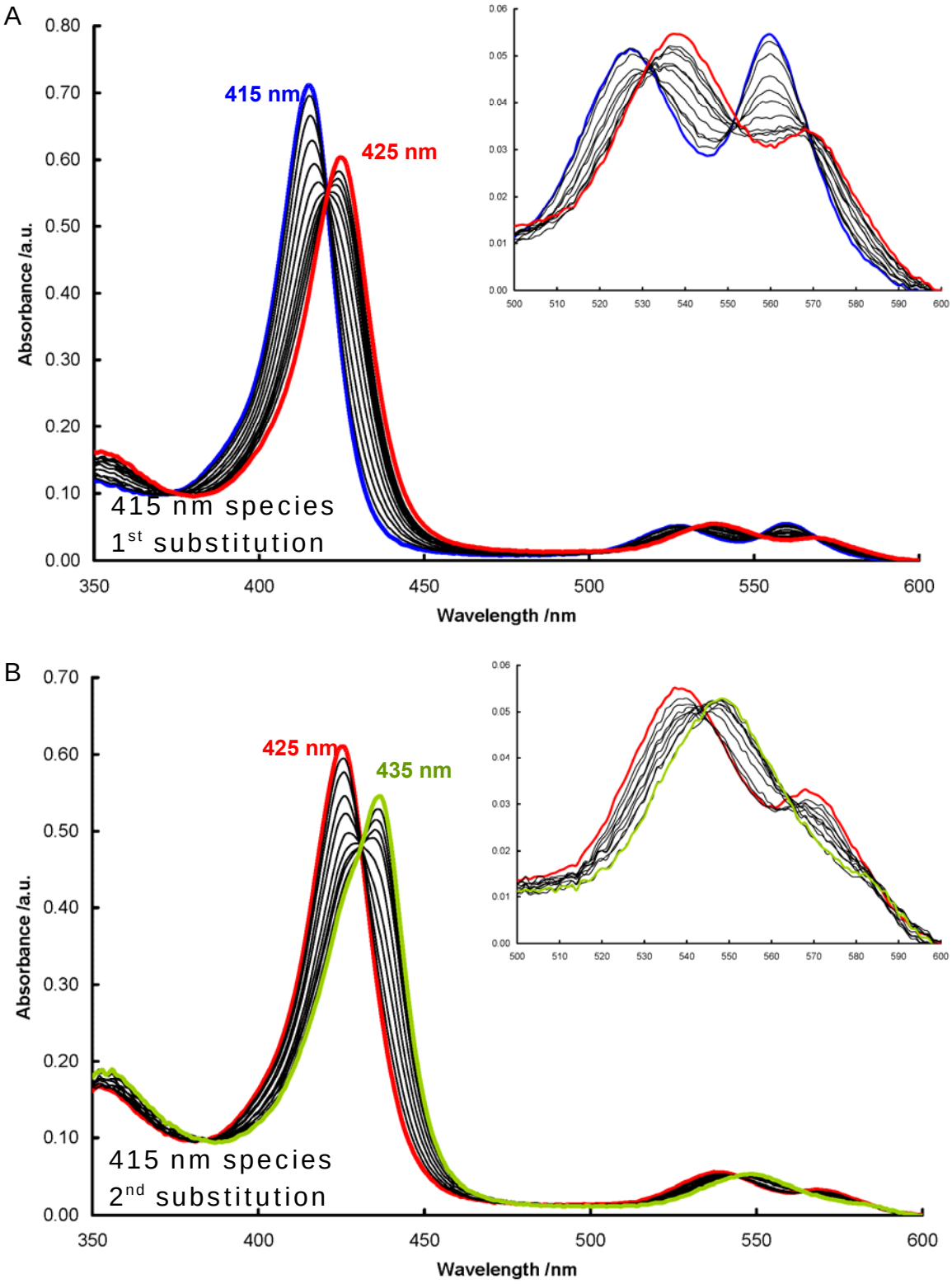


Figure 5.8 The titration of NAcCoMP8 415 nm species in MOPS buffer (0.1 M; pH 6.8; 25 °C) with NaCN (0.1 M) showing 1st (**A**) and 2nd axial substitution (**B**). Refer to Table 5.1 for isosbestic points.

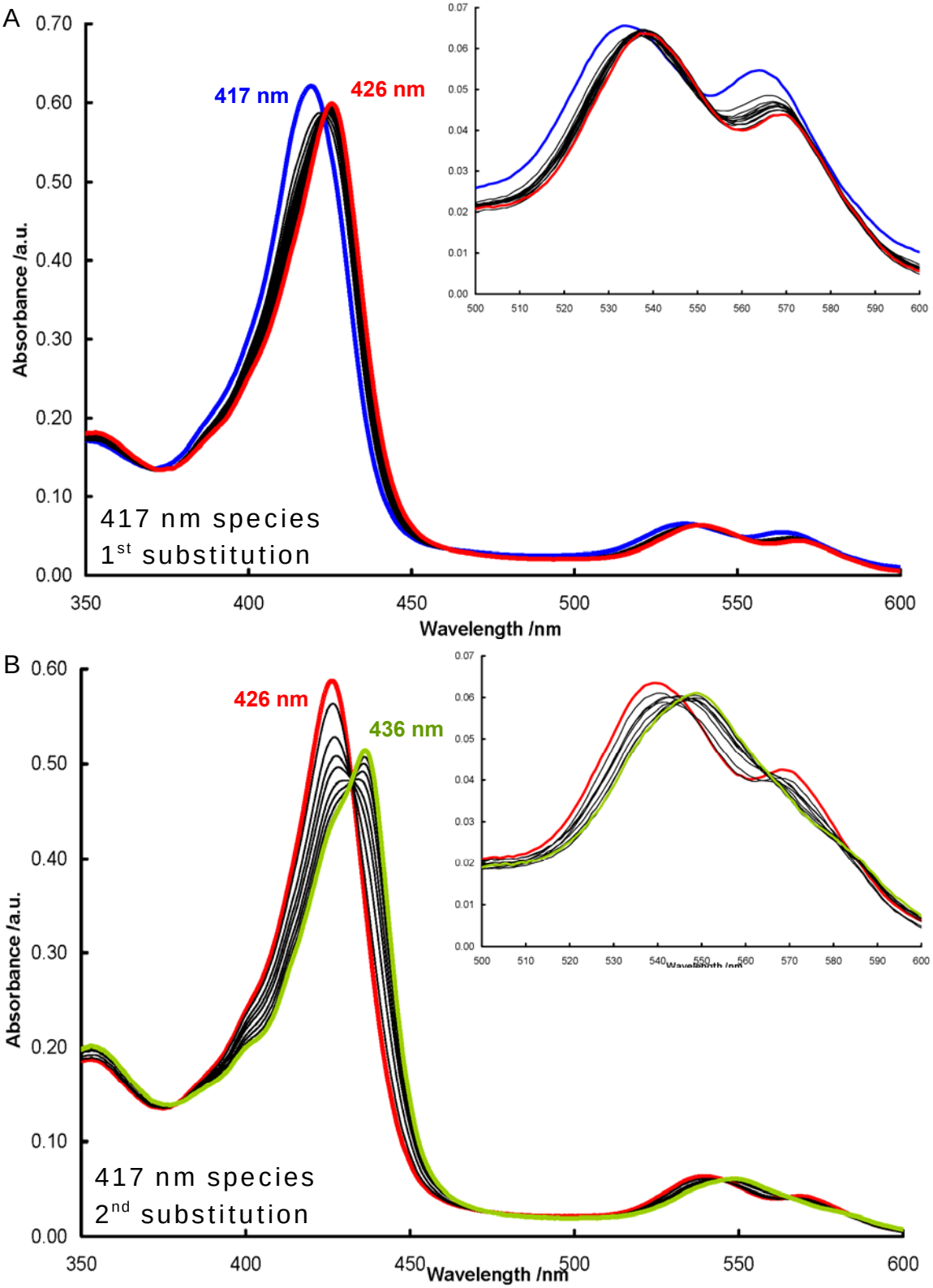


Figure 5.9 The titration of NAcCoMP8 417 nm species in MOPS buffer (0.1 M; pH 6.8; 25 °C) with NaCN (0.1 M) showing 1st (**A**) and 2nd axial substitution (**B**). Refer to Table 5.1 for isosbestic points.

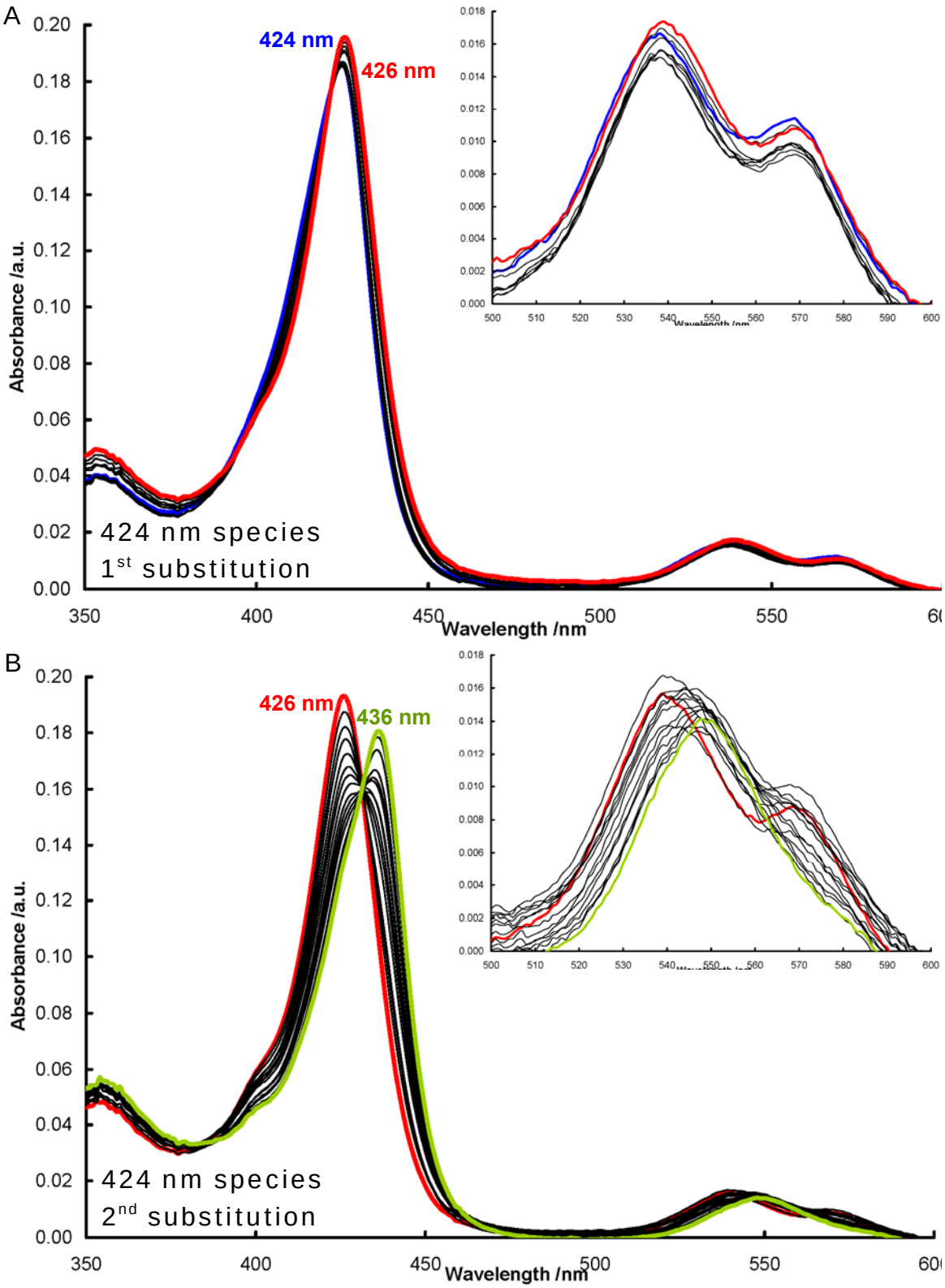


Figure 5.10 The titration of NAcCoMP8 424 nm species in MOPS buffer (0.1 M; pH 6.8; 25 °C) with NaCN (0.1 M) showing 1st (**A**) and 2nd axial substitution (**B**). Refer to Table 5.1 for isosbestic points.

Equilibrium constants (log K) for the binding of cyanide to each NAcCoMP8 species were obtained (25 ^{o}C; pH 7; μ = 0.1 M). Each species had two sets of spectral data, **A** and **B**, presumably corresponding to the first and second ligand substitution. The first substitution is clearly cyanide replacing the distally coordinated water on Co(III) in NAcCoMP8 (**Equation 5.1**). The equilibrium constants corresponding to this substitution were anticipated to be similar given the structural similarities of the various species (**Table 5.2**). These were (6.06 ± 0.06, 6.32 ± 0.05 and 5.77 ± 0.10) for the 415, 417 and 424 nm species, respectively. It is interesting to note that for this substitution the 415 and 417 nm species have a similar binding affinity for cyanide suggesting perhaps a similar coordination environment. On the other hand, the 424 nm species has the lowest log K. This would be consistent with an oligomer, possibly a tetramer with a less accessible axial water molecule (see **Section 4.2.4**)

The second substitution is ascribed to the substitution of the proximally coordinated histidine ligand on Co(III) by cyanide (**Equation 5.3**). The log K values were considerably lower than for the first substitution (**Table 5.2**). These were (3.50 ± 0.08, 4.02 ± 0.10 and 3.96 ± 0.07) for the 415, 417 and 424 nm species, respectively. This was anticipated since the Co-His bond would be stronger than the Co-OH_2 bond. In contrast to the first substitution, here it is the 417 and 424 nm species that appear to share a similar coordination environment based on the similarity in log K values (see later **Figure 5.11**).

Table 5.2 A comparison of isosbestic points for the replacement of coordinated water with CN^- in three NAcCoMP8 species (pH 7; 25 ^{o}C; μ = 0.1M)

Species	Substitution	Isosbestic points	Log K
415	First	373; 420; 500; 532; 551; 596	6.06 ± 0.06
	Second	383; 431; 544; 564	3.50 ± 0.08
417	First	371; 423; 431; 465; 551; 580	6.32 ± 0.05
	Second	433; 450	4.02 ± 0.10
424	First	388; 425; 507; 537; 558; 578	5.77 ± 0.10
	Second	389; 431; 469; 546; 563	3.96 ± 0.07

NAcCoMP8 exists as three concentration-dependent species (**Chapter 4**). The evidence thus far suggests that these species, 415, 417 and 424 nm, likely correspond to a monomer, dimer and tetramer, respectively (**Section 3.2.2.3**; **4.2.1**; **4.2.4**) which is not uncommon for these types of molecules.[31-33]

It is possible to envisage a variety of routes that lead to the formation of these oligomers. Based on the spectral and thermodynamic evidence amassed in this Chapter, two models describing the monomer → dimer → tetramer formations are proposed (**Figure 5.11**). Model One is facilitated by the head-to-tail side-on packing arrangement (A1-D1). Model Two is a head-to-*head* and side-on conformation (A2-D2). Both models begin with monomers that form reversible π-π stacks. As concentration increases these stacks pack closer and form irreversible metal–side-chain aggregates. Both models are discussed concurrently as monomers, dimers and tetramers.

The monomer formation in both models is straightforward with two possible orientations (**Figure 5.11**). This may be 'head-up' (A1) or 'tail-up' (A2); both are common in non-protein-bound, near-planar porphyrins.[34-37] Since the disparity is spatial these monomers have the same spectral (both λ_{max} = 415 nm) and binding properties. Both axial positions are equally accessible especially the axial water. Thus, from a purely steric perspective, the substitution of water by exogenous ligands should be fairly unhindered (log K = 6.0 for CN^-; **Table 5.2**). These monomers are also prone to π-π stacking depending on concentration, ionic strength and temperature (**Sections 4.2.1**; **4.2.4**; **4.2.7**). This propensity towards stacking then allows for two unique dimer conformations.

The dimer forms two possible conformations through the π-π stacking of two monomers (**Figure 5.11**). This may be head-to-tail side-on (B1) or head-to-head side-on (B2). In this instance λ_{max} supposedly occurs at 417 nm. The steric crowding around the axial water becomes apparent especially in B1. In B2, the axial waters are less hindered thus the binding of CN- is still high (log K = 6.3). This conformation may also order the ligand molecules by hydrogen bonding thus allowing for a marginally higher log K than the monomer (**Table 5.2**).

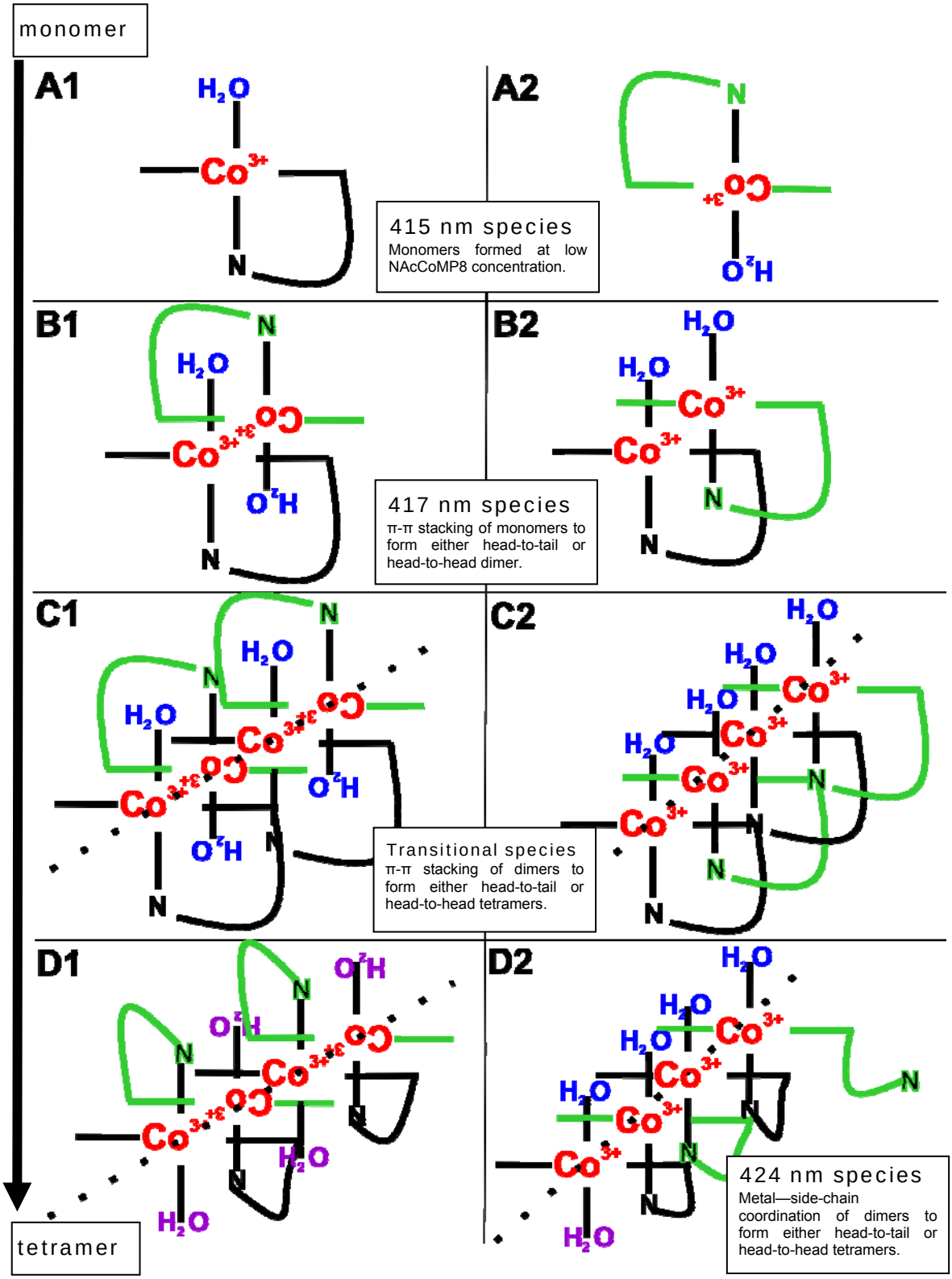


Figure 5.11 Possible methods of tetramer formation. Route A1-D1 suggests a head-to-tail side-on conformation whilst Route A2-D2 suggests a head-to-head side-on conformation. The water molecules originally coordinated by the molecule are illustrated in blue whilst the water molecules substituted during the tetramer formation are represented in purple. Monomers in A1 and A2 are indistinguishable in solution.

The nature of the oligomer, in this case the dimer, was considered. Is the dimer a π-π aggregate or a metal—side-chain aggregate? In the case of π-π aggregates monomerisation may be achieved by dilution or by the use of detergents as was observed with the 417 nm NAcCoMP8 species (See **Chapter 4**). Furthermore, the broadened spectra exhibit shifts that are small relative to the monomer (415 → 417 nm), where the extent of the shift depends on H- or J-type formations. Reviewing the evidence presented thus far suggests that the 417 nm species is likely a π-π dimer that then proceeds to stack further and form the putative tetramer species (**Sections 3.2.1.2**; **3.2.2.3**; **4.2.1** - **4.2.8**).

The formation of the putative tetramer species at sufficiently high concentration could produce two possible conformations through the π-π stacking of two dimers (**Figure 5.11**). This may be head-to-tail side-on (D1) or head-to-head side-on (D2). In this instance λ_{max} occurs at 424 nm. In contrast to the monomer and dimer species, the tetramer's steric crowding around the axial water is considerably large, certainly in the case of D1. This would significantly decrease the binding of exogenous ligands such as cyanide relative to the other species (lowest log K = 5.8; **Table 5.2**).

Once again, the nature of the oligomer, in this case the tetramer was considered. Is this a π-π aggregate or a metal—side-chain aggregate? Metal—side-chain aggregation in NAcCoMP8 would involve the coordination of an N-donor histidine ligand to Co(III). The coordination of an N-donor ligand is expected to exhibit larger spectral shifts relative to the monomer similar to those observed with the putative tetramer (415 → 424 nm). A coordinated aggregate would also be irreversible by dilution and detergents alone as was the case with the 424 nm NAcCoMP8 species (**Chapter 4**). The evidence thus far infers that the 424 nm species is a metal—side-chain aggregate (**Section 4.2.4**).

ESI-MS evidence was found to be inconclusive for the detection of both coordinated- or π-π aggregates. In the case of coordinated aggregates the total mass would be beyond the high-mass limit of the instrumentation available (> 3000 $g.mol^{-1}$). It was anticipated that the spectra would be irreproducible and

comprise a plethora of detectable ions depending on the charges of the various species in solution at the time of data-collection. This was observed with the putative metal—side-chain 424 nm tetramer in a time-dependent experiment which exhibited different masses for the same stock sample over a *ca*. 40 minute study. However in the case of π-π aggregation it was anticipated that these aggregates would disperse in the chamber and reflect only the monomer mass. This was observed in the case of the putative 417 nm π-π dimer which remained undetected by ESI-MS in both positive and negative modes.

It is appreciated that the tetramer formation in NAcCoMP8 is complex and that the outlined steps represent a probable and simplistic set of events (**Figure 5.11**). That said it is not inconceivable that the tetramer formation would first proceed through a 'transitional' π-π aggregation step (C1, C2). Here two π-π dimers associate to form a π-π tetrameric intermediate. This species would be expected to share similar spectroscopic and binding properties with B1 and B2. As the dimer concentration increases the packing of these tetramers become tighter. This close-packing of porphyrin electron densities then destabilises the tetramer and facilitates the formation of an irreversible aggregate.

It was also considered that this irreversible 424 nm species is a μ-oxo dimer. This is however, unlikely as the solution conditions do not favour the formation of such a dimer (**Chapter 2**). The data for the low spin cobalt(III) system were generally obtained at neutral pH and the aqueous system was degassed using argon.[38,39] Furthermore, a μ-oxo dimer should be stable enough to be reproducibly detected by ESI-MS.

This type of aggregation-dependent spectral behaviour is not uncommon in acetylated microperoxidases.[40-43] Work pertaining to NAcFeMP11 revealed absorbance spectra that were exceptionally aggregation-dependent and complex. In fact, these were later shown to have a strong correlation with ionic strength, not unlike the NAcCoMP8 system. The aggregation in the NAcFeMP11 system is so spectacularly complex that not only is its formation a function of the ionic strength but the nature of that aggregation is heavily dependent on the

identity of the anion promoting that aggregation.[42,43]

Using absorbance spectroscopy, Munro and Marques showed that the NAcFeMP8 system was only marginally simpler.[40] This system formed π stacked dimers as a function of ionic strength where Na^+ promoted first a loosely packed dimer (*ca*. 2 Na^+) and then a tighter dimer (*ca*. 4 Na^+). These findings were not unlike those observed here with NAcCoMP8 (**Section 4.2.4**). Their subsequent exciton theory and Gaussian analysis work revealed fascinating conformational insights.[41] Their analysis suggested that the second dimer has stronger dipole-dipole interactions than the first dimer but not necessarily coordinated through metal—side-chain. However, whilst these models provide a theoretical basis for the NAcCoMP8 system, the identity of the metal ion (Fe(III) vs. Co(III)), and possible spin switch over in the Fe(III) system, means the model may not necessarily be applicable to the trivalent NAcCoMP8 .

5.2.1.2 Structural Evidence (from the CSD)

Before embarking on a description of the ligand binding studies, a brief review of information available from solid state studies is appropriate. The solid state evidence that adequately verifies the structural effect of the different macrocyclic steric demands is limited. For example, dicyano-corrin complexes are common whilst the corresponding porphyrin data are not; several pyridine complexes of Co(III) porphyrins are known, but have yet to be reported for a corrin. The difficulty in selecting appropriate comparisons becomes apparent when considering the electronic *trans* influence; thus the ligand *trans* to the ligand of interest in the corrin and the porphyrin must have similar electronic properties. Within these constraints, some porphyrin and corrin complexes were compared (**Table 5.3**) using data available in the CSD.

Coordination with nitrites has been detailed (**Table 5.3**). There are three reports of nitrocobalamin (NO_2Cbl) where the coordination is through N rather than O since the former is a better donor ligand for Co(III).[7,54] The corresponding porphyrin data have nitrite coordinated to the metal, *trans* to an aromatic N-

donor ligand (imidazole or pyridine). This makes it electronically similar to the DMB ligand in vitamin B_{12a} and thus a suitable choice for comparison.

NO_2^- is expected to be relatively sterically undemanding given its structure and orientation.[44] On analysis (**Table 5.3**), the wide range in Co—NO_2 bond length data in both corrins and porphyrins, suggest that this type of bond is sensitive to the crystal environment; bond lengths seem to be affected by the presence of other salts and by solvent. The average Co(III)—N bond length in porphyrins (1.92(2) Å) is statistically identical to that in cobalamins (1.93(2) Å) where the *trans* ligand is an aromatic N donor (**Table 5.3**).

Imidazole is likely to be more sterically demanding than NO_2^-. Imidazole is a rigid 5-membered ring with two H atoms on the C neighbours of the coordinating N-donor. Again there is a great deal of variability in Co—L bond lengths (**Table 5.3**). Nevertheless, the bond length to imidazole in a corrin (1.95(1) Å) does appear to be somewhat longer than in a porphyrin (1.93(2) Å), but again this may not be statistically significant.

Unfortunately there are no data for pyridine cobalamins available. A pyridine should be sterically more demanding than an imidazole (the C—N—C angle is wider, *viz*., 117(3)^o (from 1306 observations in 775 compounds in which at least one free pyridine is present in the crystal lattice) compared to 105(3)^o for imidazole (460 observations in 304 compounds where the imidazole is not coordinated to a metal ion). Thus, caution has to be exercised when comparing log K values for binding of larger ligands such as pyridines and imidazoles to porphyrins and corrins because the steric effect in the latter may very well decrease log K. Smaller and less sterically demanding ligands such as NO_2^- are not expected to be subject to this caveat.

Table 5.3 Bond length data for some selected corrins and porphyrins.

Macrocycle	Ligand (L)	Trans Ligand (T)	Complex	Co(III)-L /Å	Co(III)-T /Å	CSD Ref.
Corrin	NO_2	DMB	NitroCbl	1.913	2.013	[a]HUSPEQ[45]
	NO_2	DMB	NitroCbl	1.940	2.008	[b]EJADOI[54]
	NO_2	DMB	NitroCbl	1.942	1.993	[c]HUSPAM[45]
			Average (σ)	*1.93(2)*		
Porphyrin	NO_2	Pyr	[CoTPP(NO_2)(Pyr)]	1.921	2.032	YEQMIQ[46]
	NO_2	3,5-Cl_2Pyr	[CoTPP(NO_2)(3,5-Cl_2Pyr)]	1.912	2.044	YEQMOW[46]
	NO_2	3,5-Me_2Pyr	[CoTPP(NO_2)(3,5-Me_2Pyr)]	1.948	2.037	NTPOLC[47]
	NO_2	3,5-Me_2Pyr	[CoTPP(NO_2)(3,5-Me_2Pyr)]	1.925	2.017	NTPOLC01[48]
	NO_2	1,2-Me_2Im	[Co(PicketFence)(NO_2)(1,2-Me_2Im)]	1.917	2.090	[d]XAFJOD[49]
	NO_2	1-MeIm	[Co(PicketFence)(NO_2)(1-MeIm)]	1.899	1.994	[d]XAFJIX[49]
			Average (σ)	*1.92(2)*		
Corrin	His	DMB	HisCbl	1.951	1.979	GIFYAW[50]
	Im	DMB	ImCbl	1.939	2.006	GIFYEA[50]
			Average (σ)	*1.95(1)*		
Porphyrin	1-MeIm	1-MeIm	$[CoTCP(1\text{-}MeIm)_2]^+$	1.941	1.943	PACLIO[51]
	Im	Im	[e]$[CoTPP(Im)_2]^+$	1.905	1.905	[e]TPORCO10[52]
	Im	Im	[e]$[CoTPP(Im)_2]^+$	1.945	1.945	[e]TPORCO10[52]
	Im	Im	$[CoTPA(Im)_2]^{5+}$	1.920	1.963	VEGRAA[53]
			Average (σ)	*1.93(2)*		

a NaCl in lattice
b Acetone solvated
c LiCl in lattice
d Disordered imidazole
e Two independent molecules in the unit cell
Pyr = Pyridine
Im = Imidazole
Cbl = Cobalamin
His = Histidine
Me = Methyl
TPP = 5,10,15,20-tetraphenylporphyrin
TCP = 5,10,15,20-tetrakis(2,6-dichlorophenyl)porphyrin
TPA = 5,10,15,10-tetrakis(N,N,N-trimethylanilinyl)porphyrin

5.2.2 Ligand Binding

Equilibrium constants (log K) for the substitution of coordinated water by selected ligands in NAcCoMP8 and B_{12a} (H_2OCbl^+) were determined spectroscopically as a function of temperature (**Section 5.2.2.1**). From these values the ΔH and ΔS parameters were obtained using van't Hoff plots. These values were then compared between the two Co(III) systems (**Section 5.2.2.2**).

5.2.2.1 Log K trends

Log K data for the binding of selected anionic (**Table 5.4**) and neutral (**Table 5.5**) ligands with NAcCoMP8 (and with B_{12a}) were obtained as a function of temperature. Two trends were evident amongst the anionic ligand binding data. Firstly, the log K values for the anionic ligands generally decreased with increasing temperature in both macrocycles (**Table 5.4**). These observations suggest that the binding of anionic ligands to Co(III) in this system is exothermic in nature (see later **Section 5.2.2.2**), except in the case of bisulfite. The binding of bisulfite in both macrocycles exhibits log K values that increased with temperature suggesting an endothermic reaction. Secondly, the log K values were considerably larger for B_{12a} than for NAcCoMP8 indicating that the corrin is the preferred macrocycle for the binding of anions to Co(III) (see later in this Section).

The binding of neutral ligands to Co(III) exhibited strikingly different log K trends as compared to the anionic ligands (**Table 5.5**). Firstly, with the exception of MOA, the exothermicity in the neutral ligand-binding data appears to be heavily dependent upon the identity of the macrocycle encapsulating the Co(III). For example, whilst the binding of pyridine is endothermic in the corrin, it is exothermic in the porphyrin. On the other hand, the binding of the anionic ligands appeared to be generally exothermic regardless of the macrocycle's identity. Secondly, unlike the data for the anionic ligands, the log K values for the neutral ligands were generally larger in NAcCoMP8 than in B_{12a} indicating that in this case it is the porphyrin that is preferred.

Table 5.4 Equilibrium Constants for the Substitution of Coordinated H_2O in NAcCoMP8 by Some Anionic Ligands

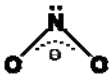
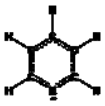
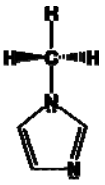
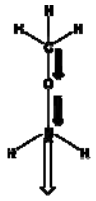
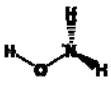
Ligand	B_{12a}					NAcCoMP8				
	T /°C	*K* /M^{-1}	log *K*	ΔH /kJ mol^{-1}	ΔS /J K^{-1} mol^{-1}	*T* /°C	*K* /M^{-1}	log *K*	ΔH /kJ mol^{-1}	ΔS /J K^{-1} mol^{-1}
N_3^-	15.0	1.70×10^5	5.23(4)	-29(1)	-1(3)	15.0	2.45×10^2	2.39(3)	-20(1)	-23(5)
	20.0	1.35×10^5	5.13(3)			20.0	2.09×10^2	2.32(6)		
	25.0	**1.05×10^5**	**5.02(5)**			**25.0**	**1.91×10^2**	**2.28(6)**		
	35.0	7.59×10^4	4.88(3)			30.0	1.74×10^2	2.24(7)		
	40.0	6.31×10^4	4.80(2)			35.0	1.38×10^2	2.14(5)		
						40.0	1.29×10^2	2.1(1)		
CN^-	15.0					5.6	4.37×10^6	6.64(4)	-47(2)	-42(6)
	20.0					15.4	2.00×10^6	6.30(5)		
	25.0		**≥12**[55]			18.0	1.82×10^6	6.26(6)		
	30.0					20.0	1.41×10^6	6.15(7)		
	35.0					**25.0**	**1.10×10^6**	**6.04(5)**		
	40.0					28.0	1.00×10^6	6.0(1)		
						35.0	5.37×10^5	5.7(1)		
						45.0	3.72×10^5	5.6(1)		
NO_2^-	15.0	1.74×10^6	6.2(3)	-47(3)	-44(9)	5.0	1.51×10^3	3.18(7)	-20(2)	-12(8)
	20.0	9.77×10^5	6.0(2)			10.0	1.35×10^3	3.13(9)		
	25.0	**7.24×10^5**	**5.9(1)**			15.0	1.17×10^3	3.07(6)		
	30.0	5.37×10^5	5.73(9)			**25.0**	**1.00×10^3**	**3.00(4)**		
	35.0	4.27×10^5	5.63(7)			35.0	6.31×10^2	2.80(6)		
	40.0	3.09×10^5	5.49(5)			40.0	5.62×10^2	2.75(8)		
HSO_3^-	15.0	2.14×10^5	5.3(1)	156(9)	644(31)	20.0	3.98×10^3	3.6(2)	22(2)	143(7)
	20.0	6.31×10^5	5.8(1)			**25.0**	**4.47×10^3**	**3.7(1)**		
	**25.0**	**2.88×10^6**	**6.5(3)**			30.0	5.62×10^3	3.75(1)		
	30.0	8.13×10^6	6.9(4)			35.0	6.17×10^3	3.8(1)		
	35.0	1.38×10^7	7.1(4)			40.0	6.92×10^3	3.84(1)		
	40.0	2.95×10^7	7.5(5)							

Table 5.5 Equilibrium Constants for the Substitution of Coordinated H_2O in NAcCoMP8 by Some Neutral Ligands

Ligand	B_{12a}					NAcCoMP8				
	T /°C	*K* /M^{-1}	log *K*	ΔH /kJ mol^{-1}	ΔS /J K^{-1} mol^{-1}	*T* /°C	*K* /M^{-1}	log *K*	ΔH /kJ mol^{-1}	ΔS /J K^{-1} mol^{-1}
Pyr	15.0	0.96 x 10^1	0.98(4)	6.2(0.5)	40(2)	15.0	1.58 x 10^5	5.20(6)	-30(3)	-6(9)
	20.0	1.00 x 10^1	1.00(4)			20.0	1.17 x 10^5	5.07(5)		
	**25.0**	**1.02 x 10^1**	**1.01(3)**			**25.0**	**8.51 x 10^4**	**4.93(5)**		
	30.0	1.10 x 10^1	1.04(2)			30.0	7.41 x 10^4	4.87(4)		
	35.0	1.12 x 10^1	1.05(2)			35.0	6.61 x 10^4	4.82(3)		
	40.0	1.17 x 10^1	1.07(5)			40.0	5.50 x 10^4	4.74(4)		
NMI	15.0	7.59 x 10^4	4.9(1)	-62(3)	-122(11)	10.0	1.82 x 10^5	5.26(7)	42(3)	250(11)
	20.0	3.98 x 10^4	4.6(1)			15.0	3.09 x 10^5	5.49(9)		
	**25.0**	**2.69 x 10^4**	**4.43(7)**			**25.0**	**5.75 x 10^5**	**5.76(8)**		
	30.0	1.70 x 10^4	4.23(4)			35.0	8.51 x 10^5	5.93(4)		
	35.0	1.20 x 10^4	4.08(4)			40.0	1.07 x 10^6	6.03(7)		
	40.0	8.91 x 10^3	3.95(5)							
MOA	15.0	2.40 x 10^6	6.4(3)	-81(7)	-161(23)	10.0	3.02 x 10^4	4.48(5)	-64(6)	-138(20)
	20.0	8.13 x 10^5	5.9(1)			15.0	2.88 x 10^4	4.46(9)		
	**25.0**	**6.03 x 10^5**	**5.78(7)**			20.0	1.12 x 10^4	4.05(7)		
	30.0	3.72 x 10^5	5.6(1)			**25.0**	**6.46 x 10^3**	**3.81(9)**		
	35.0	1.66 x 10^5	5.22(4)			30.0	5.50 x 10^3	3.74(8)		
	40.0	1.29 x 10^5	5.11(4)			35.0	3.89 x 10^3	3.59(7)		
						40.0	2.82 x 10^3	3.5(1)		
HA	5.5	5.62 x 10^3	3.75(6)	100(9)	428(30)	12.0	1.78 x 10^6	6.3(6)	-105(13)	-248(44)
	10.0	5.25 x 10^3	3.72(6)			15.0	1.78 x 10^6	6.3(6)		
	15.0	1.26 x 10^4	4.10(6)			18.0	1.29 x 10^6	6.1(5)		
	20.0	3.47 x 10^4	4.54(6)			20.0	4.47 x 10^5	5.7(3)		
	**25.0**	**5.25 x 10^4**	**4.72(4)**			**25.0**	**3.47 x 10^5**	**5.5(2)**		
	30.0	1.51 x 10^5	5.2(2)			30.0	2.45 x 10^5	5.4(2)		
	35.0	3.98 x 10^5	5.6(1)			35.0	4.37 x 10^4	4.6(2)		
	40.0	3.72 x 10^5	5.6(2)			40.0	5.25 x 10^4	4.7(1)		

The log K values obtained for vitamin B_{12a} are consistent with those reported in literature for both sets of ligands.[7, 12, 55-59] Further comparisons and references to these values will be made later on when the ligands are discussed under the relevant sections.

Examples of the spectroscopic changes observed for the substitution of coordinated water by NMI are illustrated for NAcCoMP8 and B_{12a}, respectively, (**Figure 5.12**; **5.13**). Absorbance data obtained during the course of the titration of NAcCoMP8 with NMI (25 ^{o}C, pH 6.85, 0.1 M MOPS) were recorded (**Figure 5.12A**), and similarly for B_{12a} (**Figure 5.13A**). These data were then analysed at various wavelengths by fitting according to Equations 2.6-2.7 which take free ligand concentration into account (**Figure 5.12B** and **5.13B** for NAcCoMP8 and B_{12a}, respectively). Forty such fits gave a weighted average of log K = 5.76(8) for NAcCoMP8, and 4.43(7) for B_{12a} at 25 ^{o}C. Similarly, log K values were obtained at various temperatures (10-40 ^{o}C) and used to construct van't Hoff plots in order to find ΔH and ΔS (**Figure 5.12C** and **5.13C** for NAcCoMP8 and B_{12a}, respectively). A similar approach was used for studying the reaction of NAcCoMP8 (and of B_{12a}) with the other ligands listed previously.

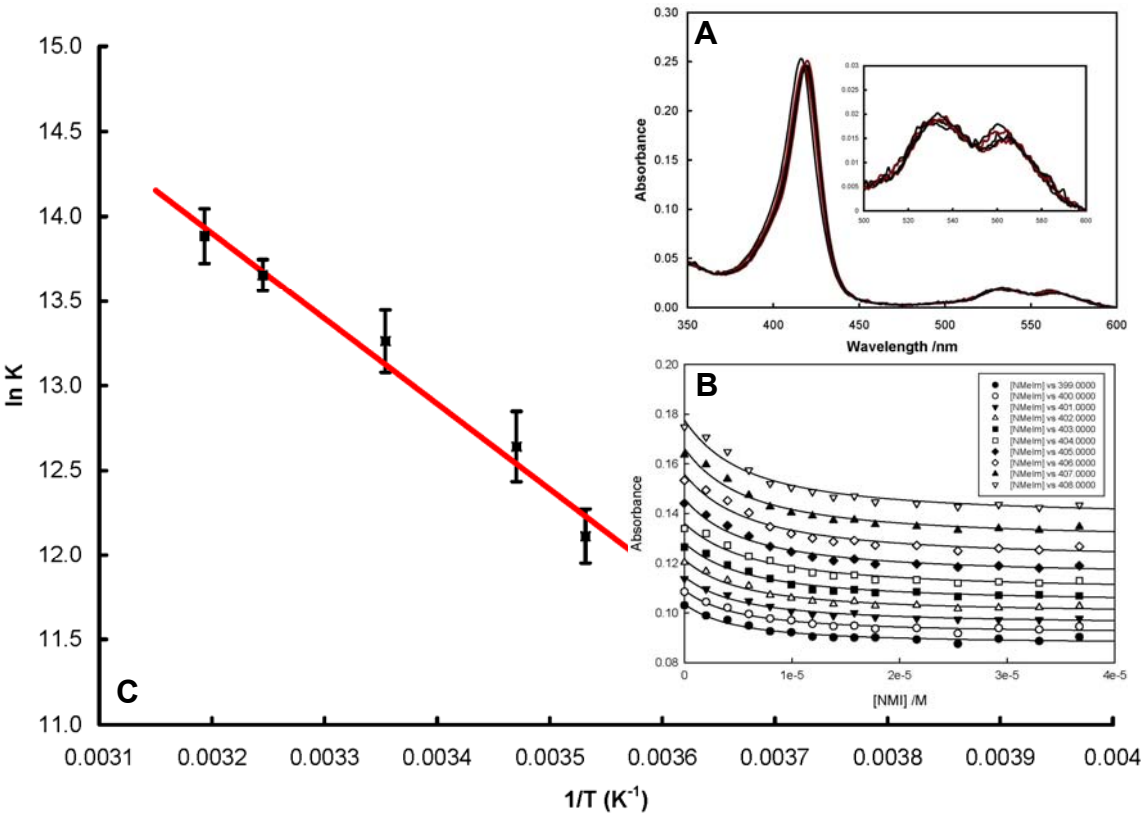


Figure 5.12: Examples of spectroscopic data obtained in this work. Absorbance data obtained in the titration of NAcCoMP8 with NMI (25 ^{o}C, pH 6.85, 0.1 M MOPS) (**A**) were fitted according to Equation 2.6-2.7 in order to find log K (**B**). Similarly log K values were obtained at various temperatures between 10 – 40 ^{o}C and used to construct van't Hoff plots (**C**) in order to find ΔH and ΔS.

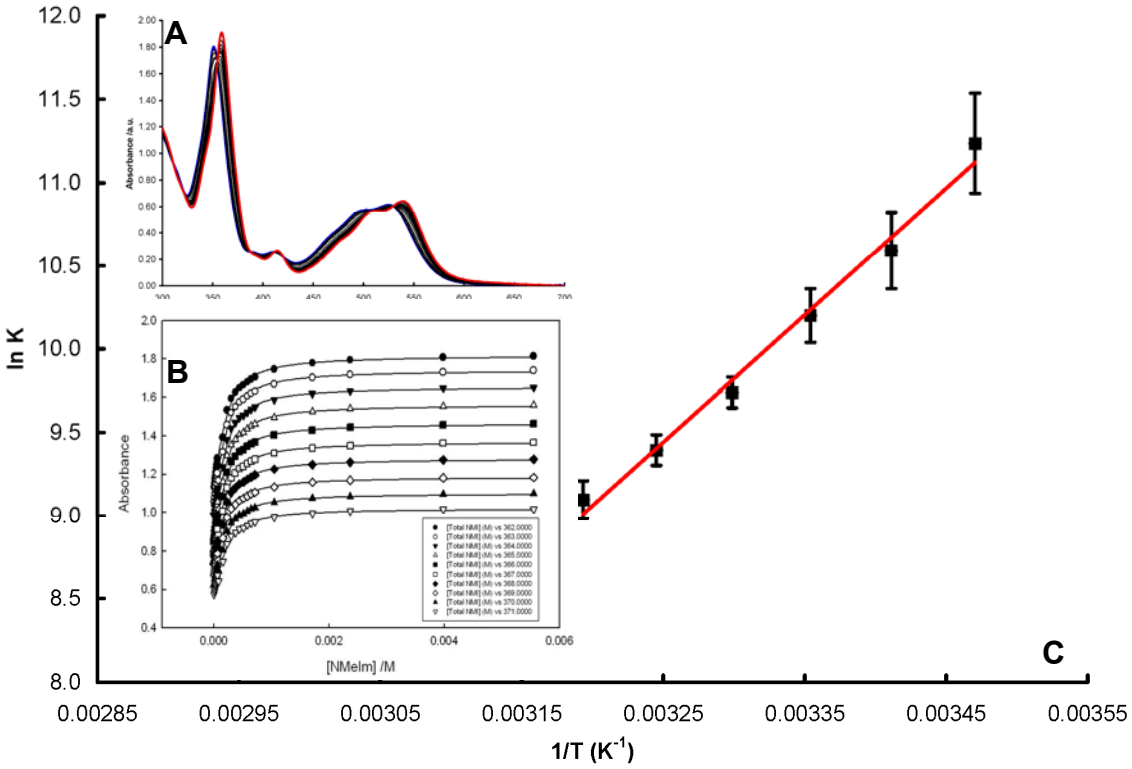


Figure 5.13: Examples of spectroscopic data obtained in this work. Absorbance data obtained in the titration of B_{12a} with NMI (25 °C, pH 6.85, 0.1 M MOPS) (**A**) were fitted according to Equations 2.6-2.7 in order to obtain log K (**B**). Similarly log K values were obtained at various temperatures between 10 – 40 °C and used to construct van't Hoff plots (**C**) in order to find ΔH and ΔS.

The log K values at 25 °C for the substitution of coordinated water in NAcCoMP8 and in B_{12a} are compared (**Figure 5.14**). The binding trends exhibited by anionic ligands are considered (**Figure 5.14**, red dots). A striking feature of this plot is that all the anionic ligands bind more strongly with the corrin than the porphyrin. Furthermore, the plot also shows a positive linear correlation between the corrin and the porphyrin log K values; this suggests that the binding behaviour in the two systems parallel each other. Another prominent feature pertains to the anomalously high log K value estimated for the coordination of CN^- by B_{12a}. The value is too large to be reliably determined but is estimated at log K > 12; literature values range from >12[55] to 12.3(5)[60] in 80% MeOH and 14.1.[61] The binding of cyanide to Co(III) in both macrocycles will be discussed further below (**Section 5.2.2.2**).

In contrast, the binding trends exhibited by the neutral ligands to Co(III) in both macrocycles are opposite to those exhibited by the anionic ligands (**Figure 5.14**, blue dots). The most notable contrasting feature here is that the neutral ligands bind more strongly with the *porphyrin* rather than the corrin. A further contrast is that the plot exhibits a *negative* linear relationship between the corrin and the porphyrin log K values implying an inverse relationship in the binding behaviour of the two systems. Another prominent feature is the anomalously low log K value for binding of Pyr to Co(III) in B_{12a} (log K = 1.01(3)). Bauriedel[58] observed the binding but was unable to quantify it, whilst Knapton and Marques[59] found log K = 1.23(7) at 25 ^{o}C. The binding of pyridine to Co(III) in both macrocycles will be discussed further below (**Section 5.2.2.2**).

A further consideration of the log K trends for the binding of anionic ligands is warranted (**Figure 5.14**; **Table 5.4**, 25 ^{o}C data in bold). A number of conclusions can be drawn. Firstly, both macrocycles preferentially bind ligands with softer donor atoms: (softer) $\underline{C}N^-$ > $H\underline{S}O_3^-$ > $\underline{N}O_2^-$ > $\underline{N}_3^-$ (harder) (**Figure 5.14**). Secondly, despite this shared preference, each macrocycle binds the anionic ligand differently as suggested by the log K range. NAcCoMP8 data range from log K = 6.0 to 2.3 whilst the range for B_{12a} is wider, from log K = ~12[10,55] to 5.0. This implies that the electronic influence exerted by the porphyrin onto Co(III) decreases the binding affinity by a remarkable six orders of magnitude! Lastly, there is considerable difference in log K values with softer ligands between B_{12a} and NAcCoMP8 (Δlog K[§] for HSO_3^- and CN^- = 2.8 and ~6, respectively) than with harder ligands (Δlog K for N_3^- and NO_2^- = 2.7; 2.9, respectively). Again this brings to light the rather large log K value for the binding of CN^- to Co(III) in B_{12a} in contrast to NAcCoMP8.

[§] Defined here as Δ Log K = |Log K_{B12a} - Log $K_{NAcCoMP8}$|

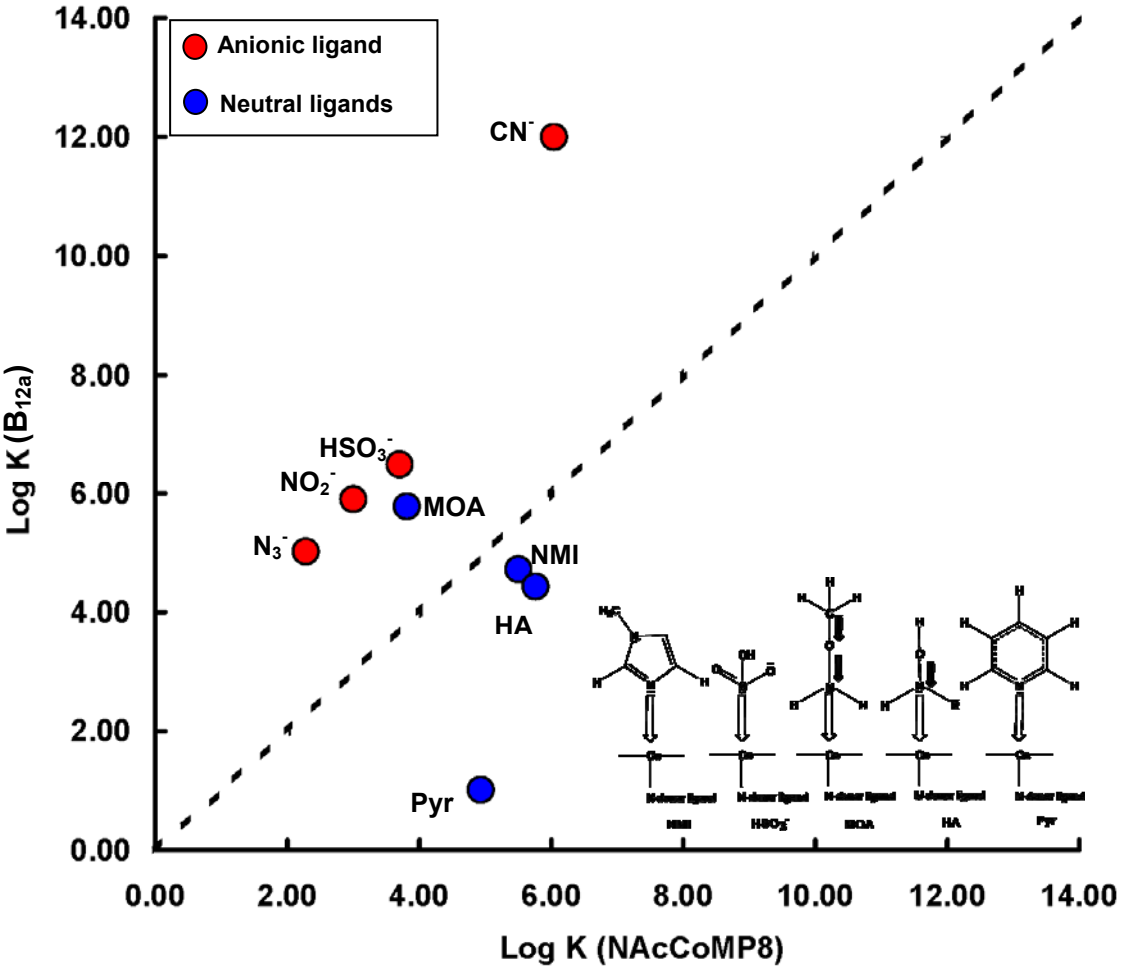


Figure 5.14 Log K of B_{12a} vs. NAcCoMP8 for neutral (blue) and anionic (red) ligands. The binding of neutral ligands (and HSO_3^-) are schematically illustrated (inset) where N-donor ligand refers to DMB or His for vitamin B_{12a} or NAcCoMP8, respectively. The dotted equivalence line for which log K (B_{12a}) = log K (NAcCoMP8).

These ligand binding trends seem counter-intuitive. In the case of NAcCoMP8, the fully conjugated system allows for more electron density to be distributed onto the metal ion. This would suggest that the metal ion has a softer, more Co(II)-like nature. Being partially conjugated, the opposite would be anticipated in B_{12a}. Furthermore, assuming electronic isolation of the cobalt(III) metal ion from the peripheral substituents,[§§] the net charge on the monoanionic corrin is (+2) and (+1) in the dianionic porphyrin. Thus it would seem reasonable to assume a harder Co(III)-like nature in B_{12a}. However, B_{12a} exhibits a clear preference for the softer ligands, suggesting that in fact it is the cobalt ion in

[§§] The charges on the phosphates in B_{12a} are some 9 Å away. The charges on NAcCoMP8's propionate side chains are between 5.5 - 8.5 Å away, depending on the side chain orientation.

B_{12a} that is softer and somewhat Co(II)-like in nature.[1,62] These data suggest that the ligand binding is far more complex than to be attributed to simply net charge effects or ligand charge density distribution in isolation. These trends suggest that Co(III)'s binding affinity in B_{12a} depends on the extent to which the anionic ligand can *donate* any *available* charge density (electronic effects) and secondly, the extent to which the macrocycle can *distribute* that donation.[3,12]

The effective distribution of charge density may be attributed to the smaller macrocyclic cavity size in corrins than in porphyrins.[7,12,63-68] Corrins have one less methine bridge and more sp^3 carbons than porphyrins allowing for greater flexibility and buckling around the metal ion. Whilst it has indeed been shown that porphyrins too are flexible,[69,70] the larger cavity size works against the effective distribution of that charge. Rovira *et al*., presented compelling DFT evidence to suggest that the metal-macrocycle specificity is motivated by metal-size.[71] This 'closer fit' may allow for a more efficient distribution of electron density around the metal ion, albeit having lower electron density for distribution than the porphyrin. Thus, comparatively, the metal ion in porphyrin appears more Co(III)-like in nature than in corrins barring any steric influences. The steric influences may be considered in the absence of additional ligand charges.

Log K trends for the binding of neutral ligands was examined further (**Figure 5.14**; **Table 5.5**). Several observations were noted in contrast to the data obtained for the anions. Firstly, the *porphyrin* exhibited a generally higher binding affinity for the neutral ligands than the corrin. Secondly, the B_{12a} values still exhibit a wider range (log K = 1.0 to 5.8) than NAcCoMP8 (log K = 3.8 to 5.8). However, these ranges were comparatively smaller in both macrocycles than observed for the anionic ligands. Nevertheless, the corrin strongly binds a wider range of ligands suggesting that it is the preferred macrocycle. Thirdly, in contrast to the anionic ligands, the NAcCoMP8 ligand binding trends (NMI > HA> Pyr > MOA) do not mirror those of B_{12a} (MOA > HA > NMI > Pyr). Lastly, there is considerable difference in log K values with Pyr between B_{12a} and NAcCoMP8 (Δlog K = 3.9) than with the other neutral ligands (Δlog K for NMI, MOA and HA = 1.3, 2.0 and 0.8, respectively).

N-donor ligands are known to have a complex binding behaviour.[56,57,72-77] These complexities are particularly common in the case of neutral ligands such as primary amines, pyridines and azoles. Often these complexities are rationalised as a combination of steric (either on macrocycle or on axial ligand), electronic (dπ-pπ backbonding) or solvent effects.[73,76] However, without enthalpic or entropic information, those rationalisations often remain unclear. Thus it becomes apparent that log K data, particularly at a single temperature, are not always sufficient for substantiating those rationalisations; this was found to be particularly true in the case of the neutral ligands (**Table 5.5**). Therefore by determining log K as a function of temperature, and hence being able to calculate ΔH and ΔS values for these ligand substitution reactions, further insight would be gained into the factors that control the magnitude of log K and establish whether enthalpic or entropic effects were primarily responsible for discrimination between the two systems (**Section 5.2.2.2**).

5.2.2.2 ΔH and ΔS trends

Values for ΔH and ΔS were obtained for the substitution of water axially coordinated to Co(III) with various exogenous ligands in NAcCoMP8 and B_{12a} (**Section 2.3.1**; **5.2.2.1**). These values were obtained in order to help rationalise the underlying enthalpic and entropic contributions influencing log K in each macrocyclic system. The subscript $_{Cor}$ and $_{Por}$ denotes data pertaining to corrin (B_{12a}) and porphyrin (NAcCoMP8), respectively.

The values for ΔH and ΔS are reported for the binding of anionic (**Table 5.4**) and neutral ligands (**Table 5.5**) in NAcCoMP8 and B_{12a}. Some trends are observed. Firstly, the binding of anionic ligands exhibit ΔH and ΔS values that are generally larger in B_{12a} than in NAcCoMP8; azide is the exception (in J K^{-1} mol $^{-1}$: ΔS_{por} = -23(5) and ΔS_{cor} = -1(3)). In the case of the neutral ligands, the values are still generally larger in B_{12a} than in NAcCoMP8 though less obvious than with the anionic ligands. This trend together with the corresponding log K trends (**Section 5.2.2.1**) suggests that the corrin is the more energetically favoured macrocycle especially when it comes to the binding of anionic ligands.

Secondly, with the binding of anionic ligands, ΔH is generally larger and more negative than ΔS in both macrocycles. This indicates that the binding of anionic ligands to Co(III) in both systems is exothermic and enthalpically-driven. Bisulfite is the obvious exception where the binding in both macrocycles is clearly endothermic and entropically-driven (in J K^{-1} mol $^{-1}$: ΔS_{por} = 143(7) and ΔS_{cor} = 644(31)). In contrast the binding of neutral ligands to Co(III) exhibit larger Δ*S* in both macrocycles, implying that the reaction is more entropically-driven in contrast to the anionic ligands. The binding of pyridine in NAcCoMP8 is the exception and the reaction is clearly enthalpically-driven (ΔH_{por} = -30(3) kJ mol^{-1} and ΔS_{cor} = -6(9) J K^{-1} mol $^{-1}$). Nevertheless, these observations indicate an overall correlation between ΔH and ΔS regardless of macrocycle or ligand-set.

The correlation between ΔH and ΔS in both macrocycles alludes to a type of enthalpic-entropic 'compensation effect' which is common in many systems.[20,78-84] There are good correlations between ΔH and ΔS where r^2 > 0.9 in both macrocycles (**Figure 5.15**). As ΔH becomes more negative (thereby favouring complex formation), ΔS becomes more negative as well (thereby disfavouring complex formation). This appears to be true for both anions and neutral ligands. This inverse relationship in turn has a 'levelling-off' effect on the log K value thereby masking the underlying factors that contribute to the binding. The 'levelling-off' is particularly evident in the neutral ligand data for both macrocycles (**Table 5.5**) whereby the log K values are generally similar whilst the enthalpic or entropic contributions are very different. The ΔH values (and hence ΔS values, because of their correlation, **Figure 5.15**) for the anionic ligands vary in a similar fashion (HSO_3^- > N_3^- > NO_2^-) in the two systems. This is not the case for the neutral ligands (HA > NMI > MOA for B_{12a} but NMI > MOA > HA for NAcCoMP8). For this reason, log K values parallel each other in the two systems when binding anions, but appear to be inversely correlated for the binding of the neutral ligands It is unfortunate that ΔH and ΔS values are seldom reported in literature. The current work therefore presents the opportunity to delve further and build upon pre-existing log K information.

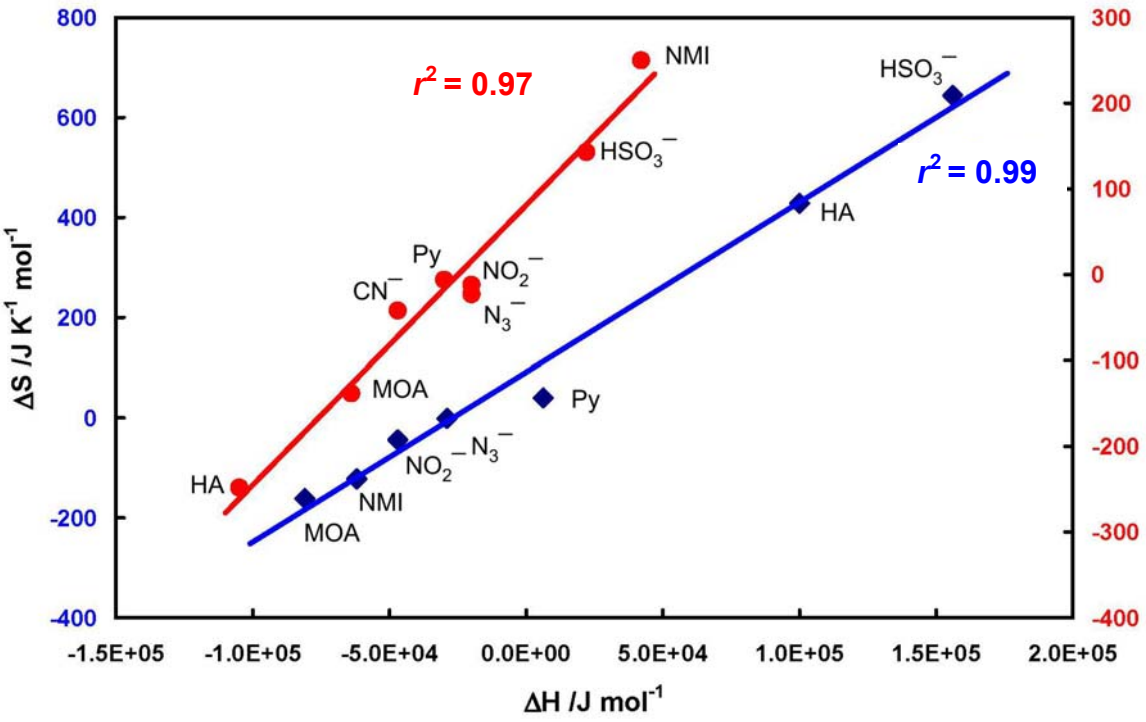


Figure 5.15 Correlation between ΔH vs ΔS for the substitution of coordinated water in B_{12a} (blue, left axis) and NAcCoMP8 (red, right axis) by neutral and anionic ligands illustrating the enthalpic-entropic compensation effect.

The thermodynamic data (log K, ΔH, ΔS) for the binding of anionic ligands to Co(III) are complex and were therefore examined separately in order to fully appreciate the macrocyclic influences on the binding process (**Table 5.4**). In the case of azide, ΔH and ΔS are both negative for each macrocycle. This suggests that the binding of azide to Co(III) in both instances is spontaneous at lower temperatures (highest log K values at 15 °C). Whilst in the porphyrin system the internal energies were well compensated (if only marginally entropically-driven), the binding of azide in B_{12a} is clearly enthalpically driven ($\Delta H_{cor} >> \Delta S_{cor}$). It was also noted that the entropic contribution in B_{12a} is smaller yet more positive than in the porphyrin ($\Delta S_{por} \approx 20\Delta S_{cor}$). These observations indicate very different driving influences in the binding of azide to Co(III) in each macrocycle.

Azide is a small, hard, centrosymmetric, highly water soluble ion capable of donating electron density to Co(III) through possible σ donation. The small size and abundant electron density makes azide a favourable ligand in the corrin system (log K = 5.02(5); ΔH_{cor} large and negative relative to ΔS_{cor}), despite

some of that density being less accessible to Co(III) due to azide's internal resonance stabilisation. It is the same abundance of electron density and weak π acceptor tendencies that makes azide a poor ligand for Co(III) in the porphyrin (log K_{por} = 2.28(6)). The values for ΔH_{por} and ΔS_{por} were anticipated given the porphyrin's relatively unobstructed upper surface. The small yet more positive ΔS_{cor} suggests a degree of disorder around Co(III) in the corrin, possibly even weaker/longer Co-L bonds; desolvation effects afforded by azide's hydrophilicity would be common in both macrocycles.

The binding of the small strong field CN^- ligand to Co(III) on the other hand, is significantly more favourable in both macrocycles; in fact it is the highest log K value for each macrocycle across both sets of ligands (**Table 5.4**, **5.4**). In the case of the porphyrin log K for the binding of CN^- was 6.04(5), consistent with similar porphyrin studies (Log K_{CoTPPS} = 6.54(2);[109] Log K_{CoTAP} = 6.34(4);[109] Log $K_{NAcFeMP8}$ = 6.76;[82] Log $K_{NAcFeMP11}$ = 6.55[86]).*** The values for ΔH and ΔS are high and negative suggesting that the reaction is spontaneous at low temperatures. On the other hand, the binding of CN^- to Co(III) in B_{12a} is too large for a reliable determination of K let alone ΔH and ΔS. Estimations of log K for the binding of cyanide vary from >12[55] to 12.3 in 80% MeOH[60] to 14.1[61] Despite this variation, it is interesting to note that the binding of CN^- in B_{12a} is significantly higher than NAcCoMP8 (log K_{cor} > 12;[55] log K_{por} = 6.04(5)).

The favourable binding of cyanide to Co(III) in the corrin system may be interpreted in terms of synergistic bonding between metal and ligand. Accepting that Co(III) in B_{12a} is a low spin O_h d^6 ion with pseudo C_{4v} symmetry then the binding of CN^- to Co(III) may occur in two ways. Firstly, CN^- donates electron density to Co(III) through σ bonding; it was previously established that Co(III) in B_{12a} favours σ donor ligands.[7] Secondly, the bond is fortified by Co(III) donating electron density back to CN^-(**Figure 5.16**). Firth[12] *et al*., suggested that that the effect of π backbonding in B_{12a} was less influential in the binding process as their log K values for methyl isocyanide and azide were statistically similar (log

*** CoTPPS = cobalt(III)-tetrakis(4-sulfonatophenyl)porphyrin; CoTAP = cobalt(III)-tetrakis(4-N,N,N-trimethylanilinium)porphyrin; NAcFeMP8 = *N*-acetyl iron(III) microperoxidase-8; NAcFeMP11 = *N*-acetyl iron(III) microperoxidase-11.

K = 4.8 and 4.9, respectively). By analogy, they expected π backbonding in cyanide to be the same. Methyl isocyanide is the least capable of participating in π backbonding. Azide, though small, has its electron density stabilised through resonance (less accessible) and is a poor π acceptor. CN^- on the other hand, has all the favourable characteristics to afford a very stable binding scenario in the case of Co(III) in B_{12a} (small, soft donor atom, large amounts of accessible electron density, no resonance stabilisation, strong field ligand).

By the same rationale the binding of CN^- to Co(III) in NAcCoMP8 is lower than B_{12a} whilst being the most favourable within NAcCoMP8. The cobalt ion in NAcCoMP8 appears to prefer less electron dense environments thus small ligands with less accessible electron density and with resonance stabilisation would be favoured. Whilst CN^- is electron rich σ donor (less favourable for the porphyrin), that density is efficiently shunted away from Co(III) through π backbonding making it more favourable. This suggests that in the porphyrin the adequate dispersal of electron density away from Co(III) and a decrease in donor strength are significant driving forces towards stable ligand binding[87]

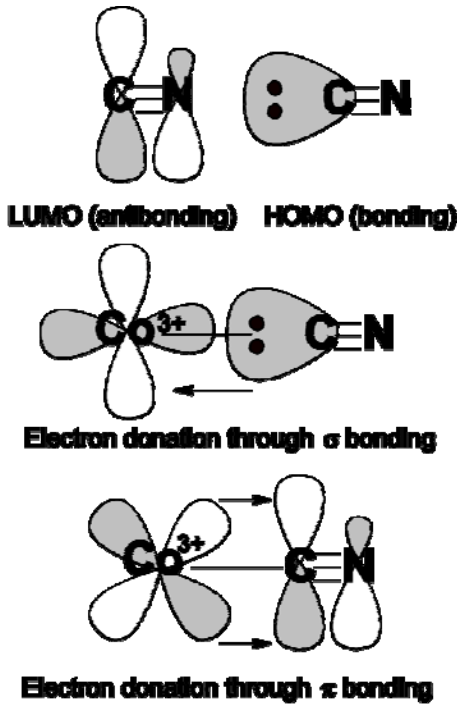


Figure 5.16 Diagrammatic representation of synergistic bonding between cyanide and Co(III) in B_{12a} in order to explain the remarkable binding affinity in this reaction.

The binding of HSO_3^- to Co(III) revealed some interesting thermodynamic insight into the influences of both macrocycles on the binding process (**Table 5.4**). Firstly, the binding of bisulfite to Co(III) is higher in the corrin than the porphyrin (log K_{cor} = 6.5(3); log K_{por} = 3.7(1)). Large amounts of accessible electron density from a strong σ-donor coupled to a soft S-donor atom makes bisulfite favourable to B_{12a} and consequently less so to NAcCoMP8. Secondly, it is striking that both macrocycles have large and positive ΔH and ΔS values indicating that the binding of bisulfite is endothermic and spontaneous at high temperatures. Thirdly, ΔS >> ΔH in both cases indicating an entropically-driven reaction. These findings were in direct contrast to the other anionic ligands that were enthalpically-driven with negative ΔH and ΔS values. Thirdly, ΔS is significantly larger in the corrin ($\Delta S_{cor} \approx 4.5\Delta S_{por}$); the disorder in the binding of bisulfite to Co(III) is more pronounced in the corrin than the porphyrin.

Two theories may account for the significant disorder in the binding of bisulfite to Co(III) (**Table 5.4**). Firstly, the disorder may arise from the desolvation of hydrophilic bisulfite. This may be verified by conducting further binding studies in a variety of solvents. Alternatively, the ΔS value might suggest a longer/weaker Co-L bond as a result of overcoming hydrogen-bonding (**Figure 5.17**). Bisulfite is more inclined to undergo hydrogen bonding with neighbouring bisulfite molecules (or with the macrocycle itself) as a result of the OH-group(s). This is likely since ΔH and ΔS values are large and positive in *both* macrocycles. The steric crowding of hydrogen bonded HSO_3^- molecules in conjunction with possible desolvation effects allows for a greater level of disorder (large, positive ΔS) around the coordination centre and thus longer M-L bonds. These observations are exacerbated in B_{12a} due to the *β*-face crowding hence the considerably larger ΔS value than NAcCoMP8. Nevertheless, it is interesting to note the amount of energy B_{12a} is prepared to expend in order to overcome the hydrogen bonding and bind bisulfite (ΔH_{cor} = 156(9) kJ mol^{-1} as opposed to ΔH_{por} = 22(2) kJ mol^{-1} in the porphyrin; **Table 5.4**). This again alludes to the corrin's preference (and the porphyrin's aversion) for softer σ donor ligands[7] that have large amounts of *accessible* electron density.

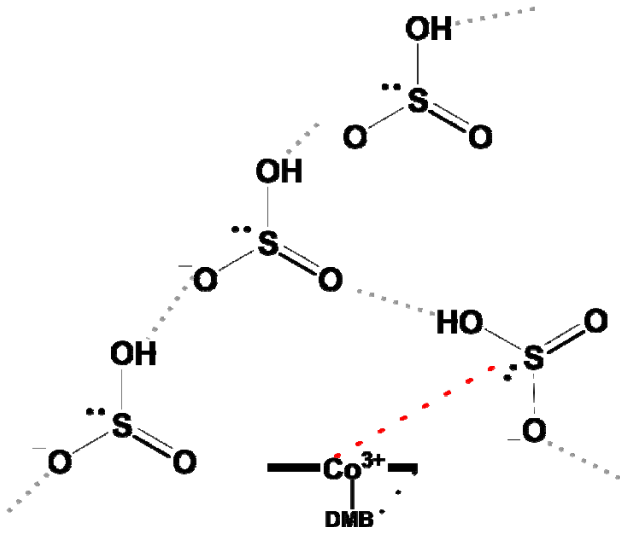


Figure 5.17 Diagrammatic representation of hydrogen-bonding between bisulfite molecules in relation to Co(III) in B_{12a} to explain the large entropic value in this reaction.

The analysis of ΔH and ΔS data is essential for the interpretation of the neutral ligand-binding data in each macrocycle. The log K values for the binding of neutral ligands were found to be generally similar within and between macrocycles (see **Section 5.2.2.1**). In the case of B_{12a} the log K values for the binding of neutral ligands range from *1.0* to 5.8 and 3.8 to 5.8 in NAcCoMP8. The most notable exception pertains to the binding of pyridine.

There are obvious disparities in the binding of pyridine to Co(III) between the porphyrin and the corrin (**Table 5.5**). The binding of pyridine in the NAcCoMP8 system was considerably higher than B_{12a} (log K_{por} = 4.93(5); log K_{cor} = 1.01(3)). These findings were consistent with other synthetic porphyrins where pyridine replaced the axially bound water *trans* to an N-donor ligand (log $K_{Co(III)TMPyP}$ = 4.68(2);[87] log $K_{Co(III)TPPS}$ = 5.06(9);[87,88] log $K_{Co(III)TCPP}$ = 4.98(1)[88]). The poor binding of pyridine in B_{12a} is often attributed to steric repulsions caused by the angle of pyridine's annular hydrogens against the macrocycle (see **Figure 5.18A**).[72,89] However, these steric repulsions do not appear to greatly effect the porphyrin's affinity for pyridine. It may be argued that unlike NAcCoMP8, the Co(III) in B_{12a} is 'sterically fenced-in' by having a crowded β-face with upward directed acetamide chains,[7,63,90] mitigating against the binding of the ligand. Therefore, the binding of substituted pyridines to Co(III) in B_{12a} would be lower regardless of where those substituents are located (**Figure 5.18A**). However,

preliminary data for the binding of 4-dimethylaminopyridine (DMAP) to Co(III) in B_{12a} revealed log K = 3.99(2) in 80% MeOH.[85] DMAP is a stronger base (pKa = 9.2) than pyridine (pKa = 5.2) and would be preferentially coordinated by B_{12a}[7] suggesting that the binding of pyridines are influenced by more than steric effects.

The ΔH and ΔS values reported for the binding of pyridine to Co(III) in each macrocycle clearly indicate that there are different driving influences (**Table 5.5**). Firstly, in B_{12a} both ΔH and ΔS are positive indicating a disordered reaction that is spontaneous at high temperatures. In contrast, the NAcCoMP8 values are negative indicating a more ordered and exothermic reaction. Secondly, the reaction in NAcCoMP8 is enthalpically-driven whilst being entropic in $B_{12a;}$ the latter being consistent with a more disordered system (see bisulfite, **Table 5.4**). In addition to the steric hindrance mentioned earlier, it is also not uncommon for aromatic ligands such as pyridines to π-π stack in solution (**Figure 5.18B**).[91-94] It is certainly plausible at the pyridine concentrations required in the B_{12a} study (neat pyridine as compared to μM concentrations in NAcCoMP8). The energy required to overcome the stacking in addition to the resulting longer/weaker Co-L bonds may account for the positive ΔH and ΔS values. On the other hand, the porphyrin's preference for less accessible electron dense ligands compels the more negative ΔH and ΔS values. Although pyridine is an electron dense conjugated 6-membered ring structure, it is that ring that stabilises the available density away from Co(III), allowing for a more stable Co(III)-Pyr ($\Delta H_{por} \approx 6\Delta H_{cor}$).

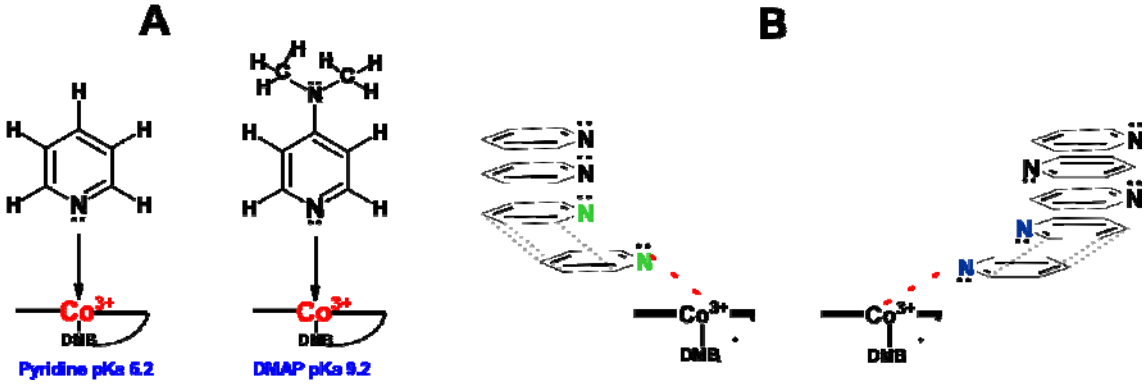


Figure 5.18 Sources of steric hindrance in the binding of pyridine to Co(III) in B_{12a}. Annular hydrogens and substituents may cause steric interactions against macrocycle or its sentinel groups (**A**). Pyridine may also π-π stacking in several conformations (**B**).

Pyridine ligand bindings studies with both porphyrin and corrin type macrocycles were conducted in the 1990s and revealed some interesting insights, particularly concerning entropy.[73,74,76,82,95,96] It was suggested that the unusual entropy may be as a result of several cooperating factors *e.g*. steric effects and π-π interactions. Pyridine, being both π donor and π acceptor ligand in the case of low spin Fe(III) porphyrins implies that these thermodynamic trends were as a result of π-donor-acceptor type interactions between the conjugated porphyrin ring and the phenyl group.[95,96] Additionally, the formation of pyridine adducts with the metalloporphyrin are common. However such a formation would imply a considerable spectroscopic change, of which there was no evidence, both in their work and in NAcCoMP8.[95,96] It has to be noted that whilst these reported systems have some rather interesting implications, they are in fact, very different systems to that of NAcCoMP8. Some of the studies were conducted using KCl, a potential ligand, (*ca*. 0.1 M) or an unacetylated microperoxidase species; others included iron which has access to more than one spin state.

The binding of NMI to Co(III) was challenging to interpret in light of the available literature (**Section 5.2.1.2**). For example, most studies did not include ΔH and ΔS experiments. Those that did generally used a competing ligand as a background electrolyte such as Cl^-; Cl^- has been shown to coordinate at high concentrations.[97-99] Other systems had the macrocycle embedded within a protein. In some instances the metal ion was Fe(III), having at least two spin states available or Cr(III)[100] In other cases, the incoming ligand was imidazole. It is noted that whilst imidazole and substituted imidazole data may, to a degree, be comparable, the identity and orientation of those substituents uniquely affect basicity, sterics, tautomerism and ultimately, the binding.[75,101] Comparisons were nevertheless attempted whilst being cognisant of these differences in each of the systems surveyed.

The binding of NMI to Co(III) in both macrocycles were compared (**Table 5.5**). NAcCoMP8 binds NMI better than B_{12a} (log K_{por} = 5.76(8) and log K_{cor} = 4.43(7), respectively). These findings were plausible considering NAcCoMP8's preference for less electron dense ligands; NMI has its electron density

stabilised within the azole ring structure. The values for B_{12a} were consistent with those of Eilbeck and West[75] (log K = 4.40; μ = 0.1 M by KNO_3). Marques[101] *et al*., obtained slightly higher values likely due to high ionic strength by KCl (log K = 4.90; μ = 1.0 M KCl). Similarly, the findings of Cregan[57] *et al*., were higher still (log K = 5.17; μ = 1.5 M $NaClO_4$). Analogous experiments with imidazole were conducted by Eilbeck and West[75] (log K = 4.61) as well as by Marques[101] *et al.,* (log K = 4.59) (**Table 5.6**). Eilbeck and West[75] found imidazole to be the preferred ligand whilst the opposite was observed by Marques[101] *et al*., a disparity likely attributable to elevated KCl concentration. Eilbeck and West[75] speculated that whilst steric factors were negligible, imidazole may in fact be stabilised through hydrogen bonding on the corrin's amide side chains.[56] This degree of ordering would allow for a more negative ΔS (see later).

Table 5.6 Thermodynamic trends in some B_{12a}-related compounds with NMI-type ligands.

[a]Complex	[b]X—Co(III)—Y + Z			μ /M (electrolyte)	Log K (25 °C)	[h]ΔH kJ mol^{-1}	[h]ΔS K^{-1}mol^{-1}
	X	Y	Z				
B_{12a}	H_2O	[c]DMB	[d]NMI[57]	1.5 ($NaClO_4$)	5.17		
			[d]Im[75]	0.1 (KNO_3)	4.61	-29.3	-10.2
			NMI[75]	0.1 (KNO_3)	4.40	-23.0	+6.9
			Im[56]	0.042 (NaCl)	4.59	-30.1	-13.4
			Im[101]	1.0 (KCl)	4.59		
			NMI[101]	1.0 (KCl)	4.90		
			Im[59]	2.2 ($NaClO_4$)	4.63		
			[g]*NMI*	*0.1 ($NaNO_3$)*	*4.44*	*-62*	*-122*
[g]*NAcCoMP8*	*H_2O*	[d]*His*	*NMI*	*0.1 ($NaNO_3$)*	*5.69*	*42*	*250*
[e]NAcFeMP11	H_2O	His	Im[43]	0.1 (KCl)	4.16	-29.5	-19.3
[f]metMb	H_2O	His	Im[43]	0.1 (KCl)	2.23	-16.7	-13.2
[f]NAcFeMP8	H_2O	His	Im[82]	0.1 (NaCl)	4.08		
	H_2O	His	NMI[82]	0.1 (NaCl)	4.17		

a Refers to the identity of the macrocycle as well as the metal ion.
B X, Y and Z are distal, proximal and incoming ligands, respectively and Z replaces X.
c DMB = 5,6-dimethybenzimidazole.
D NMI = n-methylimidazole (1-methylimidazole); Im = imidazole; His = histidine.
E NAcFeMP11 = *N*-acetyl iron(III) microperoxidase-11.
F metMb = Metmyoglobin; NAcFeMP8 = *N*-acetyl iron(III) microperoxidase-8.
G Refers to this work (in italics).
H Reported where available.

On the other hand, comparable porphyrin evidence was limited (**Table 5.6**). The most relevant data pertain to the binding of NMI (and imidazole) to Fe(III) in the analogous, NAcFeMP8.[82] Whilst the system contains NaCl as well as Fe(III) with two spin states, some key observations were noted. Firstly, the binding of NMI in NAcFeMP8[82] (log K = 4.17; μ = 0.1 M) was considerably lower than in NAcCoMP8 suggesting that the binding is heavily dependent on the identity of the metal ion. In fact, the binding preference for NMI, NAcCoMP8 > B_{12a} > NAcFeMP8, suggests that the Co(III)-NMI system is most stable. This trend persists with imidazole; B_{12a} was energetically more favourable than the iron porphyrins (log K_{metMb} = 2.23;[43] log $K_{NAcFeMP8}$ = 4.08;[82] log $K_{NAcFeMP11}$ = 4.16;[43] log K_{B12a} = 4.59[101]). Secondly, in both the B_{12a}[101] and NAcFeMP8[82] systems it was generally the bulkier NMI ligand that was preferred, not the potentially tautomeric imidazole. This suggests that the binding may be more electronically than sterically influenced; steric influences typically lower binding constants as noted in the protein-bound metMb (log K = 2.23).[43]

The underlying thermodynamic factors governing the binding of NMI to Co(III) are again remarkably different in each macrocycle (**Table 5.5**). NAcCoMP8 exhibited ΔH and ΔS values that were both positive; ΔS_{por} is larger and more positive than ΔH_{por}. This suggests that the reaction is endothermic and distinctly entropically driven. The marginally comparable data were for the binding of imidazole to NAcFeMP11[43] (log K = 4.16; μ = 0.1 M by KCl) (**Table 5.6**). The ΔH and ΔS values were negative, and like NAcCoMP8, ΔS was more positive than ΔH. The NAcCoMP8 findings were thus distinctly unusual and were remotely analogous to the binding of NMI in cytochrome *c* which was monitored using ^{1}H NMR analysis.[102] Although the binding constant was very low (*ca*. log K = 1.54) the ΔH and ΔS values were 39.5 kJ mol^{-1} and 154 J mol^{-1} K^{-1}, respectively. Their findings were rationalised structurally since the porphyrin was still embedded within the native protein. Additionally, NMI's propensity for π-π stacking[57] may also contribute to the large and positive ΔS values.

In contrast, B_{12a} values were both *negative*; ΔS_{cor} is larger and more *negative* than ΔH_{cor} indicating an ordered and *exothermic* reaction. The values reported

here for ΔH and ΔS are not in agreement with B_{12a} literature values (**Table 5.6**). Eilbeck and West[75] found that the binding of NMI in B_{12a} was enthalpically driven; ΔS was more positive than ΔH, and in fact ΔS was positive. Hanania and Irvine's[56] study with imidazole (μ = 0.042 M by NaCl) was also enthalpically driven; ΔS was more positive than ΔH. They suggested that the binding was more electronic in nature than steric.[56] Interestingly, the iron porphyrins[43] (μ = 0.1 M by KCl) also exhibited a similar trend. This is fascinating as it implies (though unlikely) that the internal thermodynamic influences are fairly consistent despite the identity of the macrocycle, electrolyte and metal ion.[56,75,43] Eilbeck and West's findings[75] share a particular congruency with those having Cl^- as a background electrolyte. Contamination by Cl^- may be overlooked if the absorbance was only monitored at one wavelength especially if the shifts are small; the γ shift due to the binding of Cl^- is small (350 → 352 nm).[7]

The binding of primary amines (MOA and HA) to Co(III) provide an excellent opportunity to observe what each macrocycle does with the electron density. Sterically, both MOA and HA are small with similar steric influences so relatively large binding constants are anticipated. Electronically however, HA has three heteroatoms as compared to two in MOA; the electronic contributions are anticipated to be different. Both ligands donate electron density through the same N-donor atom but there are no ring-structures or resonance stabilisations so the binding preferences between the macrocycles should be pronounced.

Interestingly, MOA seems to be the only neutral ligand in the series that preferentially binds Co(III) in the *corrin* rather than the porphyrin (**Table 5.5**). In fact, it's the weakest bound ligand amongst the porphyrin data (log K_{por} = 3.81(9)) whilst being the highest amongst the corrin (log K_{cor} = 5.78(7)). The binding of MOA to Co(III) in both macrocycles appear to be under the same thermodynamic influences. ΔH and ΔS in both macrocycles are large and negative where ΔS is more negative than ΔH, indicating that the reaction is exothermic, entropically driven. Steric influences seem unlikely and if significant, would be pronounced in B_{12a} due to β-face crowding.[7] However this is unlikely since ΔS_{cor} is large and negative indicating an ordered system.

In contrast, the binding of HA by Co(III) is more favourable in the *porphyrin* than the corrin (**Table 5.5**). NAcCoMP8 binds HA (log K = 5.5(2)) better than B_{12a} (log K = 4.72(4)) by *ca*. 0.8 log units. However, in this instance, there are distinctly different internal thermodynamic parameters suggesting that the binding of HA is influenced differently in each macrocycle. In the case of NAcCoMP8, both ΔH and ΔS are large and negative where ΔS is more negative than ΔH. This suggests that, similar to MOA, the binding is exothermic and highly ordered. However, the binding of HA in B_{12a} is distinctly different. Here, ΔH and ΔS are both large and positive where ΔS is more *positive* than ΔH. This suggests that the binding of HA to Co(III) in B_{12a} is *endothermic* and dominated by entropy. These values are reminiscent of those observed with B_{12a} and bisulfite (**Table 5.4**) where the large positive ΔH and ΔS contributes signalled the possibility of longer/weaker M-L bonds due to hydrogen bonding between ligand molecules; the disorder is uniquely exacerbated by B_{12a}'s crowded β-face (see bisulfite explanation for large and positive ΔS values).

It was anticipated that MOA would be the preferred ligand for B_{12a} whilst HA would be preferentially bound by NAcCoMP8. It was earlier stated (**Section 5.2.2.1**) that the Co(III) in B_{12a} has a preference for more *accessible* electron dense ligands and less so in the case of NAcCoMP8. With the primary amines selected, MOA has the additional electronic contribution of a methyl group whilst HA has that of a single hydrogen. The log K values for the binding of MOA (and of HA) to Co(III) in NAcCoMP8 (and in B_{12a}) support these anticipations (**Table 5.5**). A precedent for this can be observed with cobinamide despite the different *trans* ligands.[73] If accessible electron density is important in the corrin system then it would be expected that methylamine would have a higher log K than HA (log $K_{methylamine}$ = 3.4; log K_{HA} = 2.46).[73] The opposite would be expected with iron porphyrins[82] (log $K_{methoxylamine}$ = 2.14; log K_{HA} = 2.91). Both methylamine and methoxylamine have more electron density to contribute than HA.

The binding of N-donor ligands, especially amines (sp^3), are notoriously complex.[56,57,72-77] Byfield *et al*., noted this and attempted to delineate amine's anomalous behaviour using iron porphryins.[95] They speculated that the various

factors influencing amine binding such as inductive effects, polarisability and steric effects, should not viewed in isolation but rather as a composite. Here, factors that typically decrease and increase log K have been broadly grouped as steric- and α-effects, respectively.

Steric effects have two parts: the incoming ligand and the macrocycle. Byfield *et al*., have shown that amine steric effects in corrin-type macrocycles are important when they afford a branched or lateral structure as opposed to successive additions of methyl groups in a linear fashion.[95] Branching by the addition of methyl groups significantly diminishes the binding of amines to corrin-type structure as observed with the binding of glycine and alanine.[95] Additionally, Baldwin *et al*., noted that steric effects in corrins increase as the donor power of the *trans* ligand decreases and applies to substitution on both faces of the corrin.[74] Although pertaining to ring-structures, Byfield[95] *et al.* and Marques[82] *et al*., have commented on the significance of ligand steric effects as a result of ligands π-π stacking and/or adduct formation. Hydrogen bonding interactions are also sterically possible.[73] Ligands capable of hydrogen bonding exert a steric effect either by interaction with macrocyclic side-chains or by steric repulsions on the macrocyclic face.

The α-effect is considerably more difficult to interpret. It is a term given to the excess reactivity (*e.g.* in ligand substitution reactions) above that expected from basicity alone; the donor atom is also attached directly to an electronegative atom with lone pair electrons.[73,103] This 'excess reactivity' is quantified by establishing a 'baseline' of log K values for a particular family of compounds in relation to their pKa.[73,103] As applicable to amines, MOA and HA are often used to test the α-effect's applicability in a study.[95,104] Whilst this effect was initially applied to rates of reactions,[103,105] it has recently been shown to have a significant thermodynamic component,[73,106,107] notably in microperoxidases.[95,104] Interestingly, it has always been assumed that HA coordinates the metal ion through a single atom; however there is insufficient structural evidence to substantiate this. In contrast, the formation of η^2 complexes with some metal ions is well established and may be a structural implication of the α-effect.[73]

5.3 SUMMARY AND CONCLUSIONS

The work in this Chapter qualitatively and quantitatively assessed the *cis* influences exerted by the macrocycle on the metal ion in both NAcCoMP8 and $B_{12a.}$

A systematic qualitative analysis of the various spectra was conducted in order to find any spectral relationships between the macrocycles. This was attempted in two ways. Firstly, the porphyrin and corrin absorbance spectra were compared both with and without the metal ion. As anticipated, the spectra of the Co(III)-macrocycles were analogous given the chromophores' structural similarities. These observations indicated a certain degree of electronic similarity between the metal complexes. The corrin's spectrum however, exhibited a more pronounced blue shift relative to the porphyrin, likely due to the corrin's interrupted conjugation. The metal-free spectra on the other hand exhibited significant differences. Whilst the metal-free spectrum in each macrocycle exhibits a blue shift relative to the metal complex, the removal of Co(III) appears to have a more significant effect on the porphyrin's absorbance spectrum than on the corrin's. This effect manifests in the porphyrin's Q-band region where there are subsequently four peaks after Co(III) is removed. The corresponding αβ band in the corrin remains relatively unaffected by the absence of Co(III). This evidence suggests that there is a more pronounced metal-macrocycle electronic relationship in the porphyrin than the corrin.

Secondly, NAcCoMP8 (and B_{12a}) was reacted with selected anionic and neutral ligands and the absorbance spectra for these complexes were qualitatively assessed. The replacement of the axial water by any of the ligands studied caused a red shift in both macrocycles; the shifts were more pronounced in the corrin than the porphyrin suggesting a more prominent *cis* influence. It was also noted that the anionic ligands caused significantly larger spectral shifts than the neutral N-donor ligands in both macrocycles. Additionally, the relationship between wavelength shifts (*ca*. 400 nm region) for each macrocycle shows a reasonably positive linear correlation. Both trends indicate that the systems are

sensitive to the donor power of the axial ligand. The softer ligands caused the greatest shift towards longer wavelength which is consistent with a narrowing of the HOMO-LUMO gap of the delocalised π electron system of the macrocycles.

As a consequence of this work the three previously mentioned NAcCoMP8 species were isolated: the putative monomer (415 nm), the intermediate dimer (417 nm) and the tetramer (424 nm). These species were reacted with a probe ligand, cyanide, to test for reproducibility. The 415 nm species was the only species that showed reproducible binding data with cyanide and was used in subsequent experiments. The binding of cyanide with each species exhibited approximately the same binding constants whereby the second substitution was *ca*. 3 log units less than that of the first substitution. This suggests that they each species binds cyanide similarly possibly due to a similar conformation or structure. Also, the Co-His bond would be stronger than the Co-OH_2 bond. Thus, two possible modes of aggregation were proposed.

Bond lengths and angles for various porphyrins and corrins were examined from the Cambridge Structural Database to help rationalise these observed spectral trends. This examination showed that there is a considerable lack of directly comparable data. Furthermore, within the set of available comparable structures, there needs to be electronically suitable *trans* ligands in order to keep the *trans* influences the same. Within those constraints, examples for nitrites, imidazoles and pyridines were found. Based on these data, nitrites were expected to be less sterically demanding than imidazoles. Both nitrite and imidazole datasets reflected considerable variability in Co-L bond lengths. Bond lengths in the nitrite study were statistically identical between the macrocycles. However, in the case of imidazoles, the corrin exhibits a marginally smaller bond length than the porphyrin, suggesting a stronger bond. There are no crystal structures for a pyridine complex with B_{12a}. However, the Co-N bond lengths were found to be statistically similar in a variety of sterically unhindered complexes such as pentammine, porphyrins, cobaloximes and corroles.

The quantitative thermodynamic binding properties of selected ligands to Co(III)

in NAcCoMP8 and B_{12a} proved to be remarkably complex to rationalise. A significant finding is that the anionic ligands bind more strongly to Co(III) in the corrin than in the porphyrin, and that the log K values for both macrocycles parallel each other. Neutral ligands on the other hand, show a greater affinity for Co(III) in the porphyrin rather than the corrin (with the exception of MOA). There also appears to be an inverse relationship between the log K values in the two systems. Further ligand-binding studies with a larger variety of neutral ligands would have to be conducted in order to verify this. The binding of neutral ligands to Co(III) in both macrocycles were difficult to interpret thereby emphasising the importance of conducting log K experiments as a function of temperature to obtain ΔH and ΔS values.

By obtaining log K values as a function of temperature, ΔH and ΔS values for these ligand substitution reactions were obtained. A comparison of these values affords insight into the enthalpic and entropic factors underlying log K in each macrocyclic system. Firstly a strong compensation effect between ΔH and ΔS was observed in both systems whereby negative ΔH values were offset by positive ΔS values. This is commonly observed in many biological systems. Secondly, it was noted that both ΔH and ΔS obtained for the anionic ligands vary in the same way in both macrocycles ($HSO_3^- > N_3^- > NO_2^-$). However, this is not the case with the neutral ligands (HA > NMI > MOA for B_{12a} but NMI > MOA > HA for NacCoMP8). This evidence supports the log K findings whereby the binding of anionic ligands in both macrocycles parallel each other whilst the binding of neutral ligands exhibit an inverse relationship in both systems.

It was previously posited that the binding of exogenous ligands to the metal ion in either macrocycle is dependent on the amount of available and *accessible* electron density that ligand can provide. It was suggested that the metal ion in the corrin, due to its interrupted conjugation, would have less electron density from the macrocycle directed towards it and is thus more Co(II)-type in nature. It follows that the cobalt ion in the corrin macrocycle would then preferentially bind to ligands that have large amounts of *accessible* electron density; accessibility being influenced by softer donor atoms, σ-donation, resonance stabilisation,

ring stabilisation, cavity size and steric hindrance. It was further posited that strong binding as attributed by *accessibility* is influenced more by a selection of features working cooperatively rather than by one feature in isolation. Porphyrins on the other hand, have sufficient electron density from a fully conjugated system directed towards the cobalt ion thus inferring a Co(III)-type nature. It would be expected that the Co(III) porphyrin would then exhibit a preference for less electron dense ligands that have a diminished capacity to donate that density.

5.4 REFERENCES FOR CHAPTER 5

1. Pratt, J. M.; Thorp, R. G., *J. Chem. Soc. (A)*, **1966**, 187.
2. Perry, C. B.; Marques, H. M., *S. Afr. J. Chem.,* **2005**, *58*, 9.
3. Firth, R. A.; Hill, H. A. O.; Pratt, J. M.; Thorp, R. G.; Williams, R. J. P., *J. Chem. Soc.*, **1968**, *(A)*, 2428.
4. Rovati, G. E., *Trends in Pharmacological Sciences*, **1998**, *19*, 365.
5. Eldik, R. van., *Chem. Rev.*, **2005**, *105(6)*, 1917.
6. Sannasy, D., M.Sc. Dissertation, University of the Witwatersrand, Johannesburg, South Africa, **2005**.
7. Pratt, J. M.; *Inorganic chemistry of vitamin* B_{12}, Academic Press, London 1972 (and references therein).
8. Munro, O. Q.; Marques, H. M., *Inorg. Chem.*, **1996**, *35*, 3752
9. Marques, H.M., Ph. D. Thesis, University of the Witwatersrand, Johannesburg, South Africa, **1986**.
10. Reenstra, W. W.; Jencks, W. P., *J. Am. Chem. Soc.,* **1979**, *101(19)*, 5780.
11. Firth, R. A.; Hill, H. A. O.; Pratt, J. M.; Thorp, R. G., *J. Chem. Soc.*, **1968**, *(A)*, 453.
12. Firth, R. A.; Hill, H. A. O.; Pratt, J. M.; Thorp, R. G.; Williams, R. J. P., *J. Chem. Soc.(A)*, **1969**, 381.
13. *SigmaPlot,* 11.0; Systat Software, Inc.: San Jose, CA, **2008**.
14. Winzor, D. J.; Jackson, C. M., *J. Mol. Recognit.,* **2006**, *19*, 389.
15. Frederick, J.; *Statistical Methods in Experimental Physics* (2nd ed.); World Scientific; Singapore. 2006.
16. Day, P., *Theoretica Chimica Acta (Berlin),* **1967**, *7*, 328.
17. Hill, J. A.; Pratt, J. M.; Williams, R. J. P., *J. Theor. Biol.,* **1962**, *3*, 423.

18. Kuhn, H.; Drexhage, K. H.; Martin, H., *Proc. Roy. Soc.,* **1965**, *A288*, 348.

19. Hill, H. A. O.; Pratt, J. M.; Williams, R. J. P., *J. Chem. Soc.,* **1965**, 2859.

20. Knapton, L.; Ph. D. Thesis, University of the Witwatersrand, Johannesburg, South Africa, **2005**.

21. Gouterman, M.; in D. Dolphin (ed.), *The Porphyrins,* Physical Chemistry, Part C, Volume 3, Academic Press, New York, San Francisco, London, 1978.

22. Milgrom, L. R.; *The Colours of Life: An introduction to the chemistry of porphyrins and related compounds,* Oxford University Press, Oxford, 1997.

23. Loew, G. H.; in A. B. P Lever and H. B. Gray (eds.), *Iron Porphyrins,* Part 1, Physical Bioinorganic Chemistry Series, Addison-Wesley, Reading, Mass., 1983, pp 1-87.

24. Firth, R. A.; Hill, H. A. O.; Pratt, J. M.; Williams, R. J. P.; Jackson, W. R., *Biochemistry*, **1969**, *(6)*, 2178.

25. Toohey, J. I.; *Proc. Nat. Acad. Sci.*, **1965**, *54*, 934.

26. Perry, C. P.; Fernandes, M. A.; Brown, K. L.; Zou, X.; Valente, E. J.; Marques, H. M., *Eur. J. Inorg. Chem.,* **2003**, 2095.

27. Hill, H. A. O.; Pratt, J. M.; Thorp. R. G.; Ward, B.; Williams, R. J. P., *Biochem. J.,* **1970**, 120, 263.

28. Perry, C. B.; Ph. D. Thesis, University of the Witwatersrand, Johannesburg, South Africa, **2004**.

29. Vashi, P. R.; Ph. D. Thesis, University of the Witwatersrand, Johannesburg, South Africa, **2004**.

30. Ni, W. T.; Tezcan, F. A., *Angew. Chem. Int. Ed.,* **2010**, *49*, 7014.

31. Hannak, R. B.; Farber, G; Konrat, R, Krautler, B., *J. Am. Chem. Soc.,* **1997**, *119,* 2313.

32. Wang, R.; MacGillivray, B. C.; MacCartnery, D. H., *Dalton Trans.*, **2009**, 3589

33. Zhou, K.; Zelder, F., *Chem.Commun.*, **2011**, *47*, 11999.

34. Shelnutt, J. A.; Song, X.; Ma, J.; Jentzen, W.; Medforth, C. J., *Chem. Soc. Rev.,* **1998**, *27(31)*, 39.

35. Kano, K.; Fukuda, K.; Wakami, H.; Nishiyabu, R.; Pasternack, R. F., *J. Am. Chem. Soc.,* **2000**, *122*, 7494.

36. Melchionna, S.; Barteri, M.; Ciccotti, G., *J. Phys. Chem.,* **1996**, *100*, 19241.

37. Hunter, C. A.; Sanders, J. K. M., *J. Am. Chem. Soc.,* **1990**, *112*, 5525.

38. James, B. R.; in D. Dolphin (ed.), *The Porphyrins,* Physical Chemistry, Part C, Volume 5, Academic Press, New York, San Francisco, London, 1978.

39. Strong, J. D.; Hartzell, C. R., *Bioinorg. Chem.*, **1976**, *5*, 219.

40. Munro, O. Q.; Marques, H. M., *Inorg. Chem.*, **1996**, *35(13)*, 3752.

41. Munro, O. Q.; Marques, H. M., *Inorg. Chem.*, **1996**, *35(13)*, 3768.

42. Marques, H. M.; Perry, C. B., *J. Inorg. Biochem.*, **1999**, *75*, 281.

43. Perry, C. B.; Chick, T.; Ntlokwana, A.; Davies, G.; Marques, H. M., *J. Chem. Soc. Dalton Trans.,* **2002**, 449.

44. Chemaly, S. M.; Florczak, M.; Dirr, H.; Marques, H. M., *Inorg. Chem.* **2011**, *50*, 8719.

45. Garau, G.; Geremia, S.; Marzilli, L. G.; Nardin, G.; Randaccio, L.; Tauzher, G., *Acta Cryst., Sec. B,* **2003**, 51.

46. Goodwin, J.; Bailey, R.; Pennington, W.; Rasberry, R.; Green, T.; Shasho, S.; Yongsavanh, M.; Echevarria, V.; Tiedeken, J.; Brown, C.; Fromm, G.; Lyerly, S.; Watson, N.; Long, A.; De Nitto, N., *Inorg. Chem.,* **2001**, *40*, 4217.

47. Kaduk, J. A.; Scheidt, W. R., *J. Am. Chem. Soc.,* **1974**, *13*, 1875.

48. Annoni, E.; Pizzotti, M.; Ugo, R.; Quici, S.; Morotti, T.; Casati, N.; Macchi, P., *Inorg. Chim. Acta,* **2006**, *359*, 3029.

49. Jene, P. G.; Ibers, J. A., *Inorg. Chem.,* **2000**, *39*, 3838.

50. Hannibal, L.; Bunge, S. D.; Eldik, R. van.; Jacobsen, D. W.; Kratky, C.; Gruber, K.; Brasch, N. E., *Inorg. Chem.,* **2007**, *46*, 3613

51. Bang, H.; Edwards, J. O.; Kim, J.; Lawler, R. G.; Reynolds, K.; Ryan, W. J.; Sweigart, D. A., *J. Am. Chem. Soc.* **1992**, 114, 2843.

52. Lauher, J. W.; Ibers, J. A., *J. Am. Chem. Soc.* **1974,** 96, 4447.

53. Guangdi, Y.; Xizhang, C.; Fengshan, W.; Guodong, Z., *Jilin Daxue Ziran Kex. Xue.* **1988,** 118, 118-121.

54. Perry, C. B.; Fernandes, M. A.; Brown, K. L.; Zou, X.; Valente, E. J.; Marques, H. M., *Eur. J. Inorg. Chem.,* **2003**, 2095

55. Hayward, G. C.; Hill, H. A. O.; Pratt, J. M.; Vanston, N. J.; Williams, R. J. P.; *J. Chem. Soc.,* **1965**, 6485.

56. Hanania, G. I. H.; Irvine, D. H., *J. Chem. Soc.,* **1964**, 5694.

57. Cregan, A. G.; Brasch, N. E.; Eldik, R. van., *Inorg. Chem.,* **2001**, *(40)*, 1430.

58. Bauriedel, W. R., *Iowa State Coll. J. Sci.*, **1956**, *(30)*, 321.

59. Knapton, L.; Marques, H. M., *Dalton Trans.,* **2005**, 889.

60. Zipp, C.F.; Mathura, S.; Michael, J. P.; Fernandes, M. A.; Marques, H.M., unpublished results.

61. de Tacconi, N. R.; Lexa, D.; Saveant, J. M., *J. Am. Chem. Soc.*, **1979**, *101*, 467.

62. Rubinson, K. A.; Parekh, H.; Mark, h. B., *Inorg. Chem.,* **1983**, *22*, 458.

63. Pratt, J. M., *Pure and Appl. Chem.,* **1993**, *65(7)*, 1513.

64. Jensen, K. P.; Ryde, U., *Coord. Chem. Rev.*, **2009**, *253,* 769.

65. Jensen, K. P.; Ryde, U., *Chem. Biochem.*, **2003**, *4,* 413.

66. Fruasto da Silva, J. J. R.; Williams, R. J. P., *The Biological Chemistry of the Elements,* Clarendon Press, Oxford, p403, 1994.

67. Liccoccia, S.; Paolesse, R., *Struct. Bonding*, **1995**, *84*, 71.

68. Geno, M. K.; Halpern, J., *J. Am. Chem. Soc.*, **1987**, *109*, 1238.

69. Munro, O. Q.; Bradley, J. C.; Hancock, R. D.; Marques, H. M.; Marsicano, F.; Wade, P. W., *J. Am. Chem. Soc.,* **1992**, *114*, 7218.

70. Munro, O. Q.; Marques, H. M.; Debrunner, P. G.; Mohanrao, K.; Scheide, W. R., *J. Am. Chem. Soc.*, **1995**, *117*, 935.

71. Rovira, C.; Kune, K.; Hutter, J.; Parrinello, M., *Inorg. Chem.,* **2001**, *40(1)*, 11.

72. Choi, K-H.; Lee, H-J.; Karpfen, A.; Yoon, C-J.; Park, J.; Choi, Y-S., *Chem. Phys. Letters.,* **2001**, *345(3)*, 338.

73. Hamza, M. S. A.; Pratt, J. M., *J. Chem. Soc. Dalton Trans.,* **1994**, 1377. (and references therein).

74. Baldwin, D. A.; Betterton, E. A.; Pratt, J. M., *J. Chem. Soc. Dalton Trans.,* **1983**, 2217.

75. Eilbeck, J. W.; West, M. S., *J. Chem. Soc. Dalton Trans.,* **1976**, 274.

76. Hamza, M. S. A.; Pratt, J. M., *J. Chem. Soc. Dalton Trans.,* **1994**, 1373.

77. Reddy, D. S.; Reddy, N. R. K.; Sridhar, V.; Satyanarayana, S., *Proc. Indian. Acad. Sci. (Chem. Sci.)*, **2002**, *114(1)*, 1.

78. Lumry, R.; Rajendra, S., *Biopolymers,* **1970**, *9*, 1125.

79. Williams, K. R., *J. Theor. Comp. Chem.,* **2004**, *3(4)*, 511.

80. Sharp, K., *Protein Science*, **2001**, *10*, 661.

81. Perozzo, R.; Folker, G.; Scapozzo, L., *J. Recept. Sig. Transd.*, **2004**, *24(1)*, 1.

82. Marques, H. M.; Munro, O. Q.; Munro, T.; de Wet, M.; Vashi, P., *Inorg. Chem.,* **1999**, *38(10)*, 2312.

83. Searle, M. S.; Westwell, M. S.; Williams, D. H., *J. Chem. Soc., Perkins Trans.,* **1995**, *2*, 141.

84. Williams, D. H.; Searle, M. S.; Mackay, J. P.; Gerhard, U.; Mapelstone, R. A., *Proc. Natl. Acad. Sci. U.S.A.,* **1993**, *90*, 1172.

85. Zipp, C. F., University of the Witwatersrand, personal communication.

86. Perry, C. B.; Chick, T.; Ntlokwana, A.; Davies, G.; Marques, H. M. , *J. Chem. Soc., Dalton Trans.* **2002**, 449.

87. Pasternack, R. F.; Cobb, M. A.; Sutin, N., *Inorg. Chem.,* **1975**, *14(4)*, 866.

88. Ashley, K. R.; Leipoldt, J. G., *Inorg. Chem.*, **1981**, *20*, 2326.

89. Seeman, J.; Ennis, D. M.; Sector, H. V.; Clawson, L.; Palen, J., *Chem. Senses.*, **2000**, *25(4)*, 429.

90. Glusker, J. P. In B_{12}; Dolphin, D., Ed.; Wiley: New York, 1982; Vol. 1, p 23.

91. Shimohigashi, Y.; Yamauchi, Y.; Ikesue, K.; Maeda, I.; Kawahara, M.; Nose, T*., Pept. Sci.: Present Future, Proc. Int. Pept. Symp., 1st* **1997***,* 649.

92. Kashima, A.; Inoue, Y.; Sugio, S.; Maeda, I.; Nose, T.; Shimohigashi, Y*., Eur. J. Biochem.* **1998**, *255*, 12.

93. Afshar, C.; Berman, H. M.; Sawzik, P.; Lessinger, L.; Lim, B. B.; Hosmane, R. S., *J. Crystallogr. Spectrosc. Res.* **1987**, *17*, 533.

94. Mitchell, J. B. O.; Nandi, C. L.; McDonald, I. K.; Thornton, J. M.; Price, S. L., *J. Mol. Biol.* **1994**, *239*, 315.

95. Byfield, M. P.; Hamza, M. S. A.; Pratt, J. M., *J. Chem. Soc. Dalton Trans.,* **1993**, 1641.

96. Marques, H. M.; Byfield, M. P.; Pratt, J. M., *J. Chem. Soc. Dalton Trans.,* **1993**, 1633.

97. Marques, H. M.; Egan, T. J.; Marsh, J. H.; Mellor, J. R.; Munro, O. Q., *Inorg. Chim. Acta*, **1989**, *166*, 249.

98. Marques, H. M.; Knapton, L., *J. Chem. Soc. Dalton Trans.,* **1997**, 3827.

99. Prinsloo, F. F.; Breet, E. L. J.; Eldik, R. van.; *J. Chem. Soc. Dalton Trans.,* **1995**, 685.

100. Ashley, K. R.; Kuo, J.; *Inorg. Chem.,* **1988**, *27*, 3556.

101. Marques, H. M.; Marsh, J. H.; Mellor, J. R.; Munro, O. Q., *Inorg. Chim. Acta*, **1990**, *170*, 259.

102. Shao, W.; Liu, G.; Tang, W., *J. Inorg. Biochem.,* **1995**, *57*, 103.

103. Edwards, J. O.; Pearson, R. G., *J. Am. Chem. Soc.,* **1962**, *84*, 16.

104. Hamza, M. S. A.; Pratt, J. M., *J. Chem. Soc. Dalton Trans.,* **1993**, 1647.

105. Fina, N. J.; Edwards, J. O., *Int. J. of Chem. Kinetics*, **1973**, *1(26)*, 1.

106. Jencks, W. P.; Carriuolo, J., *J. Am. Chem. Soc.,* **1960**, *82*, 1778.

107. Abraham, M. H.; Duce, D. P.; Prior, D. V.; Barratt, D. G.; Morris, J. J.; Taylor, P. J., *J. Chem. Soc., Perkin Trans.* **1989*,*** *2*, 1355.

108. Chipperfield, J. R.; in N. B. Chapman and J. Shorter (eds.), *Advances in Linear Free Energy Relationships,* Plenum, London, 1972, pp. 321.

109. Hambright, P.; Langley, R., *J. Inorg. Biochem.,* **1988**, *32*, 197.

CHAPTER 6
KINETICS of the LIGAND SUBSTITUTION REACTIONS of NAcCoMP8

6.1 INTRODUCTION

Part of the elegance of metalloproteins is the synergistic relationship that exists between the metal ion, the macrocyclic ligand and the native protein to which they are both attached. The metal ion affords a wide range of available chemical reactions[1,2] whilst the macrocycle asserts a particular steric and/or electronic selectivity;[1] then finally, the protein[3] directs the exchange towards achieving the optimal metabolic function particular to the physiological environment. The intricacies of this type of metalloprotein relationship have fascinated researchers for years, particularly in the case of the extensively explored biological cobalt(III) metalloprotein cofactor, vitamin B_{12} and its derivatives.[1,3,4]

In research on the cobalt corrins, the nature of the relationship that exists between metal ion, macrocycle and protein have been explored in many ways.[4] In this work, for example, the central focus has been to explore how the macrocycle influences the binding properties of the metal ion (*cis* effects). Previously, several corrin chemical equilibria were investigated alongside those of a cobalt(III) porphyrin in order to compare the differences in free energy between the ground states of each macrocycle (Equilibrium Constants, **Chapter 5**). In this Chapter, kinetics data for the replacement of water *trans* to an imidazole-type moiety with probe ligands were obtained as a function of temperature in a simple biologically-derived cobalt(III) porphyrin, *NAcCoMP8*. NAcCoMP8, serves as a biomimetic model for B_{12a} (**Chapter 1**). B_{12a} is a cobalt(III) corrin macrocycle with dimethylbenzimidazole

(DMB) and water in α and β positions, respectively[4,5]. By contrast, NAcCoMP8 is a porphyrin with histidine (His) and water, respectively.[6,7] The axial water can be replaced by a variety of ligands and in B_{12a} these reactions were found to be surprisingly fast for a traditionally inert Co(III) complex; the fast rates are presumably due to the *cis* effect of the delocalized π-electron system of the corrin ring.[15] Thus the similarity of the coordination environment of Co(III) in each macrocycle provides a unique opportunity of evaluating what effect the equatorial macrocycle (porphyrin *vs.* corrin) has on the ligand binding properties of Co(III).

The probe ligands selected were the strong field cyanide anion and the neutral NMI ligand. Cyanide was selected as an anionic probe ligand in the NAcCoMP8 study since there are analogous data for comparison with both B_{12a}-type[8,9] and heme-type[10,11] compounds. Similarly, the neutral probe ligand NMI was selected since there was literature available for comparison.[12] NMI is less sterically hindered than a 2- substituted imidazole such as 2-methyl imidazole. Furthermore, NMI does not exhibit complex kinetics due to tautomerism as in the case of imidazole.[12] Thus available kinetic data for CN^- and NMI were compared in both macrocycles in order to illustrate how changing the macrocycle affects the lability of the Co(III) centre.

The kinetics of ligand reactions were also briefly explored with pyridine as an alternative to the neutral NMI. It was assumed that any steric hindrance afforded by the annular hydrogen atoms (or by π-π stacking of pyridine) would result in the reaction kinetics being slow enough to be captured on a UV-vis spectroscopy timescale. However, in the case of NAcCoMP8, only an estimated rate was obtained.

The aim of the work in this Chapter was therefore to quantitatively assess the *cis* effects of the equatorial ligand on the lability of the Co(III)-OH_2 bond in B_{12a}. This was achieved by comparing the rates of ligand substitution reactions of H_2O bound to Co(III) in NAcCoMP8 to that obtained for vitamin B_{12a}. In this way the differences between ground- and transition states may be observed for each macrocycle. Thus

the kinetics of substitution of axially bound water by probe ligands CN^- and NMI were determined as a function of temperature for NAcCoMP8 under pseudo first-order conditions using UV-vis spectroscopy (pH 7; μ = 0.1 M by $NaNO_3$). The second-order rate constants were determined from plots of the pseudo first-order rate constant against ligand concentration and the values of $\Delta H^{\ddagger}$ and $\Delta S^{\ddagger}$ were found from Eyring plots. These were then compared to similar available or experimental vitamin B_{12a} data (**Investigation 2.2**, **Figure 5.1**).

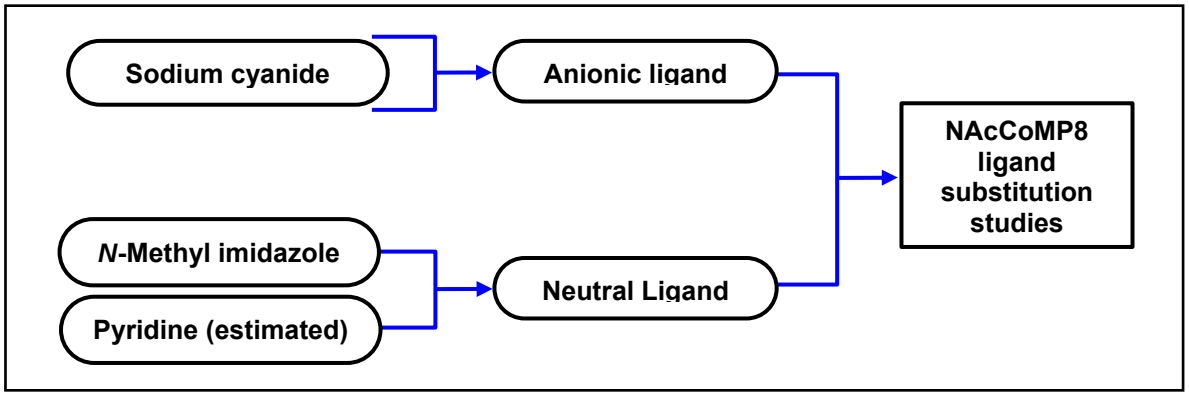


Figure 6.1 A flow diagram of the kinetics results focussed on in Chapter 6. Ligand substitution studies were performed as a function of temperature with anionic and neutral probe ligands, cyanide and NMI, respectively (pyridine kinetics were estimated in NAcCoMP8).

6.2 RESULTS AND DISCUSSION

For a monomeric Co(III) macrocycle (NAcCoMP8 or B_{12a}) in aqueous solution, the kinetics of substitution reactions with probe ligands is described by (**Equation 2.5**):

$$CoH_2O + L \xrightarrow{k_{II}} CoL + H_2O \qquad \textbf{Equation 2.5}$$

where L represents the incoming exogenous probe ligand that replaces the axial water with a second order rate constant k_{II}. The rate was monitored spectrophotometrically at selected wavelengths as described below. For brevity, sources of reagents (**Section 2.4**), technical specifications (**Section 2.4**), specialized (**Sections 2.2.2; 2.2.3**) and general techniques (**Section 2.5**) may found elsewhere (**Chapter 2**).

Freshly prepared and degassed solutions of cyanide were reacted with NAcCoMP8 (*ca*. 1 - 2 μM) under pseudo first order conditions as a function of temperature (*ca*. 15 - 35 ^{o}C). This was achieved by monitoring the decrease in absorbance at 415 nm and the increase in absorbance at 429 nm as a function of [CN^{-}] (pH 7; 0.1 M MOPS; **Figure 6.2A**). The observed pseudo first order rate constant, k_I^{obs}, was obtained by fitting a standard exponential function to the absorbance/time traces obtained for each titration and corrected for the pK_a of NAcCoMP8 (**Equations 2.8-2.10**). Between five and eight different cyanide solutions with an effective [CN^{-}] (after correction for the pK_a of HCN) of typically between 10 and 150 μM were used at each temperature. The second order rate constant, k_{II}, was obtained from the gradient of a plot of corrected k_I against [CN^{-}]. The average value of k_{II} obtained at the two monitoring wavelengths was used in Eyring plots of $\ln(k_{II}h/k_BT)$ against T^{-1} (h and k_B are the Plank and Boltzmann constants, respectively) to obtain the activation parameters $\Delta H^{\ddagger}$ and $\Delta S^{\ddagger}$ from the gradient and intercept, respectively. The corresponding study pertaining to the kinetics of the reaction of CN^{-} with H_2OCbl^{+} is available for comparison.[8]

A similar approach was used for studying the reaction of NAcCoMP8 with NMI. The maximum absorbance changes were found to occur at 413 and 424 nm (at which wavelengths the absorbance decreases and increases, respectively) and these wavelengths were used to monitor the reaction (**Figure 6.2B**). Unfortunately, the very small absorbance changes accompanying the ligand exchange made the data quite noisy. The reactions were studied at between five and eight NMI concentrations between 3 and 35 μM (after correction for the pK_a of NMI) at pH 7 (0.1 M MOPS) with [NAcCoMP8] *ca*. 0.5 μM.

The reaction of H_2OCbl^{+} with NMI was monitored at 351 and 360 nm (**Figure 6.2C**), with [NMI] typically between 0.3 and 3 mM (after correction for the pK_a of NMI), [H_2OCbl^{+}] *ca*. 30 μM, pH 7 (0.1 M MOPS). The observed pseudo first order rate constants were corrected for the pK_a of H_2OCbl^{+}.

In the case of the substitution of axial water with pyridine in NAcCoMP8 (*ca*. 1 μM) the reactions proceed rapidly under pseudo first order conditions. These rapid reactions and the very small absorbance changes made it difficult to acquire reliable data. Furthermore, the very low NAcCoMP8 concentrations together with the absorbance contributions from pyridine made the data quite noisy. In this case, the k_{II} was estimated using similar methods as for cyanide and NMI previously. The reaction was monitored at the point of maximum absorbance change with the lowest noise which was at 414 nm where the absorbance decreases (**Figure 6.2D**). A detailed study of the kinetics of the reaction of pyridine with H_2OCbl^+ is available for comparison.[13]

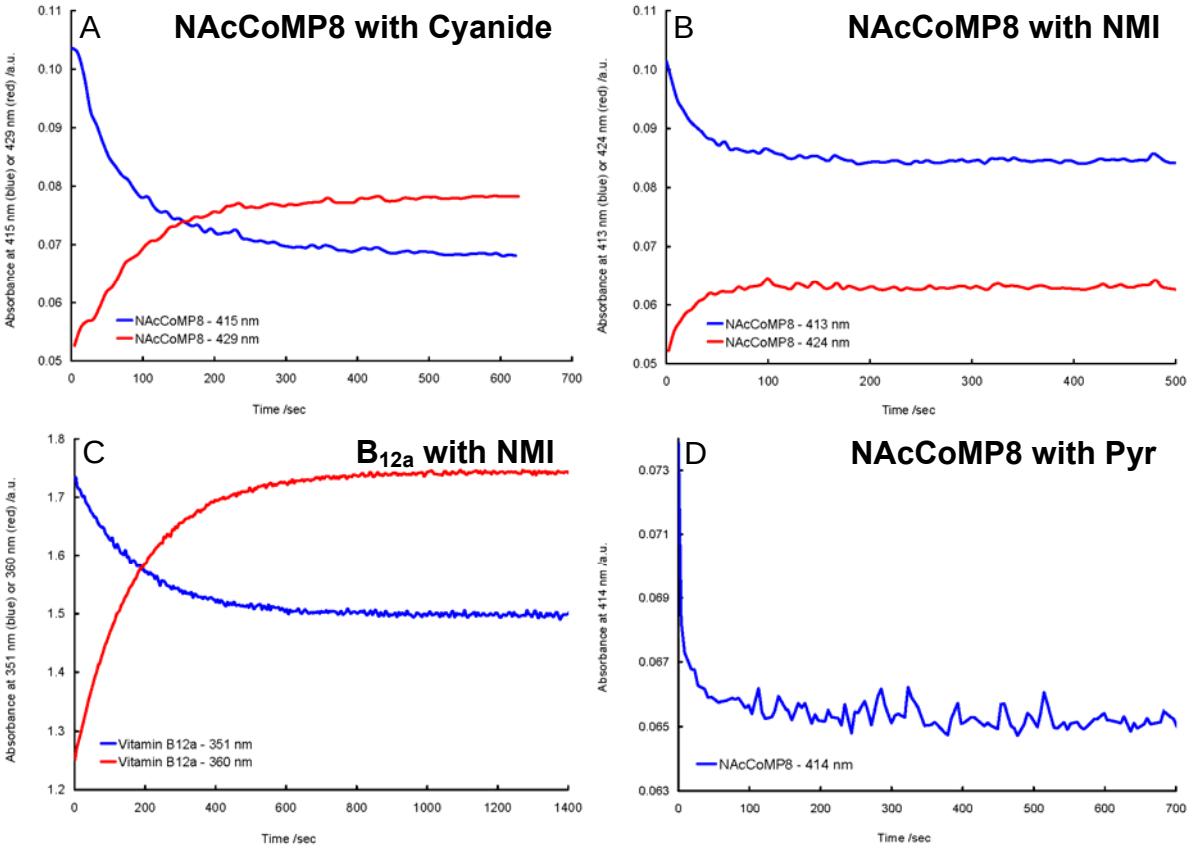


Figure 6.2 Examples of corrected monophasic absorbance/time traces obtained from Cary 300 Bio for the substitution of axially coordinated water with selected probe ligands in NAcCoMP8 (or B_{12a}). Substitutions illustrated here were conducted under pseudo first order conditions at 25 ^{o}C in MOPS (0.1 M) at neutral pH where $NaNO_3$ was used as the background electrolyte (μ_{total} = 0.1 M).

Examples are shown of absorbance traces fitted to the exponential functions described previously (**Equations 2.9** and **2.10**; **Section 2.3.2**) in order to obtain values for k_I^{obs} (**Figure 6.3**).

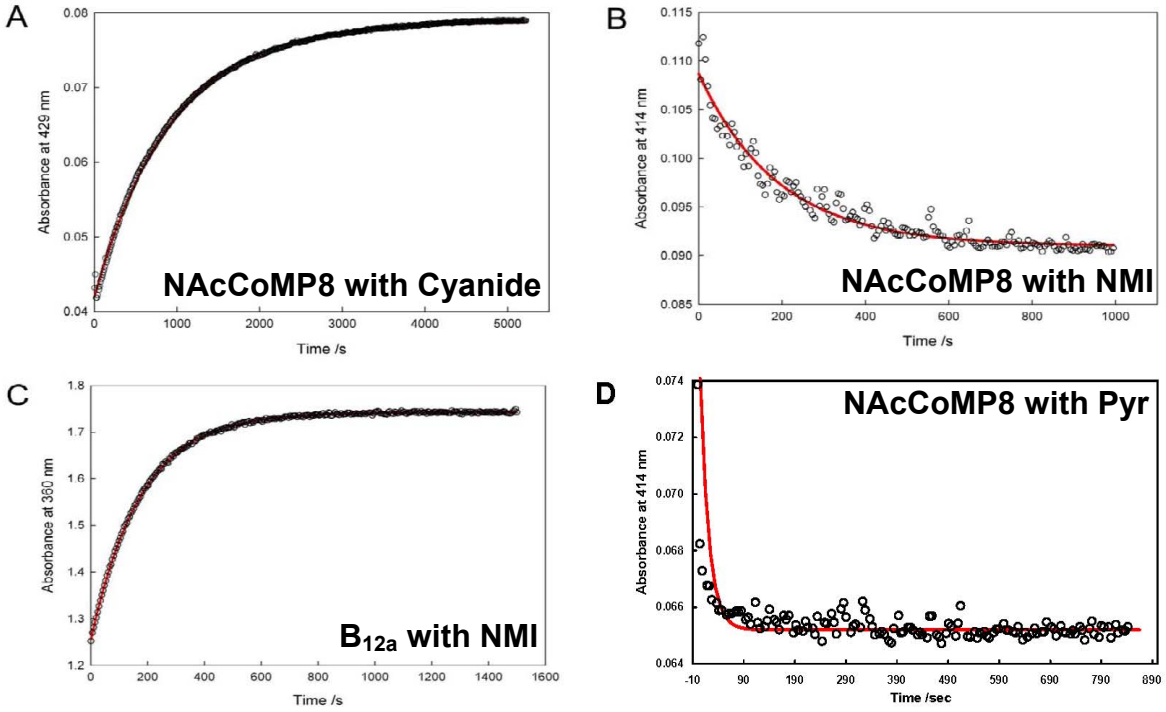


Figure 6.3 The absorbance/time traces were fit to an equation of the form $A = A_0 + A_1 e^{-k_I^{obs} t}$ for the reaction with selected probe ligands at 25 °C. Fits of (A) cyanide with NAcCoMP8, (B) NMI with NAcCoMP8; (C) NMI with H_2OCbl^+ and (D) Pyr with NAcCoMP8. In (A): r^2 = 0.9995, k_I^{obs} = 1.08(3) × 10^{-3} s^{-1}, [CN^-] (corrected of pH) = 11.3 μM, pH 7.00. In (B): r^2 = 0.97, k_I^{obs} = 5.2(2) × 10^{-3} s^{-1}, [NMI] (corrected of pH) = 2.84 μM, pH 6.69. In (C): r^2 = 0.9996, k_I^{obs} = 5.71(2) × 10^{-3} s^{-1}, [NMI] (corrected for pH) = 334 μM, pH 6.88. In (D): r^2 = 0.8348, k_I^{obs} = 0.11(2) × 10^{-3} s^{-1}, [Pyr] (corrected for pH) = 19.93 μM, pH 6.70.

The k_I values were subsequently corrected for pH (**Equation 2.8**; **Section 2.3.2**). These k_I values were then plotted against [L]. Examples of corrected k_I against [L] are shown for CN^- and NMI at 25 °C as examples (**Figure 6.4**). Values for k_{II} were then used to construct weighted linear least squares Eyring plots of $\ln(k_{II}h/k_BT)$ against T^{-1} (h and k_B are the Plank and Boltzmann constants, respectively) in order to find $\Delta H^‡$ and $\Delta S^‡$ from the slope and intercept, respectively (**Figure 6.5**).

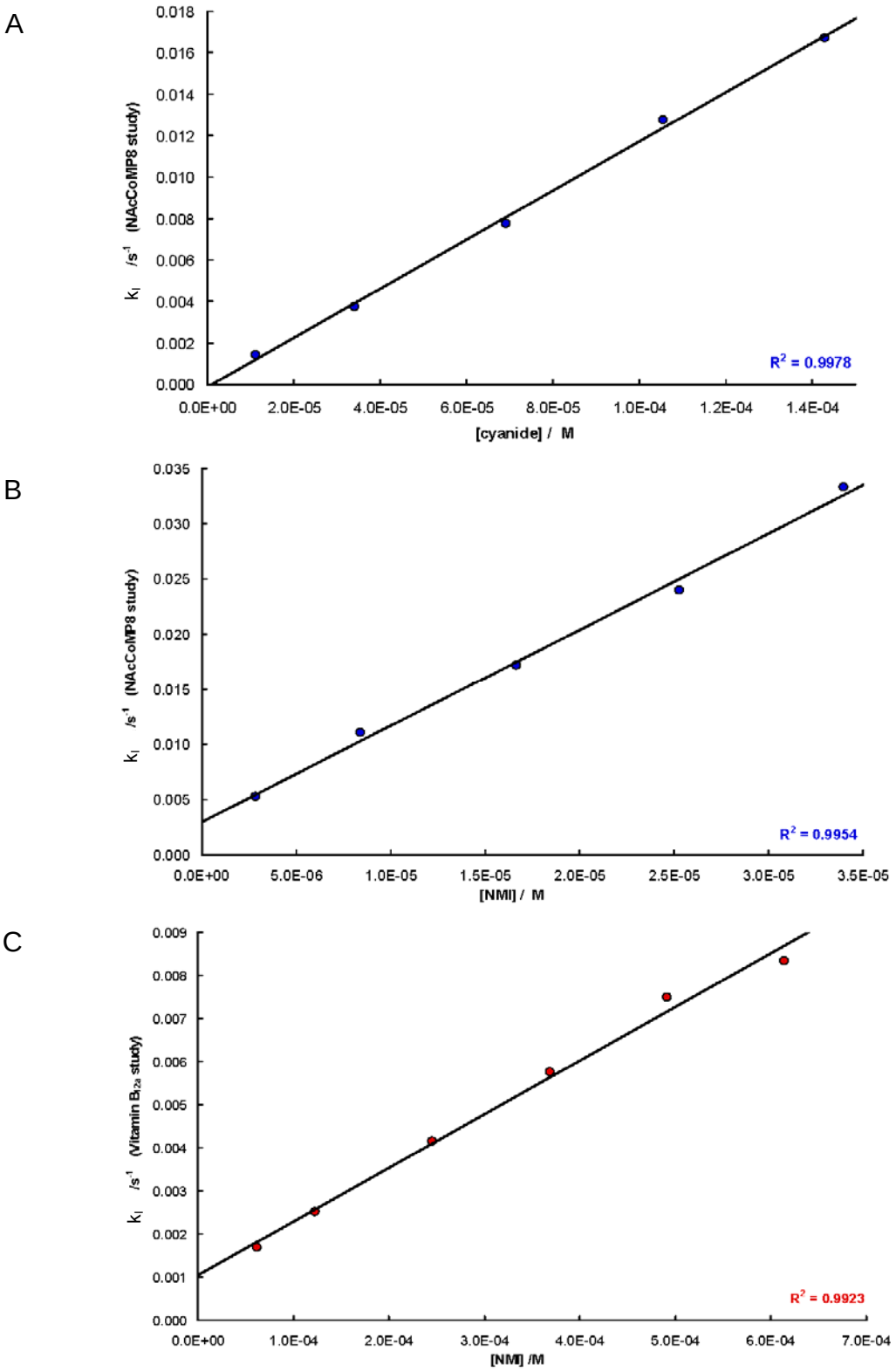
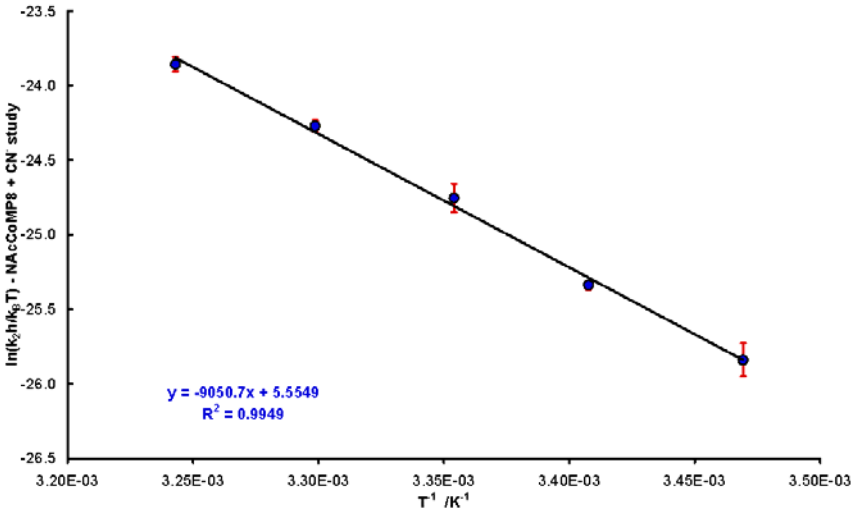
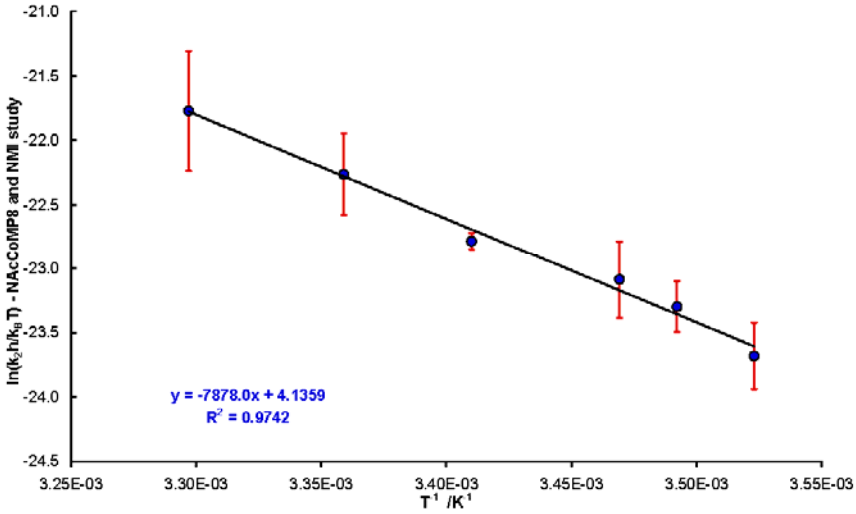


Figure 6.4 Plots of pH-corrected pseudo first order rate constants k_I against [L] plots (25 ^oC; pH 7; MOPS (0.1 M); μ = 0.1 M by $NaNO_3$) where L is the exogenous probe ligand cyanide with NAcCoMP8 (**A**), NMI with NAcCoMP8 (**B**) and NMI with vitamin B_{12a} (**C**).

A



B



C

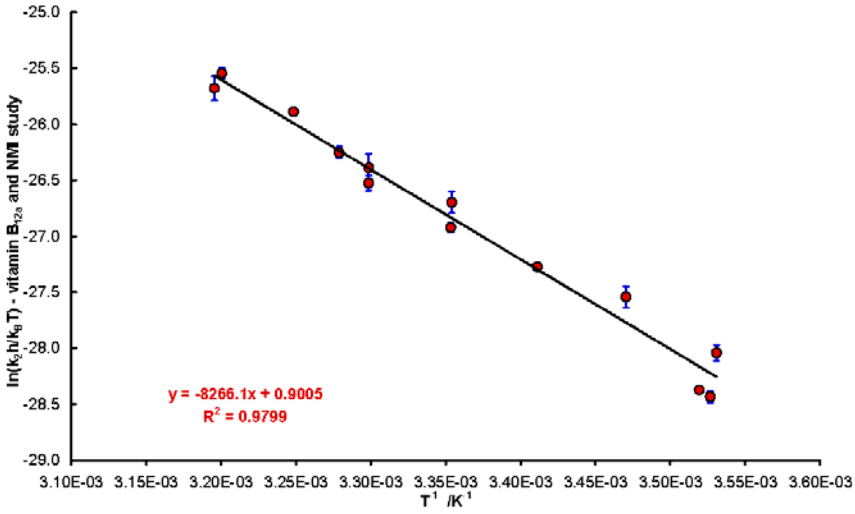


Figure 6.5 Eyring plots of corrected $\ln(k_2h/k_BT)$ against T^{-1} (pH 7; MOPS (0.1 M); μ = 0.1 M by $NaNO_3$) where L is the exogenous probe ligand CN^- with NAcCoMP8 (**A**), NMI with NAcCoMP8 (**B**) and NMI with vitamin B_{12a} (**C**).

Plots of the pH-corrected pseudo first order rate constants, k_l, against ligand concentration are shown as examples (**Figure 6.4**). The plots for the reaction of CN^- with NAcCoMP8 pass very close to the origin, whereas those for the reaction of NMI with both NAcCoMP8 and H_2OCbl^+ do not, i.e., the reverse rate constant, k_r, for dissociation of the ligand from the metal is not negligible. Eyring plots were also obtained for these reactions (**Figure 6.5**). Similarly, the Eyring plots for the reverse rate constant for the reaction of NMI with H_2OCbl^+ and with NAcCoMP8 are shown (**Figure 6.6**). The kinetics data are listed (**Table 6.1**).

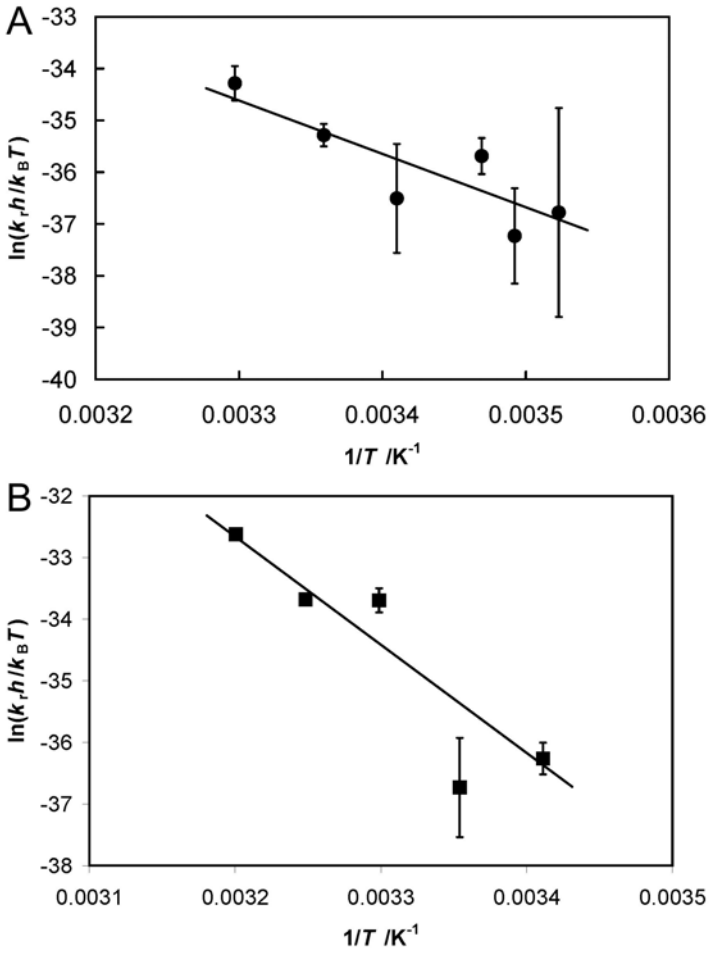


Figure 6.6 Eyring plots for the rate constant for the reverse reaction of NMI with (**A**) NAcCoMP8 and (**B**) with H_2OCbl^+. The reverse rate constants are from the intercepts of plots such as in Figure 6.4B and C. In the case of the reaction of NMI with H_2OCbl^+ the intercepts were not statistically different from zero for reactions at T < 20 ^oC and the data were omitted from the plot in (**B**).

Table 6.1 Rate constants and activation parameters for the reaction of Cyanide, N-Methylimidazole and Pyridine with NAcCoMP8 and Aquacobalamin (B_{12a} or H_2OCbl^+).

Reaction	Temp /°C	k_{II} /M^{-1} s^{-1}	$\Delta H^{\ddagger}$ /kJ mol^{-1}	$\Delta S^{\ddagger}$ /J K^{-1} mol^{-1}	k_{II} (25 °C) /M^{-1} s^{-1}	k_r^* /s^{-1}	$\Delta H^{\ddagger}$ /kJ mol^{-1}	$\Delta S^{\ddagger}$ /J K^{-1} mol^{-1}	k_r (25 °C) /s^{-1}
CN^- + NAcCoMP8[†]		(× 10^2)							
	15.1	0.36(2)	75(3)	46(9)	112				
	20.3	0.61(2)							
	25.0	1.10(4)							
	30.0	1.82(5)							
	35.2	2.8(2)							
CN^- + B_{12a}[8]			51.9(1.3)	-25.3(3.8)	237				
CN^- + HC-B_{12a}[‡]			56.9(0.4)	-33.5(0.2)	11.4(0.6)				
NMI + NAcCoMP8[†]		(× 10^2)				(× 10^{-4})			
	10.7	3.1(9)	66(5)	34(16)	1.0 × 10^3	6(41)	86(25)	-5(99)	3.3 × 10^{-3}
	13.2	4.5(9)				4(6)			
	15.1	5.6(2.0)				19(7)			
	20.1	7.8(5)				8(16)			
	24.5	13.3(5)				29(7)			
	30.5	2.2(1.3)				82(32)			
NMI + B_{12a}[†]						(× 10^{-4})			
	10.4	2.6(1)	73(3)	21(11)	12		146(26)	196(83)	1.2 × 10^{-2}
	11.0	2.82(9)							
	15.0	6.6(7)							
	20.0	8.72(3)				19(3)			
	25.0	16(2)				7(9)			
	30.0	20(2)				147(32)			
	34.7	37(1)				152(7)			
	39.3	52(3)				443(15)			
Pyr + NAcCoMP8[§†]					6.2 x 10^3				
Pyr + B_{12a}[13]			84.5(2.9)	68(10)	34(7)				

*Rate constant for the reverse reaction; [‡]Protein-bound B_{12a} where HC refers to haptocorrin; see Ref.(9);

[§]Estimate data (25 °C). [†]This work.

The rate constants and activation parameters for the substitution of H_2O coordinated to Co(III) *trans* to an imidazole derivative by CN^- and by NMI are reported (**Table 6.1**). In the case of the substitution of the axial water with CN^-, k_{II} for H_2OCbl^+ is more than double that of NAcCoMP8 at 25 ^oC indicating that the former is more labile in this reaction (k_{II} at 25 ^oC = 237; and 112 M^{-1} s^{-1} for $H_2OCbl^+$and NAcCoMP8, respectively). The difference arises from a much smaller $\Delta H^‡$ value for the reaction on H_2OCbl^+ (51.9 kJ mol^{-1}), which is compensated for by a much more negative $\Delta S^‡$ (-25.3 J K^{-1} mol^{-1}). If the latter value were the same in both systems, then k_{II} would be 10^4 larger for the reaction with H_2OCbl^+ than for that with NAcCoMP8. It was previously observed that this compensation effect masks a very significant change in the electronic properties of the equatorial ligand which is then observed in the rate of substitution of the axial ligand.[14] Chemaly *et al*., showed in their study of aquacyanocobester and a cobester in which the conjugation of the corrin is interrupted at the C5 position, that this electronic change is reflected in the very different values of $\Delta H^‡$.[14]

A survey of early B_{12} literature seems to suggest that the ligand substitution reactions of H_2OCbl^+ proceeded through a strictly dissociative (D) mechanism whereby the unimolecular dissociation of water from the metal ion's coordination sphere is rate limiting.[4,13,15,18,29-31] This view is based on the observation that the rate of substitution, regardless of the ligand's identity, often varies by at most two orders of magnitude whilst formation constants vary by over 11 orders.[16-20] There also seems to be a linear free energy relationship between log k and log K for the aquation of a wide range of cobalamin complexes further implying a D mechanism.[13,20,29-31] However, Randall and Alberty demonstrated that the significantly slower rate of substitution of imidazole (27 dm^3 mol^{-1} s^{-1} as compared to (0.1 - 7.1) x 10^3 dm^3 mol^{-1} s^{-1} for other smaller ligands) might suggest that the reaction does not simply proceed through the unimolecular release of water followed by fast binding of the incoming ligand, that is, the reaction may be more complex than a straightforward D mechanism.[17]

Further evidence against a strictly D mechanism were amassed when Stochel and van Eldik demonstrated that at high pyridine concentrations (*ca*. > 0.5 M) the rate constants saturate to a limiting value (k_{sat}).[13] Marques *et al*., subsequently found values for k_{sat} where L = pyridine, 4-methylpyridine, histamine (imidazole-4-ethanamine), imidazole or methyl glycinate; their values were all different which invariably demonstrated that the limiting value is in fact dependent on the identity of the incoming ligand. From this they concluded that the reactions did not proceed through an exclusively D mechanism but their evidence rather supported the presence of a dissociative interchange mechanism (I_d).[21]

The intimate mechanism of the ligand substitution reactions of H_2OCbl^+ may described as an interchange mechanism under dissociative activation, I_d.[8,13,21,22] This type of mechanistic behaviour is likely to be very similar in Co(III) porphyrins as well. [23-25] Thus, the transition state of the rate determining step will feature significant bond breaking between Co(III) and departing H_2O, and some extent of bond formation between the metal and the entering ligand. The $\Delta H^{\ddagger}$ value for the reaction of H_2OCbl^+ with CN^- is less positive than for its reaction with NAcCoMP8, whilst conversely $\Delta S^{\ddagger}$ is more negative. This type of kinetic behaviour is consistent with a transition state that occurs earlier along the reaction coordinate and in which there is greater participation of incoming CN^- in that transition state. This is also consistent with the log K observations for the coordination of anionic CN^- by H_2OCbl^+ which is larger than log K for its coordination by NAcCoMP8 (see **Chapter 5**).

As an aside, it is interesting to note how the rate of substitution of water coordinated to Co(III) by an exogenous ligand in a macrocycle is affected by the presence of the native protein. A comparison of rate constants with free- and protein-bound B_{12a}-type compounds may provide mechanistic insight as to how the protein itself influences the reaction rates at the metal centre (**Table 6.1**). In the case of free-B_{12a} the substitution of CN^- with the axial water is about 22-fold faster than that of the protein-bound B_{12a} derivative (k_{II} = 240 and 11.4 M^{-1} s^{-1} for free and

protein-bound B_{12a}, respectively).[9] Marques *et al*., demonstrated that whilst there is this difference in rates of substitution between the two types of B_{12a}, the mechanism of replacement of water by CN^- is the same and involves the attack of both CN^- and HCN on Co(III). Their kinetic findings supported the view that the metal ion is readily accessible to the solvent despite the presence of the protein; in fact the protein appears to facilitate more ordered transition states suggesting the Co-O bond is strengthened by the protein.[9] These findings are in stark contrast to those seen in hemoproteins where the protein-bound derivatives have a significantly slower rate than the free complex; the slower rate being attributed to steric crowding.[11,26-28]

On the other hand, the substitution of the axial water with NMI is considerably different to the anion (**Table 6.1**). The value for k_{II} for H_2OCbl^+ is significantly smaller than that of NAcCoMP8 at 25 ^oC (k_{II} at 25 ^oC = 12; and 1.0 x 10^3 M^{-1} s^{-1} for $H_2OCbl^+$and NAcCoMP8, respectively). This evidence suggests that it is the Co(III) in the porphyrin that is labile to this substitution than in the corrin. This is again likely due to the smaller $\Delta H^‡$ and a somewhat larger value of $\Delta S^‡$. These findings are seen once again to parallel the log K values. This may suggest that the greater thermodynamic stability of the NMI complex with the cobalt porphyrin compared to its complex with the cobalt corrin causes a greater involvement of the entering ligand in the transition state.

It seemed likely that this trend would persist with the other neutral ligand pyridine, as well. An estimate of k_{II} at 25 ^oC is available for the substitution of pyridine with Co(III) in NAcCoMP8 (**Table 6.1**). Here k_{II} was found to be 6.2 x 10^3 M^{-1} s^{-1}. Stochel and van Eldik's corresponding value for the substitution of NMI in B_{12a} was 34(7) M^{-1} s^{-1} which is considerably lower than the porphyrin thereby demonstrating that Co(III) in the porphyrin is more labile to this substitution than in the corrin.[13] This was similar to the findings with the other neutral ligand, NMI. Further studies would have to be conducted with NAcCoMP8 and pyridines (as well as other neutral ligands) in order to confirm these preliminary observations.

It is also interesting to note that the reverse reaction rate constant, k_r, for the dissociation of the ligand from the metal ion is negligible with the anion but significant with the neutral ligand (**Table 6.1**). The plots of k_l against [CN-] for NAcCoMP8 pass very close to the origin, whereas those for the reaction of NMI with both NAcCoMP8 and H_2OCbl^+ do not. The values for k_r were 3.3 x 10^{-3} and 1.2 x 10^{-2} s^{-1} for the substitution of NMI in NAcCoMP8 and H_2OCbl^+, respectively. Similarly, Stochel and van Eldik noted significant reverse reaction rates for the dissociation of the neutral pyridine ligand from Co(III) in B_{12a}.[13]

6.3 SUMMARY AND CONCLUSIONS

In this work, the central focus has been to explore how the macrocycle influences the binding properties of the metal ion (*cis* effects). In this Chapter particularly, the emphasis has been to evaluate the effect that the macrocycle has on the rate of substitution of coordinated water by an incoming probe ligand. These reactions were found to be surprisingly fast in the B_{12a} corrin containing the classically inert Co(III) ion. Since the biologically-derived Co(III) porphyrin NAcCoMP8 serves as a biomimetic model for B_{12a}, it provided an excellent opportunity to evaluate the effect the equatorial macrocycle (porphyrin *vs.* corrin) has on the ligand binding properties of Co(III).

The kinetics of ligand substitution (k_{II}, $\Delta H^{\ddagger}$ and $\Delta S^{\ddagger}$) of water coordinated to Co(III) by incoming probe ligands (CN^-, NMI and Pyr) were obtained as a function of temperature for NAcCoMP8 and compared to the available B_{12a} data. In the case of the substitution with CN^-, it was found that the anion reacts faster with H_2OCbl^+ than with NAcCoMP8 (k = 237 M^{-1} s^{-1} and 112 M^{-1} s^{-1} at 25 ^oC, respectively) because $\Delta H^{\ddagger}$ is lower (52 vs 75 kJ mol^{-1}) although $\Delta S^{\ddagger}$ is more negative (-25 vs 46 J K^{-1} mol^{-1}). These findings were consistent with an earlier transition state involving nucleophilic participation of the entering ligand in an I_d intimate mechanism.

On the other hand, the neutral NMI ligand reacts faster with NAcCoMP8 than with H_2OCbl^+ (k = 1.0 x 10^3 and 12 M^{-1} s^{-1}, respectively) because $\Delta H^{\ddagger}$ is lower and $\Delta S^{\ddagger}$ is larger (34 vs 21 J K^{-1} mol^{-1}, respectively). This is consistent with better Co–ligand binding in the transition state between the neutral ligand and Co(III) in the porphyrin system than in the corrin system.

It was also noted that there is a significant reverse rate constant contribution for the substitution of the neutral NMI ligand in both macrocycles. This was found to be faster in the porphyrin (3.3 x 10^{-3} s^{-1}) than in the corrin (1.2 x 10^{-2} s^{-1}). The reverse

reaction was not observed with the substitution of cyanide in NAcCoMP8. Whilst the substitution of pyridine in B_{12a} is known to exhibit a pronounced reverse rate constant, there was no such comparison available for NAcCoMP8 as the reaction was considerably fast; in fact only an estimate was obtained for the forward reaction.

The neutral ligand pyridine also exhibited greater lability with NAcCoMP8 than with H_2OCbl^+ ($k_{estimated}$ = 6.2 x 10^3 for NAcCoMP8 and 35 M^{-1} s^{-1} for B_{12a}).[13] Stochel and van Eldik demonstrated that the studies pertaining to the substitution of pyridines were not straightforward since the values for the rate constants saturated to a limiting value. This finding may provide evidence to support a dissociative interchange mechanism.[13] A more extensive investigation of NAcCoMP8 with a range of pyridines as well as other anionic ligands is therefore warranted and would serve to confirm these necessarily preliminary observations and conclusions.

It was further observed that the kinetics of ligand substitution parallels the thermodynamic stability of the product complex because of involvement of the incoming ligand in the transition state of the reaction. The equatorial macrocyclic ligand in Co(III) complexes appears to modify both the thermodynamics and the kinetics of substitution reactions of the axial ligand. Thus *cis* effects, often overlooked, are important in the chemistry of these complexes. It is therefore concluded that there is a correlation between the thermodynamic stability of the Co(III) complexes of corrin and porphyrins and of the rate of substitution of the axially coordinated water to form these complexes. The Co(III) is certainly more labile in these two macrocycles relative to other acyclic Co(III) complexes. However, Co(III) is not necessarily more labile in the corrin than the porphyrin. The lability of the metal ion here is dependent on the identity of the incoming ligand. A more complete investigation with a wider range of anions and neutral ligands will be investigated in the future.

6.4 REFERENCES FOR CHAPTER 6

1. Pratt, J. M., *Pure and Appl. Chem.,* **1993**, *65(7)*, 1513.
2. Jensen, K. P.; Ryde, U., *Chem. Biochem.*, **2003**, *4,* 413.
3. Jensen, K. P.; Ryde, U., *Coord. Chem. Rev.*, **2009**, *253,* 769.
4. Brown, K. L., *Chem. Rev*., **2005**, *105*, 2075 (and references therein).
5 Pratt, J. M.; *Inorganic chemistry of vitamin B_{12}*, Academic Press, London 1972 (and references therein).
6 Munro, O. Q.; Marques, H. M., *Inorg. Chem.*, **1996**, *35*, 3752
7 Sannasy, D., M.Sc. Dissertation, University of the Witwatersrand, Johannesburg, South Africa, **2005**.
8. Reenstra, W. W.; Jencks, W. P., *J. Am. Chem. Soc.,* **1979**, *101*, 5780.
9. Marques, H. M.; Brown, K. L.; Jacobsen, D. W., *J. Biol. Chem.*, **1988**, *263*, 12378.
10. Marques, H. M., Ph.D. Dissertation, University of the Witwatersrand, Johannesburg, South Africa, **1986**.
11. Marques, H. M.; Baldwin, D. A.; Pratt, J. M., *J. Inorg. Biochem.*, **1987**, *29*, 77.
12. Marques, H. M.; Egan, T. J.; Marsh, J. H.; Mellor, J. R.; Munro, O. Q., *Inorg. Chim. Acta.*, **1989**, *166*, 249.
13. Stochel, G.; Eldik, van R., *Inorg. Chem.,* **1990**, *29*, 2075.
14. Chemaly, S. M.; Florczak, M.; Dirr, H.; Marques, H. M., *Inorg. Chem.*¸**2011***, 50*, 8719.
15. Marques, H. M., *J. Chem. Soc. Dalton Trans.*, **1991**, 339.
16. Randall, W. C.; Alberty, R. A., *Biochemistry*, **1966**, *5*, 3189.
17. Randall, W. C.; Alberty, R. A., *Biochemistry*, **1966**, *6*, 1520.

18. Thusius, D., *J. Am. Chem. Soc.,* **1971**, *93*, 2629.

19. Thusius, D., *J. Am. Chem. Soc. Chem. Commun.,* **1968**, 1183.

20. Poon, C. K., *Coord. Chem. Rev.*, **1973**, *10*, 1.

21. Marques, H. M.; Bradley, J. C.; Campbell, L. A., *J. Chem. Soc., Dalton Trans.,* **1992**, 2019.

22. Marques, H. M.; Munro, O. Q., Cumming, B. M.; Nysschen, C. de, *J. Chem. Soc., Dalton Trans.,* **1994**, 297.

23. Pasternack, R. F.; Cobb, M. A., *J. Inorg. Nucl. Chem.,* **1973**, *35*, 4327.

24. Pasternack, R. F.; Cobb, M. A.; Sutin, N., *Inorg. Chem.,* **1975**, *14*, 866.

25. Fleischer, E. B.; Jacobs, S.; Mestichelli, L., *J. Am. Chem. Soc.,* **1967**, *90,* 2527.

26. Awad, E. S.; Badro, R. G., *Biochemistry*, **1967**, *6*, 1785.

27. Goss, D. J.; LaGow, J. B.; Parkurst, L. J., *Comp. Biochem. Physiol.*, **1982**, *71B*, 229.

28. Seybert, D. W.; Mofat, K.; Gibson, Q. H., *J. Biol. Chem.*, **1976**, *251*, 45.

29. Stochel, G.; Eldik, van R.; Kunkley, H.; Vogler, A., *Inorg. Chem.*, **1989**, *28*, 4314.

30. Nome, F.; Fendler, J. H., *J. Chem. Soc., Dalton Trans.*, **1976**, 1212.

31. Baldwin, D. A.; Betterton, E. A.; Pratt, J. M., *S. Afr. J. Chem.*, **1982**, *35*, 173.

CHAPTER 7
CONCLUSIONS AND FUTURE WORK

7.1 INTRODUCTION

The main results and conclusions of this work are summarised in this Chapter. More detailed summaries are provided at the end of the individual Chapters.

Vitamin B_{12a} is a Co(III)-containing cofactor with a corrin equatorial ligand that is essential to many fundamental biological processes.[1-3] The main aim of this work was to determine how the equatorial ligand modifies the electronic properties of the coordinated metal ion. To this end, a metal complex, NAcCoMP8, was synthesised as a biomimetic model for vitamin B_{12a} and its kinetic and thermodynamic properties were investigated and compared with data for B_{12a}.

B_{12a} is a cobalt(III) corrin macrocycle with dimethylbenzimidazole (DMB) and water in α and β positions, respectively.[1] By contrast, NAcCoMP8 is a *porphyrin* with histidine (His) and water, respectively.[4,5] The axial water can be replaced by a variety of ligands and in B_{12a} these reactions were found to be surprisingly fast for a traditionally inert Co(III) complex, certainly faster than Co(III) porphyrins; the fast rates are presumably due to the *cis* effect of the delocalized π-electron system of the corrin ring.[6] Thus the similarity of the coordination environment of Co(III) in each macrocycle provides a unique opportunity of evaluating what effect the equatorial macrocycle (porphyrin *vs.* corrin) has on the ligand binding properties of Co(III).

7.2 STRATEGY USED IN THIS WORK

The strategy employed in this research project was as follows and illustrated accordingly (**Figure 7.1**):

Investigation 1

The qualitative identification and assessment of aggregation effects in NAcCoMP8 was investigated. This study was approached as two separate investigations:

Investigation 1.1

Firstly, the optimisation of the synthesis, isolation and characterisation of NAcCoMP8 was investigated. Preliminary optimisations included the utilisation of cost-effective options such as synthetic trivalent cobalt-substituted porphyrins.

Investigation 1.2

Secondly, the qualitative assessment of NAcCoMP8's behaviour in solution was investigated. Preliminary studies included procedures for the preparation of monomeric NAcCoMP8.

Investigation 2

A quantitative assessment of the *cis* effect of the equatorial ligand on the properties of Co(III) metal ion was undertaken by comparing the ligand binding properties of Co(III) in NAcCoMP8 and in vitamin B_{12a}. This study was approached as two separate investigations in which the axial H_2O ligand was substituted by a variety of exogenous ligands:

Investigation 2.1

The temperature-dependence of the thermodynamics of ligand substitution reactions.

Investigation 2.2

The temperature-dependence of the kinetics of ligand substitution reactions.

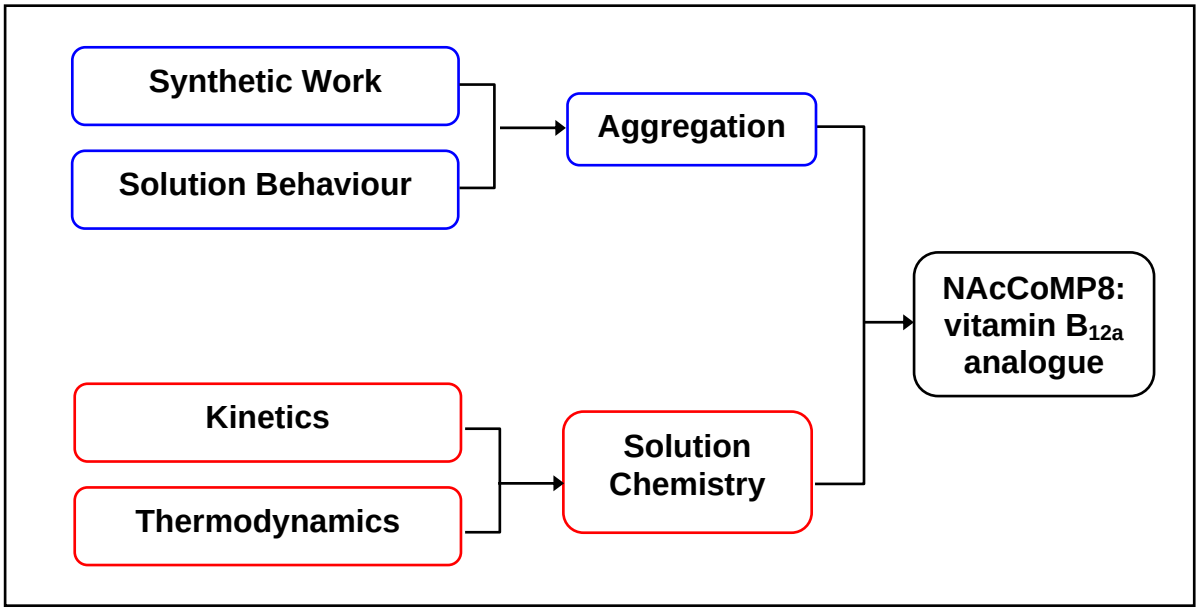


Figure 7.1 Flow diagram of the strategy undertaken in this work. The blue pathway reflects methods pertaining to the monomerisation of NAcCoMP8 whilst the red pathway reflects the study of the solution chemistry of NAcCoMP8.

7.3 MONOMERISATION OF NAcCoMP8: Synthesis Aspects

The synthesis methods were optimised in order to diminish aggregation and to improve yields. These optimisations included ways to limit metal–side-chain aggregation as well as aggregation as a result of π-π stacking.

The following were noted:

(i) Acetylation of the N-terminus of the Cys-14 amino group was necessary in order to limit the metal–side-chain aggregation observed in CoMP8 thereby forming NAcCoMP8;

(ii) The optimal synthetic route was found to be Cytochrome *c* → FeMP11 → NAcFeMP11 → NAcMP11 → NAcCoMP11 → NAcCoMP8; the improved yield was 77% (by mass);

(iii) Three cobalt microperoxidases were identified as an artefact of the

isolation process: CoMP11, CoMP8, CoMP6; these were also acetylated;

(iv) The improved synthesis avoided the use of extreme pH, high concentrations and temperature where possible; the use of SepPak® C-18 cartridges instead of the Amicon® pressure cell was integral to this process;

Future Work

It is recommended that NAcCoMP11 be screened as a possible biomimetic model for B_{12a} since the process will require fewer synthetic steps and is present in larger quantities.

7.4 MONOMERISATION OF NAcCoMP8: Solution Behaviour

NAcCoMP8 in solution is extremely sensitive to aggregation and degradation. Reproducible solution chemistry data relies upon NAcCoMP8 being stable and monomeric in solution. Therefore one of the strategies employed in this work was to qualitatively investigate the conditions under which a spectroscopically stable and monomeric NAcCoMP8 solution may be prepared.

Factors contributing to aggregation were qualitatively assessed and the following were noted:

(i) Three NAcCoMP8 species were identified: the putative monomer with a Soret at 415 nm; the transient and reversible 417 nm intermediate which is likely a π-π dimer; and the irreversible 424 nm species that is possibly

a coordinated tetramer. The 424 nm species eventually precipitates as dark pink thread-like aggregates. Possible modes of formation were proposed.

(ii) The 415 nm species, when titrated with CN^- as a test ligand, gave reproducible spectra and solution chemistry data and was subsequently used for further experiments;

(iii) Aggregation is dependent on: the length of time NAcCoMP8 remains in solution, the concentration of NAcCoMP8, the ionic strength, pH and temperature of the solution;

(iv) At high NAcCoMP8 concentration, the appearance of 424 nm and disappearance of the 417 nm species follows first order kinetics at a rate of k_1 = 0.096 ± 0.002 and 0.087 ± 0.002 min^{-1}, respectively, and a half life of between 7.2 and 8.0 min;

(v) At low NAcCoMP8 concentrations, appearance of 415 nm and the disappearance of 417 nm species is complex and the estimated rates were therefore averaged: k_{1ave} = 0.030 ± 0.010 and 0.080 ± 0.03 min^{-1}, respectively, with apparent half life values between 8.7 and 23.1 min;

(vi) Monomeric NAcCoMP8 is strongly influenced by ionic strength. The dimer formation at low concentration (415 → 417 nm) is driven by the binding of 3 cations (n = 3.4 ± 0.3) and the putative tetrameric species (417 → 424 nm), is driven by the binding of approximately 4 further cations (j = 3.7 ± 0.1);

(vii) NAcCoMP8 is monomeric at low concentrations (1-5 μM) with Soret at 415 nm ($\varepsilon = 1.61(3) \times 10^5$ M^{-1} cm^{-1});

(viii) The monomeric 415 nm species is favoured at low temperature (10 ^oC) and increasing the temperature above 45 ^oC produces the 425 nm species.

(ix) NAcCoMP8 has five spectroscopically observable pK_as at 1.74 ± 0.04 (which may consist of more than one closely overlapping pK_a) is attributed to protonation and displacement of His-18 either by H_2O or a carboxylate from the peptide; at 4.08 ± 0.02 and 5.80 ± 0.05 due to

ionisation of the heme carboxylate groups; at 7.81 ± 0.03 is due to ionisation of coordinated H_2O and at 12.00 ± 0.03 due to ionisation of His-18 to form an imidazolate. The pK_a for the ionisation of coordinated H_2O does not change significantly with temperature between 10 and 40 ^oC, and has an average value of 7.5 $\pm$ 0.2 in this temperature range.

Factors contributing to degradation were qualitatively assessed and the following were noted:

(i) NAcCoMP8 degrades (possibly to bilins) on exposure to light with apparent half life for the overall process being $t_{1/2apparent}$ = 478 min for k_1 = 0.0015 ± 0.0002 min^{-1};

(ii) NAcCoMP8 degrades (possibly to bilins) on exposure to oxygen with apparent half life for the overall process being $t_{1/2apparent}$ = 7.81 min for k_1 = 0.089 ± 0.009.;

(iii) The detergents were found to cause spectroscopic interference and SDS 5% was shown to coordinate with NAcCoMP8;

(iv) HEPES buffer was shown to coordinate with NAcCoMP8 (415 → 413 nm);

(x) On the addition of $NaBH_4$, NAcCoMP8 exhibited spectral changes that were consistent with the metal being reduced[10,11] (Co(III)→ Co(II)→ Co(I)); on exposure to air, the spectrum started to revert back to the original.

A stable monomeric solution of NAcCoMP8 may therefore be prepared at neutral pH, low ionic strength (<0.1 M), low concentration (1-5 μM) ideally using degassed MOPS buffer (0.1 M). The distinctly pink monomeric solution should be freshly prepared and allowed to reach equilibrium for an hour. Samples should be clarified and routinely stored at 4 ^oC in a dark container.

Future Work

A wider range of detergents need to be tested in order to find a more efficient way to monomerise NAcCoMP8.

The 415 nm system appears to be complex; gathering more information about the other two species will therefore help to detect or eliminate any unusual behaviour that may occur whilst working with the monomer. In this light, it would be interesting to determine the temperature dependent pK_a values for the 417 nm and 424 nm species even if only for comparison with the 415 nm species.

Similarly, the exposure to light and oxygen tests were attempted on relatively low NAcCoMP8 concentrations. It would be interesting to see what decay rates are observed at higher NAcCoMP8 concentrations.

7.5 EQUILIBRIUM CONSTANTS FOR NAcCoMP8 (Thermodynamics)

Equilibrium constants for the replacement of water axially coordinated to Co(III) by selected incoming ligands were obtained as a function of temperature in NAcCoMP8 and B_{12a} (*ca*. 15 – 40 ^{o}C; pH 7; u_{total} = 0.1 M by $NaNO_3$). The anionic ligands selected for this study were CN^-, HSO_3^-, NO_2^- and N_3^-; the neutral ligands were NMI, HA, MOA and Pyr. By comparing these chemical equilibria, the difference in free energy between the ground states of Co(III) in these two macrocycles were observed.

The equilibrium constants for the binding of the selected ligands to Co(III) showed that:

(i) the anionic ligands bind more strongly to Co(III) in the *corrin* (log K at 25 ^{o}C for CN^{-}, HSO_3^{-}, NO_2^{-}; N_3^{-}= >12;[7] 6.5(3); 5.9(1); 5.02(5), respectively) than in the porphyrin (similarly, 6.04(5); 3.7(1); 3.00(4); 2.28(6)); the converse is true for the neutral ligands;

(ii) the neutral ligands bind more strongly to Co(III) in the *porphyrin* (log K at 25 ^{o}C for NMI, HA, MOA, Pyr = 4.43(7); 4.72(4); 5.78(7); 1.01(3), respectively) than in the corrin (similarly, 5.76(8); 5.5(2); 3.81(9); 4.93(5));

(iii) the binding of anionic ligands in both macrocycles parallel each other whilst the binding of neutral ligands exhibit an inverse relationship;

(iv) there appeared to be a strong 'compensation effect'[9] between ΔH and ΔS;

(v) for the binding of anionic ligands, ΔH and ΔS vary in the same way for both macrocycles; this is not the case for the neutral ligands;

(vi) The porphyrin appears to preferentially bind ligands that have either less electron density for distribution or that on binding exhibit a tendency to distribute electron density away from the metal ion; the opposite is true for the corrin.

Future Thermodynamic Work

Extensive studies with a wider array of both neutral and anionic ligands will have to be undertaken in order to support these findings. In the case of the anionic ligands, it is recommended that a comparative study be conducted specifically on the binding of various dianionic ligands in order to observe what each macrocycle does with the additional charge. In the case of the neutral ligands, it is recommended that in NAcCoMP8, binding studies be conducted with various substituted pyridines in order to assess the validity of the idea that Co(III) in the porphyrin exhibits a preference for ligands with less *accessible* electron density .

7.6 RATE CONSTANTS FOR NAcCoMP8 (Kinetics)

Kinetics data for the replacement of water *trans* to an imidazole-type moiety with CN^-, NMI and Pyr were obtained under pseudo first order conditions as a function of temperature (*ca*. 10 – 40 ^oC) in NAcCoMP8 (pH 7; MOPS (0.1 M)). These were then compared to analogous B_{12a} data. In this way the differences between ground- and transition states were observed for each macrocycle.

The kinetics of the reaction of NAcCoMP8 with the anionic CN^- showed that:

(i) CN^- ($k = 112\ M^{-1}\ s^{-1}$) acts as a nucleophile towards Co(III);
(ii) The activation parameters are large and positive such that $\Delta H^{\ddagger} > \Delta S^{\ddagger}$ ($\Delta H^{\ddagger} = 75(3)$ kJ mol^{-1} and $\Delta S^{\ddagger} = 46(9)$ J K^{-1} mol^{-1});
(iii) No significant reverse rate constant (k_r) detected.

Comparison of these results with analogous B_{12a} data from literature[7] showed that:

(i) Co(III) is more labile in the *corrin* ($k = 237\ M^{-1}\ s^{-1}$) than in the porphyrin ($k = 112\ M^{-1}\ s^{-1}$);
(ii) The significant electronic properties of the equatorial ligand that possibly contributing to this lability may be masked by a 'compensation effect';[9] in B_{12a} $\Delta S^{\ddagger}$ (-25.3(3.8) J K^{-1} mol^{-1}) is much more negative than $\Delta H^{\ddagger}$ (51.9(1.3) kJ mol^{-1});
(iii) The binding in B_{12a} exhibits kinetic behaviour consistent with an I_d mechanism ($\Delta H^{\ddagger}$ for B_{12a} is more negative than in NAcCoMP8 whilst conversely, $\Delta S^{\ddagger}$ is more negative; this suggests that in B_{12a} the incoming ligand is closely associated with an early transition state);

Similarly, the kinetics of the reaction of NAcCoMP8 with the neutral NMI showed that:

(i) NMI ($k = 1 \times 10^3\ M^{-1}\ s^{-1}$) acts as a nucleophile towards Co(III);

(ii) The activation parameters are also large and positive such that $\Delta H^{\ddagger} > \Delta S^{\ddagger}$ ($\Delta H^{\ddagger} = 66(5)$ kJ mol^{-1} and $\Delta S^{\ddagger} = 34(16)$ J K^{-1} mol^{-1});

(iii) There is however, a significant reverse rate constant ($k_r = 3.3 \times 10^{-3}\ M^{-1}\ s^{-1}$).

Comparison of these results with analogous data obtained for B_{12a} showed that:

(i) With the neutral NMI ligand, the Co(III) appears to be more labile in the *porphyrin* ($k = 1 \times 10^3\ M^{-1}\ s^{-1}$) rather than in the corrin ($k = 12\ M^{-1}\ s^{-1}$);

(iv) Unlike the anion, $\Delta S^{\ddagger}$ is positive; $\Delta H^{\ddagger} > \Delta S^{\ddagger}$ ($\Delta H^{\ddagger} = 73(3)$ kJ mol^{-1} and $\Delta S^{\ddagger} = 21(11)$ J K^{-1} mol^{-1});

(ii) There is a significant reverse rate constant ($k_r = 1.2 \times 10^{-2}\ M^{-1}\ s^{-1}$).

However, in the case of the neutral ligand pyridine, only an estimated rate constant was obtained for the substitution of water in NAcCoMP8 ($k = 6.2 \times 10^3\ M^{-1}\ s^{-1}$); this substitution was considerably faster than in B_{12a} ($k = 34(7)\ M^{-1}\ s^{-1}$).[8] In the case of B_{12a}, a reverse rate constant (k_r) was observed and the value saturates to a limiting value (k_{sat}).[8]

In general, these preliminary findings suggest that Co(III) in the corrin is more labile to substitution reactions involving anionic ligands; conversely Co(III) in the porphyrin exhibits greater lability towards the substitution of neutral ligands. These findings parallel those observed in the log K studies.

Future Kinetic Work

These are preliminary findings based on three probe ligands. Extensive studies with a wider array of both neutral and anionic ligands will have to be undertaken in order to confirm these results. It is recommended that a study be specifically

conducted on the binding of various pyridines to Co(III) in NAcCoMP8 in order to probe the validity of an I_d mechanism in this system.

7.7 FINAL CONCLUSION AND COMMENT

This work has illustrated how profoundly the identity of the equatorial ligand, in this case either porphyrin or corrin, has modified the electronic properties of the Co (III) ion thereby influencing both its kinetic and thermodynamic ligand binding properties.

7.8 REFERENCES FOR CHAPTER 7

1. Pratt, J. M.; *Inorganic chemistry of vitamin B_{12}*, Academic Press, London 1972 (and references therein).
2. Brown, K. L., *Chem. Rev*., **2005**, *105*, 2075 (and references therein).
3. Pratt, J. M., *Pure and Appl. Chem.,* **1993**, *65(7)*, 1513.
4. Sannasy, D., M.Sc. Dissertation, University of the Witwatersrand, Johannesburg, South Africa, **2005**.
5. Marques, H. M., Ph.D. Dissertation, University of the Witwatersrand, Johannesburg, South Africa, **1986**.
6. Marques, H. M., *J. Chem. Soc. Dalton Trans.*, **1991**, 339.
7. Reenstra, W. W.; Jencks, W. P., *J. Am. Chem. Soc.,* **1979**, *101*, 5780.
8. Stochel, G.; Eldik, van R., *Inorg. Chem.,* **1990**, *29*, 2075.
9. Chemaly, S. M.; Florczak, M.; Dirr, H.; Marques, H. M., *Inorg. Chem.*¸**2011***, 50*, 8719.
10. Mosseri, S.; Neta, P.; Harriman, A.; Hambright, P., *J. Inorg. Biochem.,* **1990**, *39*, 93.
11. Pasternack, R. F.; Cobb, M. A.; Sutin, N., *Inorg. Chem.*, **1975**, *14*, 866.

APPENDIX FOR CHAPTER 2

MATERIALS AND METHODS

APPENDICES FOR CHAPTER 2

APPENDIX 2.1 *Alternative synthetic routes for NAcCoMP8*

Alternative synthetic routes were investigated in order to optimise the synthetic procedure against aggregation. Route A was investigated by Sannasy[1]; Route C was described in the text. Route B and D will be described here. All materials, chemicals and specialized procedures referred to may be found in Chapter 2.

	A	B	C	D
1	Cytochrome *c*	Cytochrome *c*	Cytochrome *c*	Cytochrome *c*
2	FeMP11	FeMP11	FeMP11	FeMP11
3	FeMP8	FeMP8	NAcFeMP11	MP11
4	MP8	NAcFeMP8	NAcMP11	CoMP11
5	CoMP8	NAcMP8	NAcCoMP11	NAcCoMP11
6	NAcCoMP8	NAcCoMP8	NAcCoMP8	NAcCoMP8

Figure AII-1 A diagrammatic representation of the four synthetic routes to attain monomeric NAcCoMP8 explored in this work. Red cells indicate the metal-free porphyrin step. Blue cells indicate primary acetylation step. Route A was used by Sannasy[3]. Routes B, C and D were alternatives explored in this work.

Route B

This route describes the synthesis of NAcCoMP8 through the acetylation and demetalation of NAcFeMP8. The first step (B1–B2) characterized by the isolation of FeMP11 from cytochrome *c* was achieved as described in the text (C1–C2). The subsequent step being the isolation of FeMP8 from FeMP11 (B2–B3) was achieved as described by Sannasy[1] (A2–A3). This route thus follows on from the acetylation of FeMP8 (B3–B4), demetalation of NAcFeMP8 (B4-B5) and remetalation of NAcMP8 to yield NAcCoMP8 (B5-B6).

Synthesis of NAcFeMP8 by the acetylation of FeMP8

The acetylation procedure was adapted from work done by Munro and Marques[2] and from work done by Sannasy[1] in NAcCoMP8. The isolation steps were adapted and modified from work of Carraway *et al*.[3].

The FeMP8 utilised in this step was previously purified using gel permeation chromatography to remove FeMP11, FeMP9 and trace FeMP6 impurities. Only samples showing >98% purity by HPLC were utilized.

FeMP8 (10 mg) was dissolved in 5 mL saturated sodium acetate solution in a thermostatted cell at 5 ^{o}C. A 300 molar excess of acetic anhydride previously cooled to *ca*. 10 ^{o}C was used to acetylate FeMP8; this was added in 5 aliquots at 5-minute intervals. It was found that cooling the acetic anhydride allowed for a more stable reaction. The reaction mixture was stirred at 5 ^{o}C for 15 minutes and *ca*. 60 minutes at 30 ^{o}C. Once the reaction was complete (monitored by HPLC and TLC[4]) the sample was lyophilized. The lyophilized NAcFeMP8 was redissolved in sodium carbonate buffer (2 mL; 0.2M; pH 9.5) and the scarlet compound was desalted on a Sep-Pak® cartridge. Neutral NAcFeMP8 was clarified using a Millex® syringe-filter before being lyophilized. The red-brown product was routinely stored at -20 ^{o}C under argon. NAcFeMP8 was identified by mass spectroscopy. Concentration was determined spectroscopicaly using[2] ε_{397}= 1.55 x 10^{5} M^{-1} cm^{-1}.

Synthesis of NAcMP8 by reductive demetalation of NAcFeMP8

The demetalation procedure was achieved as described in the text (C3–C4) with modifications in the isolation/purification step as follows:

Once the clear bright cerise solution was obtained, signalling the metal-free NAcMP8, the sample was immediately diluted (*ca*. 10 mL) using degassed methanol (30 %). The sample was then frozen with liquid nitrogen and lyophilization in the dark. Once lyophilized to dryness, metal-free NAcMP8 was redissolved in minimum volume deionised water (*ca*. 1 mL) and immediately loaded onto a Sep-Pak® cartridge for desalting and removal of any residual acids. The neutral light pink-red NAcMP8 was then clarified using a syringe-filter before being frozen with liquid nitrogen and re-lyophilized in the dark. The light pink-red spongy solid was stored briefly at -20 ^{o}C under argon before the remetalation step.

Synthesis of NAcCoMP8 by the oxidative remetallation of NAcMP8

The remetalation procedure was achieved as described in the text (C4–C5) with modifications in the isolation/purification step as follows:

After the refluxing process the sample could be exposed to white light. NAcCoMP8 was allowed to reach room temperature whilst stirring. The sample was then diluted (*ca*. 50 mL) with deionised water. This sample was gradually loaded onto a Sep-Pak® cartridge (*ca*. 5mL at a time) to ensure minimal aggregation by lowering total salt concentration. Once desalted, the neutral dark-pink band was eluted with 30% acetonitrile, clarified using a Millex® syringe-filter and then lyophilized. The pink spongy NAcCoMP8 was routinely stored under argon at -20 ^{o}C and protected from unnecessary light. Concentration was determined spectroscopically using[1] ε_{415} = 1.61 x 10^5 M^{-1} cm^{-1}

Route D

This route describes the synthesis of NAcCoMP8 through the demetalation of FeMP11 and the subsequent cobalt-insertion of MP11. The first step (D1–D2) characterized by the isolation of FeMP11 from cytochrome *c* was achieved as described in the text (C1–C2). The subsequent step (D2-D3) removes Fe(III) from FeMP11 to yield metal-free MP11. This is then remetalated with Co(III) to yield CoMP11 (D3-D4) followed by the acetylation of CoMP11 to yield NAcCoMP11 (D4-D5). Finally, NAcCoMP8 is obtained by the trypic digestion of NAcCoMP8 (D5-D6) which mirrors that described previously in the text (C5-C6). These steps are analogous to those proposed by Sannasy[1], using FeMP11 instead of FeMP8. Thus the steps described follow on from demetalation (D2-D3), remetalation (D3-D4) and acetylation (D4-D5).

Synthesis of MP11 by reductive demetalation of FeMP11

The demetalation procedure was achieved as described in the text (C3–C4) with modifications in the isolation/purification step as follows:

Once the clear bright purple-red solution was obtained, signalling the metal-free MP11, the sample was immediately diluted (*ca*. 50 mL) using degassed methanol (30 %). The sample was transferred under argon into a 250 mL flask and frozen along the walls with liquid nitrogen, then lyophilization in the dark. Once lyophilized to dryness, metal-free MP11 was redissolved in minimum volume deionised water (*ca*. 2 mL) and immediately loaded onto a Sep-Pak® cartridge for desalting and removal of any residual acids. The neutral light purple-red MP11 was then clarified using a syringe-filter before being frozen with liquid nitrogen and re-lyophilized in the dark. The light purple-red spongy solid was stored briefly at -20 ^{o}C under argon before the remetalation step.

Synthesis of CoMP11 by the oxidative remetallation of MP11

The remetalation procedure was achieved as described in the text (C4–C5) with modifications in the isolation/purification step as follows:

After refluxing the sample could be exposed to white light. CoMP11 was rapidly cooled in an ice bath since gradual cooling to 25 ^{o}C caused aggregation. The sample was then diluted (*ca*. 50 mL) with deionised water, sealed under argon and temporarily stored at 4 ^{o}C whilst desalting occurred in small aliquots.

Cold CoMP11 was gradually loaded onto a Sep-Pak® cartridge (*ca*. 5mL at a time) to ensure minimal aggregation and washed with copious amounts of cold deionised water. Once desalted, the neutral dark-pink band was eluted with cold 30% acetonitrile, clarified using a Millex® syringe-filter and then lyophilized. The pink spongy CoMP11 was routinely stored under argon at -20 ^{o}C and protected from unnecessary light.

Synthesis of NAcCoMP11 by the acetylation of CoMP11

The acetylation procedure was adapted from work done by Munro and Marques[2] and from work done by Sannasy[1] in NAcCoMP8. The isolation steps were adapted and modified from work of Carraway *et al*.[3].

CoMP11 (10 mg) was dissolved in 5 mL saturated sodium acetate solution in a thermostatted cell at 5 ^{o}C. A 300 molar excess of acetic anhydride previously cooled to *ca*. 10 ^{o}C was used to acetylate CoMP11; this was added in 5 aliquots at 5-minute intervals. It was found that cooling the acetic anhydride allowed for a more stable reaction. The reaction mixture was stirred at 5 ^{o}C for 15 minutes and *ca*. 60 minutes at 30 ^{o}C. Once the reaction was complete (monitored by HPLC and TLC[4]) the sample was lyophilized. The lyophilized NAcCoMP11 was redissolved in sodium carbonate buffer (2 mL; 0.2M; pH 9.5) and the scarlet compound was desalted on a Sep-Pak® cartridge. Neutral NAcCoMP11 was clarified using a Millex® syringe-filter before being lyophilized. The red-brown product was routinely stored at -20 ^{o}C under argon.

APPENDIX 2.2 *Miscellaneous Synthesis Information*

Observations

Iron microperoxidases displayed a myriad of colours during synthesis (**Figure 2II-2**). These colours are typically pH-dependant and may be observed through the various synthetic steps.

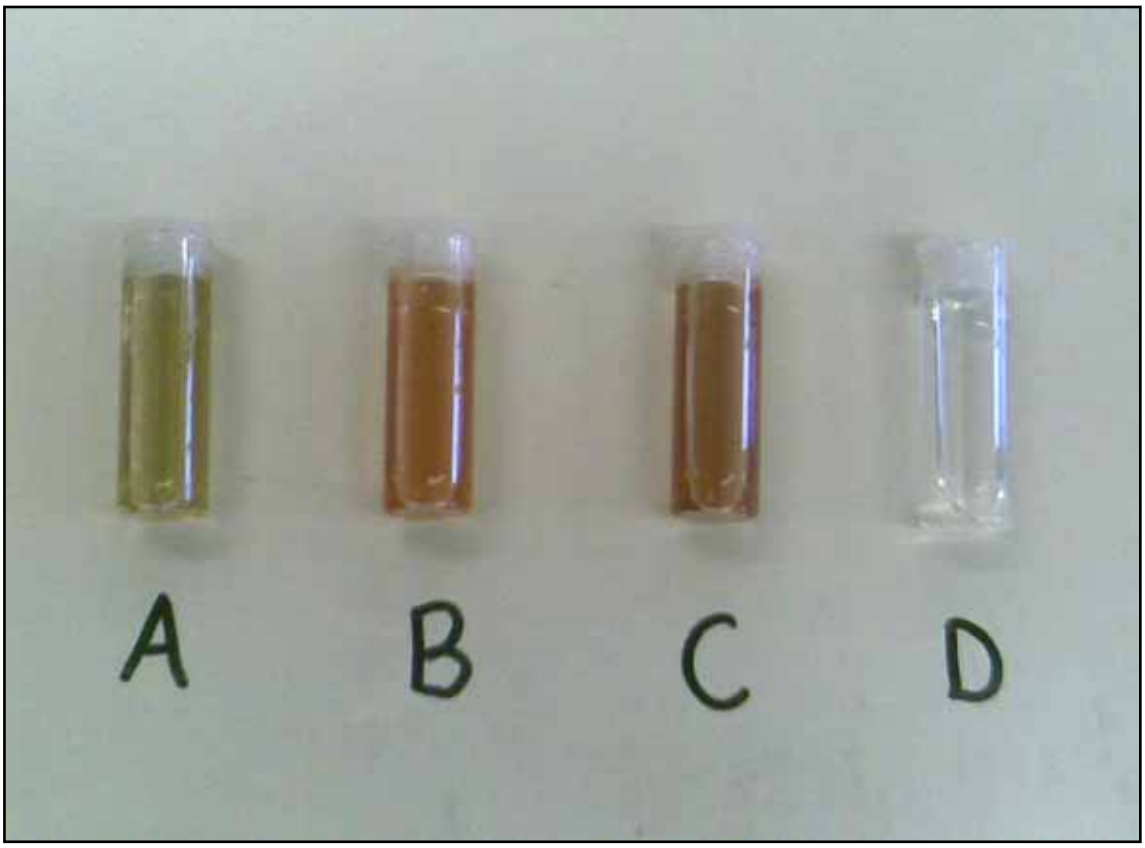


Figure AII-2 FeMP8 in deionised water at (**A**) pH 2 – 3, (**B**) pH 6 – 7, (**C**) pH 8-9. The colours were contrasted with (**D**) deionised water.

TLC R_f values

These samples were run on one system. A 10 x 5 cm silica gel plate was spotted with a concentrated sample of each compound and developed on a CH_3OH: $CHCl_3$:NH_4OH (3:5:1). The R_f values were averaged over 3 plates.

Table AII-1 Typical TLC Rf values observed in this work.

Compound	R_f
Cytochrome *c*	0.00
MP11	0.17
MP8	0.22
FeMP11	0.25
FeMP8	0.28
NAcFeMP11	0.44
NAcFeMP8	0.49
CoMP11	0.78
CoMP8	0.83
NAcCoMP11	Solvent front
NAcCoMP8	Solvent front

HPLC R_t values

Typical retention times expected relative to cytochrome *c*. These were separate experiments run over different days according to the protocol in the text.

Table AII-2 Typical HPLC retention times observed in this work

Experiment	Compound	R_t / min (averaged over 3 runs)
1	Cytochrome *c*	12.50
	FeMP11	8.20
	FeMP8	13.50
2	Cytochrome *c*	12.22
	NAcFeMP8	13.12
	FeMP8	13.44
3	Cytochrome *c*	12.59
	FeMP11	8.12
	MP11	9.22
4	Cytochrome *c*	12.32
	FeMP8	13.05
	MP8	14.17
5	Cytochrome *c*	12.55
	NAcCoMP11	8.99
	CoMP11	9.08
6	Cytochrome *c*	12.55
	NAcCoMP8	13.55
	CoMP8	14.01

Sephadex bands

Gel permeation or size exclusion chromatography is used to separate products based on size. Products of lower mass tend to retain longer and move slower whilst those of higher mass tend to move faster off the column. In this work, typically Sephadex G50 resin was used as the stationary phase with NH_4HCO_3 (0.1 M) as mobile phase at a rate of 10 mL h^{-1}. The enzymatic digestion of cytochrome *c* has a variety of products of similar size and colour. This coupled to the propensity for band-smearing/broadening makes it difficult to assess bands clearly. A typical separation is represented below (**Figure AII-2**).

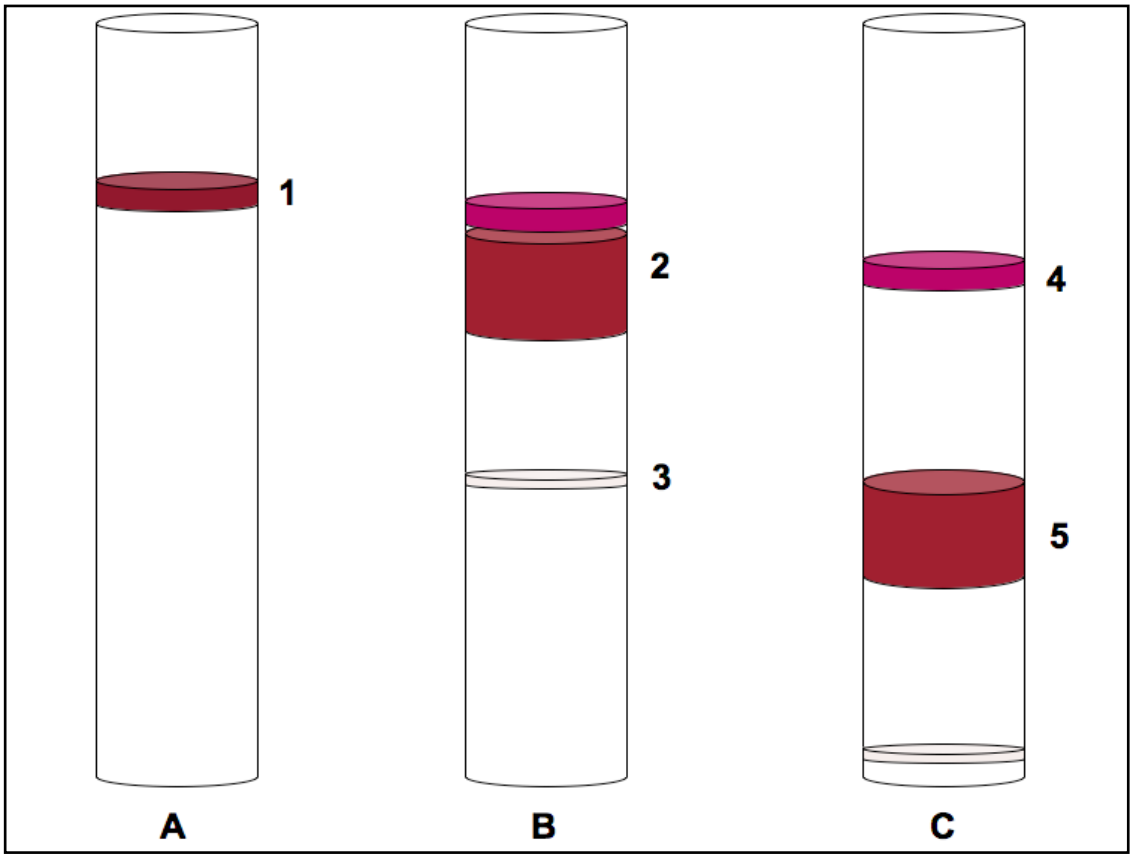


Figure AII-3 A diagrammatic representation of a typical Sephadex G50 FeMP11 band separation. (**A**) is the column on loading with initial band (*1*). (**B**) is the column after ~30 min with a major band (*2*) showing tailing and an almost imperceptible faint pink shadow (*3*). (**C**) is the column after ~ 90 min showing 'first major band' (*5*) and 'second major band' (*4*).

UV-Vis Spectra

UV-Vis spectrum showing NAcCoMP8 before and after desalting.

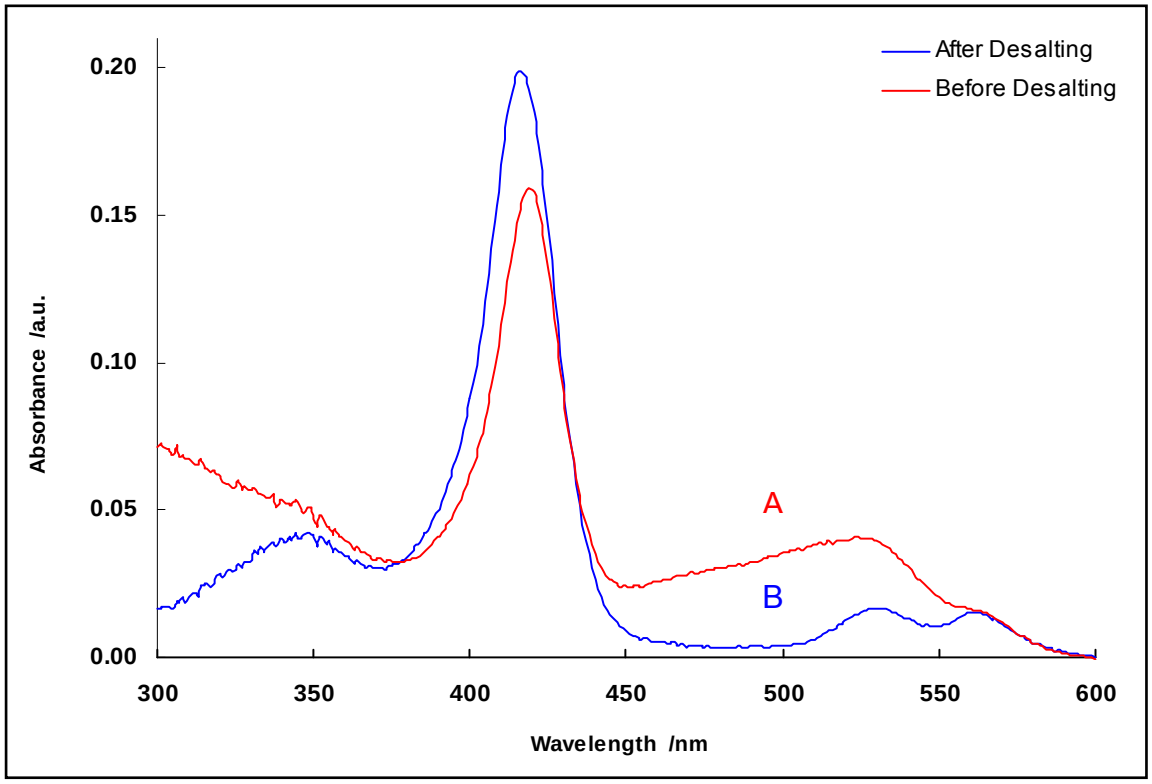


Figure AII-4 UV-Vis spectrum of NAcCoMP8 (**A**) before- and (**B**) after desalting.

APPENDIX 2.3 Derivation of Equation 2.4

$AH_4 \rightleftharpoons AH_3 + H^+ ...$ $\quad K_1 = \dfrac{[AH_3][H^+]}{[AH_4]}$

$AH_3 \rightleftharpoons AH_2 + H^+ ...$ $\quad K_2 = \dfrac{[AH_2][H^+]}{[AH_3]}$

$AH_2 \rightleftharpoons AH + H^+ ...$ $\quad K_3 = \dfrac{[AH][H^+]}{[AH_2]}$

$AH \rightleftharpoons A + H^+ ...$ $\quad K_4 = \dfrac{[A][H^+]}{[AH]}$

Now...

$$[A]_T = [AH_4] + [AH_3] + [AH_2] + [AH] + [A] \quad \text{.....(1)}$$

$$[A]_T = [AH_4] + K_1[AH_4]/[H^+] + K_2[AH_3]/[H^+] + K_3[AH_2]/[H^+] + K_4[AH][H^+]$$

$$= [AH_4]\left(1 + \frac{K_1}{[H^+]} + \frac{K_1K_2}{[H^+]^2} + \frac{K_1K_2K_3}{[H^+]^3} + \frac{K_1K_2K_3K_4}{[H^+]^4}\right)$$

$$= [AH_4]\left(\frac{[H^+]^4 + K_1[H^+]^3 + K_1K_2[H^+]^2 + K_1K_2K_3[H^+] + K_1K_2K_3K_4}{[H^+]^4}\right)$$

$\therefore$

$$[AH_4] = \frac{[A]_T\,[H^+]^4}{\alpha} \quad \text{.....(2)}$$

Where...

$$\alpha = [H^+]^4 + K_1[H^+]^3 + K_1K_2[H^+]^2 + K_1K_2K_3[H^+] + K_1K_2K_3K_4 \quad \text{.....(10)}$$

Similarly,

$$[AH_3] = \frac{[A]_T K_1[H^+]^3}{\alpha} \quad \text{.....(3)}$$

$$[AH_2] = \frac{[A]_T K_1K_2[H^+]^2}{\alpha} \quad \text{.....(4)}$$

$$[AH] = \frac{[A]_T K_1K_2K_3[H^+]}{\alpha} \quad \text{.....(5)}$$

$$[A] = \frac{[A]_T K_1K_2K_3K_4}{\alpha} \quad \text{.....(6)}$$

Writing in terms of mole fractions :

$$x_{A_T} = 1$$

$$x_{AH_4} = \frac{x_{A_T}[H^+]^4}{\alpha} = \frac{[H^+]^4}{\alpha}$$

$$x_{AH_3} = \frac{x_{A_T}K_1[H^+]^3}{\alpha} = \frac{K_1[H^+]^3}{\alpha}$$

$$x_{AH_2} = \frac{x_{A_T}K_1K_2[H^+]^2}{\alpha} = \frac{K_1K_2[H^+]^2}{\alpha}$$

$$x_{AH} = \frac{x_{A_T}K_1K_2K_3[H^+]}{\alpha} = \frac{K_1K_2K_3[H^+]}{\alpha}$$

$$x_A = \frac{x_{A_T}K_1K_2K_3K_4}{\alpha} = \frac{K_1K_2K_3K_4}{\alpha}$$

So, at some wavelength λ

$$A_\lambda = A_1x_{AH_4} + A_2x_{AH_3} + A_3x_{AH_2} + A_5x_A \text{ ....} (8)$$

Where A_i is the absorbance of the i^{th} species at wavelength λ if it were the only species present in solution.

$\therefore$

$$A_\lambda = \frac{A_1[H^+]^4}{\alpha} + \frac{A_2K_1[H^+]^3}{\alpha} + \frac{A_3K_1K_2[H^+]^2}{\alpha} + \frac{A_4K_1K_2K_3[H^+]}{\alpha} + \frac{A_5K_1K_2K_3K_4}{\alpha} \text{.....} (9)$$

$$A_\lambda = \frac{A_1[H^+]^4 + A_2K_1[H^+]^3 + A_3K_1K_2[H^+]^2 + A_4K_1K_2K_3[H^+] + A_5K_1K_2K_3K_4}{\alpha} \text{.....} (7)$$

Then from (8)...
If n is the number of successive ionisation s then (8) can be written as

$$A_\lambda = \sum_{m=1}^{n+1} A_m\beta_m \text{ ....} (11)$$

Where
A_m is the absorbance terms $A_1, A_2, ...A_n$ in (8) and
β_m term is the rest of the term in (8).

Each β term consists of a numerator and denominator as seen by (9).
The numerator consists of $[H^+]^n$ multiplied by the relevant equilibrium constants where n is the number of ionisations. The numerator can be summed as

$$[H^+]^{n+1-m}\prod_{i=1}^{n-1}K_i$$

The denominator consists of α which was defined as in (10). Using (10) α may be summed as

$$\alpha = \sum_{j=0}^{n}([H^+]^j\prod_{i=1}^{n-j}K_i)$$

Thus, β_m may be written fully as

$$\beta_m = \frac{[H^+]^{n+1-m}\prod_{i=1}^{n-1}K_i}{\sum_{j=0}^{n}([H^+]^j\prod_{i=1}^{n-j}K_i)}$$

REFERENCES FOR CHAPTER 2 - APPENDIX

1 Sannasy, D., M.Sc. Thesis, University of the Witwatersrand, Johannesburg, South Africa, **2005**.

2 Munro, O. Q.; Marques, H. M., *Inorg. Chem.*, **1996**, *35*, 3752

3 Carraway, A. D.; McCollumn, M. G.; Peterson, J., *Inorg. Chem.,* **1996**, *35,* 6885.

4 Baldwin, D. A.; Mabuya, M. B.; Marques, H. M., *S. Afr. J. Chem.,* **1987**, *40*, 103.

APPENDIX FOR CHAPTER 3 MONOMERISATION OF NAcCoMP8: SYNTHESIS ASPECTS

APPENDICES FOR CHAPTER 3

APPENDIX 3.1 *The Complex Solution Chemistry of CoMP8*

CoMP8 was the initial biomimetic model synthesised in this work (**Figure AIII-1A**). The synthesis was analogous to that of NAcCoMP8 explained elsewhere (**Chapter 2, Appendix 2.1**). A stock solution of CoMP8 was prepared using degassed deionised water (*ca*. 30 μM; pH 6.89; 25 ^{o}C) and was stored at 4 ^{o}C in the dark under argon. This stock solution was found to be monomeric[†] at *ca*. 10 μM and was thus used for further solution chemistry studies (**Figure AIII-1B**). However, preliminary thermodynamic and kinetic ligand binding data at 25 ^{o}C were found to be irreproducible when using the same CoMP8 stock solution and *N*-methyl imidazole as a test ligand (**Figure AIII-1C**, **D**).

The irreproducibility observed in CoMP8 data could be a consequence of the kinetics of its aggregation. The Beer's Law studies were conducted soon after the stock solution was prepared and gave a linear plot (**Figure AIII-1A)**. By contrast, the thermodynamic and kinetic ligand binding studies were performed a day later. The repeats 1 and 2 could be fitted to a simple single exponential function whereas *ca*. 30 minutes later (repeat 3) the reaction became significantly slower and distinctly biphasic. It seemed likely that this irreproducible and time-dependent behaviour was due to aggregation. Evidence of this aggregation thus promoted the need for acetylation of CoMP8 to produce NAcCoMP8, the biomimetic model focussed on in this study.

[†] Monomerism is based on the assumption that a species in a given solution is monomeric if Beer's Law is obeyed. Beer's Law was used as an indicator of monomerism in FeMP8 and has thus set the precedent for this work.[1-3]

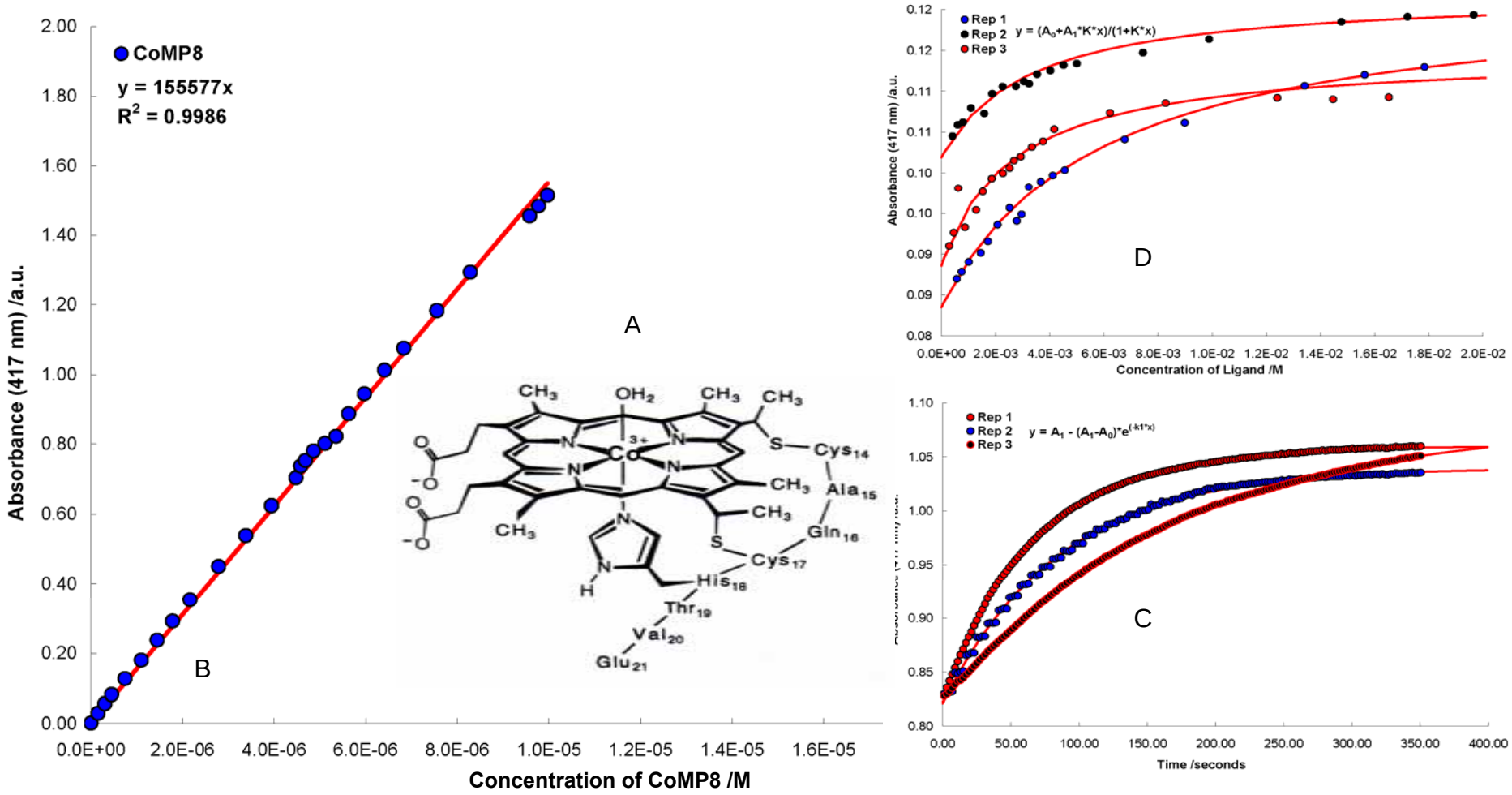


Figure AIII-1 The complex solution chemistry of CoMP8. CoMP8 (**A**) shows Beer's law behaviour and led to the initial conclusion that CoMP8 was monomeric in solution up to a concentration of over 10 μM (**B**). However, kinetics (**C**) and thermodynamics (**D**) of the substitution of coordinated H_2O by *N*-methyl imidazole gave irreproducible results for three repeat experiments (25 ^{o}C; pH 7).

APPENDIX 3.2 *Percentage Yield, ICP-OES and Absorptivity Data*

Percentage yield data were obtained for Routes A, B, C and D. Synthesis for these routes as well as sample preparation for weighing were carried out as previously described (**Chapter 2, Appendix 2.1, Chapter 3**). Percentage yields were determined for microperoxidases in each route and reported here as a percentage conversion from the microperoxidase used as the starting material for that step. The percentage yield data represent an average of three repeated syntheses for each route (**Table AIII-1**) and are in good agreement with previously reported values.[8]

Table AIII-1 Percentage yield data for Routes A-D in NAcCoMP8 (in triplicate).

Synthetic Routes	Compound	Percentage yield (by mass)				Std dev (σ)	%RSD
		Exp1	Exp2	Exp3	Ave		
A	FeMP11	84.9	85.0	83.8	84.6	0.6	0.75
	FeMP8	57.6	57.1	56.5	57.1	0.5	0.92
	MP8	69.1	68.9	68.1	68.7	0.5	0.79
	CoMP8	65.5	64.9	65.0	65.1	0.3	0.48
	NAcCoMP8	68.9	69.1	69.1	69.0	0.1	0.16
B	FeMP11	91.9	93.1	93.1	92.7	0.7	0.71
	FeMP8	58.0	57.5	57.9	57.8	0.3	0.52
	NAcFeMP8	87.8	87.0	88.0	87.6	0.5	0.61
	NAcMP8	75.8	76.0	76.1	76.0	0.2	0.23
	NAcCoMP8	71.9	72.6	72.9	72.4	0.5	0.69
C	FeMP11	92.5	93.9	92.8	93.1	0.7	0.80
	NAcFeMP11	94.6	95.3	95.5	95.1	0.5	0.52
	NAcMP11	98.2	98.2	98.0	98.1	0.1	0.12
	NAcCoMP11	95.3	95.0	95.0	95.1	0.2	0.19
	NAcCoMP8	77.4	76.6	76.0	76.7	0.7	0.94
D	FeMP11	90.2	91.4	92.2	91.3	1.0	1.13
	MP11	90.2	90.4	89.6	90.0	0.4	0.48
	CoMP11	86.5	85.8	85.3	85.9	0.6	0.65
	NAcCoMP11	65.7	67.3	67.0	66.7	0.9	1.34
	NAcCoMP8	75.2	74.6	75.0	74.9	0.3	0.44

Percentage yield data for NAcCoMP8 were also obtained using ICP-OES (**Chapter 2**). ICP-OES data were recorded for Routes A, B, C and D and are reported here based on the amount of cobalt in NAcCoMP8. (**Table AIII-2**).[8]

Table AIII-2 ICP-OES percentage yield data based on the amount of cobalt in NAcCoMP8 for Routes A-D. The focus, Route C, is highlighted in *italics*.

Route	NAcCoMP8			Co^{3+}		
	Mass	**Concentration**		**Concentration** (x10) /ppm		**%Yield**
	/mg	/ppm	(x10) /ppm	Expected	Observed	Based on Co^{3+}
A	0.205	8.200	0.820	0.031	0.0205	65.86
B	0.222	8.880	0.888	0.034	0.0218	64.68
C	*0.249*	*9.960*	*0.996*	*0.038*	*0.0298*	*78.83*
D	0.212	8.480	0.848	0.032	0.0225	69.90

Absorptivity values for NAcCoMP8 were obtained from the Beer's Law study conducted previously (**Chapter 2**, **Chapter 4**). These values were reported based on the average absorbance obtained at four different wavelengths (**Tabled AIII-3**) and are in good agreement with previously reported values.[8]

Table AIII-3 Absorptivity for NAcCoMP8 derived from Route C.

Wavelength /nm	Absorbance /a.u.	ε ($x10^5$) /M^{-1} cm^{-1}	Std dev (σ)	%RSD
347	0.1843	0.51	0.01	0.37
417	0.6255	1.63	0.03	0.22
530	0.0655	0.17	0.02	0.35
560	0.0596	0.15	0.03	0.54

APPENDIX 3.3 *FeMP5, FeMP6, FeMP8, FeMP9 and FeMP11*

The ESI-MS spectra for FeMP11, NAcFeMP11, FeMP9, FeMP8, FeMP6 and FeMP5 are reported (**Figure AIII-2-7)** with possible peak assignments (**Table AIII-4**). The microperoxidase diagrams inserts reflect the Fe(III) form with deprotonated carboxylates (referred to here as, for example, '*deprotonated*

FeMP11') and possible sodium ion pairings indicated by circles. Exact masses were calculated using ChemDraw® Ultra[4]. The observed values are in good agreement with calculated and previously reported values, where applicable.

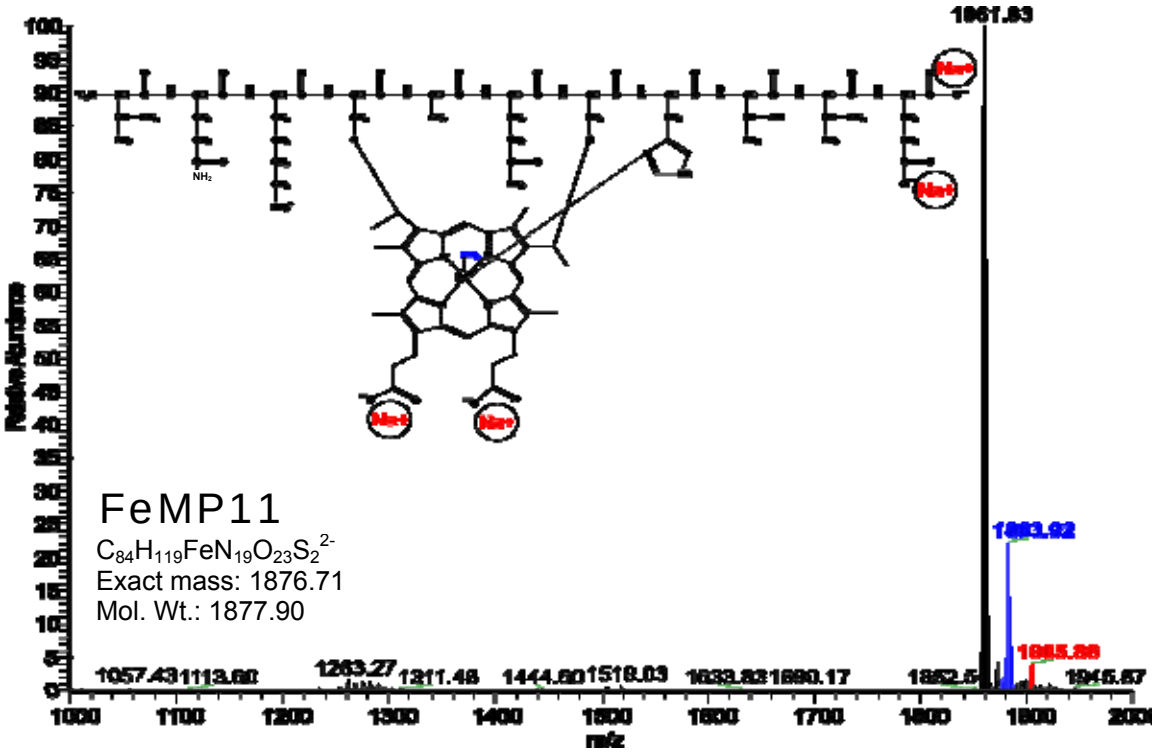


Figure AIII-2 Low resolution positive mode ESI-MS of FeMP11 in 50% methanol. Spectrum shows protonated FeMP11 with (blue) and without (black) axially coordinated water and the latter with one sodium ion (black).

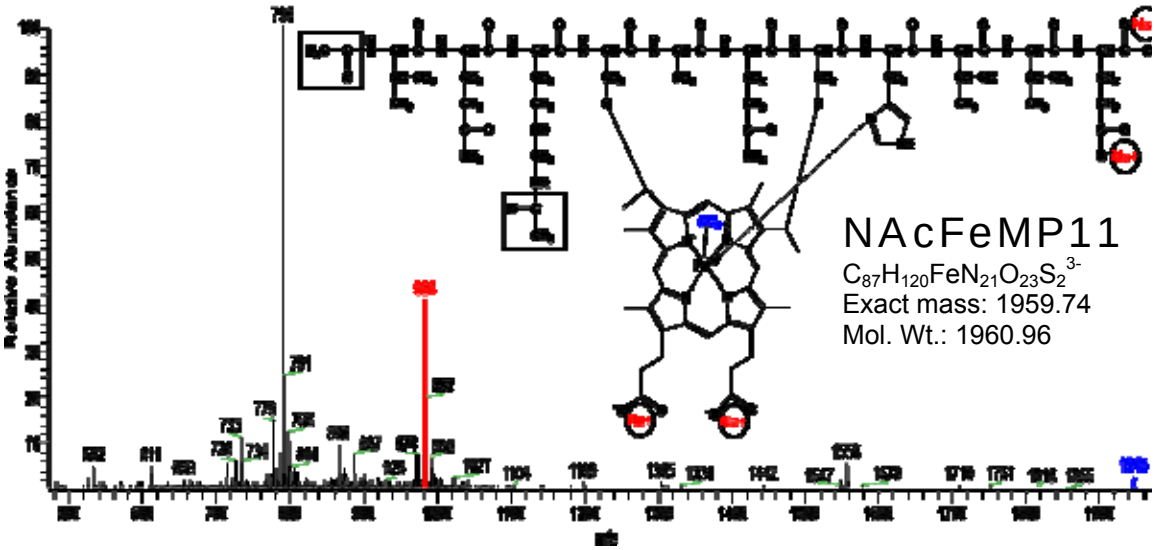


Figure AIII-3 Low resolution positive mode ESI-MS of NAcFeMP11 in 50% methanol. Spectrum shows *bis*-acetylated deprotonated NAcFeMP11 without axially coordinated water (blue); the doubly charged species (black) and the doubly charged protonated species with coordinated water (red)

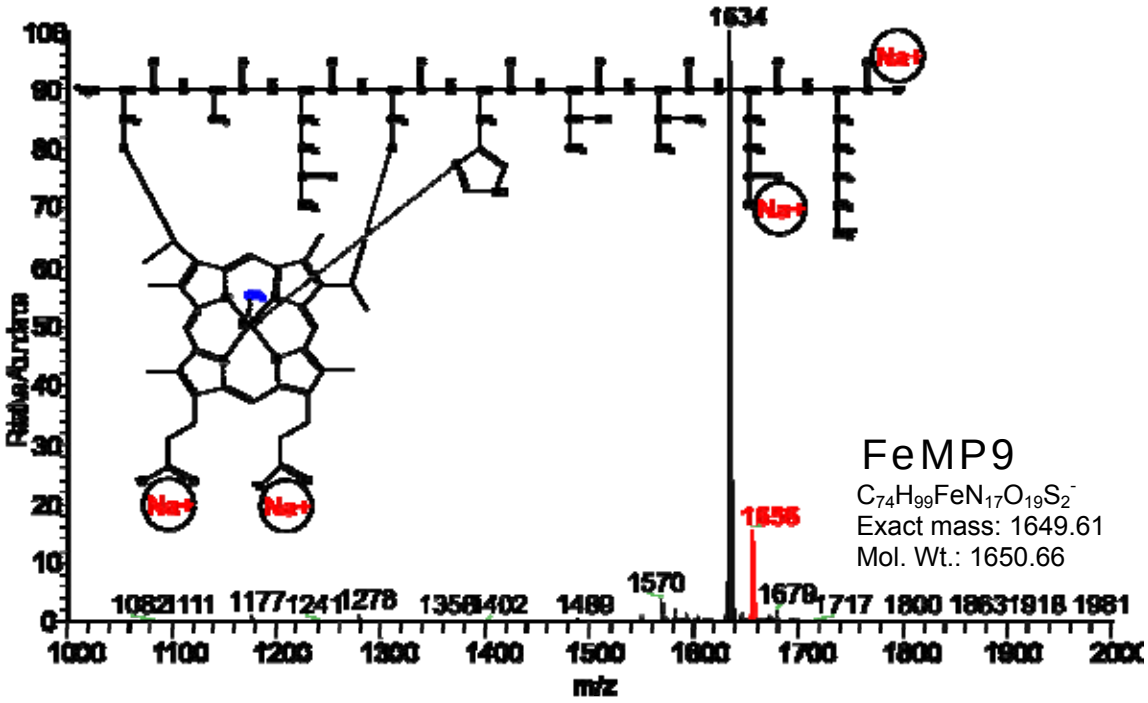


Figure AIII-4 Low resolution positive mode ESI-MS of FeMP9 in 50% methanol. Spectrum shows protonated FeMP9 with (red) and without (black) axially coordinated water.

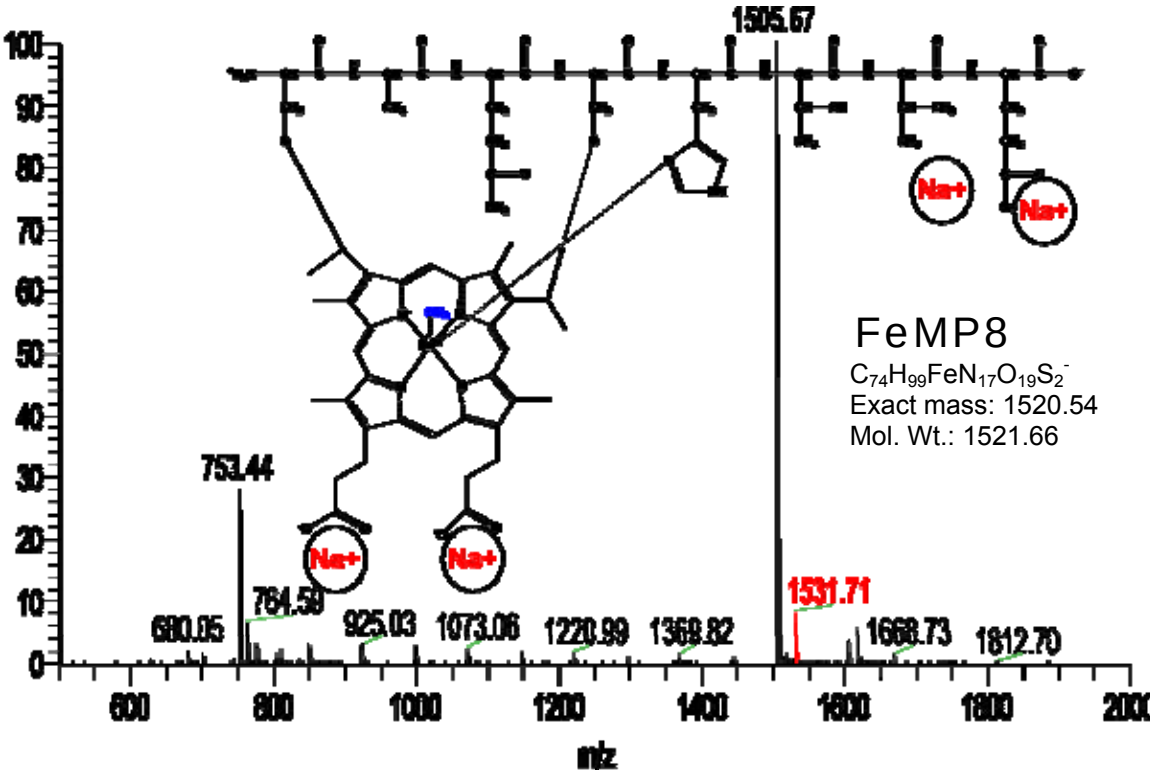


Figure AIII-5 Low resolution positive mode ESI-MS of FeMP8 in 50% methanol. Spectrum shows protonated FeMP8 with without axially coordinated water (black), the doubly charged molecular ion (black: m/z 753) and the molecular ion with sodium (red).

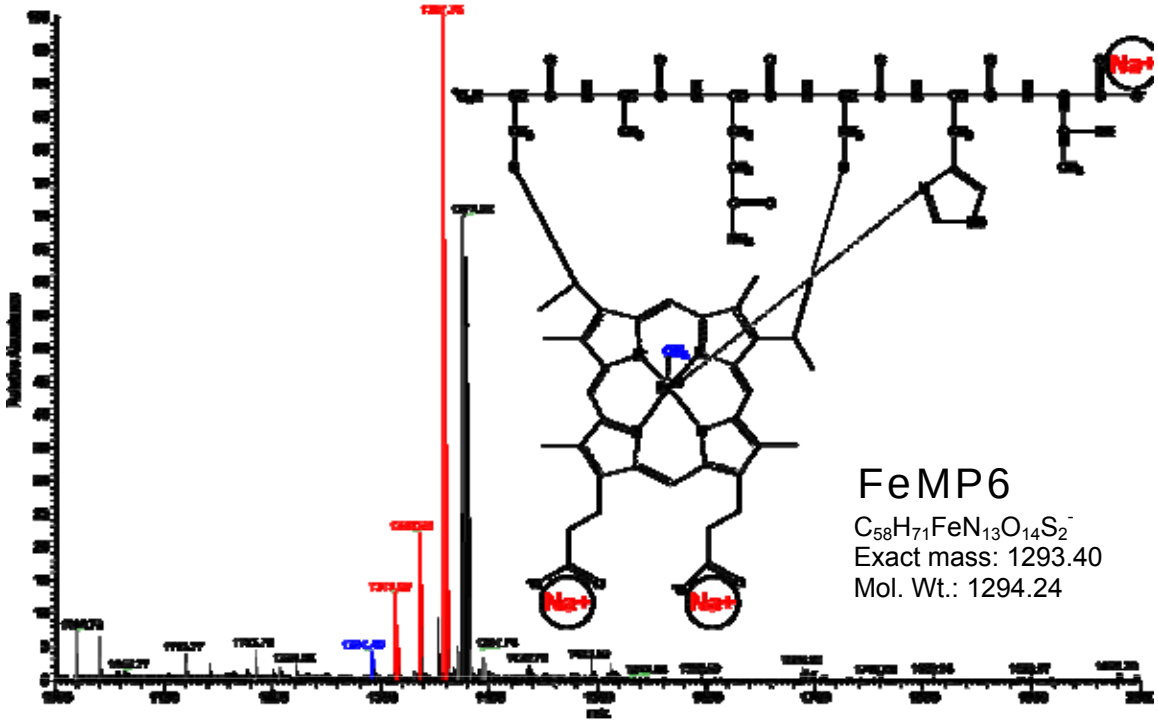


Figure AIII-6 Low resolution positive mode ESI-MS of FeMP6 in 50% methanol. Spectrum shows protonated FeMP6 with axially coordinated water (blue), with sodium ions (red) and with a further associated water molecule (black).

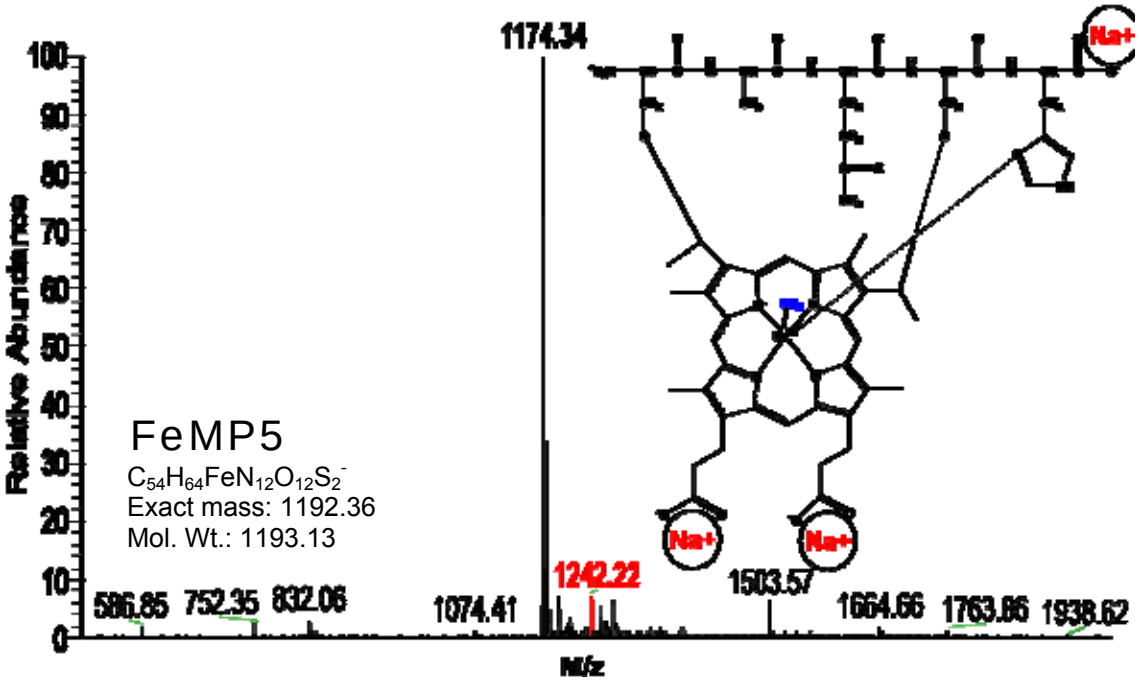


Figure AIII-7 Low resolution negative mode ESI-MS of FeMP5 in 50% methanol. Spectrum shows deprotonated FeMP5 without axially coordinated water (black) and with sodium ions (red).

Table AIII-4 Possible ESI-MS assignments for various Fe(III) microperoxidases.

Fig #	MP	Mode (+/-)	Peak /(m/z)	Possible assignment
AIII-2	FeMP11[5]	+	1905	a, f
			1883	a
			1861	b
AIII-3	NAcFeMP11[5]	+	1945	d, h
			1556	d, 3g, i(FeMP8),
			1021†	c, e, f, g, h
			993†	b, e, g, h
			984	a, e, h
			974	d, e, h
			790	d, e, g, i(NAcFeMP8)
AIII-4	FeMP9[6]	+	1656	a
			1634	b
AIII-5	FeMP8[6,7,8,‡]	+	1531	b, f
			1505	b
			753	b, e
AIII-6	FeMP6	+	1375	b, 3f, g
			1357	b, 3f
			1335	b, 2f
			1313	b, f
			1291	b
AIII-7	FeMP5[7,9]	-	1664	c, g, i(FeMP9)
			1503	d, i(FeMP8)
			1242	d, 3f
			1174	d
			1074	c, g, i(FeMP4)
			832	c, e, g, i(FeMP9)
			752	d, e, i(FeMP8)
			586	d, e

a protonated carboxylates with axial water
b protonated carboxylates without axial water
c deprotonated carboxylates with axial water
d deprotonated carboxylates without axial water
e doubly charged
f sodium, where 2f refers to $2Na^+$ and so forth.
g water, where 2g refers to $2H_2O$ and so forth.
h *bis*-acetylated
i a possible contaminating microperoxidase with likely contaminant in brackets.
† Carraway *et al*., referred to a possible tris-acetylated product, however this is unlikely as there are no other positions available for acetylation. Thus, the assignment reported here is more plausible. [5]
‡ the commonly observed $[protoheme+1]^+$ at m/z 617 was not present in this work. [6,8]

APPENDIX 3.4 *TLC Patterns*

TLC plates developed with microperoxidase samples obtained from Amicon® desalting steps were found to be irreproducible. This phenomenon was observed to a much lesser extent with microperoxidase samples obtained from the Sep-Pak® desalting procedure. The plates were developed as previously described (**Chapter 2**).

The spots on the TLC plates presented as smears from baseline to solvent front (**Chapter 3**). The irreproducible smears were found to be independent of concentration as they were also observed when the TLC spotting solution was diluted by *ca*. 50 % with deionised water. The smears patterns however, could be loosely grouped according to how long the microperoxidase stock solution had been stored since preparation. These smear patterns are grouped as feathering, tailing and eclipsing in this work (**Figure AIII-8**). These patterns are attributed to microperoxidase interacting with the solid phase at various stages of aggregation. Tailing was usually observed with microperoxidase stock solutions that were used immediately after preparation, whilst eclipsing and feathering were typically observed *ca*. 2 and 4 hours after sample preparation.

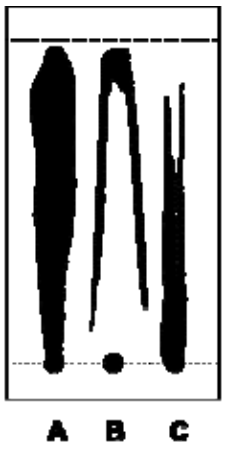


Figure AIII-8 A diagrammatic representation of TLC patterns observed in microperoxidase samples that were purified using the Amicon® cell. The patterns were independent of concentration and were grouped according to tailing (**A**) which was typically observed when the spotting solution was used immediately after preparation, eclipsing (**B**) which was typically observed when the spotting solution had been allowed to stir for *ca*. 2 hours or feathering (**C**) which was observed when the spotting solution had been allowed to stir for *ca*. 4 hours.

APPENDIX 3.5 *Amine Protection Experiments*

The protection of various amino-groups on the NAcCoMP8 peptide chain was briefly explored as a side experiment. There were primarily two reasons to protect the amino-groups in microperoxidases: firstly, to prevent the metal-side-chain aggregation on Cys-14 and secondly to promote the 'base-off' state of NAcCoMP8 by protecting the amine on the His-18 proximal ligand.

Firstly, the acetylation of CoMP9 was attempted along with that of CoMP11, CoMP8 and CoMP6 (**Chapter 3**). These cobalt microperoxidases were acetylated in order to optimise the procedure for the target compound, NAcCoMP8. However, CoMP9 was only briefly isolated as a by-product of the CoMP11 synthesis and visibly aggregated during desalting. The visible aggregation in CoMP9 appeared to be more rapid than with CoMP11. CoMP8 displayed the most resistance towards visible aggregation. This suggested that perhaps the lysine groups, specifically its orientation relative to the other amino acids, played a significant role in the aggregation process. In CoMP9 the lysine group is more accessible towards aggregation than in the case of CoMP11 which appeared to be more sterically hindered.

The acetylation process was attempted on the CoMP9 solution regardless, and characterised by HPLC and ESI-MS as previously described (**Chapter 2**, **Figure AIII-9A**). ESI-MS calculations suggested that NAcCoMP9 with protonated carboxylates should be isolated at m/z 1694 with the water elimination product at m/z 1676. The doubly charged species should be isolated at m/z 847 and 838, respectively. Analogously, the possible *bis*-acetylated products should be at m/z 1735, 1717, 867 and 858. None of these peaks were observed (**Figure AIII-9A**) HPLC data provided further evidence to support the aggregation and/or the possibility of mixed products during CoMP9 acetylation (**Figure AIII-9A**).

Secondly, the protection of the His-18 moiety was attempted in order to obtain an authentically 'base-off' NAcCoMP8 at neutral pH. The solution chemistry

studies attempted on this 'base-off' compound, the putative BOCoMP8, would then be compared to those of the 'base-on' derivative. In this way, the effect of the His-18 side-chain on NAcCoMP8's solution chemistry could be assessed in relation to porphryin *cis*-effects.

The protection of the amine group on the His-18 proximal ligand was attempted by using N-terminus protecting groups commonly used during solid-phase peptide synthesis (SPPS) with some modifications.[10-15] The particular N-terminus protecting group available was Boc (*t*-butoxycarbonyl). Three main obstacles were observed in relation to this synthesis. The first obstacle in this synthesis was the utilisation of non-aqueous solvents. Boc-protection is typically carried out in excess using CH_3CN, DMF and DMAP as solvents. NAcCoMP8 is sparingly soluble in CH_3CN. Regardless, the protection was attempted and resulted in an orange gel-like substance that could not be analysed further.

The second obstacle related to NAcCoMP8's lack of robustness towards the synthesis. The synthesis was then attempted in aqueous sodium bicarbonate (0.1 M) at reduced temperature (*ca*. 4 ^{o}C) for 15 minutes. Thereafter the solution was allowed to stir at room temperature for two hours after which it was desalted on a Sep-Pak® cartridge. The synthesis with BOC_2O was found to be too aggressive and NAcCoMP8 degraded into an insoluble black-brown solid. The solid was washed exhaustively with methanol and washings were analysed by ESI-MS and HPLC as described previously (**Chapter 2**, **Figure AIII-9B**). ESI-MS calculations suggested that deprotonated BOCoMP8 should be isolated at m/z 1665 with the water elimination product at m/z 1647. By analogy, the doubly charged species should be isolated at m/z 832 and 823, respectively. None of these peaks were observed (**Figure AIII-9B**).

FMoc (Fluorenylmethyloxycarbonyl chloride) and carboxymethylation methods were suggested as a less aggressive alternative to Boc and have been used successfully with ferricytochome *c*.[11,13,15] However, the third obstacle commonly associated with SPPS-type of syntheses[10] is the low yield which is further exacerbated by NAcCoMP8's generally low yields and aggregation.

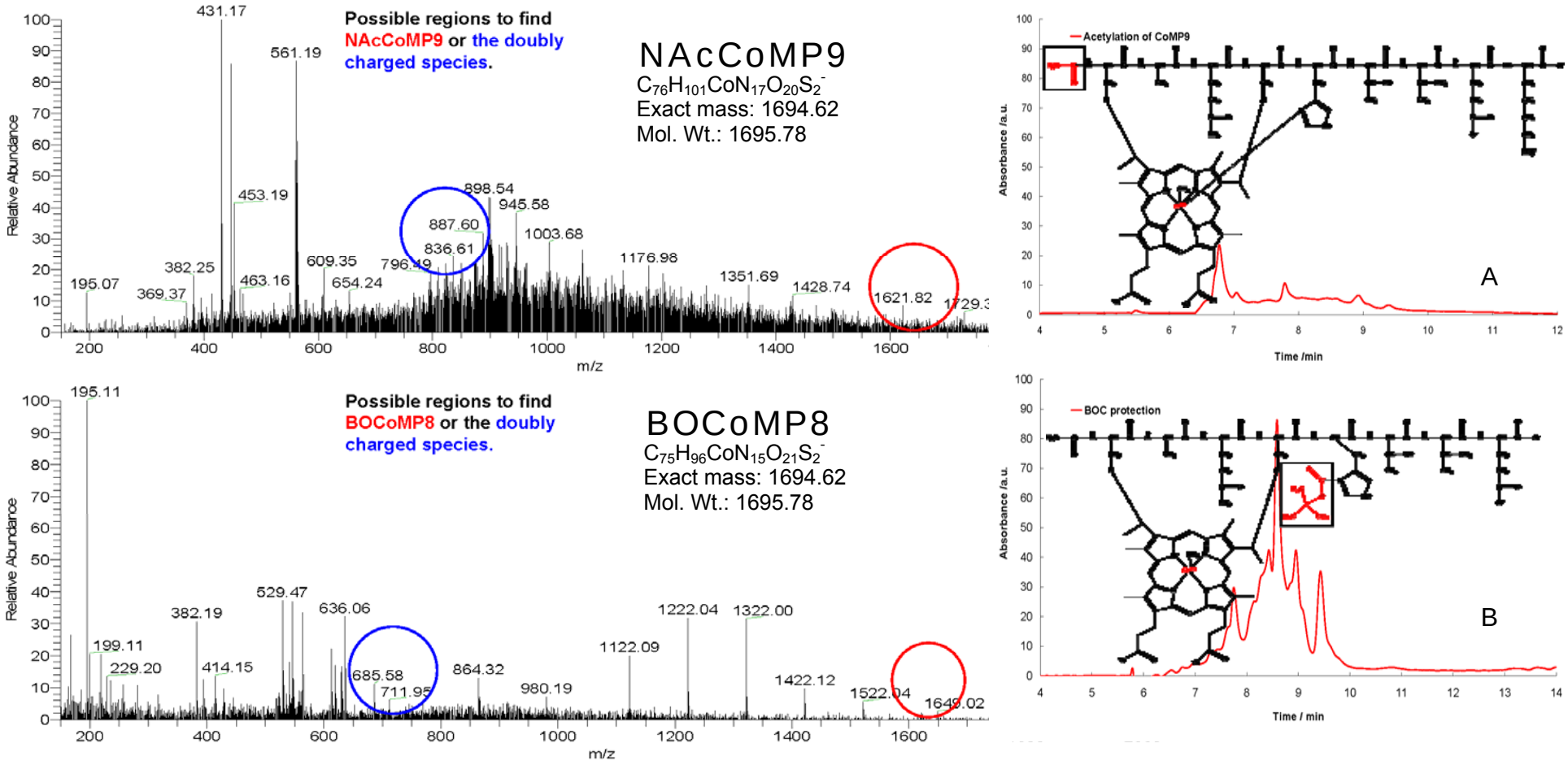


Figure AIII-9 Side experiments explored in this work. The acetylation of CoMP9 (**A**) was unsuccessful as CoMP9 appeared to aggregate in solution. The Boc-protection of His-18 (**B**) was also unsuccessful possibly due to aggregation or decomposition. The circles refer to m/z regions where products and their derivatives (red) or their doubly charged molecular ions (blue) might be found. ESI-MS and supporting HPLC data were performed as previously described (**Chapter 2, Appendix 2.1**).

APPENDIX 3.6 *Characterisation of NAcCoMP8*

NAcCoMP8 was synthesised and characterised as described previously (**Chapter 2**). The compound formed a dark pink-red spongy solid upon lyophilisation. Solid NAcCoMP8 was stored in the dark at -20 ^{o}C under argon as NAcCoMP8 is particularly susceptible to degradation and static. Stock solutions of NAcCoMP8 for characterisation purposes were freshly prepared in degassed solvents and were dilute (*ca*. 30 μM). The freshly prepared bright-pink NAcCoMP8 stock solution was allowed to stir for *ca*. 2 hours before being clarified using a Millex® syringe filter. This stock solution was then used to characterise NAcCoMP8 by UV-vis, HPLC and ESI-MS (**Figure AIII-10**). The embedded structural representation of NAcCoMP8 indicates the acetylation as well as possible points of sodium ion pairing during ESI-MS.

The isolated NAcCoMP8 was analysed by positive mode ESI-MS (**Figure AIII-10B**). Protonated NAcCoMP8 without axially coordinated water was detected at m/z 1551. The peak observed at m/z 1566 might be attributed to NAcCoMP8 with protonated carboxylates and axial water. This product with the presence of sodium might be observed at m/z 1592. These data were in good agreement with calculated values and values previously reported.[8]

The UV-vis data for NAcCoMP8 and metal-free NAcMP8 were obtained as described (**Chapter 2**). Samples were run in deionised water at *ca*. pH 7 at 25 ^{o}C (**Figure AIII-10C**). There was a distinct shift in Soret from metal-free NAcMP8 to NAcCoMP8 (378 and 415 nm, respectively). The disappearance of four Q-bands to two Q-bands indicated that the cobalt insertion had been achieved.[8] The single major peak obtained in the HPLC data suggested that CoMP8 was completely acetylated (**Figure AIII-10D**).

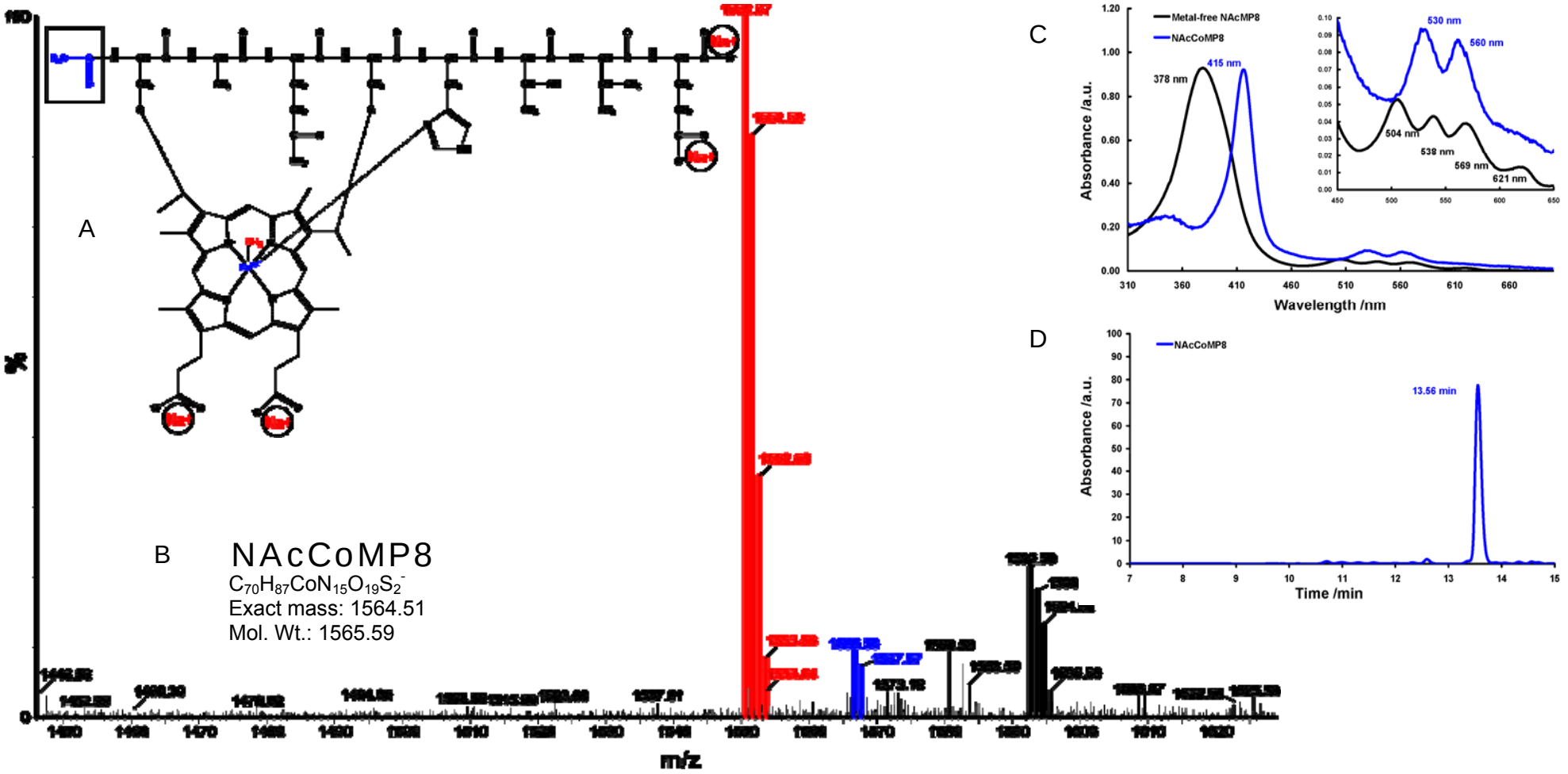


Figure AIII-10 The characterisation of NAcCoMP8 (**A**) using ESI-MS (**B**), HPLC (**C**) and UV-vis(**D**). HPLC and ESI-MS were performed as previously described (**Chapter 2, Appendix 2.1**).

APPENDIX 3.7 *Synthetic Porphyrins (Publication: Abstract only)*

Full articles may be found on the accompanying Data Disk

Inorganica Chimica Acta 392 (2012) 108–111

Contents lists available at SciVerse ScienceDirect

Inorganica Chimica Acta

journal homepage: www.elsevier.com/locate/ica

Note

5,10,15,20-Tetra-*p*-phenylsulfonyporphinatocobalt(III), a water-soluble Co(III) porphyrin

Sadhna Mathura, Alvaro S. de Sousa, Manuel A. Fernandes *, Helder M. Marques *

Molecular Sciences Institute, School of Chemistry, University of the Witwatersrand, P.O. Wits, Johannesburg, 2050 South Africa

ARTICLE INFO

Article history:
Received 8 March 2012
Received in revised form 24 April 2012
Accepted 6 May 2012
Available online 4 June 2012

Keywords:
Cobalt porphyrins
$[Co(TPPS)(H_2O)_2]$
SQUEEZE algorithm

ABSTRACT

An alternative procedure is described for producing diffraction-quality crystals of the sodium salt of the water-soluble porphyrin diaqua-5,10,15,20-tetra-*p*-phenylsulfonyporphinatocobalt(III), $Na[Co(TPPS)(H_2O)_2]\cdot 4H_2O$ by vapour diffusion of ethyl acetate into an aqueous solution of the porphyrin overlaid with a layer of acetone. The structure contains a large amount of disordered solvent in channels but application of an appropriate algorithm (SQUEEZE – an algorithm incorporated into PLATON that applies a Fourier transform of the observed density in the solvent areas and incorporates its contribution to the structure factors) permits a structure solution.

© 2012 Elsevier B.V. All rights reserved.

1. Introduction

The metal complexes of the water-soluble synthetic porphyrin 5,10,15,20-tetrakis(4-sulfonatophenyl)porphyrin (TTPS) have several interesting properties. For example, Mn(II)TTPS is a tumour-seeking MRI contrast agent [1,2]; Co(III)TTPS photocatalyses the oxidation of alcohols under anaerobic conditions [3] and has also been suggested as a useful cyanide scavenger [4]; and Fe(II)TTPS has been investigated as a peroxynitrite decomposition catalyst [5]. A great deal of work on the solution chemistry of these porphyrins has been carried out including, for example, the kinetics and thermodynamics of the substitution of coordinated H_2O in Cr(III)TTPS by imidazole [6,7], and by pyridine [8,9], I^- [10], SCN^- [9,10] and CN^- [4] in Co(III)TTPS, the kinetics of substitution of H_2O by CN^- in $[Ru(TPPS)(CO)(H_2O)]^{4-}$ [11], the reduction of Co(III)TTPS by Cr(II) [12], the dimerisation of Fe(III)TTPS [13], and the radiolytic [14,15] and electrochemical reduction of Co(III)TTPS [14]. Despite this interest, there is a single crystal structure of TTPS available in the Cambridge Structural Database [16], that of Ir(III) [17]. In this structure the counter ions are Na(benzo-18-crown-6)$^+$; the use of this particular crown ether was found to be essential to complex Na^+ and K^+ cations to produce diffraction-quality crystals. Powder patterns for $[Fe(TPPS)]^{3-}$ and $[Zn(TPPS)]^{4-}$ have been reported [18].

We report here conditions for the crystallisation of diaqua-5,10,15,20-tetrakis(4-sulfonatophenyl)porphinato-cobalt(III) in which Na^+ itself is the counter-ion. Despite the presence of a large amount of disordered solvent in the lattice, use of the SQUEEZE algorithm [19] allowed for a structure solution from the diffraction data.

2. Experimental

The preparation of CoTPPS was based on previous reports [9,20]. The free-base TPPS (Sigma–Aldrich) was contaminated by traces of the more hydrophobic di- and tri-substituted derivatives, as well as unidentified water-soluble salts. It was desalted using C18 Sep-Pak cartridges (Waters). We found this desalting step to be crucial for the successful crystallisation of the metalloporphyrin. Free-base TPPS (10 mg) was dissolved in slightly basic deionised water (ca. 2 mL; pH 9, NaOH) and refluxed with cobaltous acetate (100 M excess) under argon for 30 min in the dark. Thereafter, the reaction was cooled and stirred at room temperature for 3 h in air. The progress of the metallation was monitored by UV–Vis spectroscopy; the Soret band shifts from 413 to 425 nm. The resultant metalloporphyrin, which we shall refer to as CoTPPS, was precipitated out as dark pink flakes using cold acetone. The product gave a single peak on reverse phase HPLC.

Non-isothermal thermogravimetric analysis was performed on the crystalline CoTPPS (11.3040 mg) using a Q500 Thermogravimetric Analyzer V6.4 Build 193 at a heating rate of 10 °C min^{-1} from 10 to 600 °C under N_2. UV–Vis spectra were recorded on a Cary 300 Bio spectrometer and the temperature of the cell block was maintained with a Peltier device. NMR spectra were recorded on a Bruker 300 MHz spectrometer. Electrospray mass spectra were obtained on a Thermo Finnigan LXQ spectrometer operating in positive mode and visualised using Xcalibur 2.0.7.

* Corresponding authors. Tel.: +27 11 7176737; fax: +27 11 7176749.
E-mail addresses: Manuel.Fernandes@wits.ac.za (M.A. Fernandes), Helder.Marques@wits.ac.za (H.M. Marques).

0020-1693/$ - see front matter © 2012 Elsevier B.V. All rights reserved.
http://dx.doi.org/10.1016/j.ica.2012.05.021

APPENDIX 3.8 *Other Publications (Abstract only)*

Full articles may be found on the accompanying Data Disk

*Manuscript
Click here to download Manuscript: CoMP8_Paper 1.docx Click here to view linked References

The Preparation of *N*-Acetyl-Co(III) Microperoxidase-8 (NAcCoMP8) and its Solution Chemistry

Sadhna Mathura, Desigan Sannasy, Alvaro S. de Sousa and Helder M. Marques*

Molecular Sciences Institute, School of Chemistry, University of the Witwatersrand, P.O. Wits, Johannesburg, 2050 South Africa

Abstract

The Co(III) porphyrin octapeptide *N*-acetyl-Co(III) Microperoxidase-8 (NAcCoMP8) was prepared by the proteolytic digestion of cytochrome *c*, replacement of Fe(III) by Co(III), and protection of the N-terminal group of the peptide by acetylation. In neutral aqueous solution it is monomeric at low concentration with a Soret band at 415 nm with $\varepsilon = 1.61(3) \times 10^5$ M^{-1} cm^{-1}; higher concentrations (> 10 μM), an increase in the ionic strength of the solution, or an increase in temperature above 45 °C causes the formation of oligomeric species with a Soret band at 425 nm, usually through intermediacy of a species with a Soret band at 417 nm. Although formation of the latter can be reversed to produce the monomeric 415 nm species on dilution of the solution, or by lowering the temperature or the ionic strength, the formation of the former is irreversible and on standing eventually leads to precipitation of the metallopeptide from solution. NAcCoMP8 has five spectroscopically observable pK_as: at 1.74 ± 0.04 due to protonation and displacement of His-18 either by H_2O or a carboxylate from the peptide; at 4.08 ± 0.02 and 5.80 ± 0.05 due to ionization of the heme carboxylate groups; at 7.81 ± 0.03 is due to ionization of coordinated H_2O; and at 12.00 ± 0.03 due to ionization of His-18 to form an imidazolate. NAcCoMP8 provides a means of comparing and contrasting the chemistry of Co(III) porphyrins and corrins and so assess the influence of the macrocycle on the chemistry of the metal ion.

Keywords: Microperoxidases; cobalamins; iron porphyrins

Full articles may be found on the accompanying Data Disk

*Manuscript
Click here to download Manuscript: Co_MP8_Paper2.docx
Click here to view linked References

The Ligand Substitution Reactions of *N*-Acetyl-Co(III) Microperoxidase-8 (NAcCoMP8): a Comparison with Aquacobalamin (vitamin B_{12a})

Sadhna Mathura, Alvaro S. de Sousa, Christopher B. Perry, Isabelle Navizet and Helder M. Marques*

Molecular Sciences Institute, School of Chemistry, University of the Witwatersrand, P.O. Wits, Johannesburg, 2050 South Africa

Abstract

N-Acetyl-Co(III) Microperoxidase-8 (NAcCoMP8), a Co(III) porphyrin-containing octapeptide and aquacobalamin (H_2OCbl^+, vitamin B_{12a}) both contain Co(III), an N-donor macrocyclic equatorial ligand (porphyrin, corrin), an imidazole derivative as one axial ligand (His, 5,6-dimethylbenzimidazole) and H_2O in the other axial coordination site. This allows for an evaluation of the effect of the equatorial macrocyclic ligand on the ligand substitution reactions of Co(III). Equilibrium constants (as log *K* values) for the coordination of anionic (CN^-, N_3^-, NO_2^-, HSO_3^-) and neutral (pyridine, N-methylimidazole, methoxylamine and hydroxylamine) ligands were determined spectrophotometrically as a function of temperature and ΔH and ΔS values are reported. The log *K* value for coordination of pyridine by H_2OCbl^+ is anomalously low and DFT calculations (M06L/SVP) show that pyridine is sterically hindered for coordinating the metal ion, resulting in a long Co–N bond and a flattened corrin ring. Anionic ligands bind more strongly to H_2OCbl^+ than to NAcCoMP8 while the converse is true for the neutral ligands. It is suggested that the higher residual charge at the metal center in the corrin (+2) compared to the porphyrin (+1) is primarily responsible. The anionic and neutral ligands behave differently. Log *K* values for coordination of the anionic ligands by both NAcCoMP8 and H_2OCbl^+ parallel the pK_a of their conjugate acid. In the case of the neutral ligands, log *K* for coordination by NAcCoMP8 correlates directly with ligand basicity but there is an inverse correlation in the case of H_2OCbl^+. Log *K* and ΔH values for the reaction with anionic ligands parallel each other in the two systems, but there appears to be an inverse correlation for the neutral ligands. DFT calculations show that the bond length between the metal and the axial ligand trans to the imidazole derivative in corrin is always longer in the corrin; however, the average difference in these bond lengths is larger for the neutral ligands than for the anions. This is attributed to the increased coulombic interaction

Full articles may be found on the accompanying Data Disk

between the anionic ligands and the greater charge on the metal center in the corrin system. A QTAIM analysis of the electron density in these DFT models shows that electron-rich anionic ligands induce a significant covalency in their bond to Co(III) in both the corrin and the porphyrin, whereas the bonding between the metal and neutral N-donor ligands is predominantly ionic. The extent of the covalency appears to be an important factor in determining the stability of the resultant complex. The significant ellipticity of the bonds to a coordinated anion indicates the presence of some multiple bonding to Co(III). Kinetics measurements show that H_2OCbl^+ is significantly more labile towards substitution by CN^- than NAcCoMP8 (k_{25} = 240 and 103 M^{-1} s^{-1}, respectively) because of a much smaller value of $\Delta H^{\ddagger}$ value which is somewhat, but not completely, compensated for by a much more negative $\Delta S^{\ddagger}$. By contrast, the reaction of N-methylimidazole occurs faster with NAcCoMP8 than with H_2OCbl^+ due to a smaller $\Delta H^{\ddagger}$ and a somewhat larger $\Delta S^{\ddagger}$. Since the intimate mechanism is probably an interchange mechanism under dissociative activation, the kinetic results are rationalized by the extent of participation of the entering ligand in the transition state. CN^- forms a more stable complex with H_2OCbl^+ (log K > 12) than NAcCoMP8 (log K = 6.04). In its reaction with H_2OCbl^+ the transition state will occur earlier along the reaction coordinate than in its reaction with NAcCoMP8 leading to a lower $\Delta H^{\ddagger}$. The converse is true for N-methylimidazole where its greater affinity for the porphyrin than the corrin (log K = 5.70 and 4.49, respectively) makes its reaction with the former faster (k_{25} = 1300 M^{-1} s^{-1} compared to 14 M^{-1} s^{-1}). Therefore there is a correlation between the thermodynamic stability of Co(III) complexes of corrin and porphyrins and the rate of substitution of axially coordinated H_2O. The nature of the macrocycle in these Co(III) systems has a profound effect on the chemistry of the metal ion.

Keywords: Microperoxidases; cobalamins; vitamin B_{12a}; ligand substitution; DFT calculations; QTAIM calculations.

REFERENCES FOR CHAPTER 3 - APPENDIX

1. Aron, J. A.; Baldwin, D. A.; Marques, H. M.; Pratt, J. M.; Adams, P. A., *J. Inorg. Biochem.*, **1986**, *27*, 227.
2. Urry, D. W.; Pettegrew, J. W., *J. Am. Chem. Soc.*, **1967**, *89*, 5276.
3. Urry, D. W., *J. Am. Chem. Soc.*, **1967**, *89*, 4190.
4. *ChemDraw® Ultra*, 8.0; CambridgeSoft Corporation, Cambridge, MA 02140, USA, **2003**.
5. Carraway, A. D.; McCollumn, M. G.; Peterson, J., *Inorg. Chem.,* **1996**, *35,* 6885.
6. Carraway, A. D.; Burkhalter, R. S.; Timkovich, R.; Peterson, J., *Inorg. Biochem.,* **1993**, *52,* 201.
7. Chuang, W. J.; Chang, Y. D.; Jeng, W. Y., *J. Inorg. Biochem*., **1999**, *75(2)*, 93.
8. Sannasy, D., M.Sc. Dissertation, University of the Witwatersrand, Johannesburg, South Africa, **2005**.
9. Tullio, A. D.; Caputi, L.; Malatesta, F.; Reale, S.; Angelis, F. D., *J. Mass Spectrom.*, **2005**, *40*, 325.
10. Merrifield, R. B., *J. Am. Chem. Soc.*, **1963**, *85(14)*, 2149.
11. Nilsson, B.L.; Soellner, M. B.; Raines, R.T., *Annu. Rev. Biophys. Biomol. Struct.*, **2005**, *34*, 91.
12. Casella, L.; Gioia, L. D.; Silvestri, G. F.; Monzani, E.; Redaelli, c.; Roncone, R.; Santagostini, L., *J. Inorg. Biochem.*, **2000**, *79*, 31.
13. Stellwagen, E., *Biochemistry*, **1968**, 2496.
14. Lundbald, R. L., *Techniques in Protein Modification*, CRC Press, Inc., Florida, 1995, pp 105-124.
15. Harding, S. J.; Jones, J. H.; Sabirov, A. N.; Samukov, V. V., *J. Peptide Sci.*, **1999**, *5*, 368.

APPENDIX FOR CHAPTER 4
MONOMERISATION OF NAcCoMP8: SOLUTION BEHAVIOUR

APPENDICES FOR CHAPTER 4

APPENDIX 4.1 Derivation of Equation 4.5 and 4.9

At low [NAcCoMP8] (415 → 417 nm)

Suppose:

$$2M \rightleftharpoons D_1$$

where:

$$2M + nL^{+} \xrightarrow{K_1} D_1$$

then:

$$[M] + 2[D_1] = 1$$

$$K_1 = \frac{[D_1]}{[M]^2[L]^n}$$

$$\therefore [D_1] = K_1[M]^2[L]^n$$

$$\therefore [M] + 2K_1[M]^2[L]^n - 1 = 0$$

$$\therefore [M] = \frac{-1 + \sqrt{1 + 8K_1[L]^n}}{4K_1[L]^n}$$

$$\therefore [D_1] = \frac{1 - [M]}{2}$$

Similarly,

At high [NAcCoMP8] (417 → 424 nm)

Suppose:

$$2D_1 \rightleftharpoons T_L$$

where:

$$2D_1 + jL^+ \xrightarrow{K_2} T_L$$

then:

$$[D_1] + 2[T_L] = 1$$

$$K_2 = \frac{[T_L]}{[D_1]^2[L]^j}$$

$$\therefore [T_L] = K_2[D_1]^2[L]^j$$

$$\therefore [D_1] + 2K_2[D_1]^2[L]^j - 1 = 0$$

$$\therefore [D_1] = \frac{-1 + \sqrt{1 + 8K_1[L]^j}}{4K_2[L]^j}$$

$$\therefore [T_L] = \frac{1 - [D_1]}{2}$$